Real-Time Strategies for Enhancing Aircraft Performance in Wind

A DISSERTATION
SUBMITTED TO THE FACULTY OF THE GRADUATE SCHOOL
OF THE UNIVERSITY OF MINNESOTA
BY

Kamuran Turkoglu

IN PARTIAL FULFILLMENT OF THE REQUIREMENTS
FOR THE DEGREE OF
Doctor of Philosophy

Yiyuan J. Zhao, Adviser

August, 2012

Acknowledgements

This is the final result of a long journey. On the way, I have witnessed, experienced and learned a lot of things which helped me to improve myself at every single step of this process. But overall, this is a work, which became possible with help and support of many valuable people who took place in my life during this journey.

First and foremost, I would like to express my gratitude to my advisor Professor Yiyuan J. Zhao. Without his support in tough times, guidance in dark days and help in difficult moments, this work would not be possible. It was a true privilege to know him personally and work with him professionally. Not only is he a great educator and researcher, but also he is a good person in heart.

Second, I want to express my thankfulness to Professor Tryphon T. Georgiou. He has been a continuous support throughout my PhD studies and has been a great mentor. I'm very happy and privileged that I had a chance to know him and work with him.

I would like to thank my committee members Professor William Garrard and Professor Yohannes Ketema for the useful discussions that they had provided throughout the journey. I would also like to thank Professor Mihailo R. Jovanovic for being a part of the process with his support and encouragement.

I thank Arda Ozdemir, Pietro Ferrero, Eyoab Zegeye and Kyung-Hoon Shin for their company during my stay at the University of Minnesota. I would sincerely like to thank Brianna Jean Kendall for encouraging me throughout tough times and for showing her support no matter what the circumstances were. In addition, I will always remember FC Voyageurs soccer team for the great intramural games.

I would like to thank Cuma Yarim for his conditionless help and support from the very beginning of this journey. I'm happy to now him for the last 20years.

And my family: I don't know how to thank them, since every single word I put

here will not be enough to express my gratitude, love and thankfulness I have in my heart for them. My father, Mehmet Turkoglu; my mother, Ayse Turkoglu; and my brother, Ercument Turkoglu, have been there, for me, to support me in very challenging moments, regardless what the circumstances were. They deserve a lot more than a thank you on these pages. I only wish health for all of my family members for better days to come.

To each of above, I extend my sincere appreciation, from deep inside my heart: Thank you!

Dedication

"Fall seven times, stand up eight ... "

Abstract

This thesis presents real-time guidance strategies for unmanned aerial vehicles (UAVs) that can be used to enhance their flight endurance by utilizing *insitu* measurements of wind speeds and wind gradients. In these strategies, periodic adjustments can be made in the airspeed and/or heading angle command for the UAV to minimize a projected power requirement at some future time. In this thesis, UAV flights are described by a three-dimensional dynamic point-mass model. A stochastic wind field model has been developed not only to reflect the mean wind magnitude behaviour in both vertical and horizontal axis, but also has it been extended to characterize wind direction behaviour as well. Proposed wind field model is assumed that it is consisted of a constant term plus terms that vary sinusoidally with respect to the location and time. Onboard closed-loop trajectory tracking logics that follow airspeed vector commands are modeled using the method of feedback linearization. To evaluate the benefits of these strategies in enhancing UAV flight endurance, a reference strategy is introduced in which the UAV would follow the optimal airspeed command in a steady level flight under zero wind conditions. A performance measure is defined as the average power consumption both over a specified time interval and over different initial heading angles of the UAV. A relative benefit criterion is then defined as the percentage improvement in the performance measure of a proposed strategy over that of the reference strategy. Extensive numerical simulations are conducted to show efficiency and applicability of the proposed algorithms. Results demonstrate the efficiency, benefits and trends of power savings of the proposed real-time guidance strategies in level flights.

Contents

List of Tables

List of Figures

Chapter 1

Introduction

1.1 Introduction

Every flying object, due to the nature of flight and its interaction with the atmosphere, is subjected to (either severe or moderate) air currents and/or winds. Since it is not possible to avoid such external disturbance effect, one natural reaction towards this phenomenon is to try to come up with solution strategies that will turn the situation into advantage rather than a disadvantage.

When nature is observed, it is possible to see that birds, in that extent, are the most known experts to benefit from the wind currents! They are able to take advantage of wind currents not only to minimize their energy consumption, but also to maximize their endurance. For instance, Albatros is a seabird of the biological family Diomedeidae that is known to be able to maintain nonstop intercontinental flights (ranging from 5000 to $\sim$7500 nautical miles) just by taking advantage of *local* wind currents. One important aspect of this is that, they do not have any information and the ability to estimate the weather conditions on the path they are flying (and/or going to fly through). They solely base their decisions with respect to local and instantaneous wind conditions and optimize their trajectory based on these local and instantaneous decisions.

As humanbeings, we have learned, adapted many things from nature to revolutionize and improve the way we live. And, in long run, this is another yet simple but inspiring mechanism to learn and incorporate into our daily lives through the mechanics of flight.

Therefore, in the light of all these inspiring facts, the main motivation behind this

study becomes to answer the following ultimate questions:

- Since it is not possible to avoid air currents and/or winds during the flight of aerial objects,
  - *What are the conditions that will make it possible to utilize wind energy, benefit from the wind currents and minimize power consumption to fly with less effort?*
- Like every single dynamic system existing in nature, everything has its own limitations, and in this case,
  - *What are the advantages as well as limitations associated with this approach?*
- And finally,
  - *What are the outcomes (benefits, energy savings, ... etc) of this approach?*

To investigate such phenomenon, as an application platform, small to mid-size Unmanned Aerial Vehicles (UAVs) are of great interest for this study. UAVs are increasingly being applied in a wide range of fields and because of their generally light weight and/or small size, wind can play an important (and sometimes crucial) role in terms of endurance, range, safety and power management during the whole flight. This is specifically true for micro air vehicles. With this, given the ubiquitous nature of wind, it is imperative to understand the potential effect of the wind energy on UAV flights and, when possible, to devise UAV flight strategies that enable them to benefit from the natural energy of the wind.

Ideally, if the regional wind information is completely known in advance (with the help of a pre-determined (forecasted) weather/wind maps over the flight region), optimal flight/trajectory planning can be used to determine flight paths that minimize the total power consumption over a specified time interval, subject to various constraints. However, the main challenge for such a *pre-determined map* approach is that (due to the highly complex, coupled and nonlinear nature of the atmosphere) weather forecasting is a process which includes extensive prediction errors (sometimes up to 50%) in its estimation routine. In addition, when these errors propagate through the flight regime, and when the actual wind field changes throughout the flight, previously determined

wind map becomes invalid and erroneous. This causes the UAV to fly in a state which is thought to be optimal, but actually is completely out of the pre-determined optimal domain. Such an approach has the need to obtain not only precise and accurate, but also timely wind information in the region of flight before (or at the beginning of) the flight, which has its own drawbacks as mentioned above.

Therefore, instead of making decisions based on pre-determined (also erroneous) weather maps, with this study, it is aimed to come up with real-time guidance strategies that will make *local*, *in-situ* decisions using *on-board* instruments to benefit from the existing *local* wind conditions and minimize power consumption during the flight. The foundation of this concept had been briefly outlined by the author in Turkoglu and Zhao (2009), and in this thesis, it has been investigated thoroughly in further details.

1.2 Overview of Previous Work

Previous studies have indicated that there is a great potential for UAV to use wind energies in terms of minimizing the power consumption and maximizing the endurance of the flight.

There are pioneering works in the area of UAV flights utilizing wind energies. The developments and flight tests of practical guidance strategies for detecting and utilizing thermals by Allen (2005); Allen and Lin (2007) and Edwards (2008) have illustrated the feasibility of these concepts. Boslough (2002) demonstrated the benefits of utilizing wind gradients through dynamic soaring using radio-controlled UAVs. Patel and Kroo (2006) studied the effect of wind in determining optimal flight control conditions under the influence of atmospheric turbulence. Langelaan (2008) studied how to exploit energy from high frequency gusts in the vertical plane for UAVs. Wharington (1998, 2004) presented methods for learning the wind patterns, based on local sensing and an appropriately selected reward function, and to fly most efficiently. Pisano and Lawrence (2009) investigated the gust sensitivity on the UAV dynamics as a function of aircraft size. In addition, Langelaan (2009) presented a method for minimum energy path planning in complex wind fields using a predetermined energy map. Lawrance and Sukkarieh (2009); Lawrence and Sukkarieh (2009); Sukkarieh and Lawrence (2011)

developed a framework for an energy-based path planning that utilizes local wind estimations for dynamic soaring using the measurements and predictions from the wind patterns. Rysdyk (2007) studied the problem of course and heading changes in significant wind conditions. McNeely, Iyer, and Chandler (2007) and et al. studied the tour planning problem for UAVs under wind conditions. McGee and Hedrick (2007) presented a study of optimal path planning using a kinematic aircraft model.

Dynamic optimization methods have also been used to determine the full potential benefits of wind energy utilization when a regional wind model is known. Nachmani (2007) studied the minimum energy flight paths for UAVs using wind forecasts with approximate dynamic programming technique. Sachs, Knoll, and Lesch (1991) et al. studied optimal glider dynamic soaring in a wind gradient. Zhao and Qi (2004); Qi and Zhao (2005); Zhao (2004) showed that under appropriate conditions with a full knowledge of the wind field in a region, a UAV can greatly enhance its endurance by properly utilizing wind energies. In addition to favorable wind patterns, such as wind gradient and thermals, Zhao (2009) recently showed that even downdraft wind can be utilized to improve UAV performances. These results indicate that the utilization of wind energies for enhancing UAV flights is highly promising. Furthermore, dynamic optimization methods have also been applied to glider flights in winds by Pierson and Chen (1980); Pierson and Jong (1978); Lorenz (1985). In addition, Mueller, Zhao, and Garrard (2009) studied optimal airship ascent flights by utilizing wind energy. In these studies, the nonlinear dynamic optimization formulation was incorporated in general sense. This approach typically requires knowledge of regional winds and an iterative solution process, and thus may not be feasible for generating real-time guidance strategies due to excessive computational times (sometimes hours) and slow convergence rates. Still, they are useful in understanding fundamental patterns of optimal UAV flights in winds and providing benchmark results that can be used to evaluate wind utilization strategies. Approximate solutions may also be obtained for nonlinear dynamic dynamic optimization problems to explore and aid real-time guidance strategies.

In all of these studies, it is assumed that wind information is fully known over the region of flight. But in reality wind is a stochastic process that also needs to be addressed appropriately. One suitable approach is to devise real-time evaluation strategies of wind behaviour rather than depending on big forecasted maps with embedded errors.

Therefore when all of the stated arguments are taken into account, it is reasonable to adopt the idea of *local*, *instantaneous* measurements to utilize wind energy via the information available at that specific time instant t_0. Compared with the dynamic optimization studies, this thesis presents real-time guidance strategies that use *in-situ* wind measurements alone with no regional wind information, to reduce power consumptions. Then, the main goal of this study becomes *to develop such real-time guidance strategies that will utilize wind energy through instantaneous wind measurements: In this way try to minimize power consumption and enhance the endurance of UAV flights based on in-situ wind information.*

This thesis presents such real-time guidance strategies in which optimal adjustments are made to the airspeed, heading angle and/or flight path angle commands to minimize a projected power consumption at some future time to prolong a UAV flight, based on the *instantaneous*, *local* wind conditions. The onboard feedback control system then tracks these modified commands, and this process is repeated periodically throughout the entire flight.

These strategies periodically adjust airspeed vector commands (i.e. airspeed, heading angle and flight path angle) to take advantage of changes in the mean wind profile. Wind energies in the changing mean wind profile are generally of lower frequency compared with gust energies. As a result, the proposed real-time guidance strategies complement the previous works on real-time guidance and control methods that utilize gust energies.

1.3 Outline of Thesis

The objective of this thesis is to study autonomous optimal flight guidance strategies that will benefit from local wind conditions to minimize power consumption through periodic adjustments on airspeed, heading angle and/or flight path angle.

In Chapter 2, UAV models have been obtained based on 3D point-mass equations. Performance constraints, together with practical and operational constraints are listed. In Chapter 3, a statistics based stochastic wind model has been derived to characterize wind behaviour. Moreover, a stochastic wind magnitude model has been obtained together with stochastic wind direction characteristics. In Chapter 4, UAV flights are

formulated as non-linear optimal control problems that minimizes power consumption at terminal states. Given problem has been presented as a static optimization problem and solution strategies has been given for 3-dimensional and level flights in Chapters 5 and 6. Necessary optimization strategies to solve such problem has been devised in Chapter 7. In Chapter 8, models of closed loop tracking strategies has been derived which will make sure that once the optimal states are calculated they will be tracked appropriately. Numerical and simulational results are presented in Chapter 9. Important features and power saving flight patterns are discussed. In particular, it has also been shown that combination of guidance strategies serves well for power minimization strategies in restricted flight zones as well. Conditions of energy extraction from the wind conditions are discussed in further details, while with Chapter 10 summary of real-time optimal flight strategies is given. With several key suggestions in Chapter 11, the thesis has been finalized.

With this thesis it is concluded that, using suggested real-time guidance strategies, significant power savings can be obtained by utilizing wind energy.

Chapter 2

UAV Modeling and Analysis

In control systems design, modeling of the plant dynamics plays an essential role in terms of obtaining meaningful results. Modeling of the plant dynamics should be accurate and precise enough to reflect the true nature of plant in hand, so that the designed control system can respond and produce accurate control effort to achieve desired performance measures. Therefore, in trajectory optimization studies modeling of UAV (or any air-vehicle) dynamics is a vital task in accomplishing meaningful results.

In flight dynamics, it is a common practice to use 6DOF rigid-body models to study/analyze the instantaneous (or short term) behaviour of the aircraft. The nature of the 6DOF rigid-body models is highly complex, but provides valuable insight into the short term behaviour of the longitudinal and/or lateral dynamics of the aircraft.

When the nature of trajectory optimization problems is taken into account, it is possible to see that there are six main components which are vital in determining (and also analyzing) the flight trajectory: airspeed (V), heading angle (Ψ), flight path angle (γ) and location of the aircraft in terms of x, y and h coordinates. Once these quantities are known (and/or provided), trajectory planning becomes a relatively easy task. In trajectory optimization community, it is a common practice to model and study the flight trajectory of the air-vehicle as a 3D dynamic point mass model. With this approach, not only is it possible to provide all the listed flight trajectory components (i.e. V, Ψ, γ, x, y and h), but also is able to provide more simple and less cumbersome dynamic structure than the rigid-body model for thorough analysis.

If rigid-body dynamics and 3D dynamic-point-mass modeling approaches and results

are compared with each other, it is possible to see (as shown in Kinoshita and Imado (2006a,b)) that even if the short term transient response may slightly vary from case to case, the overall steady state behaviour of aircraft dynamics remains identical. This fact has also led trajectory optimization community to inherit the usage of 3D dynamic point mass model in problem formulations instead of cumbersome and complex structure of 6 DOF rigid-body models.

In this study, the main goal is to observe, analyze and investigate the long term characteristic behaviour of UAV trajectories in presence of wind. For this purpose, it is desired to benefit from simple, but yet unique and compact characteristics of 3D dynamic-point-mass-model to devise real-time optimal guidance strategies. Therefore, in this thesis, for the purpose of developing optimal guidance strategies, UAV flights are represented using a 3D dynamic-point-mass model, and the detailed structure is provided in further detail in the following sections.

2.1 Equations of Motion

For a propeller-driven UAV, corresponding equations of motion (EoM) (taken from Jackson, Zhao, and Slattery (1999)) are as

$$m\dot{V} = T - D - mg\sin\gamma - m\dot{W}_V \tag{2.1}$$

$$mV\cos\gamma\dot{\Psi} = L\sin\mu - m\dot{W}_\Psi \tag{2.2}$$

$$mV\dot{\gamma} = L\cos\mu - mg\cos\gamma + m\dot{W}_\gamma \tag{2.3}$$

$$\dot{x} = V\cos\gamma\sin\Psi + W_x \tag{2.4}$$

$$\dot{y} = V\cos\gamma\cos\Psi + W_y \tag{2.5}$$

$$\dot{h} = V\sin\gamma + W_h \tag{2.6}$$

where the UAV mass is assumed to be constant. Here, wind acceleration terms are expressed as

$$\dot{W}_V = \dot{W}_x\cos\gamma\sin\Psi + \dot{W}_y\cos\gamma\cos\Psi + \dot{W}_h\sin\gamma \tag{2.7}$$

$$\dot{W}_\Psi = \dot{W}_x\cos\Psi - \dot{W}_y\sin\Psi \tag{2.8}$$

$$\dot{W}_\gamma = \dot{W}_x\sin\gamma\sin\Psi + \dot{W}_y\sin\gamma\cos\Psi - \dot{W}_h\cos\gamma \tag{2.9}$$

and complete derivation of given equations of motion is presented in Appendix-A for further, detailed investigation.

In the equations above lift (L), drag (D) and power (P), can be expressed as

$$L = \frac{1}{2}\rho V^2 S C_L, \quad D = \frac{1}{2}\rho V^2 S C_D, \quad P = TV \tag{2.10}$$

and the drag coefficient is modeled by the parabolic drag polar (as shown in Anderson (1989))

$$C_D = C_{D_0} + K C_L^2 \tag{2.11}$$

The induced drag factor (K) can be determined from the aerodynamic efficiency and the zero-lift drag coefficient as

$$E_{\max} = \left(\frac{C_L}{C_D}\right)_{\max} \quad \Rightarrow \quad K = \frac{1}{4E_{\max}^2 C_{D_0}} \tag{2.12}$$

For these equations, trajectory control variables are power (P), lift coefficient (C_L), bank angle (μ), and trajectory state variables are airspeed (V), heading angle (Ψ), flight path angle (γ), x-location (x), y-location (y) and h-location (h).

Generally, the wind terms depend not only on location, but also on time,

$$W_x(x, y, h, t), \quad W_y(x, y, h, t), \quad W_h(x, y, h, t) \tag{2.13}$$

and in this formulation, winds are considered as exogenous inputs to the system, where the specific models of the wind field are discussed below, in Chapter 3.

2.2 Normalized Equations of Motion

In non-trivial numerical analysis, quantities can (and usually do) differ in magnitude by great amounts. In presence of such drastic variation, numerical precision is affected immensely and concurrent errors propagate into the solution. This not only leads the solution itself to be unreliable, but also causes the solution to be infeasible. However, it is possible to avoid this issue, to certain extent, by scaling all variables and by making them close to one (1) in value. Then, any change in a variable becomes comparable (in magnitude) to a change in any other component. In this way, algorithm not only is able to function better, but this move also helps to reduce the computational cost, extensively.

Following to this, it is also beneficial to transform all the variables to a *unit-less/normalized* form, which can be derived through simple algebraic manipulations of some of the fundamental parameters of given problem. Through such *normalization* procedure, valuable insight is gained into how the problem depends on those *chosen* normalizing set of parameters. With the correct combination, the normalizing parameters should contain all possible units to allow the normalization of a variable with any possible unit.

Thus, in order to increase numerical efficiency in the simulation studies and to reduce computational complexity, the above equations of motion are normalized by specifying a characteristic air-speed V_n and mass m. In this thesis, characteristic *normalization speed-*V_n is selected to be the maximum speed of the aircraft (i.e. $V_n = V_{max}$).

Following to some algebraic manipulations, it is possible to obtain normalized state, rate and time components as

$$\bar{V} = \frac{V}{V_n}, \quad (\bar{x}, \bar{y}, \bar{h}) = \frac{(x, y, h)}{V_n^2/g}, \quad \bar{t} = \frac{t}{V_n/g} \tag{2.14}$$

$$(\ )' = \frac{d(\ )}{d\bar{t}} = \frac{V_n}{g}\frac{d(\ )}{d\bar{t}} \tag{2.15}$$

where normalized air density is given as

$$\bar{\rho} = \frac{\rho S V_n^2}{2mg} = \frac{\rho V_n^2}{2(mg/S)} \tag{2.16}$$

Above, the normalized air-density, $\bar{\rho}$, represents the combined effect of air density (ρ) and wing loading (mg/S) on UAV flights. More specifically, a smaller $\bar{\rho}$ corresponds to a larger wing loading (a heavier UAV) and/or thinner air, where a larger $\bar{\rho}$ represents a lighter UAV (with a smaller wing loading) and/or thicker air.

Using these normalization quantities, the normalized lift, drag and power become

$$\bar{L} = \frac{L}{mg} = \bar{\rho}\bar{V}^2 C_L, \quad \bar{D} = \frac{D}{mg} = \bar{\rho}\bar{V}^2 C_D, \quad \bar{P} = \frac{P}{mgV_n}, \tag{2.17}$$

and normalized wind components are defined as

$$\bar{W}_{x,y,h} = \frac{W_{x,y,h}}{V_n}, \quad \bar{W}'_{V,\gamma,\Psi} = \frac{\dot{W}_{V,\gamma,\Psi}}{g}, \quad \bar{W}'_{x,y,h} = \frac{\dot{W}_{x,y,h}}{g} \tag{2.18}$$

Following to this, the set of normalized equations of motion are obtained as

$$\bar{V}' = \frac{\bar{P}}{\bar{V}} - \bar{\rho}\bar{V}^2(C_{D_0} + KC_L^2) - \sin\gamma - \bar{W}_V'(\bar{V}, \Psi, \gamma, \bar{x}, \bar{y}, \bar{h}) \tag{2.19}$$

$$\Psi' = \frac{\bar{\rho}\bar{V}C_L}{\cos\gamma}\sin\mu - \frac{1}{\bar{V}\cos\gamma}\bar{W}_\Psi'(\bar{V}, \Psi, \gamma, \bar{x}, \bar{y}, \bar{h}) \tag{2.20}$$

$$\gamma' = \bar{\rho}\bar{V}C_L\cos\mu - \frac{\cos\gamma}{\bar{V}} + \frac{1}{\bar{V}}\bar{W}_\gamma'(\bar{V}, \Psi, \gamma, \bar{x}, \bar{y}, \bar{h}) \tag{2.21}$$

$$\bar{x}' = \bar{V}\cos\gamma\sin\Psi + \bar{W}_x(\bar{x}, \bar{y}, \bar{h}) \tag{2.22}$$

$$\bar{y}' = \bar{V}\cos\gamma\cos\Psi + \bar{W}_y(\bar{x}, \bar{y}, \bar{h}) \tag{2.23}$$

$$\bar{h}' = \bar{V}\sin\gamma + \bar{W}_h(\bar{x}, \bar{y}, \bar{h}) \tag{2.24}$$

and

$$\bar{W}_V' = \bar{W}_x'\cos\gamma\sin\Psi + \bar{W}_y'\cos\gamma\cos\Psi + \bar{W}_h'\sin\gamma \tag{2.25}$$

$$\bar{W}_\Psi' = \bar{W}_x'\cos(\Psi) - \bar{W}_y'\sin(\Psi) \tag{2.26}$$

$$\bar{W}_\gamma' = \bar{W}_x'\sin(\gamma)\sin(\Psi) + \bar{W}_y'\sin(\gamma)\cos(\Psi) - \bar{W}_h'\cos(\gamma) \tag{2.27}$$

where the functional dependencies of the wind terms are shown in parenthesis, for convenience. Here, the normalized rates of wind speeds follow similar expressions as given in Eqs.(2.7-2.9).

Complete set of derivation of normalized wind components is given in Appendix-B and can be investigated in further detail.

Constraints on states and controls can also be expressed using normalized values which is presented in the following chapters.

Chapter 3

Wind Profile and Analysis

In previous chapter, equations of motion that governs UAV dynamics have been provided together with the normalized equations of motion. The normalization procedure will aid to enhance the numerical efficiency of the proposed strategies and, moreover, will decrease the computational cost for real-time guidance strategies.

Following to these, in this chapter, a statistics based stochastic wind model is introduced. With the derivation of statistics based stochastic wind model, it is aimed to characterize not only the global wind magnitude behaviour, but also the nature of wind direction. The following sections present the detailed analysis and derivation of the process.

3.1 Statistics Based Stochastic Wind Model

In real-time guidance strategies, the characteristics of the wind and wind modeling plays an important role in obtaining reasonable results from the devised algorithm (especially if the wind is the main driving mechanism of the trajectory optimization routine). It is desired to have as realistic as possible wind model to reflect the real nature and the true outcome of proposed guidance strategies (which are going to be introduced in the next chapter). Therefore, in this section, it is aimed to come up with a statistics based stochastic wind model that will reflect observed, true nature of the wind characteristics. This will provide a tool that could be used in simulations to obtain meaningful and more realistic results in trajectory optimization calculations.

For this study, existing/recorded meteorological data (from weather stations located at airports in whole continental US) and publicly accessible NOAA (and IGRA) archives has been used. Based on these real data sets, it desired to devise an approximate wind model that will represent wind behaviour around the continental US.

In this specific study (to reflect the global behaviour of wind characteristics), wind data sets from two East coats locations (namely from Albany, NY and Pittsburg, PA), two Mid-West locations (Green Bay, WI and Minneapolis, MN) and two West coast locations (Tucson, AZ and San Diego, CA) have been considered. With this, the intent is to demonstrate the global, long term and low-frequency wind behaviour over different locations in continental US (varying from East Coast, to Mid-West and to West Coast). Moreover, the expectation with deriving such statistics based stochastic wind model is that it can be used with simplicity in not only aerospace engineering, but also in several other areas and applications. Some of these possible application areas may be wind turbines (wind load models), environmental engineering (atmospheric dispersion models) and so on. Thus, the main emphasis was given on obtaining an approximate wind model, which will aid to demonstrate the overall outcome of the proposed strategies in general wind conditions.

Obtaining an analytical wind model is still an ongoing research effort in *Meteorological and Wind Engineering society* and is a very complicated, highly challenging task. Derivation of a purely analytical expression for wind behaviour as a function of pressure (gradients), temperature, humidity, surface roughness and density is an elaborate procedure and relates itself to Navier-Stokes, Conservation of Mass and Conservation of Momentum equations as well as Heat Equation and Diffusion Equations. To avoid such complex nature of airflow, to simplify the evaluation procedures and to increase the applicability of the proposed wind model in the field of engineering, a statistical study has been conducted to obtain a wind model expression. For this purpose, monthly data (for the year of 2010) from each (above mentioned) location has been considered and compared. In this process, not only monthly *wind magnitude* characteristics are evaluated, but also *wind direction* characteristics (for each location) have been investigated to devise a meaningful pattern for the analysis of wind behaviour.

Here, analysis has been broken into two parts: First, the change of wind magnitude

and wind direction characteristics with respect to altitude has been analyzed. Second, horizontal wind magnitude and wind direction characteristics are examined. The following two sections discuss the insights of these procedures in further detail.

3.2 Vertical Wind Profile

3.2.1 Wind Magnitude

The analysis starts with investigating recorded wind data sets extracted from weather stations. For the above mentioned stations, obtained wind data plots are given in Fig-3.1, which characterizes the change in wind magnitude with respect to altitude up to 20km ($\sim$ 65,600 [ft]). In Fig-3.1, coloured dots are observations from locations

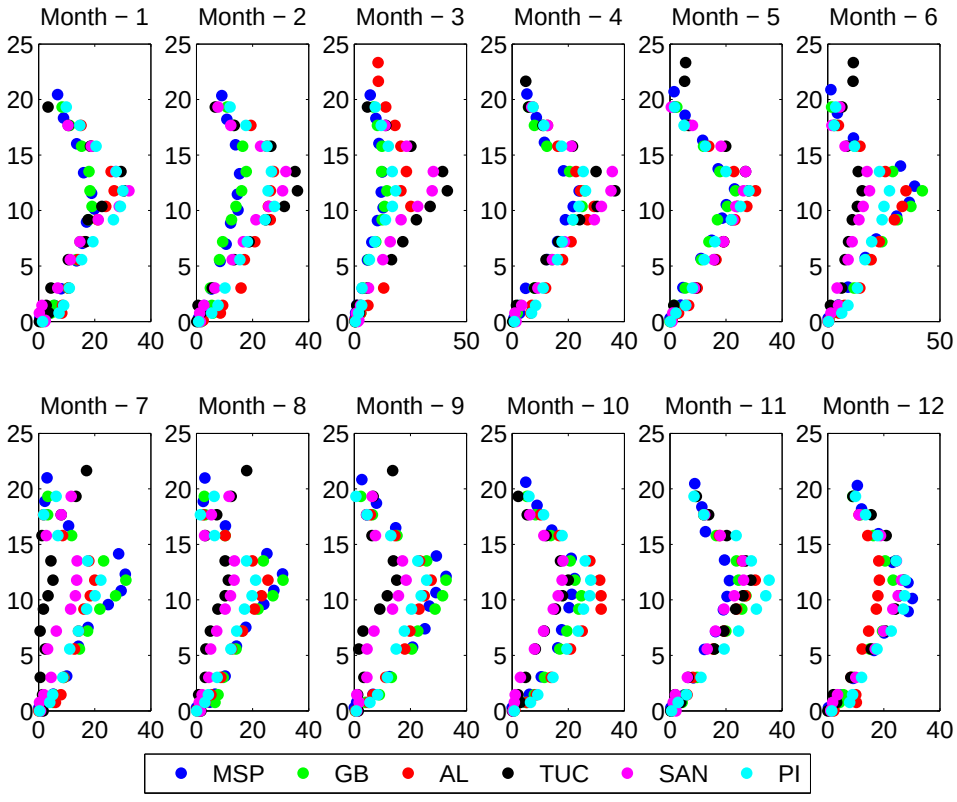

Figure 3.1: 12months statistical wind data obtained from 6 different states for year 2010. X-label: Wind magnitude [m/sec] and Y-label: Altitude [km]

as specified in legends.

With careful investigation of Fig-3.1, it is possible to see that for each month and altitude, the maximum and minimum wind magnitude values are varying from location to location, as well as from altitude to altitude. This brings the concept of uncertainty into the picture. This also introduces the benefit of describing the statistical wind model as a function of uncertainties around the mean value. To address this, next, *mean value* and *uncertainty* characteristics for vertical wind profile has been obtained.

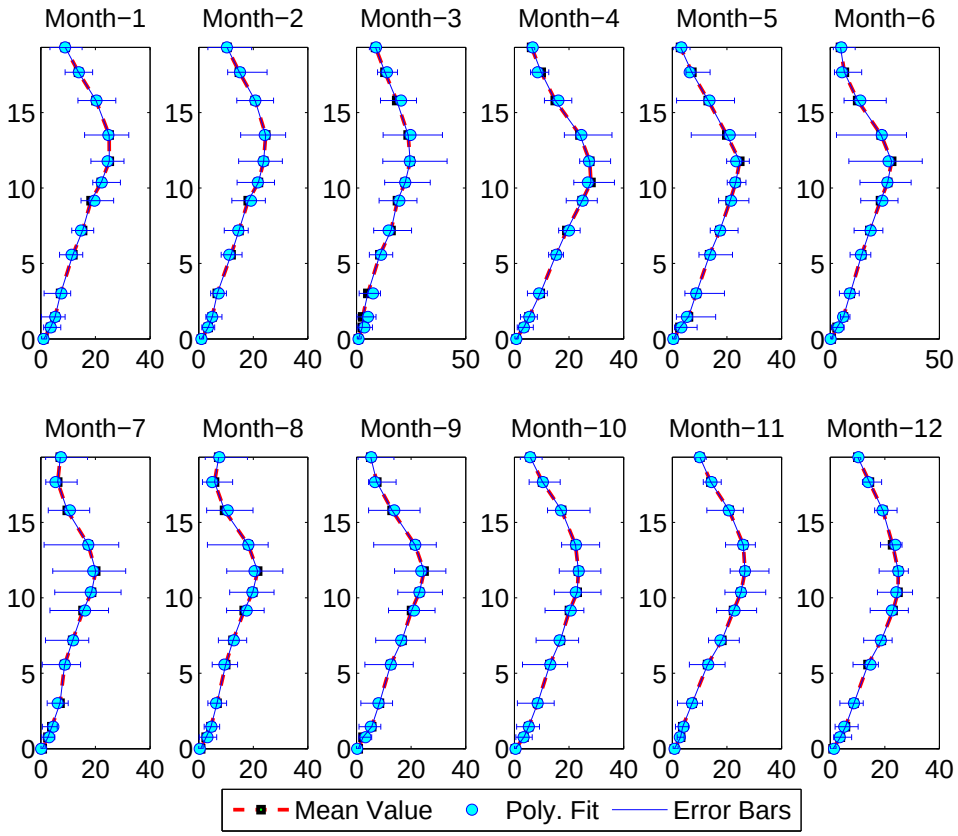

Figure 3.2: 12months statistical average wind data fit obtained from 6 different states for year 2010. X-label: Wind magnitude [m/sec] and Y-label: Altitude [km]

Associated uncertainties can also be defined with respect to an upper and lower

bound as a function of maximum and minimum observed values, at each specific altitude. With this, it is appropriate to plot mean value characteristics together with uncertainty bounds (error bars) for each specific month (during the year of 2010). The results are as given in Fig-3.2.

Using all this information, in order to obtain an approximate model of observed wind magnitude data, it is possible to fit several linear/nonlinear curves to match the observed wind characteristics. In our case, for its simplicity and use of algebraic manipulations, a polynomial fit is obtained to specify changes in wind magnitude with respect to altitude.

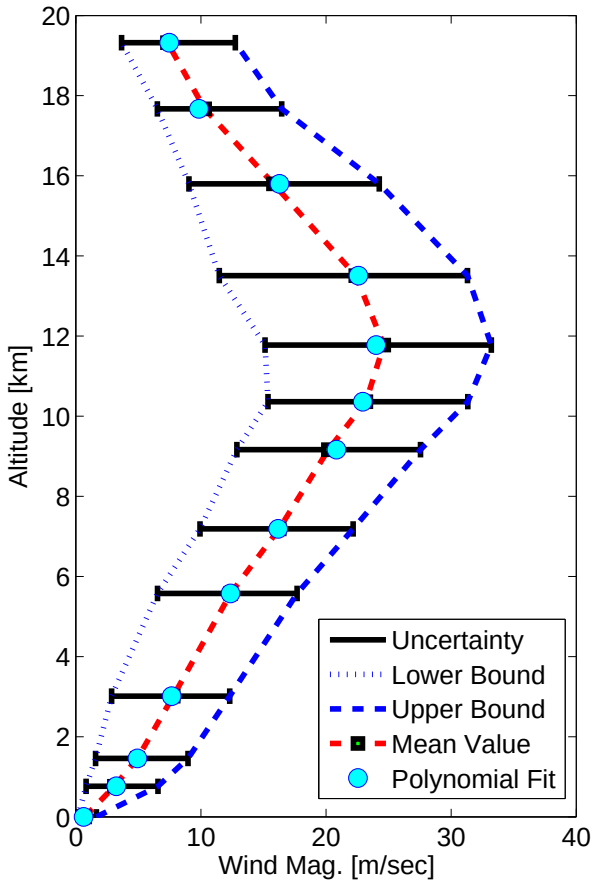

Figure 3.3: Average vertical wind magnitude profile for selected location over the year of 2010.

Finally, if all the measured data sets are combined, obtained average vertical wind profile (with given uncertainty bounds) is as given in Fig-3.3. Each uncertainty region is consisted of an upper bound which defines the maximum overall observed wind magnitude at that altitude, while the lower bound defines the overall minimum observed wind magnitude at that specific altitude. For clarification, the boundaries of uncertainty regions are also marked with blue (dashed and solid) lines to specify "the bandwidth of the change in wind magnitude with respect to altitude". As a result, obtained fit for the mean of the observed vertical wind magnitude is a $5^{th} - order$ polynomial and is given in Eq.(3.1).

$$P_{W_{avg}} = 0.0003h^5 - 0.0127h^4 + 0.1814h^3 - 1.0250h^2 + 4.0995h + 0.6336 \qquad (3.1)$$

Graphical representation of fitted polynomial model is given in Fig-3.3 and can be observed with cyan dotted points. This model will be used to generate wind magnitude data for a specific flight altitude.

As a further and more detailed study, it is also possible to obtain mean values for a collection of several (like 10) years of statistical data and associated uncertainties at each location with respect to different altitudes. With this extended approach, it will also be possible to define the vertical wind model for change magnitude as a function of altitude, which is based on statistically obtained wind data. This may further be extended to the 52 states all around the continental US, but since this is out of the scope of the intended study, it is left aside for future research and is not pursued in this thesis.

3.2.2 Wind Direction

Following to the analysis of wind magnitude for vertical profiles, same analysis is conducted for the wind direction. The corresponding data for the above selected locations is plotted and obtained results are as given in Fig-3.4

In order to be able to derive meaningful wind models, the average of the observed wind direction characteristics over different altitudes has been taken. Obtained results are given in Fig-3.5.

As it is justifiable from Fig-3.5, wind direction up to 9[km] changes significantly. Starting from 9[km] up to 16[km], wind magnitude pretty much remains constant and

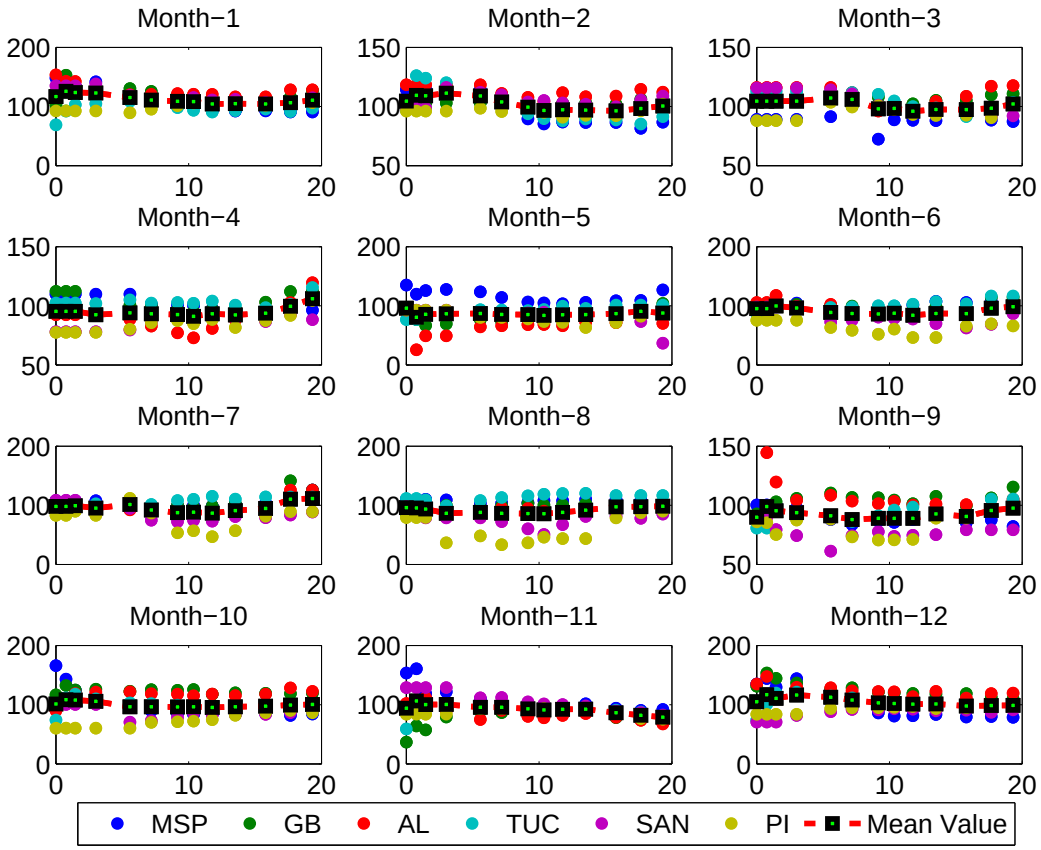

Figure 3.4: Vertical wind profile characteristics for selected locations over 2010. X-label: Altitude [km] and Y-label: Wind direction (w.r.t. true north) [deg].

deviates around a constant value of 90^o (with very small amount of variations [i.e. $\sim 1^o - 4^o$]).

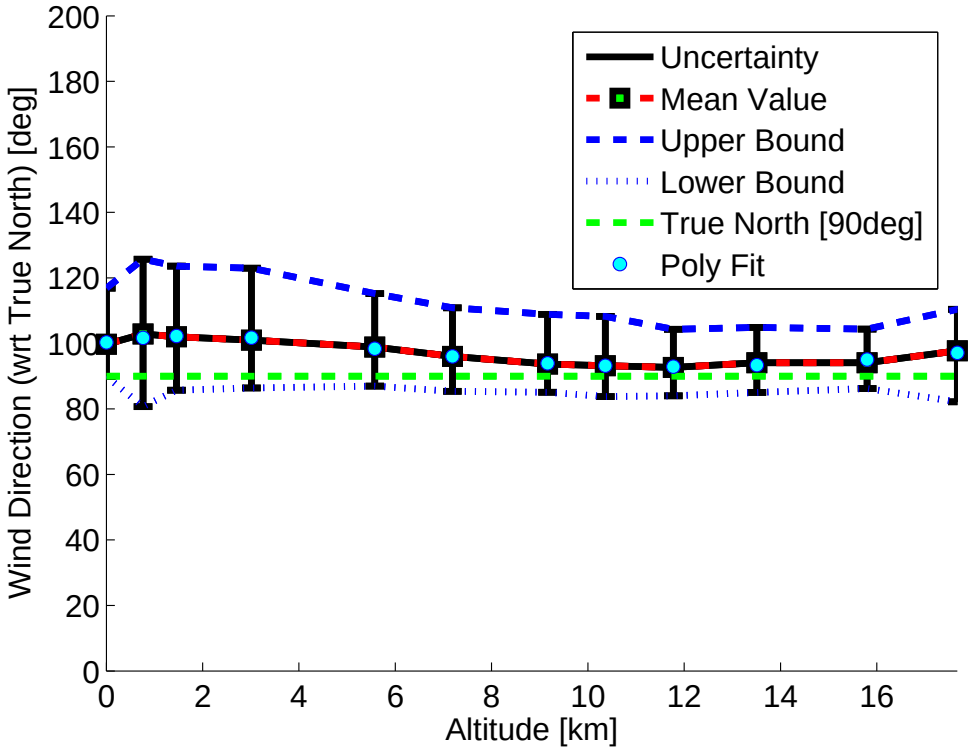

Figure 3.5: Average wind direction profile with associated uncertainties for selected location over the year of 2010.

This clearly gives the opportunity to the designer that, if the specific operation region is within the range of (9-16km), it is fair to assume that the wind direction is approximately constant and deviates around the mean with certain negligible amount of error ($\sim [1^o - 4^o]$). If it is favourable, this condition could be used in derivations and may also aid to further simplify the proposed wind model, increase the efficiency of algebraic manipulations and reduce the computational cost of real-time calculations. In the following sections it will be observed that this approach has not been used for this study, but has been provided here as an intuitive detail about the study. The operational region of flight that is defined in this study is way below the discussed

constant wind region (i.e. $9 - 16$[km]) and this assumption will not be used in the derivation of proposed wind model. But based on given observation data, it is a fair and legitimate approach to simplify wind model for a desired vertical region of flight, if it is in favour of designer.

$$\Psi_{W_{avg}} = 0.0007h^5 - 0.0195h^4 + 0.2772h^3 - 1.9711h^2 + 5.1323h + 102.1122 \tag{3.2}$$

Once the mean value of observed wind direction data is obtained, corresponding polynomial fit results in a $5^{th} - order$ polynomial and is as given in Eq.(3.2). Moreover, it is also possible to plot the deviations (uncertainties) around the mean value in terms of *error-bars*. Resulting uncertainty trends (with corresponding upper and lower bounds at each altitude) are also given in Fig-3.5.

Having defined uncertainties (deviations) around the mean values of both wind magnitude and wind direction, next step is to investigate the core of the wind model, which is the *analytical modeling of wind uncertainty (deviation) around the mean value*. This analysis has been conducted in the following section and detailed explanations are provided.

3.3 Modeling of Wind Uncertainty

3.3.1 Uncertainty in Wind Magnitude

As it is possible to see from Fig-3.3 and from Fig-3.5, uncertainty characteristics (i.e. deviation around the mean) can be defined based on observed upper and lower limits, for both wind magnitude and wind direction.

At this point, it is important to obtain a *stochastic uncertainty model* which will help to generate distributed stochastic data in simulations. For this purpose, it is assumed that, the wind magnitude and wind direction are consisted of two main parts: *mean value* ($\bar{}$) and *uncertainty (deviation)* around the mean. This has been formulated in an efficient manner as shown in Eq.(3.3),

$$\begin{aligned} W_m &= \bar{W}_m(h) + \omega_m \\ \Psi_w &= \bar{\Psi}_w(h) + \psi_w \end{aligned} \tag{3.3}$$

where $\bar{W}_m(h)$ and $\bar{\Psi}_w(h)$ depicts the mean values of wind magnitude and wind direction, respectively. In addition, ω_m with ψ_w stands for variations (uncertainties) around the mean value, for wind magnitude and wind direction, all at once.

As it was shown before, it is possible to devise models that specifies vertical wind magnitude characteristics. Having achieved that step, next step will be to derive models that will aid to define wind uncertainties (deviations) around the mean value, as a *stochastic process.*

For simplicity in design and modeling, without the loss of generality, variations (uncertainties) around the mean value will be modeled as a *first order stochastic differential equation system driven by white noise.* In that sense, it is logical to write the *first order stochastic differential equation* for uncertainty dynamics in wind magnitude as

$$\tau_h \frac{d\omega_m}{dh} + \omega_m = \omega_{mw} \tag{3.4}$$

where τ_h is a specified constant and ω_{mw} defines the white noise that drives the process. Here, Eq.(3.4) defines a first order differential equation with a stochastic nature, therefore it has to be dealt within the concept of *Stochastic Differential Equations (SDEs)*, which will constitute the next step of derivation.

Ornstein-Uhlenbeck Process:

In literature, stochastic differential equations has been studied extensively since 1960ies and still is an ongoing research topic. Throughout the years, stochastic differential equations has found ground for many applications varying from statistical physics to finance, from molecular dynamics to aerospace applications, and still are extensively used in numerous areas and applications.

In that context (as stated in Krapivsky et al. (2010), in Evans (2010), in Sauer (2010) and in many other literature sources) one of the vastly studied stochastic differential equation is *Langevin equation* which is given in Eq.(3.5).

$$dX(t) = -\mu X(t)dt + \sigma dW_t \tag{3.5}$$

or in more compact form,

$$\begin{aligned} \frac{dX(t)}{dt} &= -\mu X(t) + \sigma \frac{dW_t}{dt} \\ &= -\mu X(t) + \sigma v \end{aligned} \tag{3.6}$$

Here, μ and σ are positive constants peculiar to the system itself, and v is the white noise. Since, the main interest in this section is to model vertical wind (magnitude and/or direction) behaviour with respect to the altitude, it is clear that for the case of *modeling of wind uncertainties*, *Langevin equation* becomes a function of altitude as given in Eq.(3.7).

$$\frac{dX(h,t)}{dh} = -\mu X(h,t) + \sigma v \tag{3.7}$$

But unfortunately, with this form of *Langevin equation*, it is not possible to come up with an exact analytical solution in terms of a simple stochastic process. Instead, as stated in Sauer (2010), the solution to the *Langevin equation* (Eq.(3.7)) is provided numerically. This specific numerical solution is named as *Ornstein-Uhlenbeck process* in mathematics literature, after Leonard Ornstein and George Eugene Uhlenbeck. Once the stochastic system is converted to a *Ornstein-Uhlenbeck process*, such system can be solved using several numerical techniques (such as Euler-Maruyama approximation, as stated in Pinsky and Karlin (2011)) with ease.

The *Ornstein-Uhlenbeck process* is a unique process, which satisfies three unique properties: it is *Stationary*, it is *Gaussian* and it is *Markovian*. In other words, it is a *stationary process* meaning that when the stochastic process is shifted in time, the joint probability distribution function does not change. It is a *gaussian process*, meaning that random variables associated with the process inherits the characteristics of normal distribution. And finally, it is *markovian* meaning that the prediction for the future states of the process solely and only depends on the current states and not on the states in the past. In that sense, it can be considered as a "memoryless" process, as well. *Ornstein-Uhlenbeck process* is the only non-trivial stochastic process which satisfies these three conditions, and therefore it is of great interest and a perfect match for the intended studies on stochastic uncertainty modeling, which also inherits those three properties. The *Ornstein-Uhlenbeck process* is also considered to be a modified version of *random walk* in continuous time systems.

On the other hand, in *Arithmetic Ornstein-Uhlenbeck process* the characteristics has been changed, so that there is a driving force which enforces the system dynamics to go back to a steady-state (mean) value with time. Thus, the *Arithmetic Ornstein-Uhlenbeck process* is considered as the continuous branch of the discreet-time AR(1) process and is discussed in further detail in Brockwell and Davis (1991).

Arithmetic Ornstein-Uhlenbeck process is solved by applying *Itō-Doeblin's formula.* The derivation of the analytical solution is beyond the scope of this study, thus is omitted here. But the complete solution is given in Oksendal (1995, 4th Ed.) and can be investigated in further detail.

In this study, the emphasis is given on the implementation of *Arithmetic Ornstein-Uhlenbeck process*, and therefore, the main concentration will be focused on obtaining numerical recipes to implement the problem in computer (thus, in real-time on-board instruments). In order to be able to implement *Arithmetic Ornstein-Uhlenbeck process* in computer, it is a general practice to discretize with respect to the dependent variable (in our case altitude).

For that reason, it is desired to discretize *Arithmetic Ornstein-Uhlenbeck process*, which is defined as in Eq.(3.8).

$$\frac{dX(t)}{dh} = -\theta(X(h) - \mu) + \sigma v \tag{3.8}$$

Here, Eq.(3.8) dictates that the state variable is being *pulled* towards a steady state equilibrium level (μ) through an *intensity parameter* (θ). Due to this reason, it is also named as the *Mean-Reverting Ornstein-Uhlenbeck process.* Here, the *intensity* of *pulling towards the equilibrium* (or in other words, the intensity of mean-reverting) is controlled by the *intensity parameter-*θ. This stochastic differential equation is explicitly solveable and has the solution in terms of Itō's Integral as given in Eq.(3.9). The solution itself is given in Kloeden and Platen (1992) and can be investigated in further details, if desired.

$$X(H) = X(0)\exp(-\theta H) + (1 - \exp(-\theta H))\mu + \sigma \int_0^H \exp(\theta h) dz(h) \tag{3.9}$$

Following to this exact, discreet numerical solution, it is possible to apply the result in computer simulations. The process, as elaborated in further detail in Dixit and Pindyck (1994), is defined as given in Eq.(3.10)

$$X_h = X_{h-1} exp(-\theta \Delta h) + \mu(1 - exp(-\theta \Delta h)) + \sigma \sqrt{\frac{1 - exp(-2\theta \Delta h)}{2\theta}} \mathcal{N}(0, 1) \tag{3.10}$$

This, provides a numerical recipe that can be applied with ease in any computational platform. After obtaining such an exact numerical solution for desired uncertainty model (with the help of *Mean-Reverting Ornstein-Uhlenbeck process*), the next aim is to come up with *mean* and *standard deviation* characteristics (μ and σ, respectively), which will complete the stochastic uncertainty model analysis.

At this point, it is necessary to characterize the nature of the uncertainty in wind magnitude (namely the characteristics of the variation around the mean value). For this purpose, it is benefited from the *gaussian distribution* of the uncertainty characteristics associated with the wind behaviour. Here, Fig-3.6 constitutes a very good starting point, where all the observed data points (for different altitudes among the year of 2010) are given together with the observed upper and lower bounds and the mean value of the observations.

Using data sets given in Fig-3.6, it is possible to obtain and define the *gaussian distribution* of the uncertainties around the mean value for each specific altitude. Corresponding results are given in Fig-3.7. Obtained Gaussian fit has the characteristics of normal distribution as given in Eq.(3.11)

$$f(x;\mu,\sigma^2) = \frac{1}{\sigma\sqrt{2\pi}}\left[\exp -\frac{(x-\mu)^2}{2\sigma^2}\right] \tag{3.11}$$

A closer investigation on Fig-3.7 will reveal the fact that every single altitude will have different uncertainty distribution characteristics. In order to avoid complexity in the proposed wind model, it is assumed that wind is a stationary process for each observation altitude, and remains stationary between two different measurements in two different altitudes. In addition, between two observations, vertical wind magnitude maintains its stationary characteristics. Also, wind is considered piece-wise continuous within each segment and inherits gaussian distributions specified in Fig-3.7 and Fig-3.8. These assumptions also supports the main three characteristics of *Ornstein-Uhlenbeck process*. Therefore, it is a consistent and a reasonable assumption. finally, obtained standard deviation (σ) values are given in Table-3.1.

Having derived all the necessary components (μ and all σ characteristics) for the stochastic wind model, conducted 100 monte carlo simulations lead to stochastic wind model results as given in Fig-3.9. It is possible to see from Fig-3.9 that obtained stochastic wind model is a very good fit and approximation. It is not only able to

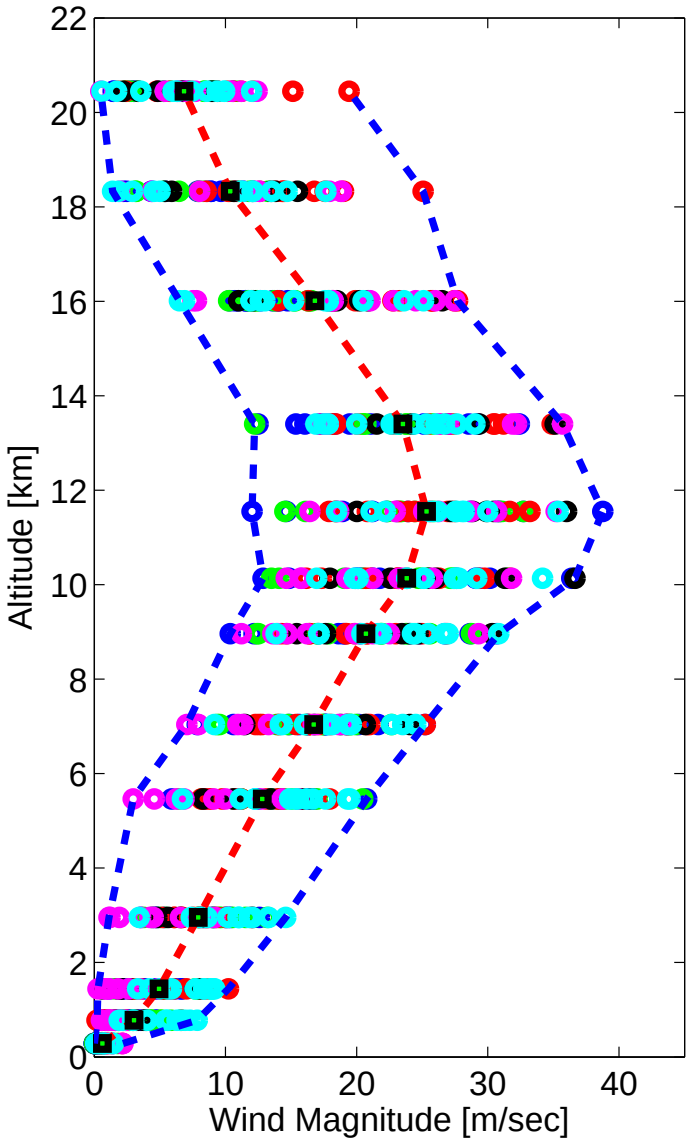

Figure 3.6: Data points for selected 6 locations among continental US.

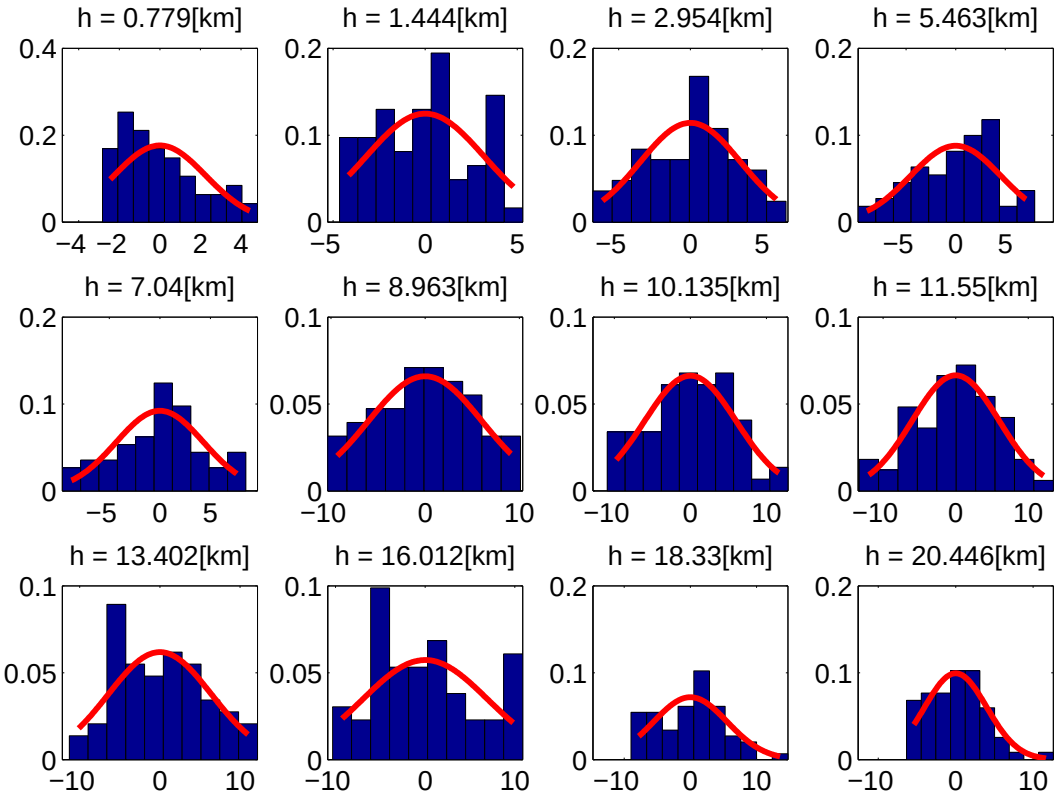

Figure 3.7: Normalized gaussian distributions (blue) and obtained fits (red) for the variation around the mean wind magnitude.

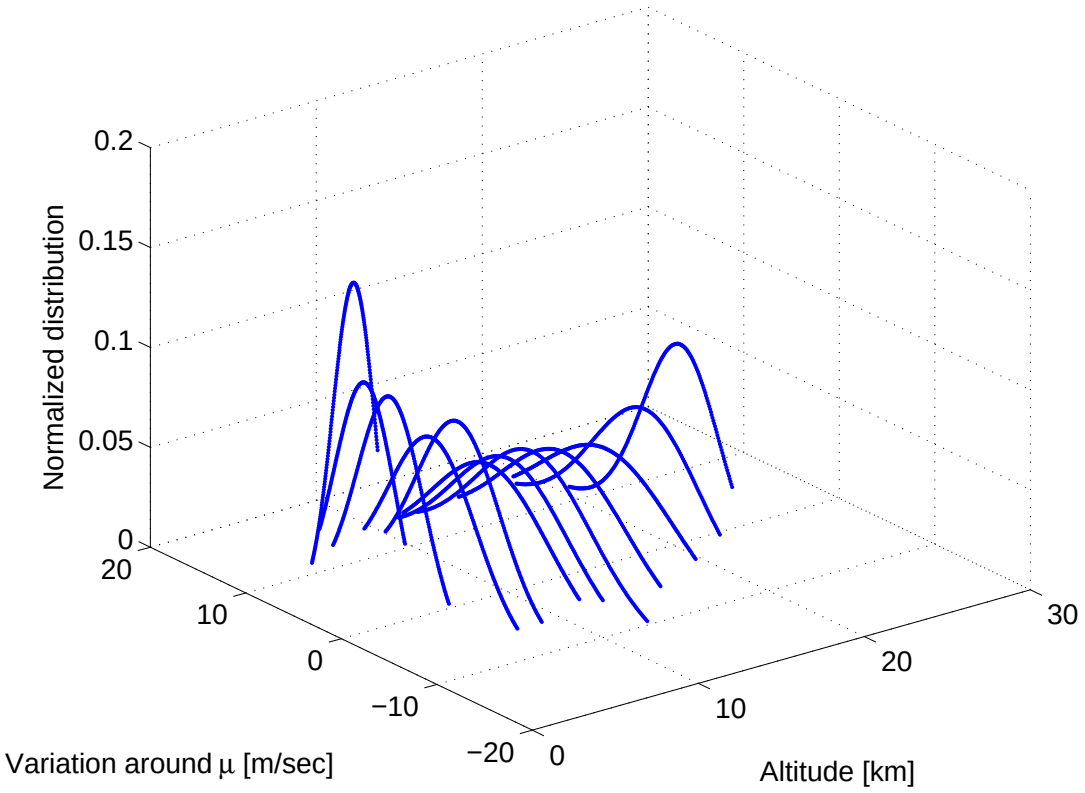

Figure 3.8: 3D - Normalized gaussian distribution fits for the variation around the mean wind magnitude.

Table 3.1: Numerical values of corresponding standard deviations (σ's): Modeling uncertainty in wind magnitude.

Altitude	σ
Alt.1	2.2631
Alt.2	3.1989
Alt.3	3.4955
Alt.4	4.5447
Alt.5	4.3313
Alt.6	6.0526
Alt.7	6.0246
Alt.8	6.0038
Alt.9	6.449
Alt.10	6.9627
Alt.11	5.5551
Alt.12	4.0169

cover the general stochastic nature of the wind behaviour, but also able to maintain the observed upper and lower bounds.

Here, it is good to note that "the nature of the given 100 monte carlo simulations" and "how well it maintains the observed upper and lower bounds", heavily depends on the intensity parameter-θ. With respect to different values of θ in Eq.(3.8), outcomes will also be slightly different, where a corresponding (sample) scenario is shown in Fig-3.10, for four sample cases.

As it is possible to see from Fig-3.10, an increasing value of θ leads stochastic wind magnitude dynamics to be more stable (i.e. steady-state-like-behaviour), and forces the state dynamics to stay around the long term equilibrium (i.e. mean value). This phenomenon will have an effect on the outcome of the guidance strategies and will be discussed in further detail in Chapter 9.

3.3.2 Uncertainty in Wind Direction

It is possible to follow the same procedure for the derivation of mean and uncertainty values in wind direction, as well. If the data points are plotted together with the corresponding wind direction values, obtained results are as given in Fig-3.11.

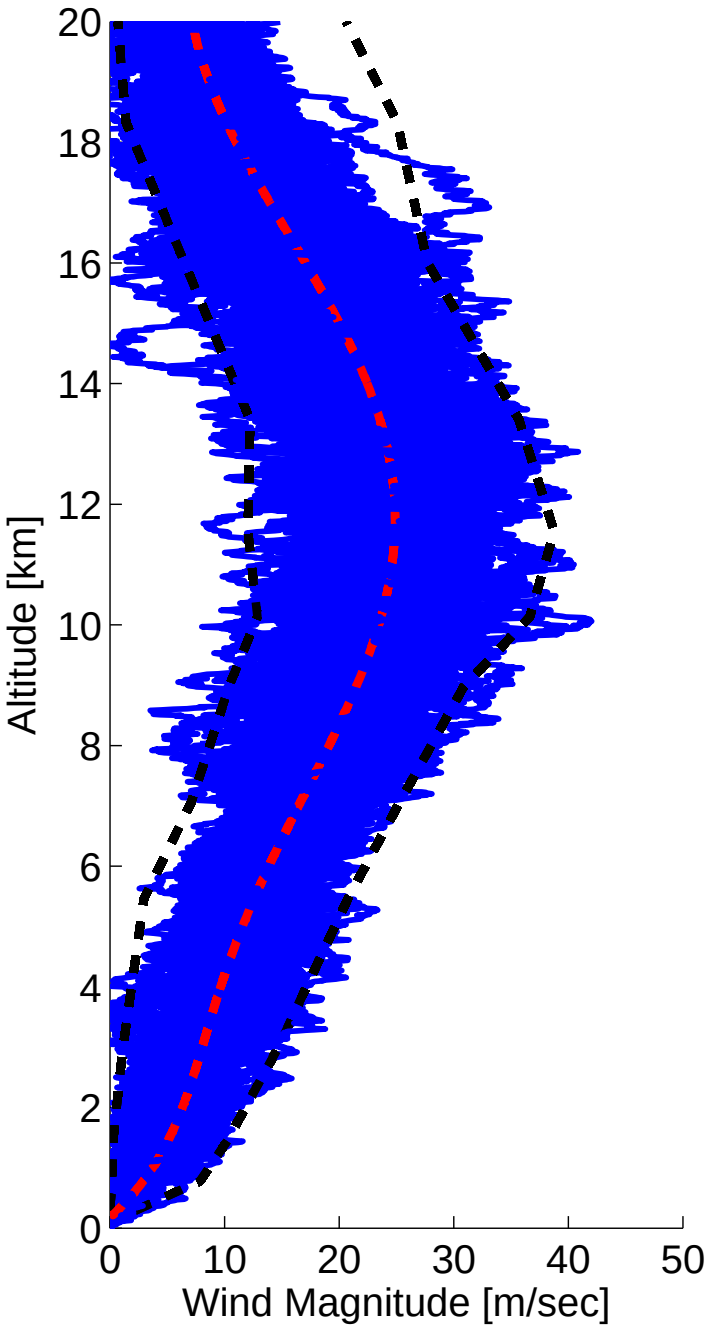

Figure 3.9: 100 monte carlo simulations of obtained stochastic wind model for vertical wind magnitude with $\theta = 1$.

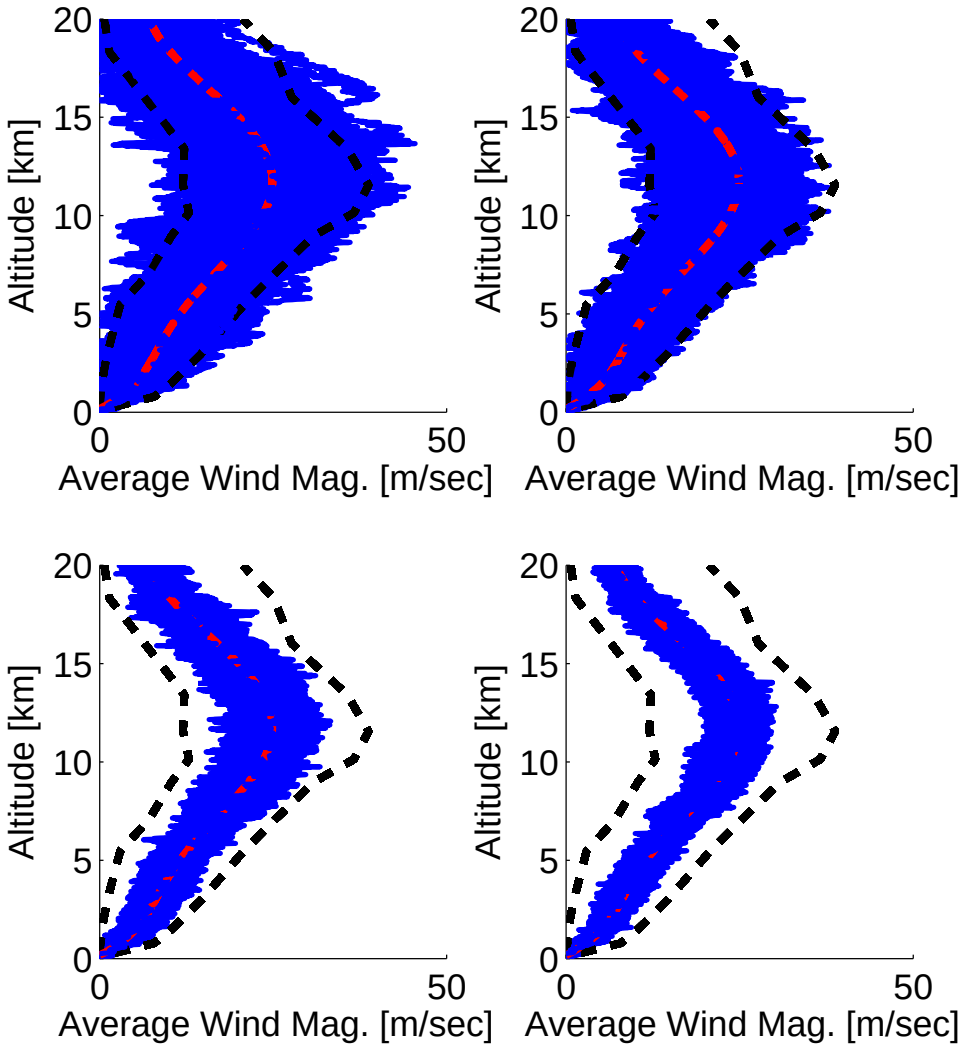

Figure 3.10: 100 monte carlo simulations of stochastic wind model for vertical wind magnitude and for different θ values. For the graphs above, in (2,2,1) $\theta = 0.5$, in (2,2,2) $\theta = 1$, in (2,2,3) $\theta = 4$ and , in (2,2,4) $\theta = 8$

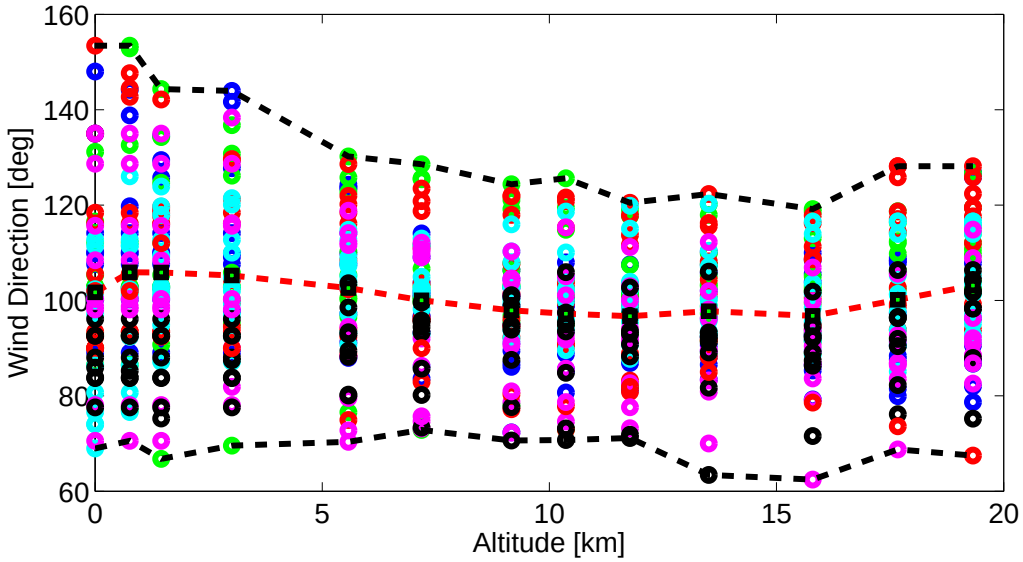

Figure 3.11: Data points for selected 6 locations among continental US.

If Fig-3.11 is investigated in further detail, it is possible to see that using the uncertainty bandwidth, not only the mean value (red dashed line) can be defined, but also the characteristic deviation around the mean can also be derived. Obtained 5^{th} order polynomial fit, characterizing mean wind direction behaviour, was already presented in Eq.(3.2) and corresponding *normalized* distributions are given in Fig-3.12 and Fig-3.13.

Using Fig-3.12, it is also possible to come up with gaussian distribution fits, which will help to characterize the uncertainty in wind direction around the mean value. Obtained uncertainty fits are given with red colour in Fig-3.12, where the corresponding σ values are presented in Table-3.2.

Having derived all the necessary components for a stochastic wind direction model, if 100 monte carlo simulations are ran, obtained results of stochastic wind direction model are as given in Fig-3.14. It is possible to see from Fig-3.14 that obtained stochastic wind model for wind direction is a very good fit and obtained results are able to mimic the nature of the stochastic wind direction characteristics very well. It is not only able to reflect the general stochastic nature of the wind direction but also is able to maintain the observed upper and lower bounds in wind direction profile.

As it was shown beforehand for the case of wind magnitude, again, it is also good

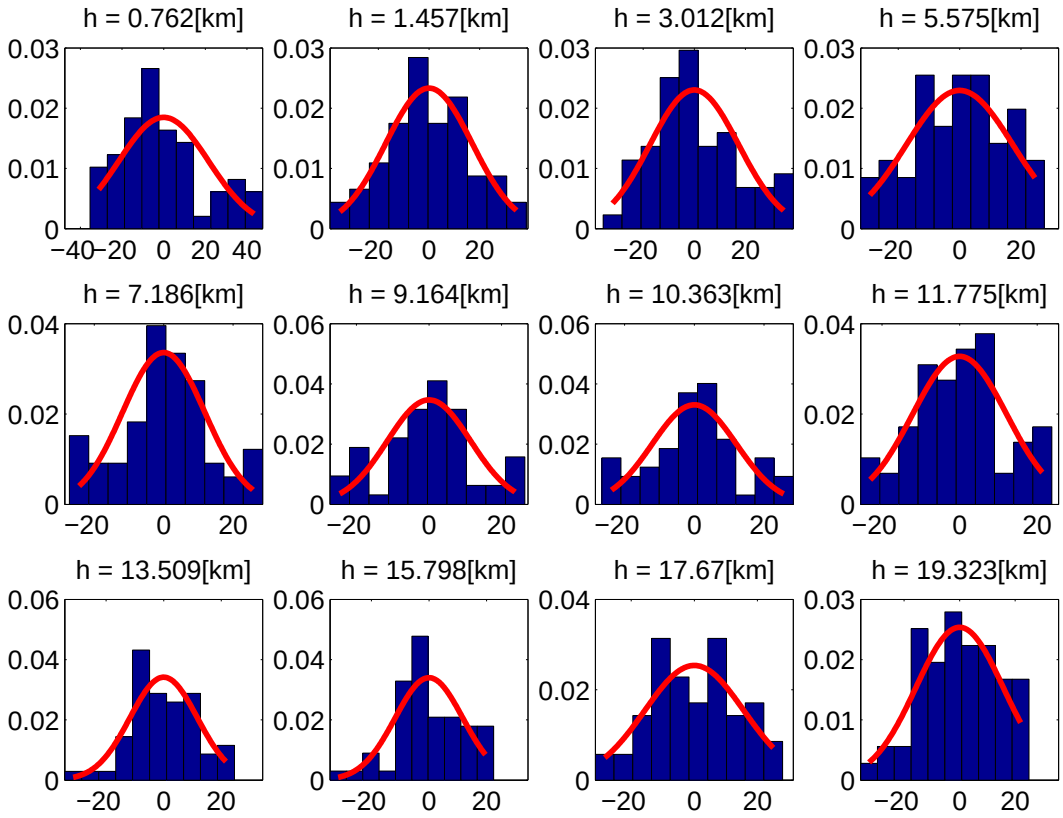

Figure 3.12: Normalized gaussian distributions (blue) and obtained fits (red) for the variation around the mean wind direction.

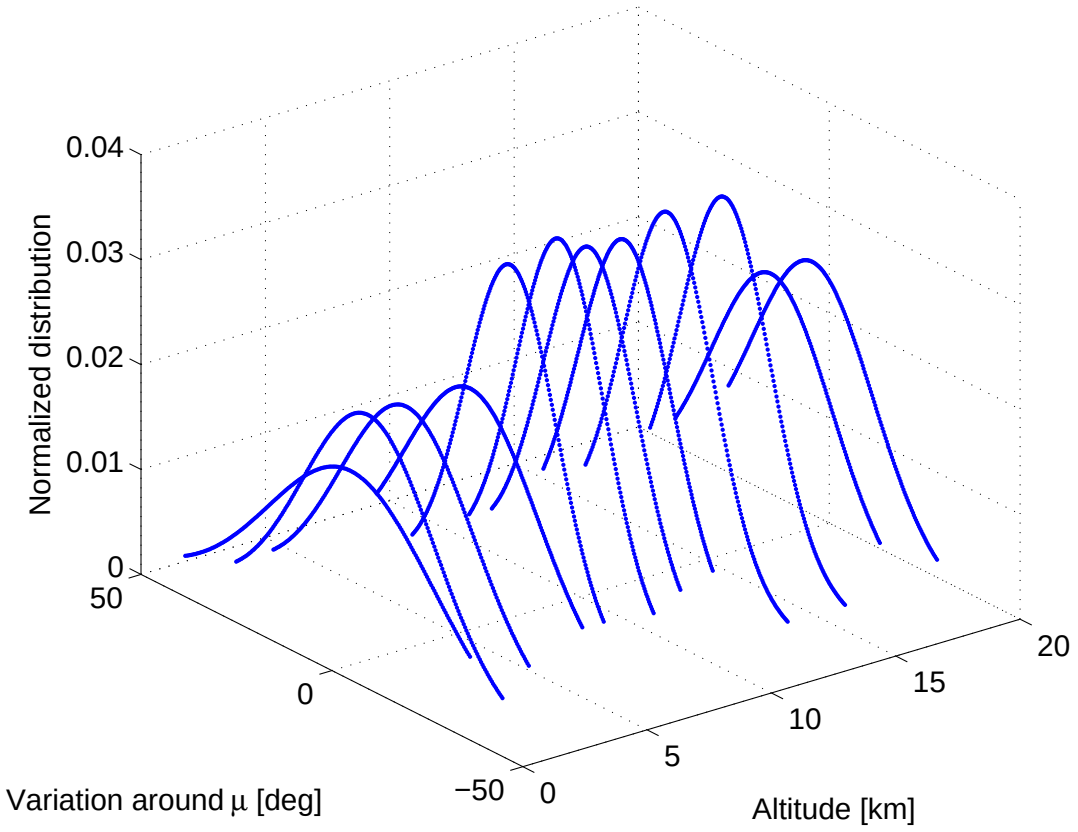

Figure 3.13: 3D - Normalized gaussian distribution fits for the variation around the mean wind direction.

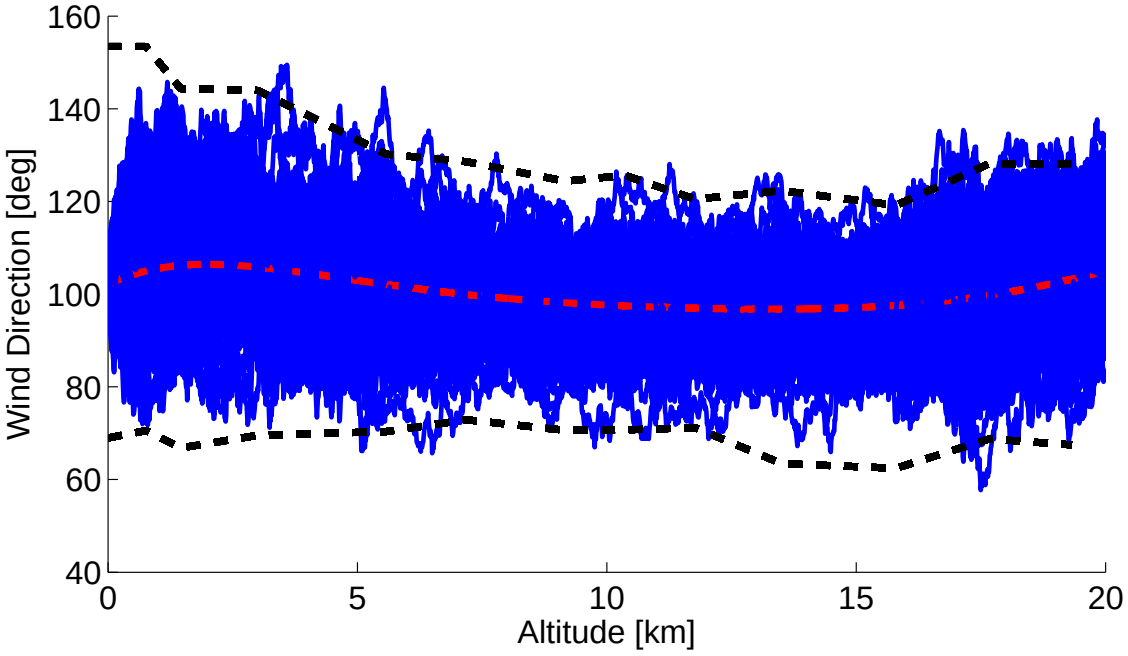

Figure 3.14: 100 monte carlo simulations of obtained stochastic wind model for horizontal wind direction with $\theta = 1$.

Table 3.2: Numerical values of corresponding standard deviations (σ's): Modeling uncertainty in wind direction.

Altitude	σ
Alt.1	21.591
Alt.2	17.099
Alt.3	17.327
Alt.4	17.388
Alt.5	11.871
Alt.6	11.502
Alt.7	12.072
Alt.8	12.175
Alt.9	11.677
Alt.10	11.733
Alt.11	15.718
Alt.12	15.73

to note that "the nature of the given 100 monte carlo simulations" and "how well it maintains the observed upper and lower bounds", heavily depends on the intensity parameter-θ. With respect to different values of θ in Eq.(3.8), outcomes will also be slightly different, and corresponding scenario is shown in Fig.3.15 for four sample cases.

As it is possible to see from Fig.3.15, an increasing value of θ leads stochastic wind direction dynamics to maintain *steady-state-like-behaviour*, and demands the state dynamics to stay around the long term equilibrium (i.e. mean value). This phenomenon will have an effect on the outcome of the guidance strategies and will be discussed in further detail in Chapter 9.

With all the aforementioned derivations and analysis, modeling of vertical wind profile characteristics is completed. Next, the details of horizontal wind profile will be discussed in further detail.

3.4 Horizontal Wind Profile

In engineering applications, the modeling and analysis of horizontal wind profile is one of the open (and most challenging) problems. Nonetheless, scientists have proposed several different approaches to model horizontal wind profiles for different applications.

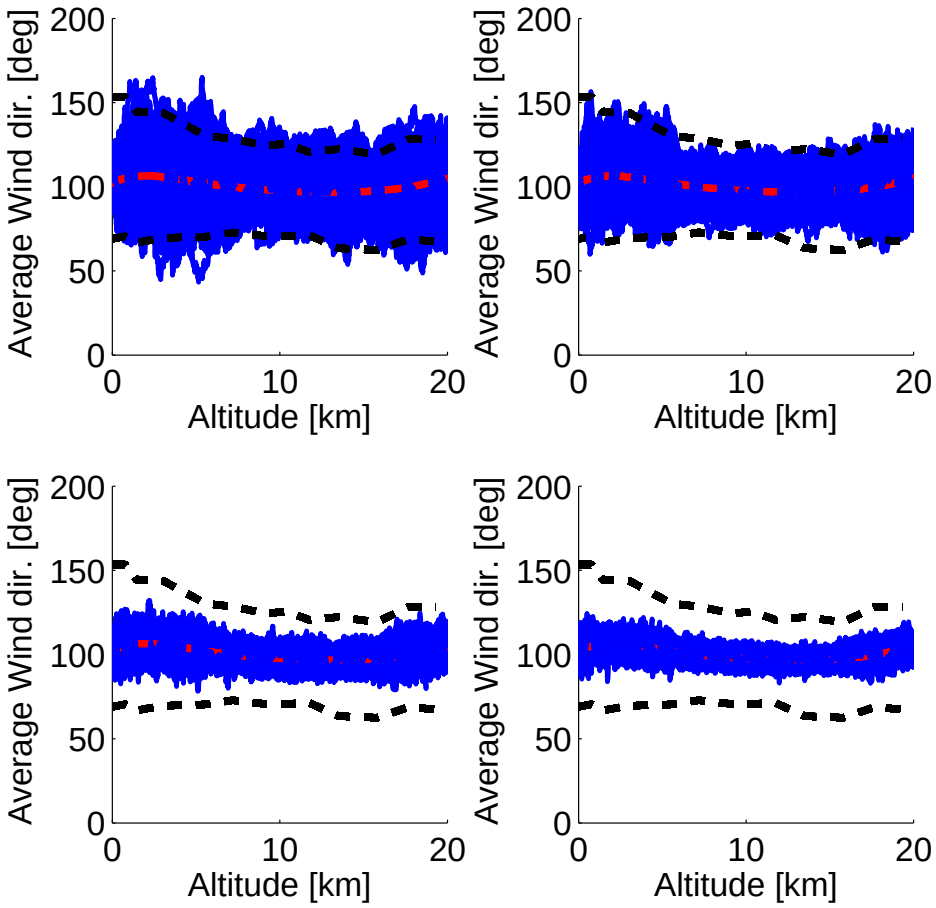

Figure 3.15: 100 monte carlo simulations of obtained stochastic wind model for horizontal wind direction and for different θ values. For the graphs above, in (2,2,1) $\theta = 0.5$, in (2,2,2) $\theta = 1$, in (2,2,3) $\theta = 4$ and , in (2,2,4) $\theta = 8$

General approach in engineering applications (such as analysis of effect of horizontal wind on buildings, skyscrapers, bridges, ...etc) is to take into account the wind effects as "sinusoidal excitations" and has been iterated further in detail in Ruscheweyh (1990), in Scruton (1981) and in Simiu and Scanlan (1996). This is a very good starting point to derive wind models for horizontal wind profiles.

Sinusoidal variations of magnitude with time, as taken from Holmes (2001), can be expressed as

$$\begin{aligned} W_m &= W_{m_0} + a_0 \sin(\omega t) \\ W_x &= W_m \sin \Psi_w \\ W_y &= W_m \cos \Psi_w \end{aligned} \tag{3.12}$$

where W_{m_0} is the constant part of the wind magnitude, ω is the wind frequency as $\omega \in \mathbb{R}[-\omega, \omega]$ and a is the ratio of the variable part to constant part of the wind as $a_0 \in \mathbb{R}[-a, a]$.

But this simple model has its disadvantages. It is a very well known fact that wind not only changes with respect to time but also changes with respect to location, therefore given definition in Eq.(3.12) needs to be extended to include not only temporal but also spatial effects of wind as well. This leads to an improved form of horizontal wind behaviour as shown in Eq.(3.13).

$$\begin{aligned} W_m &= W_{m_0} + a_x \sin(\omega x) + a_y \sin(\omega y) + a_y \sin(\omega t) \\ W_x &= W_m \sin \Psi_w \\ W_y &= W_m \cos \Psi_w \end{aligned} \tag{3.13}$$

where, again

$$\begin{aligned} \omega &\in \mathbb{R}[-\omega, \omega] \\ a_{x,y} &\in \mathbb{R}[-a, a] \end{aligned} \tag{3.14}$$

Here, a_x, a_y and a_t define the ratio of the variable part to the constant part of the wind magnitude in x, y direction and time, respectively. Also W_x and W_y represent the wind component along East-x axis and wind component along North-y axis, respectively. Ψ_W is the corresponding wind direction.

With this definition, it is possible to incorporate the effects of spatial coordinates together with temporal changes in a wind profile model. And this definition finalizes the

horizontal wind modeling part. With the following supporting assumptions, a complete wind model has been obtained to be used in the following derivations and simulations.

Concluding assumptions & suggestions on the use of proposed wind profile: The following assumptions are considered to be useful to increase the efficiency and applicability of the proposed wind models:

- *Constant Wind Direction* - 90^o*:* If Fig-3.5 is investigated further in detail, with a given *fictitious* restricted flight zone (9[km] ($\sim 29,530$[ft]) from below and 16[km] ($\sim$52,495 [ft]) from above), it is possible to see that wind direction is approximately staying in the neighbourhood of 90^o. Therefore, if devised strategies and specified UAV dynamics permits, it may be possible (in some circumstances) to inherit the overall wind direction as $\approx 90^o$ from True North (y-axis), which means that wind direction is going to be only a function of x-direction with small variations ($[1^o - 4^o]$) around the mean value of 90^o. Thus, as long as specified aircraft (and/or (UAV)) flies within the specified flight zone and based on the evidence provided in Fig-3.5, it may be beneficial to assume that experienced wind direction *on average* is going to be 90^o and will stay (approximately) constant. This approach and assumption has the potential to further simplify the following power minimization analysis in great aspect. *However, since the vast majority of UAV dynamics do not allow them to fly in such high altitudes, this (constant wind direction) approach will* **not** *be taken into account in this study. It is given here as an intuitive engineering approach and presented solely for the purpose of* **food-for-thought for further application of this concept in high-altitude commercial flights**.

- *Constant Wind Gradient Assumption:* as stated in Tiwari and Ghosal (2010), it will be assumed that the rate of change of wind components (i.e. wind gradients) remains constant and does not change after 1[km].

- *Constant Pressure Assumption:* It is assumed that the pressure gradient is constant through the complete wind profile.

- *Temperature Variations:* It is assumed that the changes in temperature are incorporated within the density function and reflected into the model dynamics through

the variation of air-density.

With the given assumptions, the derivation of an applicable and easy to use analytical wind model has been obtained. This wind model will be used accordingly for the evaluation of proposed real-time guidance strategies in the following chapters.

Chapter 4

Problem Statement

The main objective of this study is to develop real-time guidance strategies that will enhance the endurance and optimize the performance of UAV flights based on *insitu*, *local* wind information.

Ideally, if the regional wind information is completely known in advance, optimal flight planning can be used to determine UAV flight trajectories which can minimize the total power consumption over a specified time interval, subject to various constraints.

However, in real life, obtaining accurate and precise regional wind information is usually not possible. That is why in most of the cases, the aerial vehicle in hand is restricted to use only *local* and *instantaneous* wind information. For this reason, to reflect the true nature of flight missions, it is assumed that only *local* and *instantaneous* wind information (at the current location and at the current time) is available. This information includes values of wind speeds as well as wind gradients.

In general, different guidance strategies may be grouped into three basic categories: **action strategy**, **velocity strategy**, and **trajectory strategy**. In this thesis, **action strategies** refer to the *direct specifications* of some (or all) of the control variables $z_U = (P, C_L, \mu)$ (i.e. power, lift coefficient, bank angle) over a certain period of time, where they represent open-loop control schemes. In comparison, **velocity strategies** specify some or all of the desired velocity components $z_V = (V_c, \Psi_c, \gamma_c)$ (i.e. airspeed, heading angle, flight path angle) over a certain time interval (Δt) as flight commands, where these commands are then followed via closed-loop tracking. Finally as its name suggests, **trajectory strategies** specify a flight trajectory of desired positions as functions

of time over a certain time interval: $x_c(t), y_c(t), h_c(t)$ where $t \in [t_0, t_f]$. These different categories of guidance strategies can be used to harvest wind energies of different frequencies or types, and/or be used in combination.

A **complete** guidance strategy needs to uniquely and consistently specify three flight commands at a given time, respectively along the longitudinal, lateral, and vertical direction. The guidance command along each direction can be from any of the three groups. Here, a high-level picture of a complete guidance strategy is provided in Fig-4.1.

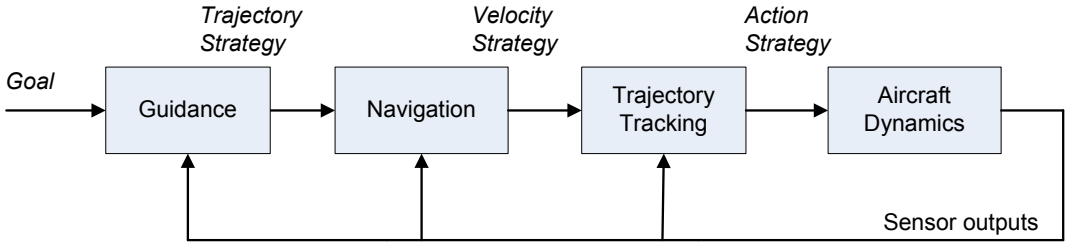

Figure 4.1: High-level architecture of guidance strategies.

In this thesis, it is desired to study **velocity guidance strategies** in combination with **trajectory strategies**. This powerful combination not only utilizes *in-situ* wind information to enhance UAV endurance, but also advocates the minimization of power consumption while verifying that UAV is still flying within the specified region. This is accomplished successfully by executing consecutive and appropriate commands throughout the entire flight, which is explained in further detail in Chapter 5 and 6.

4.1 General Formulation of an Optimal Control Problem

The main idea behind optimization is to find the best possible solution within either *global* scale or *local* scale of the given domain. In that sense, a general non-linear optimal control problem can be formulated as follows:

Define

$$\min_{\vec{u}} \bar{I} = \phi(\bar{x}(\bar{t}_f), \bar{t}_f) + \int_{\bar{t}_0}^{\bar{t}_f} L(\bar{x}(\bar{t}), \bar{u}(\bar{t}), \bar{t}) d\bar{t} \tag{4.1}$$

subject to system dynamics

$$\bar{x}' = f(\bar{x}(\bar{t}), \bar{u}(\bar{t}), \bar{t}) \tag{4.2}$$

initial conditions

$$\bar{X}(\bar{t}_0) = \bar{X}_0 \tag{4.3}$$

and path constraints

$$\begin{aligned} S_e(\bar{x}(\bar{t}), \bar{u}(\bar{t}), \bar{t}) &= 0 \\ S_i(\bar{x}(\bar{t}), \bar{u}(\bar{t}), \bar{t}) &\leq 0 \end{aligned} \tag{4.4}$$

where $\bar{x}(\bar{t})$ and $\bar{u}(\bar{t})$ are state and control vectors, $\phi(\bar{x}(\bar{t}_f), \bar{t}_f)$ is the cost associated with the terminal state, $L(\bar{x}(\bar{t}), \bar{u}(\bar{t}), \bar{t})$ is the cost associated with the transient state within the given time horizon ($\Delta\bar{t} = \bar{t}_f - \bar{t}_0$), respectively.

If the nature of the problem is examined carefully, one can see that throughout the entire flight of the UAVs, only *in-situ* and *local* wind information is available. This enforces the fact of seeking for *local* optimal solutions rather than global solutions. In that sense, global optimal solution requires the knowledge of the wind field that the mission is going to be executed, which is not readily available. As explained in Chapter 1, global optimal solution based on pre-determined wind maps includes extensive errors. Another important point of this problem is that since only local and instantaneous wind (and state) measurements are available, one may not be able to construct a meaningful transient cost function, (L) for the analysis. This is due to the reason that any transient cost function (L) will purely depend on the knowledge of not only state variables, but also wind components within the given time horizon, $\Delta\bar{t} = \bar{t}_f - \bar{t}_0$, which is not readily available. One approach in constructing the *transient cost function* may be to come up with an estimate of the wind field. But any estimation regarding the wind information, will only give a rough approximate solution, whose accuracy is debatable. To avoid this, the cost function to be evaluated is chosen as the one associated with the terminal cost. Then, the non-linear optimal control problem in hand reduces to

$$\min_{\vec{u}} \bar{I} = \phi(\bar{x}(\bar{t}_f), \bar{t}_f) \tag{4.5}$$

subject to system dynamics

$$\bar{x}' = f(\bar{x}(\bar{t}), \bar{u}(\bar{t}), \bar{t}) \tag{4.6}$$

initial conditions

$$\bar{X}(\bar{t}_0) = \bar{X}_0 \tag{4.7}$$

and path constraints

$$\begin{aligned} S_e(\bar{x}(\bar{t}), \bar{u}(\bar{t}), \bar{t}) &= 0 \\ S_i(\bar{x}(\bar{t}), \bar{u}(\bar{t}), \bar{t}) &\leq 0 \end{aligned} \tag{4.8}$$

This formulation, (i.e. minimizing the terminal cost) is the ultimate problem formulation of defined static minimization problem.

4.2 Problem Formulation of Real-Time Guidance Strategies:

In this study, as a test-bed, a propeller-driven UAV (with a constant mass) is assumed, for which maximum endurance corresponds to minimum power consumption, as defined in Anderson (1989). Thus, with this approach, it is desired to determine optimal adjustments in airspeed ($\bar{V}$), heading angle (Ψ) and flight path angle(γ) that will minimize the power consumption projected sometime into the future. In other words, it is aimed to minimize the cost function expressed at the terminal cost based on local, in-situ wind measurements.

Mathematically,

$$\min_{z_V} \ \bar{I} = \bar{P}(\bar{t}_0 + \Delta\bar{t}) \tag{4.9}$$

which is subject to all applicable constraints. As a result, a projected power consumption expressed at the terminal state (i.e. at $(\bar{t}_0 + \Delta\bar{t})$) is used to be minimized instead of the current power at initial state (i.e. $(\bar{t}_0)$).

Feasible UAV flights must satisfy constraints due to UAV performance and operational limits. These constraints can typically be expressed as bounds on trajectory states and controls. For the current problem, these constraints are

$$V_{\min} \leq V \leq V_{\max}, \quad P_{\min} \leq P \leq P_{\max} \tag{4.10}$$

$$C_{L_{\min}} \leq C_L \leq C_{L_{\max}}, \quad |\mu| \leq \mu_{\max} \tag{4.11}$$

Following to the optimal solutions that are attained with respect to given constraints, the UAV will be directed to track optimal state commands ($\bar{V}^* = \bar{V}_0 + \Delta\bar{V}_c$), ($\Psi^* = \Psi_0 + \Delta\Psi_c$) and ($\gamma^* = \gamma_0 + \Delta\gamma_c$). For *velocity guidance strategies*, all adjustments ($\Delta\bar{V}$, $\Delta\Psi$ and/or $\Delta\gamma$) are the optimal increments(or decrements) to be determined with respect to *local*, *instantaneous* and *on-board* wind measurements. As for trajectory strategies, desired commands ($x_c(t)$, $y_c(t)$, $h_c(t)$) are the coordinates of designated flight region (such as circle, ellipsoid, rectangle or 3D cylindrical area).

Once optimal adjustments in airspeed, heading angle and flight path angle are obtained, it takes some finite time for the UAV to achieve the desired changes via closed-loop tracking. This is a phenomenon that has to be taken into account and it is explained in further detail in the following chapter.

Chapter 5

Solution Strategies for 3D Flights

In control systems design, tracking of a desired reference signal is an important concept. Such concept leads the control system to track a reference value which will make sure that aimed state characteristics will be attained. While system dynamics tries to accomplish such task through the designed control algorithm, it takes certain amount of time (Δt) to achieve perfect tracking of a desired reference signal. This is a phenomenon which exists in the nature of every control system and is depicted in further detail in Fig-5.1.

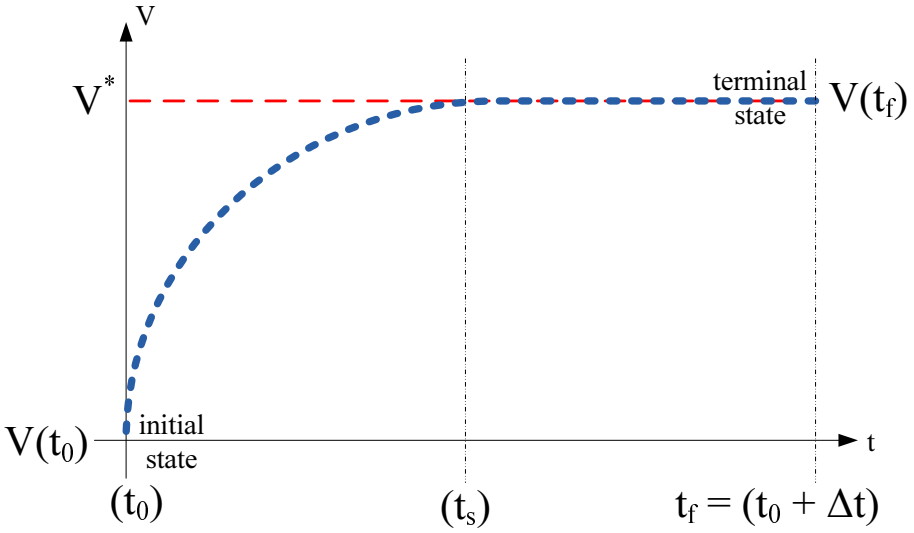

Figure 5.1: Settling time and achieving tracking conditions for a desired reference signal.

The characteristics of *how fast the dynamic system can respond to a given input* is peculiar to a system and changes from one system dynamics to another, and essentially has to be taken into account.

In the light of this information, once optimal adjustments in corresponding states are calculated, it is known that it will take certain amount of time to achieve the optimal reference signal ($\bar{V}^* = \bar{V}_0 + \Delta\bar{V}$, $\Psi^* = \Psi_0 + \Delta\Psi$ and/or $\gamma^* = \gamma_0 + \Delta\gamma$). This will also make sure that, once the reference signal is tracked, the power is minimized for *terminal cost function* (i.e. $\bar{P}(\bar{t}_0 + \Delta\bar{t})$ at *terminal state* $((\bar{t}_0 + \Delta\bar{t}))$.

At this point, a key to solve the aforementioned problem is to develop an expression for the power required at the terminal state (which corresponds to time instant at $(\bar{t}_0 + \Delta\bar{t})$) based on values of the current trajectory state variables as well as the current wind information. This requires the projection (i.e. approximation) of current states (at $\bar{t}_0$) to the terminal state (at $\bar{t}_0 + \Delta\bar{t}$). In this case, update interval $\Delta\bar{t}$ should neither be too large or too small. It certainly needs to be larger than the typical settling time of inner closed-loop controls in order to ensure that any adjustments in airspeed and heading commands will have been achieved. At the same time, too large of a $\Delta\bar{t}$ would reduce the accuracy of power consumption projections (at *terminal state*) using the current state and wind information.

It is also assumed that by the time $(\bar{t}_0 + \Delta\bar{t})$, any commanded changes in airspeed $(\bar{V})$, heading angle (Ψ) and/or flight path angle (γ) will be mostly achieved via closed-loop tracking, and the system will maintain steady-state dynamics. Therefore, when tracking of optimal control commands is achieved, vehicle will basically be in a steady state condition corresponding to $\bar{V}' \approx 0$, $\bar{\Psi}' \approx 0$, $\bar{\gamma}' \approx 0$ and $\mu \approx 0$. As a result, it is desired to minimize the power function at steady state condition (i.e. when the command inputs are achieved, and when the system is ready to execute next control command set).

For the derivation of power consumption term at terminal state (i.e. $\bar{P}_{t_f} = \bar{P}(\bar{t}_0 + \Delta\bar{t})$), acceleration $(\bar{V}')$ term has been set as a starting point. As a first step, it is possible to obtain an expression for the power at time $\bar{t}_0$, which corresponds to time instant the measurements are taken, as

$$\begin{aligned} \bar{P} &= \bar{V}\bar{V}' + \bar{\rho}\bar{V}^3(C_{D_0} + KC_L^2) + \bar{V}\sin\gamma + \bar{V}\bar{W}_V' \\ &\approx \bar{\rho}\bar{V}^3(C_{D_0} + KC_L^2) + \bar{V}\sin\gamma + \bar{V}\bar{W}_V' \end{aligned} \tag{5.1}$$

where

$$\begin{aligned}
\bar{W}'_V =& \bar{W}'_x \cos\gamma \sin\Psi + \bar{W}'_y \cos\gamma \cos\Psi + \bar{W}'_h \sin\gamma \\
\bar{W}'_V =& \left(\frac{\partial \bar{W}_x}{\partial \bar{y}} + \frac{\partial \bar{W}_y}{\partial \bar{x}}\right) \bar{V} \cos^2\gamma \sin\Psi \cos\Psi \\
&+ \left(\frac{\partial \bar{W}_x}{\partial \bar{h}} + \frac{\partial \bar{W}_h}{\partial \bar{x}}\right) \bar{V} \sin\gamma \cos\gamma \sin\Psi \\
&+ \left(\frac{\partial \bar{W}_y}{\partial \bar{h}} + \frac{\partial \bar{W}_h}{\partial \bar{y}}\right) \bar{V} \sin\gamma \cos\gamma \cos\Psi \\
&+ \frac{\partial \bar{W}_x}{\partial \bar{x}} \bar{V} \cos^2\gamma \sin^2\Psi + \frac{\partial \bar{W}_y}{\partial \bar{y}} \bar{V} \cos^2\gamma \cos^2\Psi + \frac{\partial \bar{W}_h}{\partial \bar{h}} \bar{V} \sin^2\gamma \\
&+ \frac{\partial \bar{W}_x}{\partial \bar{\Delta}} \cos\gamma \sin\Psi + \frac{\partial \bar{W}_y}{\partial \bar{\Delta}} \cos\gamma \cos\Psi + \frac{\partial \bar{W}_h}{\partial \bar{\Delta}} \sin\gamma
\end{aligned} \tag{5.2}$$

and

$$\frac{\partial(\ )}{\partial \Delta} = \bar{W}_x \frac{\partial(\ )}{\partial \bar{x}} + \bar{W}_y \frac{\partial(\ )}{\partial \bar{y}} + \bar{W}_h \frac{\partial(\ )}{\partial \bar{h}} + \frac{\partial(\ )}{\partial \bar{t}} \tag{5.3}$$

In steady state (i.e. when $\bar{V}' \approx 0$, $\bar{\Psi}' \approx 0$, $\bar{\gamma}' \approx 0$ and $\mu \approx 0$), lift coefficient, C_L can be expressed as a function of wind components as

$$\begin{aligned}
\Psi' \approx 0 = \frac{\bar{\rho}\bar{V} C_L}{\cos\gamma} \sin\mu &= \frac{1}{\bar{V}\cos\gamma} \bar{W}'_\Psi(\bar{V}, \Psi, \gamma, \bar{x}, \bar{y}, \bar{h}) \\
C_L \sin\mu &= \frac{1}{\bar{\rho}\bar{V}^2} \bar{W}'_\Psi(\bar{V}, \Psi, \gamma, \bar{x}, \bar{y}, \bar{h})
\end{aligned} \tag{5.4}$$

and

$$\begin{aligned}
\gamma' \approx 0 = \bar{\rho}\bar{V} C_L \cos\mu &= \frac{\cos\gamma}{\bar{V}} - \frac{1}{\bar{V}} \bar{W}'_\gamma(\bar{V}, \Psi, \gamma, \bar{x}, \bar{y}, \bar{h}) \\
C_L \cos\mu &= \frac{1}{\bar{\rho}\bar{V}^2} \left(\cos\gamma - \bar{W}'_\gamma(\bar{V}, \Psi, \gamma, \bar{x}, \bar{y}, \bar{h})\right)
\end{aligned} \tag{5.5}$$

leading to the final expression of C_L (as a function of wind terms) as

$$C_L = \frac{\sqrt{\bar{W}'_\Psi(\bar{V}, \Psi, \gamma, \bar{x}, \bar{y}, \bar{h})^2 + \left(\cos\gamma - \bar{W}'_\gamma(\bar{V}, \Psi, \gamma, \bar{x}, \bar{y}, \bar{h})\right)^2}}{\bar{\rho}\bar{V}^2} \tag{5.6}$$

In Eq.(5.6), $\bar{W}'_{\Psi}$ and $\bar{W}'_{\gamma}$ terms are obtained as

$$\begin{aligned}\bar{W}'_{\Psi} = &\left(\frac{\partial \bar{W}_x}{\partial \bar{x}}\cos(\Psi) - \frac{\partial \bar{W}_y}{\partial \bar{x}}\sin(\Psi)\right)\left(\bar{V}\cos(\gamma)\sin(\Psi) + \bar{W}_x\right)\\ &+\left(\frac{\partial \bar{W}_x}{\partial \bar{y}}\cos(\Psi) - \frac{\partial \bar{W}_y}{\partial \bar{y}}\sin(\Psi)\right)\left(\bar{V}cos(\gamma)cos(\Psi) + \bar{W}_y\right)\\ &+\left(\frac{\partial \bar{W}_x}{\partial \bar{h}}\cos(\Psi) - \frac{\partial \bar{W}_y}{\partial \bar{h}}\sin(\Psi)\right)\left(\bar{V}sin(\gamma) + \bar{W}_h\right)\\ &+\left(\frac{\partial \bar{W}_x}{\partial \bar{t}}\cos(\Psi) - \frac{\partial \bar{W}_y}{\partial \bar{t}}\sin(\Psi)\right)\end{aligned} \tag{5.7}$$

and

$$\begin{aligned}\bar{W}'_{\gamma} = &\left(\frac{\partial \bar{W}_x}{\partial \bar{x}}\sin(\gamma)\sin(\Psi) + \frac{\partial \bar{W}_y}{\partial \bar{x}}\sin(\gamma)\cos(\Psi) - \frac{\partial \bar{W}_h}{\partial \bar{x}}\cos(\gamma)\right)\left(\bar{V}cos(\gamma)sin(\Psi) + \bar{W}_x\right)\\ &+\left(\frac{\partial \bar{W}_x}{\partial \bar{y}}\sin(\gamma)\sin(\Psi) + \frac{\partial \bar{W}_y}{\partial \bar{y}}\sin(\gamma)\cos(\Psi) - \frac{\partial \bar{W}_h}{\partial \bar{y}}\cos(\gamma)\right)\left(\bar{V}cos(\gamma)cos(\Psi) + \bar{W}_y\right)\\ &+\left(\frac{\partial \bar{W}_x}{\partial \bar{h}}\sin(\gamma)\sin(\Psi) + \frac{\partial \bar{W}_y}{\partial \bar{h}}\sin(\gamma)\cos(\Psi) - \frac{\partial \bar{W}_h}{\partial \bar{h}}\cos(\gamma)\right)\left(\bar{V}sin(\gamma) + \bar{W}_h\right)\\ &+\left(\frac{\partial \bar{W}_x}{\partial \bar{t}}\sin(\gamma)\sin(\Psi) + \frac{\partial \bar{W}_y}{\partial \bar{t}}\sin(\gamma)\cos(\Psi) + \frac{\partial \bar{W}_h}{\partial \bar{t}}\cos(\gamma)\right)\end{aligned} \tag{5.8}$$

where complete derivations can be investigated in further detail at Appendix-B.

Once the expression for the power function at time instant $\bar{t}_0$ is obtained (i.e. $\bar{P}(\bar{t}_0)$), next step is to derive an expression for the projected power function, which is explained in the following section.

5.1 An Expression for Projected Wind Rate

Since the main aim is to minimize terminal cost $\bar{P}_{t_f} = \bar{P}(\bar{t}_0 + \Delta\bar{t})$ (i.e. power consumption at terminal state at time instant $\bar{t}_0 + \Delta\bar{t}$,), next it is necessary to obtain expressions

for $\bar{W}'_V(\bar{t}_0+\Delta\bar{t})$, $\bar{W}'_\Psi(\bar{t}_0+\Delta\bar{t})$ and $\bar{W}'_\gamma(\bar{t}_0+\Delta\bar{t})$, at terminal state, which leads to

$$\begin{aligned}
\bar{W}'_V(\bar{t}_0+\Delta\bar{t}) = \Bigg[&\frac{\partial\bar{W}_x}{\partial\bar{x}}\left((\bar{V}_0+\Delta\bar{V})\cos(\gamma_0+\Delta\gamma)\sin(\Psi_0+\Delta\Psi)+\bar{W}_x(\bar{t}_0+\Delta\bar{t})\right)\\
&+\frac{\partial\bar{W}_x}{\partial\bar{y}}\left((\bar{V}_0+\Delta\bar{V})\cos(\gamma_0+\Delta\gamma)\cos(\Psi_0+\Delta\Psi)+\bar{W}_y(\bar{t}_0+\Delta\bar{t})\right)\\
&+\frac{\partial\bar{W}_x}{\partial\bar{h}}\left((\bar{V}_0+\Delta\bar{V})\sin(\gamma_0+\Delta\gamma)+\bar{W}_h(\bar{t}_0+\Delta\bar{t})\right)\\
&+\frac{\partial\bar{W}_x}{\partial\bar{t}}\Bigg]\cos(\gamma_0+\Delta\gamma)\sin(\Psi_0+\Delta\Psi)\\
&+\Bigg[\frac{\partial\bar{W}_y}{\partial\bar{x}}\left((\bar{V}_0+\Delta\bar{V})\cos(\gamma_0+\Delta\gamma)\sin(\Psi_0+\Delta\Psi)+\bar{W}_x(\bar{t}_0+\Delta\bar{t})\right)\\
&+\frac{\partial\bar{W}_y}{\partial\bar{y}}\left((\bar{V}_0+\Delta\bar{V})\cos(\gamma_0+\Delta\gamma)\cos(\Psi_0+\Delta\Psi)+\bar{W}_y(\bar{t}_0+\Delta\bar{t})\right)\\
&+\frac{\partial\bar{W}_y}{\partial\bar{h}}\left((\bar{V}_0+\Delta\bar{V})\sin(\gamma_0+\Delta\gamma)+\bar{W}_h(\bar{t}_0+\Delta\bar{t})\right)\\
&+\frac{\partial\bar{W}_y}{\partial\bar{t}}\Bigg]\cos(\gamma_0+\Delta\gamma)\cos(\Psi_0+\Delta\Psi)\\
&+\Bigg[\frac{\partial\bar{W}_h}{\partial\bar{x}}\left((\bar{V}_0+\Delta\bar{V})\cos(\gamma_0+\Delta\gamma)\sin(\Psi_0+\Delta\Psi)+\bar{W}_x(\bar{t}_0+\Delta\bar{t})\right)\\
&+\frac{\partial\bar{W}_h}{\partial\bar{y}}\left((\bar{V}_0+\Delta\bar{V})\cos(\gamma_0+\Delta\gamma)\cos(\Psi_0+\Delta\Psi)+\bar{W}_y(\bar{t}_0+\Delta\bar{t})\right)\\
&+\frac{\partial\bar{W}_h}{\partial\bar{h}}\left((\bar{V}_0+\Delta\bar{V})\sin(\gamma_0+\Delta\gamma)+\bar{W}_h(\bar{t}_0+\Delta\bar{t})\right)\\
&+\frac{\partial\bar{W}_h}{\partial\bar{t}}\Bigg]\sin(\gamma_0+\Delta\gamma)
\end{aligned} \tag{5.9}$$

and

$$\begin{aligned}\bar{W}'_{\Psi}(\bar{t}_0+\Delta\bar{t}) = &\left(\frac{\partial\bar{W}_x}{\partial\bar{x}}\cos(\Psi_0+\Delta\Psi)-\frac{\partial\bar{W}_y}{\partial\bar{x}}\sin(\Psi_0+\Delta\Psi)\right)\\ &\big((\bar{V}_0+\Delta\bar{V})\cos(\gamma_0+\Delta\gamma)\sin(\Psi_0+\Delta\Psi)+\bar{W}_x(\bar{t}_0+\Delta\bar{t})\big)\\ &+\left(\frac{\partial\bar{W}_x}{\partial\bar{y}}\cos(\Psi_0+\Delta\Psi)-\frac{\partial\bar{W}_y}{\partial\bar{y}}\sin(\Psi_0+\Delta\Psi)\right)\\ &\big((\bar{V}_0+\Delta\bar{V})\cos(\gamma_0+\Delta\gamma)\cos(\Psi_0+\Delta\Psi)+\bar{W}_y(\bar{t}_0+\Delta\bar{t})\big)\\ &+\left(\frac{\partial\bar{W}_x}{\partial\bar{h}}\cos(\Psi_0+\Delta\Psi)-\frac{\partial\bar{W}_y}{\partial\bar{h}}\sin(\Psi_0+\Delta\Psi)\right)\\ &\big((\bar{V}_0+\Delta\bar{V})\sin(\gamma_0+\Delta\gamma)+\bar{W}_h(\bar{t}_0+\Delta\bar{t})\big)\\ &+\left(\frac{\partial\bar{W}_x}{\partial\bar{t}}\cos(\Psi_0+\Delta\Psi)-\frac{\partial\bar{W}_y}{\partial\bar{t}}\sin(\Psi_0+\Delta\Psi)\right)\end{aligned} \tag{5.10}$$

and

$$\begin{aligned}\bar{W}'_{\gamma}(\bar{t}_0+\Delta\bar{t}) = &\left(\frac{\partial\bar{W}_x}{\partial\bar{x}}\sin(\gamma_0+\Delta\gamma)\sin(\Psi_0+\Delta\Psi)+\frac{\partial\bar{W}_y}{\partial\bar{x}}\sin(\gamma_0+\Delta\gamma)\cos(\Psi_0+\Delta\Psi)\right.\\ &\left.-\frac{\partial\bar{W}_h}{\partial\bar{x}}\cos(\gamma_0+\Delta\gamma)\right)\big((\bar{V}_0+\Delta\bar{V})\cos(\gamma_0+\Delta\gamma)\sin(\Psi_0+\Delta\Psi)+\bar{W}_x(\bar{t}_0+\Delta\bar{t})\big)\\ &+\left(\frac{\partial\bar{W}_x}{\partial\bar{y}}\sin(\gamma_0+\Delta\gamma)\sin(\Psi_0+\Delta\Psi)+\frac{\partial\bar{W}_y}{\partial\bar{y}}\sin(\gamma_0+\Delta\gamma)\cos(\Psi_0+\Delta\Psi)\right.\\ &\left.-\frac{\partial\bar{W}_h}{\partial\bar{y}}\cos(\gamma_0+\Delta\gamma)\right)\big((\bar{V}_0+\Delta\bar{V})\cos(\gamma_0+\Delta\gamma)\cos(\Psi_0+\Delta\Psi)+\bar{W}_y(\bar{t}_0+\Delta\bar{t})\big)\\ &+\left(\frac{\partial\bar{W}_x}{\partial\bar{h}}\sin(\gamma_0+\Delta\gamma)\sin(\Psi_0+\Delta\Psi)+\frac{\partial\bar{W}_y}{\partial\bar{h}}\sin(\gamma_0+\Delta\gamma)\cos(\Psi_0+\Delta\Psi)\right.\\ &\left.-\frac{\partial\bar{W}_h}{\partial\bar{h}}\cos(\gamma_0+\Delta\gamma)\right)\big((\bar{V}_0+\Delta\bar{V})\sin(\gamma_0+\Delta\gamma)+\bar{W}_h(\bar{t}_0+\Delta\bar{t})\big)\\ &+\left(\frac{\partial\bar{W}_x}{\partial\bar{t}}\sin(\gamma_0+\Delta\gamma)\sin(\Psi_0+\Delta\Psi)\right.\\ &\left.+\frac{\partial\bar{W}_y}{\partial\bar{t}}\sin(\gamma_0+\Delta\gamma)\cos(\Psi_0+\Delta\Psi)+\frac{\partial\bar{W}_h}{\partial\bar{t}}\cos(\gamma_0+\Delta\gamma)\right)\end{aligned} \tag{5.11}$$

It should be carefully noted that in Eqs.(5.9-5.11), not only current states (at time instant $\bar{t}_0$) are projected to the terminal state ($\bar{t}_f=\bar{t}_0+\Delta\bar{t}$), but also corresponding wind components (namely $\bar{W}_x$, $\bar{W}_y$ and $\bar{W}_h$) are also projected to reflect the corresponding state at the terminal state (i.e. at ($\bar{t}_f=\bar{t}_0+\Delta\bar{t}$)).

Another important point to note is, due to the reason that only *insitu*, local wind information is available, it is assumed that the current wind gradients shall stay constant over the immediate neighborhood of the current position of the UAV in the near future. This assumption shall be called the *constant wind gradient assumption*, as stated before in Chapter 3.

With the constant wind gradient assumption over $[\bar{t}_0, \bar{t}_0 + \Delta\bar{t}]$, we also have

$$\begin{aligned}
\bar{W}_x(\bar{t}_0 + \Delta\bar{t}) &\approx \bar{W}_{x_0} + \frac{\partial \bar{W}_x}{\partial \bar{x}}\Delta\bar{x} + \frac{\partial \bar{W}_x}{\partial \bar{y}}\Delta\bar{y} + \frac{\partial \bar{W}_x}{\partial \bar{h}}\Delta\bar{h} + \frac{\partial \bar{W}_x}{\partial \bar{t}}\Delta\bar{t} \\
\bar{W}_y(\bar{t}_0 + \Delta\bar{t}) &\approx \bar{W}_{y_0} + \frac{\partial \bar{W}_y}{\partial \bar{x}}\Delta\bar{x} + \frac{\partial \bar{W}_y}{\partial \bar{y}}\Delta\bar{y} + \frac{\partial \bar{W}_y}{\partial \bar{h}}\Delta\bar{h} + \frac{\partial \bar{W}_y}{\partial \bar{t}}\Delta\bar{t} \\
\bar{W}_h(\bar{t}_0 + \Delta\bar{t}) &\approx \bar{W}_{h_0} + \frac{\partial \bar{W}_h}{\partial \bar{x}}\Delta\bar{x} + \frac{\partial \bar{W}_h}{\partial \bar{y}}\Delta\bar{y} + \frac{\partial \bar{W}_h}{\partial \bar{h}}\Delta\bar{h} + \frac{\partial \bar{W}_h}{\partial \bar{t}}\Delta\bar{t}
\end{aligned} \tag{5.12}$$

These expressions solely depend on ($\Delta\bar{x}$, $\Delta\bar{y}$, $\Delta\bar{h}$), which depend on $\Delta\bar{V}_c$, $\Delta\Psi_c$, $\Delta\gamma_c$ and $\Delta\bar{t}$ through Eqs.(2.22)-(2.24), and reciprocally on the wind components over the specified time interval. Therefore, in order to complete the derivation of the projected wind rate expression, expressions for $(\Delta\bar{x}, \Delta\bar{y}, \Delta\bar{h})$ needs to be derived. This derivation process is explained in detail in the following section.

5.2 Expressions for Position Changes

It is now desired to develop expressions of ($\Delta\bar{x}$, $\Delta\bar{y}$ and $\Delta\bar{h}$) that show their dependencies explicitly on the increments in airspeed ($\bar{V}$), heading angle (Ψ) and flight path angle (γ).

From Eqs.(2.22)-(2.24), we have,

$$\begin{aligned}
\Delta\bar{x} = \bar{x}(\bar{t}_0 + \Delta\bar{t}) - \bar{x}(\bar{t}_0) &= \int_{\bar{t}_0}^{\bar{t}_0+\Delta\bar{t}} \left(\bar{V}\cos(\gamma)\sin\Psi + \bar{W}_x\right) d\bar{t} \\
\Delta\bar{y} = \bar{y}(\bar{t}_0 + \Delta\bar{t}) - \bar{y}(\bar{t}_0) &= \int_{\bar{t}_0}^{\bar{t}_0+\Delta\bar{t}} \left(\bar{V}\cos(\gamma)\cos\Psi + \bar{W}_y\right) d\bar{t} \\
\Delta\bar{h} = \bar{h}(\bar{t}_0 + \Delta\bar{t}) - \bar{h}(\bar{t}_0) &= \int_{\bar{t}_0}^{\bar{t}_0+\Delta\bar{t}} \left(\bar{V}\sin(\gamma) + \bar{W}_h\right) d\bar{t}
\end{aligned} \tag{5.13}$$

At this point, several methods can be used as a choice of designer to numerically integrate $\Delta\bar{x}, \Delta\bar{y}$ and $\Delta\bar{h}$. After experimenting with different methods, trapezoidal rule

(as explained in detail in Carnahan et al. (1969)) has been selected as the integration scheme for its simplicity and compact use.

With the assumption that both airspeed ($\bar{V}$), heading angle (Ψ) and flight path angle (γ) will have achieved their commanded values (i.e. reach to steady state) at the end of the interval and assuming the wind speeds are obtained by Eq.(5.12), applying the trapezoidal rule to integrate the above equations leads to

$$\begin{aligned}
\frac{2}{\Delta t}\Delta\bar{x} &= \bar{V}_0\cos\gamma_0\sin\Psi_0 + \bar{W}_{x_0} + (\bar{V}_0+\Delta\bar{V})\cos(\gamma_0+\Delta\gamma)\sin(\Psi_0+\Delta\Psi) \\
&\quad + \bar{W}_{x_0} + \frac{\partial\bar{W}_x}{\partial\bar{x}}\Delta\bar{x} + \frac{\partial\bar{W}_x}{\partial\bar{y}}\Delta\bar{y} + \frac{\partial\bar{W}_x}{\partial\bar{h}}\Delta\bar{h} + \frac{\partial\bar{W}_x}{\partial\bar{t}}\Delta\bar{t} \\
\frac{2}{\Delta t}\Delta\bar{y} &= \bar{V}_0\cos\gamma_0\cos\Psi_0 + \bar{W}_{y_0} + (\bar{V}_0+\Delta\bar{V})\cos(\gamma_0+\Delta\gamma)\cos(\Psi_0+\Delta\Psi) \\
&\quad + \bar{W}_{y_0} + \frac{\partial\bar{W}_y}{\partial\bar{x}}\Delta\bar{x} + \frac{\partial\bar{W}_y}{\partial\bar{y}}\Delta\bar{y} + \frac{\partial\bar{W}_y}{\partial\bar{h}}\Delta\bar{h} + \frac{\partial\bar{W}_y}{\partial\bar{t}}\Delta\bar{t} \\
\frac{2}{\Delta t}\Delta\bar{h} &= \bar{V}_0\sin\gamma_0 + \bar{W}_{h_0} + (\bar{V}_0+\Delta\bar{V})\sin(\gamma_0+\Delta\gamma) \\
&\quad + \bar{W}_{h_0} + \frac{\partial\bar{W}_h}{\partial\bar{x}}\Delta\bar{x} + \frac{\partial\bar{W}_h}{\partial\bar{y}}\Delta\bar{y} + \frac{\partial\bar{W}_h}{\partial\bar{h}}\Delta\bar{h} + \frac{\partial\bar{W}_h}{\partial\bar{t}}\Delta\bar{t}
\end{aligned} \tag{5.14}$$

Here, if we define,

$$\begin{aligned}
B_1 &= \bar{V}_0\cos(\gamma_0)\sin(\Psi_0) + 2\bar{W}_{x_0} + (\bar{V}_0+\Delta\bar{V})\cos(\gamma_0+\Delta\gamma)\sin(\Psi_0+\Delta\Psi) + \frac{\partial\bar{W}_x}{\partial\bar{t}}\Delta t \\
B_2 &= \bar{V}_0\cos(\gamma_0)\cos(\Psi_0) + 2\bar{W}_{y_0} + (\bar{V}_0+\Delta\bar{V})\cos(\gamma_0+\Delta\gamma)\cos(\Psi_0+\Delta\Psi) + \frac{\partial\bar{W}_y}{\partial\bar{t}}\Delta t \\
B_3 &= \bar{V}_0\sin(\gamma_0) + (\bar{V}_0+\Delta\bar{V})\sin(\gamma_0+\Delta\gamma) + 2\bar{W}_{h_0} + \frac{\partial\bar{W}_h}{\partial\bar{t}}\Delta t
\end{aligned} \tag{5.15}$$

we get

$$\begin{bmatrix}
\left(\frac{2}{\Delta t} - \frac{\partial\bar{W}_x}{\partial\bar{x}}\right) & -\frac{\partial\bar{W}_x}{\partial\bar{y}} & -\frac{\partial\bar{W}_x}{\partial\bar{h}} \\
-\frac{\partial\bar{W}_y}{\partial\bar{x}} & \left(\frac{2}{\Delta t} - \frac{\partial\bar{W}_y}{\partial\bar{y}}\right) & -\frac{\partial\bar{W}_y}{\partial\bar{h}} \\
-\frac{\partial\bar{W}_h}{\partial\bar{x}} & -\frac{\partial\bar{W}_h}{\partial\bar{y}} & \left(\frac{2}{\Delta t} - \frac{\partial\bar{W}_h}{\partial\bar{h}}\right)
\end{bmatrix}
\begin{bmatrix} \Delta\bar{x} \\ \Delta\bar{y} \\ \Delta\bar{h} \end{bmatrix} =
\begin{bmatrix} B_1 \\ B_2 \\ B_3 \end{bmatrix} \tag{5.16}$$

or

$$\begin{aligned}\Delta\bar{x} = \frac{1}{Q}\Bigg\{&\left[\left(\frac{2}{\Delta\bar{t}} - \frac{\partial\bar{W}_y}{\partial\bar{y}}\right)\left(\frac{2}{\Delta\bar{t}} - \frac{\partial\bar{W}_h}{\partial\bar{h}}\right) - \frac{\partial\bar{W}_h}{\partial\bar{y}}\frac{\partial\bar{W}_y}{\partial\bar{h}}\right]B_1 \\ &+ \left[\left(\frac{2}{\Delta\bar{t}} - \frac{\partial\bar{W}_h}{\partial\bar{h}}\right)\frac{\partial\bar{W}_x}{\partial\bar{y}} + \frac{\partial\bar{W}_x}{\partial\bar{h}}\frac{\partial\bar{W}_h}{\partial\bar{y}}\right]B_2 \\ &+ \left[\left(\frac{2}{\Delta\bar{t}} - \frac{\partial\bar{W}_y}{\partial\bar{y}}\right)\frac{\partial\bar{W}_x}{\partial\bar{h}} + \frac{\partial\bar{W}_x}{\partial\bar{y}}\frac{\partial\bar{W}_y}{\partial\bar{h}}\right]B_3\Bigg\}\end{aligned} \tag{5.17a}$$

$$\begin{aligned}\Delta\bar{y} = \frac{1}{Q}\Bigg\{&\left[\left(\frac{2}{\Delta\bar{t}} - \frac{\partial\bar{W}_h}{\partial\bar{h}}\right)\frac{\partial\bar{W}_y}{\partial\bar{x}} + \frac{\partial\bar{W}_y}{\partial\bar{h}}\frac{\partial\bar{W}_h}{\partial\bar{x}}\right]B_1 \\ &+ \left[\left(\frac{2}{\Delta\bar{t}} - \frac{\partial\bar{W}_x}{\partial\bar{x}}\right)\left(\frac{2}{\Delta\bar{t}} - \frac{\partial\bar{W}_h}{\partial\bar{h}}\right) - \frac{\partial\bar{W}_x}{\partial\bar{h}}\frac{\partial\bar{W}_h}{\partial\bar{x}}\right]B_2 \\ &+ \left[\left(\frac{2}{\Delta\bar{t}} - \frac{\partial\bar{W}_x}{\partial\bar{x}}\right)\frac{\partial\bar{W}_y}{\partial\bar{h}} + \frac{\partial\bar{W}_x}{\partial\bar{h}}\frac{\partial\bar{W}_y}{\partial\bar{x}}\right]B_3\Bigg\}\end{aligned} \tag{5.17b}$$

$$\begin{aligned}\Delta\bar{h} = \frac{1}{Q}\Bigg\{&\left[\left(\frac{2}{\Delta\bar{t}} - \frac{\partial\bar{W}_y}{\partial\bar{y}}\right)\frac{\partial\bar{W}_h}{\partial\bar{x}} + \frac{\partial\bar{W}_y}{\partial\bar{x}}\frac{\partial\bar{W}_h}{\partial\bar{y}}\right]B_1 \\ &+ \left[\left(\frac{2}{\Delta\bar{t}} - \frac{\partial\bar{W}_x}{\partial\bar{x}}\right)\frac{\partial\bar{W}_h}{\partial\bar{y}} + \frac{\partial\bar{W}_x}{\partial\bar{y}}\frac{\partial\bar{W}_h}{\partial\bar{x}}\right]B_2 \\ &+ \left[\left(\frac{2}{\Delta\bar{t}} - \frac{\partial\bar{W}_x}{\partial\bar{x}}\right)\left(\frac{2}{\Delta\bar{t}} - \frac{\partial\bar{W}_y}{\partial\bar{y}}\right) - \frac{\partial\bar{W}_x}{\partial\bar{y}}\frac{\partial\bar{W}_y}{\partial\bar{x}}\right]B_3\Bigg\}\end{aligned} \tag{5.17c}$$

where

$$\begin{aligned}Q = &\left(\frac{2}{\Delta\bar{t}} - \frac{\partial\bar{W}_x}{\partial\bar{x}}\right)\left(\frac{2}{\Delta\bar{t}} - \frac{\partial\bar{W}_y}{\partial\bar{y}}\right)\left(\frac{2}{\Delta\bar{t}} - \frac{\partial\bar{W}_h}{\partial\bar{h}}\right) \\ &- \left[\left(\frac{2}{\Delta\bar{t}} - \frac{\partial\bar{W}_x}{\partial\bar{x}}\right)\frac{\partial\bar{W}_y}{\partial\bar{h}}\frac{\partial\bar{W}_h}{\partial\bar{y}} + \left(\frac{2}{\Delta\bar{t}} - \frac{\partial\bar{W}_y}{\partial\bar{y}}\right)\frac{\partial\bar{W}_x}{\partial\bar{h}}\frac{\partial\bar{W}_h}{\partial\bar{x}}\right. \\ &\left. + \left(\frac{2}{\Delta\bar{t}} - \frac{\partial\bar{W}_h}{\partial\bar{h}}\right)\frac{\partial\bar{W}_x}{\partial\bar{y}}\frac{\partial\bar{W}_y}{\partial\bar{x}}\right] \\ &- \left[\frac{\partial\bar{W}_x}{\partial\bar{h}}\frac{\partial\bar{W}_y}{\partial\bar{x}}\frac{\partial\bar{W}_h}{\partial\bar{y}} + \frac{\partial\bar{W}_x}{\partial\bar{y}}\frac{\partial\bar{W}_y}{\partial\bar{h}}\frac{\partial\bar{W}_h}{\partial\bar{x}}\right]\end{aligned} \tag{5.18}$$

This completes the derivation of all position changes, which makes us eligible to express power expression at terminal state, $\bar{P}(\bar{t}_f) = \bar{P}(\bar{t}_0 + \Delta\bar{t})$, as a function of current insitu measurements at initial state (i.e. at time instant $\bar{t}_0$).

5.3 Complete Solution Algorithm

Based on the derivations presented above, now it is possible express the projected power consumption at terminal state ($\bar{t}_0 + \Delta\bar{t}$) as a function of the current command adjustments in airspeed ($\bar{V}$), heading angle (Ψ) and flight path angle (γ). Then, the problem of minimizing power consumption at terminal state ($\bar{t}_f = \bar{t}_0 + \Delta\bar{t}$) reduces to determine $\Delta\bar{V}$, $\Delta\Psi$ and $\Delta\gamma$ from

$$\min_{\Delta\bar{V},\Delta\Psi,\Delta\gamma} \bar{P}_{t_f} = \bar{P}(\bar{t}_0 + \Delta\bar{t}) = \bar{I}(\Delta\bar{V}, \Delta\Psi, \Delta\gamma; \Delta\bar{t}, \bar{X}_0) \tag{5.19}$$

subject to

$$\begin{aligned} \max\{-\Delta\bar{V}_{\max}, \bar{V}_{\min} - \bar{V}_0\} \leq \Delta\bar{V} \leq \min\{\Delta\bar{V}_{\max}, \bar{V}_{\max} - \bar{V}_0\} \\ \max\{-\Delta\Psi_{\max}, \Psi_{\min} - \Psi_0\} \leq \Delta\Psi \leq \min\{\Delta\Psi_{\max}, \Psi \leq \Psi_{\max} - \Psi_0\} \\ \max\{-\Delta\gamma_{\max}, \gamma_{\min} - \gamma_0\} \leq \Delta\gamma \leq \min\{\Delta\gamma_{\max}, \gamma \leq \gamma_{\max} - \gamma_0\} \end{aligned} \tag{5.20}$$

where $\Delta\bar{V}_{\max}$, $\Delta\Psi_{\max}$ and $\Delta\gamma_{\max}$ are the maximum allowed adjustments.

The initial state conditions required (i.e. $\bar{X}_0$) include not only initial state measurements, but also wind information as well as the wind gradient information as

$$\bar{X}_0 = \left\{ \bar{V}_0, \Psi_0, \gamma_0, \bar{W}_{x_0}, \bar{W}_{y_0}, \bar{W}_{h_0}, \frac{\partial\bar{W}_{(x,y,h)}}{\partial\bar{x}}, \frac{\partial\bar{W}_{(x,y,h)}}{\partial\bar{y}}, \frac{\partial\bar{W}_{(x,y,h)}}{\partial\bar{h}}, \frac{\partial\bar{W}_{(x,y,h)}}{\partial\bar{t}} \right\} \tag{5.21}$$

With this, the derivation of power minimization strategies in 3D flights is completed and a special case of this complete derivation will be discussed in the following chapter.

Chapter 6

Solution Strategies for Level Flights

In Chapter-5, complete flight strategies has been derived for power minimization routines in presence of wind and required conditions has been stated for 3-dimensional flights. As it is possible to observe, the process is remarkably complex and requires extensive knowledge of wind behaviour in 3-dimension, which has been discussed beforehand in further details in Chapter-3.

In this chapter, 3D equations presented in Chapter-5 will be simplified. Here, the concentration will be on level flights and minimization schemes in level flights. Different applications of proposed strategies in level flights will also be discussed. In the followings, first simplified components of the proposed 3D algorithm will be presented, and then necessary conditions to maintain level flight strategies will be derived.

6.1 Level Flight Strategies in Presence of Wind

In level flight strategies, it is assumed that the aircraft is maintaining a level flight by controlling the flight path angle as zero ($\gamma = 0$). This assumption, leads to several simplifications to the presented 3D formulation, such as $\bar{W}'_\gamma = 0$. It also sets vertical wind component as zero ($\bar{W}_h = 0$), by the nature of problem formulation.

With these assumptions, at steady state conditions (i.e. $\bar{V}' \approx 0$, $\Psi' \approx 0$ and $\gamma' \approx 0$), it is possible to obtain an expression for the power at time instant $\bar{t}_0$ for level flight

strategies as

$$\begin{aligned}\bar{P}(\bar{t}_0) &= \bar{V}\bar{V}' + \bar{\rho}\bar{V}^3(C_{D_0} + KC_L^2) + \bar{V}\sin\gamma + \bar{V}\bar{W}_V' \\ &\approx \bar{\rho}\bar{V}^3(C_{D_0} + KC_L^2) + \bar{V}\bar{W}_V'\end{aligned} \tag{6.1}$$

where, in level flights, $\bar{W}_V'$ term from Eq.(2.7) simplifies to

$$\begin{aligned}\bar{W}_V' = &\left(\frac{\partial\bar{W}_x}{\partial\bar{y}} + \frac{\partial\bar{W}_y}{\partial\bar{x}}\right)\bar{V}\sin\Psi\cos\Psi \\ &+ \frac{\partial\bar{W}_x}{\partial\bar{x}}\bar{V}\sin^2\Psi + \frac{\partial\bar{W}_y}{\partial\bar{y}}\bar{V}\cos^2\Psi \\ &+ \frac{\partial\bar{W}_x}{\partial\bar{\Delta}}\sin\Psi + \frac{\partial\bar{W}_y}{\partial\bar{\Delta}}\cos\Psi\end{aligned} \tag{6.2}$$

and

$$\frac{\partial(\ )}{\partial\Delta} = W_x\frac{\partial(\ )}{\partial x} + W_y\frac{\partial(\ )}{\partial y} + \frac{\partial(\ )}{\partial t} \tag{6.3}$$

In 2D level flight strategies, it is assumed that by the time $(\bar{t}_0+\Delta\bar{t})$, any commanded changes in airspeed $(\bar{V})$ and heading angle (Ψ) will have been achieved via closed-loop tracking (i.e. tracking error wll be within %2 error margins). As a result, the vehicle will be in a steady state condition: $\bar{V}' \approx 0$, $\bar{\Psi}' \approx 0$, $\mu \approx 0$. This leads to a control command input for lift coefficient (C_L) such as

$$\gamma' \approx 0 = \bar{\rho}\bar{V}C_L\cos\mu = \frac{\cos\gamma - \bar{W}_\gamma'}{\bar{V}} \quad \rightarrow \quad C_L = \frac{\cos\gamma - \bar{W}_\gamma'}{\bar{\rho}\bar{V}^2\cos\mu} \tag{6.4}$$

For level flight conditions, with the assumptions of $\gamma \approx 0$ and $\bar{W}_\gamma' = 0$, control command input for lift coefficient (C_L) in Eq.(6.4) simplifies to

$$C_L = \frac{1}{\bar{\rho}\bar{V}^2\cos\mu} \tag{6.5}$$

It should be carefully noted that , in steady state flight, Eq.(6.4) is the corresponding lift coefficient (C_L) which ensures that the aircraft is executing a level flight mission *in presence of winds*. Further investigation leads to the fact that, *in case of no winds* (i.e for $\bar{W}_V' = \bar{W}_\Psi' = \bar{W}_\gamma' = 0$), expression in Eq.(6.4) is equivalent to the non-normalized form of a well known level flight condition

$$C_L = \left(\frac{2m}{\rho V^2 S}\right)g \quad \rightarrow \quad \frac{\rho V^2 S}{2}C_L = L = mg = W \tag{6.6}$$

Following to the derivation of control command input for lift coefficient, using Eq. (2.19) and Eq.(6.5), power function is obtained as

$$\begin{aligned}\bar{P} &= \bar{V}\bar{V}' + \bar{\rho}\bar{V}^3(C_{D_0} + KC_L^2) + \bar{V}\bar{W}_V' \\ &\approx \bar{V}\bar{V}' + \bar{\rho}\bar{V}^3 C_{D_0} + \frac{K}{\bar{\rho}\cos^2\mu}\frac{1}{\bar{V}} + \bar{V}\bar{W}_V'\end{aligned} \tag{6.7}$$

where the projected power function (at $\bar{t}_0 + \Delta\bar{t}$) for level flight strategies is derived as

$$\bar{P}(\bar{t}_0 + \Delta\bar{t}) = \left[\bar{V}\bar{V}' + \bar{\rho}\bar{V}^3 C_{D_0} + \frac{K}{\bar{\rho}\cos^2\mu}\frac{1}{\bar{V}} + \bar{V}\bar{W}_V'\right]_{\bar{t}_0+\Delta\bar{t}} \tag{6.8}$$

It is assumed that by the time $\bar{t}_0 + \Delta\bar{t}$, any commanded changes in airspeed and heading angle will have been mostly achieved via closed-loop tracking. Therefore, the vehicle will basically be at a steady state condition at the terminal state: $\bar{V}' \approx 0$ and $\mu \approx 0$. This leads to a final projected power expression as,

$$\bar{P}(\bar{t}_0 + \Delta\bar{t}) \approx \bar{\rho}[\bar{V}_0 + \Delta\bar{V}_c]^3 C_{D_0} + \frac{K}{\bar{\rho}}\frac{1}{\bar{V}_0 + \Delta V_c} + [\bar{V}_0 + \Delta\bar{V}_c]\bar{W}_V'(t_0 + \Delta t) \tag{6.9}$$

Here, the $\bar{W}_V'(\bar{t}_0+\Delta\bar{t})$ term needs to be expressed as a function of optimal corrections and in the following section, the derivation of this term is described in further detail.

6.2 An Expression For Projected Wind Rate in Level Flights

The rate of change of any wind component can be expressed in terms of a total derivative as

$$\bar{W}_{(\ )}' = \frac{\partial\bar{W}_{(\ )}}{\partial\bar{x}}\bar{x}' + \frac{\partial\bar{W}_{(\ )}}{\partial\bar{y}}\bar{y}' + \frac{\partial\bar{W}_{(\ )}}{\partial\bar{h}}\bar{h}' + \frac{\partial\bar{W}_{(\ )}}{\partial\bar{t}} \tag{6.10}$$

Here, $(\ ) = (x, y, h)$. By substituting Eqs.(2.22)-(2.24) in Eq.(6.10), it is possible to obtain an expression for $\bar{W}_V'$ as

$$\begin{aligned}\bar{W}_V' = &\left(\frac{\partial\bar{W}_x}{\partial\bar{y}} + \frac{\partial\bar{W}_y}{\partial\bar{x}}\right)\bar{V}\cos^2\gamma\sin\Psi\cos\Psi \\ &+ \left(\frac{\partial\bar{W}_x}{\partial\bar{h}} + \frac{\partial\bar{W}_h}{\partial\bar{x}}\right)\bar{V}\sin\gamma\cos\gamma\sin\Psi \\ &+ \left(\frac{\partial\bar{W}_y}{\partial\bar{h}} + \frac{\partial\bar{W}_h}{\partial\bar{y}}\right)\bar{V}\sin\gamma\cos\gamma\cos\Psi \\ &+ \frac{\partial\bar{W}_x}{\partial\bar{x}}\bar{V}\cos^2\gamma\sin^2\Psi + \frac{\partial\bar{W}_y}{\partial\bar{y}}\bar{V}\cos^2\gamma\cos^2\Psi + \frac{\partial\bar{W}_h}{\partial\bar{h}}\bar{V}\sin^2\gamma \\ &+ \frac{\partial\bar{W}_x}{\partial\bar{\Delta}}\cos\gamma\sin\Psi + \frac{\partial\bar{W}_y}{\partial\bar{\Delta}}\cos\gamma\cos\Psi + \frac{\partial\bar{W}_h}{\partial\bar{\Delta}}\sin\gamma\end{aligned} \tag{6.11}$$

where

$$\frac{(\ )}{\partial\bar{\Delta}} = \bar{W}_x\frac{(\ )}{\partial\bar{x}} + \bar{W}_y\frac{(\ )}{\partial\bar{y}} + \bar{W}_h\frac{(\ )}{\partial\bar{h}} + \frac{(\ )}{\partial\bar{t}} \tag{6.12}$$

In level flights, with negligible flight path angle and vertical winds (i.e. $\gamma = 0$, $\bar{W}_h \approx 0$), $\bar{W}'_V$ term reduces to

$$\begin{aligned}\bar{W}'_V = &\left(\frac{\partial\bar{W}_x}{\partial\bar{y}} + \frac{\partial\bar{W}_y}{\partial\bar{x}}\right)\bar{V}\sin\Psi\cos\Psi \\ &+ \frac{\partial\bar{W}_x}{\partial\bar{x}}\bar{V}\sin^2\Psi + \frac{\partial\bar{W}_y}{\partial\bar{y}}\bar{V}\cos^2\Psi \\ &+ \left(\bar{W}_x\frac{\partial\bar{W}_x}{\partial\bar{x}} + \bar{W}_y\frac{\partial\bar{W}_x}{\partial\bar{y}} + \frac{\partial\bar{W}_x}{\partial\bar{t}}\right)\sin\Psi \\ &+ \left(\bar{W}_x\frac{\partial\bar{W}_y}{\partial\bar{x}} + \bar{W}_y\frac{\partial\bar{W}_y}{\partial\bar{y}} + \frac{\partial\bar{W}_y}{\partial\bar{t}}\right)\cos\Psi\end{aligned} \tag{6.13}$$

Since, the only available information is the *local, insitu* wind information, it is assumed that the current wind gradients will stay constant over the immediate neighborhood around the current position of the UAV in the near future, leading to an expression of $\bar{W}'_V$ at $(\bar{t}_0 + \Delta\bar{t})$ as

$$\begin{aligned}\bar{W}'_V(\bar{t}_0+\Delta\bar{t}) = &\left(\frac{\partial\bar{W}_x}{\partial\bar{y}} + \frac{\partial\bar{W}_y}{\partial\bar{x}}\right)(\bar{V}_0+\Delta V_c)\sin(\Psi_0+\Delta\Psi_c)\cos(\Psi_0+\Delta\Psi_c) \\ &+ \frac{\partial\bar{W}_x}{\partial\bar{x}}(\bar{V}_0+\Delta V_c)\sin^2(\Psi_0+\Delta\Psi_c) + \frac{\partial\bar{W}_y}{\partial\bar{y}}(\bar{V}_0+\Delta V_c)\cos^2(\Psi_0+\Delta\Psi_c) \\ &+ \bar{W}_x(\bar{t}_0+\Delta\bar{t})\left[\frac{\partial\bar{W}_x}{\partial\bar{x}}\sin(\Psi_0+\Delta\Psi_c) + \frac{\partial\bar{W}_y}{\partial\bar{x}}\cos(\Psi_0+\Delta\Psi_c)\right] \\ &+ \bar{W}_y(\bar{t}_0+\Delta\bar{t})\left[\frac{\partial\bar{W}_x}{\partial\bar{y}}\sin(\Psi_0+\Delta\Psi_c) + \frac{\partial\bar{W}_y}{\partial\bar{y}}\cos(\Psi_0+\Delta\Psi_c)\right] \\ &+ \frac{\partial\bar{W}_x}{\partial\bar{t}}\sin(\Psi_0+\Delta\Psi_c) + \frac{\partial\bar{W}_y}{\partial\bar{t}}\cos(\Psi_0+\Delta\Psi_c)\end{aligned} \tag{6.14}$$

With the *constant wind gradient assumption* over $[\bar{t}_0, \bar{t}_0 + \Delta\bar{t}]$, we also have

$$\begin{aligned}\bar{W}_x(\bar{t}_0+\Delta\bar{t}) &\approx \bar{W}_{x_0} + \frac{\partial\bar{W}_x}{\partial\bar{x}}\Delta\bar{x} + \frac{\partial\bar{W}_x}{\partial\bar{y}}\Delta\bar{y} + \frac{\partial\bar{W}_x}{\partial\bar{t}}\Delta\bar{t} \\ \bar{W}_y(\bar{t}_0+\Delta\bar{t}) &\approx \bar{W}_{y_0} + \frac{\partial\bar{W}_y}{\partial\bar{x}}\Delta\bar{x} + \frac{\partial\bar{W}_y}{\partial\bar{y}}\Delta\bar{y} + \frac{\partial\bar{W}_y}{\partial\bar{t}}\Delta\bar{t}\end{aligned} \tag{6.15}$$

These expressions depend on $(\Delta\bar{x}, \Delta\bar{y})$, which also have a dependency on $\Delta\bar{V}$, $\Delta\Psi$, and $\Delta\bar{t}$ through Eqs.(2.22)-(2.24), and reciprocally on the wind components over the

specified time interval. Now, in order to complete the derivation of the projected wind rate expression for level flight strategies, expressions for $(\Delta\bar{x}, \Delta\bar{y})$ will be developed in the following section.

6.3 Expressions for Position Changes in Level Flights

The concentration in this section will mainly be focused on developing expressions for $(\Delta\bar{x}, \Delta\bar{y})$. Their dependencies, explicitly, show on the increments of airspeed and heading angle. From Eqs.(2.22)-(2.23), and for $\gamma = 0$, it is possible to have

$$\begin{aligned} \Delta\bar{x} &= \bar{x}(\bar{t}_0 + \Delta\bar{t}) - \bar{x}(\bar{t}_0) = \int_{\bar{t}_0}^{\bar{t}_0+\Delta\bar{t}} \left(\bar{V}\sin\Psi + \bar{W}_x\right) d\bar{t} \\ \Delta\bar{y} &= \bar{y}(\bar{t}_0 + \Delta\bar{t}) - \bar{y}(\bar{t}_0) = \int_{\bar{t}_0}^{\bar{t}_0+\Delta\bar{t}} \left(V\cos\Psi + \bar{W}_y\right) d\bar{t} \end{aligned} \tag{6.16}$$

With the assumption that both airspeed $(\bar{V})$ and heading angle (Ψ) will have achieved their commanded values (i.e. reach steady state conditions) at the end of the specified time interval, and keeping in mind that wind speeds are obtained using Eq.(6.15) (through the trapezoidal rule), the numerical integration of the above equations leads to

$$\begin{aligned} \frac{2}{\Delta t}\Delta\bar{x} &= \bar{V}_0\sin\Psi_0 + \bar{W}_{x_0} + (\bar{V}_0 + \Delta\bar{V})\sin(\Psi_0 + \Delta\Psi) \\ &\quad + \bar{W}_{x_0} + \frac{\partial\bar{W}_x}{\partial\bar{x}}\Delta\bar{x} + \frac{\partial\bar{W}_x}{\partial\bar{y}}\Delta\bar{y} + \frac{\partial\bar{W}_x}{\partial\bar{t}}\Delta\bar{t} \\ \frac{2}{\Delta t}\Delta\bar{y} &= \bar{V}_0\cos\Psi_0 + \bar{W}_{y_0} + (\bar{V}_0 + \Delta\bar{V})\cos(\Psi_0 + \Delta\Psi) \\ &\quad + \bar{W}_{y_0} + \frac{\partial\bar{W}_y}{\partial\bar{x}}\Delta\bar{x} + \frac{\partial\bar{W}_y}{\partial\bar{y}}\Delta\bar{y} + \frac{\partial\bar{W}_y}{\partial\bar{t}}\Delta\bar{t} \end{aligned} \tag{6.17}$$

By defining,

$$\begin{aligned} B_1 &= \bar{V}_0\sin\Psi_0 + (\bar{V}_0 + \Delta\bar{V})\sin(\Psi_0 + \Delta\Psi) + 2\bar{W}_{x_0} + \frac{\partial\bar{W}_x}{\partial\bar{t}}\Delta\bar{t} \\ B_2 &= \bar{V}_0\cos\Psi_0 + (\bar{V}_0 + \Delta\bar{V})\cos(\Psi_0 + \Delta\Psi) + 2\bar{W}_{y_0} + \frac{\partial\bar{W}_y}{\partial\bar{t}}\Delta\bar{t} \end{aligned} \tag{6.18}$$

it is possible to obtain an expression as

$$\begin{bmatrix} \frac{2}{\Delta\bar{t}} - \frac{\partial\bar{W}_x}{\partial\bar{x}} & -\frac{\partial\bar{W}_x}{\partial\bar{y}} \\ -\frac{\partial\bar{W}_y}{\partial\bar{x}} & \frac{2}{\Delta\bar{t}} - \frac{\partial\bar{W}_y}{\partial\bar{y}} \end{bmatrix} \begin{bmatrix} \Delta\bar{x} \\ \Delta\bar{y} \end{bmatrix} = \begin{bmatrix} B_1 \\ B_2 \end{bmatrix} \tag{6.19}$$

or

$$\begin{aligned}\Delta\bar{x} &= \frac{1}{Q_{level}}\left[\left(\frac{2}{\Delta\bar{t}} - \frac{\partial\bar{W}_y}{\partial\bar{y}}\right)B_1 + \left(\frac{\partial\bar{W}_x}{\partial\bar{y}}\right)B_2\right] \\ \Delta\bar{y} &= \frac{1}{Q_{level}}\left[\left(\frac{\partial\bar{W}_y}{\partial\bar{x}}\right)B_1 + \left(\frac{2}{\Delta\bar{t}} - \frac{\partial\bar{W}_x}{\partial\bar{x}}\right)B_2\right]\end{aligned} \tag{6.20}$$

where

$$Q_{level} = \left(\frac{2}{\Delta\bar{t}}\right)^2 - \frac{2}{\Delta\bar{t}}\left(\frac{\partial\bar{W}_x}{\partial\bar{x}} + \frac{\partial\bar{W}_y}{\partial\bar{y}}\right) + \left(\frac{\partial\bar{W}_x}{\partial\bar{x}}\frac{\partial\bar{W}_y}{\partial\bar{y}} - \frac{\partial\bar{W}_x}{\partial\bar{y}}\frac{\partial\bar{W}_y}{\partial\bar{x}}\right) \tag{6.21}$$

For a sufficiently small Δt, expression in Eq.(6.21) shall always be nonzero; ensuring the existence of solutions for the position change expressions.

6.4 Guidance Algorithms for Level Flights

Based on the derivations above, the power consumption at terminal state (i.e. at time $\bar{t}_0 + \Delta\bar{t}$) can now be expressed as a function of the current command adjustments in airspeed and heading angle. Then, the problem of reducing future power consumptions reduces to determine $\Delta\bar{V}$ and $\Delta\Psi$ from

$$\min_{\Delta\bar{V},\Delta\Psi} \bar{P}_{t_f} = \bar{P}(\bar{t}_0 + \Delta\bar{t}) = \bar{I}(\Delta\bar{V}, \Delta\Psi; \Delta\bar{t}, \bar{X}_0) \tag{6.22}$$

subject to

$$\begin{aligned}\max\{-\Delta\bar{V}_{\max}, \bar{V}_{\min} - \bar{V}_0\} \le \Delta\bar{V} \le \min\{\Delta\bar{V}_{\max}, \bar{V}_{\max} - \bar{V}_0\} \\ \max\{-\Delta\Psi_{\max}, \Psi_{\min} - \Psi_0\} \le \Delta\Psi \le \min\{\Delta\Psi_{\max}, \Psi_c \le \Psi_{\max} - \Psi_0\}\end{aligned} \tag{6.23}$$

where $\Delta\bar{V}_{\max}$ and $\Delta\bar{\Psi}_{\max}$ are the maximum allowed incremental changes, and the initial state conditions required $\bar{X}_0$ include

$$\bar{X}_0 = \left\{\bar{V}_0, \Psi_0, \bar{W}_{x_0}, \bar{W}_{y_0}, \frac{\partial\bar{W}_x}{\partial\bar{x}}, \frac{\partial\bar{W}_x}{\partial\bar{y}}, \frac{\partial\bar{W}_y}{\partial\bar{x}}, \frac{\partial\bar{W}_y}{\partial\bar{y}}\right\} \tag{6.24}$$

This problem formulation completes the derivation of solution algorithms for the level flight strategies in presence of wind conditions.

6.5 Reference Strategy in Level Flight Conditions:

In addition to the afore mentioned derivations, to evaluate and compare the outcomes of the suggested solution algorithms, a reference strategy has been taken into account. In this reference strategy, it is assumed that the UAV follows a constant airspeed, at straight level flight conditions. To obtain the airspeed for the reference trajectory, zero wind conditions are assumed. In this case, the projected power expression in Eq.(6.9) becomes

$$\bar{P} = \bar{\rho}\bar{V}^3 C_{D_0} + \frac{K}{\bar{\rho}}\frac{1}{\bar{V}} \tag{6.25}$$

where the optimal reference air speed, in zero wind conditions, is derived as

$$\frac{\partial \bar{P}}{\partial \bar{V}} = 0 \quad \Rightarrow \quad \bar{V}^*_{no_w ind} = \left(\frac{K}{3\bar{\rho}^2 C_{D_0}}\right)^{\frac{1}{4}} \tag{6.26}$$

This airspeed, ($\bar{V}^*_{No\ Wind}$), corresponds to the maximum endurance under zero wind in a steady level flight.

Chapter 7

Optimization Strategies

In previous chapter, the problem of minimizing power consumption at a terminal state in presence of winds has been formulated as a static optimization problem. Following to this, in this chapter it is aimed to come up with optimization routines to solve such cumbersome problems in computationally effective manner so that they can be applied as real-time guidance strategies using on board flight instruments.

From the given problem formulation in Chapters 5 and 6, it is possible to see that the nature of the problem is very complex, extensively coupled and highly non-linear. At this point, different algorithms may be used to solve the static optimization problem defined in Eq.(5.19). But most of the existing numerical methods heavily depend on iteration routines which are not desirable in real-time applications. They impose major drawbacks from the perspective of computation time and "convergence rate in allowed computation time" (which can be extremely small in some cases and applications). To avoid this to certain extent, in this chapter, it is aimed to solve the static optimization problem in an *analytical*, and *a-single-shot* manner.

For this purpose, here, two, yet simple but powerful *gradient methods* will be presented to aid in solving the static optimization problem in hand.

First, the *first-order gradient algorithms* will be introduced. Next, some potential handicaps of *first-order gradient algorithms* will be mentioned, and some major points will be discussed over "why it is not very desirable to use such first order algorithms" for the problem in hand. Then, *second-order optimal gradient algorithm* will be presented, which is the core optimization routine that has been used to evaluate proposed optimal

guidance strategies. Major advantages of second order strategies will be discussed over first-order strategies and methodology will be presented in the following sections.

7.1 First Order Adjustment Strategies

In deriving a first-order gradient method, the projected power expression at $\bar{t}_0 + \Delta\bar{t}$ (i.e. power expression at terminal state) is approximated in the neighbourhood of initial state ($\bar{t}_0$), using Taylor series approximation as

$$\bar{I}_{2D}(\bar{V}^*, \Psi^*) \approx \bar{I}_0 + \left(\frac{\partial \bar{I}}{\partial \bar{V}^*}\right)_0 \overbrace{(\bar{V}^* - \bar{V}_0)}^{\Delta\bar{V}} + \left(\frac{\partial \bar{I}}{\partial \Psi^*}\right)_0 \overbrace{(\Psi^* - \Psi_0)}^{\Delta\Psi} + \left(\frac{\partial \bar{I}}{\partial \gamma^*}\right)_0 \overbrace{(\gamma^* - \gamma_0)}^{\Delta\gamma} \tag{7.1}$$

where

$$\begin{aligned} \bar{V}^* &= \bar{V}(\bar{t}_0 + \Delta\bar{t}) = \bar{V}(\bar{t}_0) + \Delta\bar{V} \quad \rightarrow \quad \Delta\bar{V} = \bar{V}^* - \bar{V}_0 \\ \Psi^* &= \Psi(\bar{t}_0 + \Delta\bar{t}) = \Psi(\bar{t}_0) + \Delta\Psi \quad \rightarrow \quad \Delta\Psi = \Psi^* - \Psi_0 \\ \gamma^* &= \gamma(\bar{t}_0 + \Delta t) = \gamma(\bar{t}_0) + \Delta\gamma \quad \rightarrow \quad \Delta\gamma = \gamma^* - \gamma_0 \end{aligned} \tag{7.2}$$

and $(\ )_0$ corresponds to zero commanded adjustments (i.e. $\Delta V_c = 0, \Delta\Psi_c = 0, \Delta\gamma_c = 0$).

Since level flight guidance strategies is the main topic of interest here, as a natural consequence of level flights, all flight path angle (γ) related terms diminishes in the formulation. This results in further simplification of Eq.(7.1) as

$$\bar{I}_{level}(\bar{V}^*, \Psi^*) \approx \bar{I}_0 + \left(\frac{\partial \bar{I}}{\partial \bar{V}^*}\right)_0 \overbrace{(\bar{V}^* - \bar{V}_0)}^{\Delta\bar{V}} + \left(\frac{\partial \bar{I}}{\partial \Psi^*}\right)_0 \overbrace{(\Psi^* - \Psi_0)}^{\Delta\Psi} \tag{7.3}$$

which is the main formulation that will be used to determine the *local solutions (adjustments)* through first order adjustments. In the following sub-sections, the specific calculation of these *local solutions* are explained in further detail.

7.1.1 Airspeed Adjustment Strategy

A first-order airspeed adjustment can be determined using Eq.(7.3), by investigating the gradient behaviour of the first-order derivative as

$$\Delta\bar{V} = \begin{cases} 0 & |I_{\Delta\bar{V}}| < \epsilon \\ \eta \max\{-\Delta\bar{V}_{\max}, \bar{V}_{\min} - \bar{V}_0\} & I_{\Delta\bar{V}} \geq \epsilon > 0 \\ \eta \min\{\Delta\bar{V}_{\max}, \bar{V}_{\max} - \bar{V}_0\} & I_{\Delta\bar{V}} \leq -\epsilon \end{cases} \tag{7.4}$$

where $\epsilon > 0$ is introduced to avoid numerical difficulties in implementation, and $\eta \in (0, 1)$ is the adjustment stepsize. Expanding Eq.(6.9) using Eq.(6.13) leads to

$$\begin{aligned} \bar{I}_{\Delta\bar{V}} = {} & 3\bar{\rho}C_{D_0}\bar{V}_0^2 - \frac{K}{\bar{\rho}\bar{V}_0^2} + \bar{V}_0 \sin(2\Psi_0)\left(\frac{\partial\bar{W}_x}{\partial\bar{y}} + \frac{\partial\bar{W}_y}{\partial\bar{x}} + \frac{\partial\bar{W}_x}{\partial\bar{x}}\tan\Psi_0 + \frac{\partial\bar{W}_y}{\partial\bar{y}}\cot\Psi_0\right) \\ & + \left(\frac{\partial\bar{W}_x}{\partial\bar{x}}\sin\Psi_0 + \frac{\partial\bar{W}_y}{\partial\bar{x}}\cos\Psi_0\right)\left[\left(\bar{W}_x\right)_0 + \bar{V}_0\left(\frac{\partial\bar{W}_x}{\partial\Delta\bar{V}}\right)_0\right] \\ & + \left(\frac{\partial\bar{W}_x}{\partial\bar{y}}\sin\Psi_0 + \frac{\partial\bar{W}_y}{\partial\bar{y}}\cos\Psi_0\right)\left[\left(\bar{W}_y\right)_0 + \bar{V}_0\left(\frac{\partial\bar{W}_y}{\partial\Delta\bar{V}}\right)_0\right] \\ & + \frac{\partial\bar{W}_x}{\partial\bar{t}}\sin\Psi_0 + \frac{\partial\bar{W}_y}{\partial\bar{t}}\cos\Psi_0 \end{aligned} \tag{7.5}$$

Here, the partial derivatives of wind and position changes with respect to the speed increment can be obtained from Eqs.(6.20) and (6.18) as

$$\begin{aligned} \left(\frac{\partial\bar{W}_x}{\partial\Delta\bar{V}_c}\right)_0 &= \frac{\partial\bar{W}_x}{\partial\bar{x}}\left(\frac{\partial\Delta\bar{x}}{\partial\Delta\bar{V}_c}\right)_0 + \frac{\partial\bar{W}_x}{\partial\bar{y}}\left(\frac{\partial\Delta\bar{y}}{\partial\Delta\bar{V}_c}\right)_0 \\ \left(\frac{\partial\bar{W}_y}{\partial\Delta\bar{V}_c}\right)_0 &= \frac{\partial\bar{W}_y}{\partial\bar{x}}\left(\frac{\partial\Delta\bar{x}}{\partial\Delta\bar{V}_c}\right)_0 + \frac{\partial\bar{W}_y}{\partial\bar{y}}\left(\frac{\partial\Delta\bar{y}}{\partial\Delta\bar{V}_c}\right)_0 \end{aligned} \tag{7.6}$$

and

$$\begin{aligned} \left(\frac{\partial\Delta\bar{x}}{\partial\Delta\bar{V}_c}\right)_0 &= \frac{1}{Q_{2D}}\left[\left(\frac{2}{\Delta\bar{t}} - \frac{\partial\bar{W}_y}{\partial\bar{y}}\right)\sin\Psi_0 + \left(\frac{\partial\bar{W}_x}{\partial\bar{y}}\right)\cos\Psi_0\right] \\ \left(\frac{\partial\Delta\bar{y}}{\partial\Delta\bar{V}_c}\right)_0 &= \frac{1}{Q_{2D}}\left[\left(\frac{\partial\bar{W}_y}{\partial\bar{x}}\right)\sin\Psi_0 + \left(\frac{2}{\Delta\bar{t}} - \frac{\partial\bar{W}_x}{\partial\bar{x}}\right)\cos\Psi_0\right] \end{aligned} \tag{7.7}$$

As a result, Eqs.(7.5 - 7.7) provide necessary terms to calculate the first order adjustments.

7.1.2 Heading Adjustment Strategy

Similarly, the adjustment in heading angle can be obtained from Eq.(7.3) as

$$\Delta\Psi = \begin{cases} 0 & |I_{\Delta\Psi}| < \epsilon \\ \eta \max\{-\Delta\Psi_{\max}, \Psi_{\min} - \Psi_0\} & I_{\Delta\Psi} \geq \epsilon > 0 \\ \eta \min\{\Delta\Psi_{\max}, \Psi \leq \Psi_{\max} - \Psi_0\} & I_{\Delta\Psi} \leq -\epsilon \end{cases} \tag{7.8}$$

where $\bar{I}_{\Delta\Psi}$ could be expressed in compact form as

$$\bar{I}_{\Delta\Psi} = \bar{V}_0 \left[\frac{\partial \bar{W}_V(t_0 + \Delta t)}{\partial(\Delta\Psi)}\right]_0 \tag{7.9}$$

and

$$\begin{aligned} \left[\frac{\partial \bar{W}_V(t_0 + \Delta)}{\partial(\Delta\Psi)}\right]_0 = & \left(\frac{\partial \bar{W}_x}{\partial \bar{y}} + \frac{\partial \bar{W}_y}{\partial \bar{x}}\right) \bar{V}_0 \cos 2\Psi_0 + \left(\frac{\partial \bar{W}_x}{\partial \bar{x}} - \frac{\partial \bar{W}_y}{\partial \bar{y}}\right) \bar{V}_0 \sin 2\Psi_0 \\ & + \left[\frac{\partial \bar{W}_x}{\partial \bar{x}} \left(\frac{\partial \Delta\bar{x}}{\partial \Delta\Psi_c}\right)_0 + \frac{\partial \bar{W}_x}{\partial \bar{y}} \left(\frac{\partial \Delta\bar{y}}{\partial \Delta\Psi}\right)_0\right] \left(\frac{\partial \bar{W}_x}{\partial \bar{x}} \sin\Psi_0 + \frac{\partial \bar{W}_y}{\partial \bar{x}} \cos\Psi_0\right) \\ & + \left[\frac{\partial \bar{W}_y}{\partial \bar{x}} \left(\frac{\partial \Delta\bar{x}}{\partial \Delta\Psi}\right)_0 + \frac{\partial \bar{W}_y}{\partial \bar{y}} \left(\frac{\partial \Delta\bar{y}}{\partial \Delta\Psi}\right)_0\right] \left(\frac{\partial \bar{W}_x}{\partial \bar{y}} \sin\Psi_0 + \frac{\partial \bar{W}_y}{\partial \bar{y}} \cos\Psi_0\right) \\ & + \left(\bar{W}_x\right)_0 \left(\frac{\partial \bar{W}_x}{\partial \bar{x}} \cos\Psi_0 - \frac{\partial \bar{W}_y}{\partial \bar{x}} \sin\Psi_0\right) \\ & + \left(\bar{W}_y\right)_0 \left(\frac{\partial \bar{W}_x}{\partial \bar{y}} \cos\Psi_0 - \frac{\partial \bar{W}_y}{\partial \bar{y}} \sin\Psi_0\right) \\ & + \frac{\partial \bar{W}_x}{\partial \bar{t}} \cos\Psi_0 - \frac{\partial \bar{W}_y}{\partial \bar{t}} \sin\Psi_0 \end{aligned} \tag{7.10}$$

Again, the partial derivatives of position changes with respect to the heading angle adjustment can be obtained from Eqs.(6.20) and (6.18) as

$$\begin{aligned} \left(\frac{\partial \Delta\bar{x}}{\partial \Delta\Psi}\right)_0 &= \frac{\bar{V}_0}{Q_{2D}} \left[\left(\frac{2}{\Delta\bar{t}} - \frac{\partial \bar{W}_y}{\partial \bar{y}}\right) \cos\Psi_0 - \left(\frac{\partial \bar{W}_x}{\partial \bar{y}}\right) \sin\Psi_0\right] \\ \left(\frac{\partial \Delta\bar{y}}{\partial \Delta\Psi}\right)_0 &= \frac{\bar{V}_0}{Q_{2D}} \left[\left(\frac{\partial \bar{W}_y}{\partial \bar{x}}\right) \cos\Psi_0 - \left(\frac{2}{\Delta\bar{t}} - \frac{\partial \bar{W}_x}{\partial \bar{x}}\right) \sin\Psi_0\right] \end{aligned} \tag{7.11}$$

As it is possible to see from the derivations above, first-order gradient algorithms are simple and easy to implement. They are also computationally inexpensive in optimization routines, and sometimes are preferred due to this reason. But one of the major drawbacks of first-order algorithms is that they only provide the direction information for the minimization routine. The amount of adjustment is applied *manually* and needs to be tailored by the designer, which defeats the concept of optimality. With this manual *tailoring*, specified amount of adjustment may well exceed the optimal point, or may very well fall short and may not even be able to reach to the optimal point.

Therefore, in this thesis, first order gradient algorithms have not been used and are neglected. Instead, second-order optimal gradient algorithms have been adopted as main solution algorithms. It is because of the reason that, with second-order gradient algorithms, it possible to obtain not only direction information, but also the optimal amount of adjustment that will bring us to *local minima* and will *locally* minimize the corresponding terminal cost (i.e. projected power consumption function) at terminal state.

In the following sections, second order optimal adjustment strategies have been discussed in further detail.

7.2 Second Order Optimal Adjustment Strategies

With second-order gradient algorithms, the main goal is to find *locally* optimal adjustments: $\Delta\bar{V}$, $\Delta\Psi$ and $\Delta\gamma$ using the necessary conditions for optimality. For this purpose, second order Taylor series approximation of projected power function, in the

neighbourhood of initial state $\bar{X}_0$, is taken into account as

$$\begin{aligned}\tilde{I}(\bar{V}^*,\Psi^*,\gamma^*) \approx \bar{I}_0 &+ \left(\frac{\partial \bar{I}}{\partial \bar{V}^*}\right)_0 \overbrace{(\bar{V}^*-\bar{V}_0)}^{\Delta\bar{V}} + \left(\frac{\partial \bar{I}}{\partial \Psi^*}\right)_0 \overbrace{(\Psi^*-\Psi_0)}^{\Delta\Psi} + \left(\frac{\partial \bar{I}}{\partial \gamma^*}\right)_0 \overbrace{(\gamma^*-\gamma_0)}^{\Delta\gamma} \\ &+ \frac{1}{2}\left(\frac{\partial^2 \bar{I}}{\partial \bar{V}^{*2}}\right)_0 \overbrace{(\bar{V}^*-\bar{V}_0)^2}^{\Delta\bar{V}^2} + \frac{1}{2}\left(\frac{\partial^2 \bar{I}}{\partial \Psi^{*2}}\right)_0 \overbrace{(\Psi^*-\Psi_0)^2}^{\Delta\Psi^2} + \frac{1}{2}\left(\frac{\partial^2 \bar{I}}{\partial \gamma^{*2}}\right)_0 \overbrace{(\gamma^*-\Psi_0)^2}^{\Delta\gamma^2} \\ &+ \left(\frac{\partial^2 \bar{I}}{\partial \bar{V}^* \partial \Psi^*}\right)_0 \overbrace{(\bar{V}^*-\bar{V}_0)}^{\Delta\bar{V}} \overbrace{(\Psi^*-\Psi_0)}^{\Delta\Psi} + \left(\frac{\partial^2 \bar{I}}{\partial \bar{V}^* \partial^*}\right)_0 \overbrace{(\bar{V}^*-\bar{V}_0)}^{\Delta\bar{V}} \overbrace{(\gamma^*-\gamma_0)}^{\Delta\gamma} \\ &+ \left(\frac{\partial^2 \bar{I}}{\partial \gamma^* \partial \Psi^*}\right)_0 \overbrace{(\gamma^*-\gamma_0)}^{\Delta\gamma} \overbrace{(\Psi^*-\Psi_0)}^{\Delta\Psi}\end{aligned} \tag{7.12}$$

where the analytical expressions for the *local minima in the neighbourhood of in-situ measurements* are obtained through the necessary conditions of optimality,

$$\begin{aligned}\min_{\Delta\bar{V}} \tilde{I} \rightarrow \left(\frac{\partial \tilde{I}}{\partial \bar{V}^*}\right)_0 = 0 \\ \min_{\Delta\Psi} \tilde{I} \rightarrow \left(\frac{\partial \tilde{I}}{\partial \Psi^*}\right)_0 = 0 \\ \min_{\Delta\gamma} \tilde{I} \rightarrow \left(\frac{\partial \tilde{I}}{\partial \gamma^*}\right)_0 = 0\end{aligned} \tag{7.13}$$

as follows

$$\begin{aligned}\left(\frac{\partial \bar{I}}{\partial \bar{V}^*}\right)_0 + \left(\frac{\partial^2 \bar{I}}{\partial \bar{V}^{*2}}\right)_0 (\Delta\bar{V}) + \left(\frac{\partial^2 \bar{I}}{\partial \bar{V}^* \partial \Psi^*}\right)_0 (\Delta\Psi) + \left(\frac{\partial^2 \bar{I}}{\partial \bar{V}^* \partial \gamma^*}\right)_0 (\Delta\gamma) = 0 \\ \left(\frac{\partial \bar{I}}{\partial \Psi^*}\right)_0 + \left(\frac{\partial^2 \bar{I}}{\partial \Psi^* \partial \bar{V}^*}\right)_0 (\Delta\bar{V}) + \left(\frac{\partial^2 \bar{I}}{\partial \Psi^{*2}}\right)_0 (\Delta\Psi) + \left(\frac{\partial^2 \bar{I}}{\partial \Psi^* \partial \gamma^*}\right)_0 (\Delta\gamma) = 0 \\ \left(\frac{\partial \bar{I}}{\partial \gamma^*}\right)_0 + \left(\frac{\partial^2 \bar{I}}{\partial \gamma^* \partial \bar{V}^*}\right)_0 (\Delta\bar{V}) + \left(\frac{\partial^2 \bar{I}}{\partial \gamma^* \partial \Psi^*}\right)_0 (\Delta\Psi) + \left(\frac{\partial^2 \bar{I}}{\partial \gamma^{*2}}\right)_0 (\Delta\gamma) = 0\end{aligned} \tag{7.14}$$

leading to

$$\begin{bmatrix} \left(\frac{\partial \bar{I}}{\partial \bar{V}^*}\right)_0 \\ \left(\frac{\partial \bar{I}}{\partial \Psi^*}\right)_0 \\ \left(\frac{\partial \bar{I}}{\partial \gamma^*}\right)_0 \end{bmatrix} + \begin{bmatrix} \left(\frac{\partial^2 \bar{I}}{\partial \bar{V}^{*2}}\right)_0 & \left(\frac{\partial^2 \bar{I}}{\partial \bar{V}^* \partial \Psi^*}\right)_0 & \left(\frac{\partial^2 \bar{I}}{\partial \bar{V}^* \partial \gamma^*}\right)_0 \\ \left(\frac{\partial^2 \bar{I}}{\partial \Psi^* \partial \bar{V}^*}\right)_0 & \left(\frac{\partial^2 \bar{I}}{\partial \Psi^{*2}}\right)_0 & \left(\frac{\partial^2 \bar{I}}{\partial \Psi^* \partial \gamma^*}\right)_0 \\ \left(\frac{\partial^2 \bar{I}}{\partial \gamma^* \partial \bar{V}^*}\right)_0 & \left(\frac{\partial^2 \bar{I}}{\partial \gamma^* \partial \Psi^*}\right)_0 & \left(\frac{\partial^2 \bar{I}}{\partial \gamma^{*2}}\right)_0 \end{bmatrix} \begin{bmatrix} \Delta \bar{V} \\ \Delta \Psi \\ \Delta \gamma \end{bmatrix} = 0 \tag{7.15}$$

General matrix representation of Eq.(7.15) can be given as

$$[T_1]_{(nx1)} + [T_2]_{(nxn)} [\Delta]_{(nx1)} = 0 \tag{7.16}$$

where for this case, corresponding components are obtained as

$$T_1 = \begin{bmatrix} \left(\frac{\partial \bar{I}}{\partial \bar{V}^*}\right)_0 \\ \left(\frac{\partial \bar{I}}{\partial \Psi^*}\right)_0 \\ \left(\frac{\partial \bar{I}}{\partial \gamma^*}\right)_0 \end{bmatrix},$$

$$T_2 = \begin{bmatrix} \left(\frac{\partial^2 \bar{I}}{\partial \bar{V}^{*2}}\right)_0 & \left(\frac{\partial^2 \bar{I}}{\partial \bar{V}^* \partial \Psi^*}\right)_0 & \left(\frac{\partial^2 \bar{I}}{\partial \bar{V}^* \partial \gamma^*}\right)_0 \\ \left(\frac{\partial^2 \bar{I}}{\partial \Psi^* \partial \bar{V}^*}\right)_0 & \left(\frac{\partial^2 \bar{I}}{\partial \Psi^{*2}}\right)_0 & \left(\frac{\partial^2 \bar{I}}{\partial \Psi^* \partial \gamma^*}\right)_0 \\ \left(\frac{\partial^2 \bar{I}}{\partial \gamma^* \partial \bar{V}^*}\right)_0 & \left(\frac{\partial^2 \bar{I}}{\partial \gamma^* \partial \Psi^*}\right)_0 & \left(\frac{\partial^2 \bar{I}}{\partial \gamma^{*2}}\right)_0 \end{bmatrix}, \tag{7.17}$$

$$\Delta = \begin{bmatrix} \Delta \bar{V} \\ \Delta \Psi \\ \Delta \gamma \end{bmatrix}$$

It is possible to rewrite Eq.(7.16) as

$$[T_1]_{(nx1)} - [-T_2]_{(nxn)} [\Delta]_{(nx1)} = 0 \tag{7.18}$$

This result leads to a well known least squares minimization problem

$$\inf_{x \in X} || \ y - Ax \ || \tag{7.19}$$

where the optimal solution is obtained as

$$x^{opt} = \left(A^T A\right)^{-1} A^T y \tag{7.20}$$

Therefore, the solution to second-order optimal adjustments ($\Delta \bar{V}$, $\Delta \Psi$ and $\Delta \gamma$) for the case of 3D flight in presence of wind conditions is obtained as

$$[\Delta]^{opt}_{nx1} = \left[\left(T_2^T\right)_{nxn} (T_2)_{nxn}\right]^{-1} \left(-T_2^T\right)_{nxn} (T_1)_{nx1} \tag{7.21}$$

where $(\,)^T$ and $(\,)^{-1}$ defines the transpose and inverse of a matrix, respectively. This solution methodology completes the solution strategies and provides an *analytical*, *single-shot-solution* to the static optimization problem in hand.

Chapter 8

Models of Closed-Loop Tracking

In previous chapter, optimization algorithms have been devised to solve static optimization problem with respect to local, instantaneous, in-situ measurements with the help of second-order gradient algorithms. Using the given formulation, it is possible to obtain local optimal solutions that will make sure when those obtained optimal state values (namely $\bar{V}^* = \bar{V}_c = \bar{V}_0 + \Delta\bar{V}$, $\Psi^* = \Psi_c = \Psi_0 + \Delta\Psi$ and/or $\gamma^* = \gamma_c = \gamma_0 + \Delta\gamma$) are tracked, terminal cost function associated with the power consumption at the terminal state will be minimized and it will be possible to repeat this periodically for each update interval. Therefore, when desired-states-to-be-achieved are provided (i.e. $\bar{V}_{air}$, $\bar{x}_c(\bar{t})$, $\bar{V}_I$ ... etc.) the next step is to determine "the corresponding closed-loop control commands" which will make sure that defined states are achieved, and tracking performance is satisfied.

In literature, there are various and general models of control systems to achieve tracking performance. One of them is the well known *feedback linearization method*. The method of feedback linearization is a widely used and a commonly accepted application in applied nonlinear control, and is well defined in many sources, as Slotine and Li (1991). In the following subsections, necessary control command inputs will be derived using *the method of feedback linearization* which will make sure that such desired states ($\bar{V}_c$, Ψ_c, γ_c) will be achieved and tracked accordingly.

One good point to note is that, with respect to the assigned mission objectives, the aircraft may follow *velocity guidance strategies* ($\bar{V}_c$,Ψ_c,γ_c), *trajectory strategies* ($\bar{x}_c$,$\bar{y}_c$,$\bar{h}_c$) or the specific combination of both strategies. From that perspective, it is necessary

to derive such control commands, which will make sure the corresponding strategy is executed as desired. Thus, in the following sections, necessary control commands for both *velocity guidance strategies* and *trajectory tracking strategies* will be derived in detail.

8.1 Control Commands for Velocity Strategy ($\bar{V}_{air}$, Ψ, γ):

The *method of feedback linearization* simply defines a transformation from the nonlinear system in hand into an equivalent linear system through change of variables and a suitable control input. Here, the author is fully aware of the fact that effects of plant and modelling uncertainties have an important impact on the outcome of such method. Therefore, how they are handled is an important matter and should be investigated in further detail. However, it is a topic which is out of the scope of the study presented in this thesis and is left aside for future research. As a result, such uncertainty analysis is not included in this thesis.

In follows, the procedure for the derivation of control inputs (*power*-$\bar{P}$, lift coefficient-C_L and bank angle-μ) is presented in terms of normalized EoMs.

If the derivation is started with first order approximation of air-speed tracking, it is possible to define

$$\dot{V} + K_V(V - V_c) = 0 \tag{8.1}$$

Then, using normalized variables, the closed-loop power law can be determined as

$$\frac{\bar{P}_{(vel)}}{\bar{V}} = -\bar{K}_V(\bar{V} - \bar{V}_c) + \bar{\rho}\bar{V}^2\left(C_{D_0} + KC_{L_v}^2\right) + \sin\gamma + \bar{W}'_V \tag{8.2}$$

Similarly for the heading angle control, it is

$$\dot{\Psi} + \bar{K}_\Psi(\Psi - \Psi_c) = 0 \tag{8.3}$$

which leads to

$$\bar{\rho}\bar{V}^2 C_L \sin\mu = \bar{W}'_\Psi - \bar{V}\cos\gamma\bar{K}_\Psi(\Psi - \Psi_c) \tag{8.4}$$

and the flight path angle control using

$$\dot{\gamma} + K_\gamma(\gamma - \gamma_c) = 0 \tag{8.5}$$

is obtained as

$$\bar{\rho}\bar{V}^2 C_L \cos\mu = \cos\gamma - \bar{W}'_\gamma - \bar{V}\bar{K}_\gamma t_n(\gamma - \gamma_c) \tag{8.6}$$

Using Eqs.(8.4) and (8.6), closed loop control command for bank angle, (μ) is derived as

$$\tan\mu_{(vel)} = \frac{\bar{W}'_\Psi - \bar{V}cos(\gamma)\bar{K}_\Psi(\Psi - \Psi_c)}{\cos\gamma - \bar{W}'_\gamma - \bar{V}K_\gamma(\gamma - \gamma_c)} \tag{8.7}$$

where by taking the square of Eqs.(8.4) and (8.6), closed loop control logic for lift coefficient (C_L) is obtained as

$$C_{L_{(vel)}} = \frac{\sqrt{\left[\bar{W}'_\Psi - \bar{V}\cos\gamma\bar{K}_\Psi(\Psi - \Psi_c)\right]^2 + \left[\cos\gamma - \bar{W}'_\gamma - \bar{V}\bar{K}_\gamma(\gamma - \gamma_c)\right]^2}}{\bar{\rho}\bar{V}^2} \tag{8.8}$$

In the given derivations above, the *normalized* feedback gains ($\bar{K}_V, \bar{K}_\Psi, \bar{K}_\gamma$) can be tailored to reflect typical closed-loop UAV control characteristics. It is also possible to find more detailed derivation of given control commands in Appendix-C for further investigation.

Following to the derivation of control commands for *velocity strategy*, next goal will be to obtain necessary control commands for the *trajectory strategy*, which is explained in detail in the following section.

8.2 Control Commands for Trajectory Tracking Strategy:

In this section, necessary control commands, for the case where it is desired to track a reference trajectory ($\bar{x}_c$, $\bar{y}_c$, $\bar{h}_c$) will be derived. This desired trajectory may vary from mission to mission and is peculiar to every situation. In this study, a *circular, level flight trajectory* at a specified height will be aimed to be followed and is studied in the followings. Also, a sample scenario of a desired trajectory (in this case a *circular level flight*) pattern is defined and given in Fig-8.1.

In Fig-8.1, definition of α is closely related to the nature and to the characteristics of the assigned mission, but in general it is possible to define α in two different ways:

1. If UAV is assigned to solely track a circular flight trajectory and is supposed to stay all the time on the circular flight path without doing anything else, it is possible to define α (in this case depicted as α_1) as a heading angle command, where α becomes

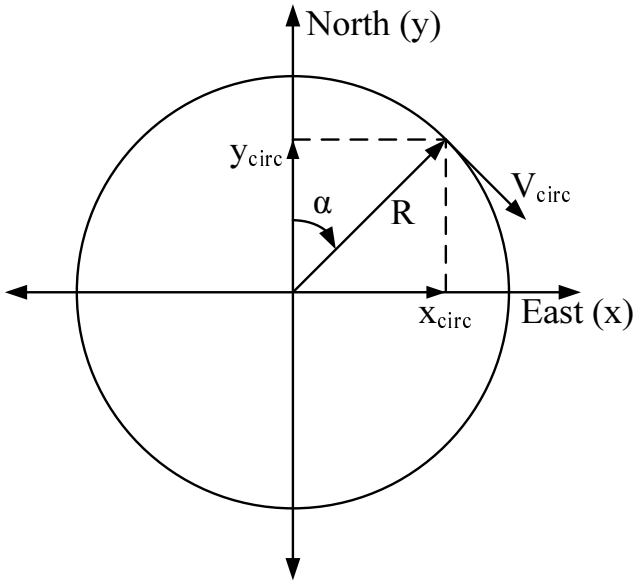

Figure 8.1: A sample circular level flight trajectory sketch at certain altitude $\bar{h}$.

$$\alpha_1 = \Psi - 90^o \tag{8.9}$$

2. If UAV is assigned with a mission to fly *freely within the given restricted zone*, then α should be defined as desired trajectory that will be enforced as boundary constraints, leading to the case where α is depicted as α_2 and become

$$\alpha_2 = 2\pi \left(\frac{\bar{t}}{\bar{t}_f} \right), \quad \alpha_2' = \frac{\bar{V}_{circ}}{\bar{R}} \tag{8.10}$$

where $\bar{t}_f$ is the total flight (i.e. simulation) time, $\bar{V}_{circ}$ is the desired airspeed to satisfy such boundary conditions and $\bar{R}$ is the radius of the circular level flight trajectory, respectively.

In this thesis, trajectory tracking constraints are selected and imposed through the scenario given in *Option-(2)*, and is iterated furthermore in Chapter 9, Section 9.5.5.

For such circular level flight trajectory, it is possible to define necessary trajectory states to be followed ($\bar{x}_c(\bar{t})$, $\bar{y}_c(\bar{t})$, $\bar{h}_c(\bar{t})$) as following:

$$\bar{x}_c = \bar{R}\sin(\alpha), \quad \bar{y}_c = \bar{R}\cos(\alpha), \quad \bar{h}_c = \bar{h}_{oper} \tag{8.11}$$

$$\bar{x}'_c = \bar{V}_{circ}\cos(\alpha), \quad \bar{y}'_c = -\bar{V}_{circ}\sin(\alpha), \quad \bar{h}'_c = 0 \tag{8.12}$$

$$\bar{x}''_c = -\frac{\bar{V}^2_{circ}}{\bar{R}}\sin(\alpha), \quad \bar{y}''_c = -\frac{\bar{V}^2_{circ}}{\bar{R}}\cos(\alpha), \quad \bar{h}''_c = 0 \tag{8.13}$$

where $\bar{h}_{oper}$ is the operation altitude of the circular level flight trajectory.

Starting from this point, one can define a second order tracking control problem as

$$(\bar{x}'' - \bar{x}''_c) + 2\zeta\bar{\omega}_n(\bar{x}' - \bar{x}'_c) + \bar{\omega}_n^2(\bar{x} - \bar{x}_c) = 0 \tag{8.14}$$

leading to

$$\bar{x}'' = \left[\bar{x}''_c - 2\zeta\bar{\omega}_n(\bar{x}' - \bar{x}'_c) - \bar{\omega}_n^2(\bar{x} - \bar{x}_c)\right] = \bar{D}_{\bar{x}} \tag{8.15}$$

where $\bar{\omega}_n$ and ζ_n are coefficients that designer can use to tailor the flight trajectory characteristics as desired.

Thus, expressions for $\bar{D}_{\bar{y}}$ and $\bar{D}_{\bar{h}}$ can be obtained similarly as

$$\begin{aligned}(\bar{y}'' - \bar{y}''_c) + 2\zeta\bar{\omega}_n(\bar{y}' - \bar{y}'_c) + \bar{\omega}_n^2(\bar{y} - \bar{y}_c) = 0\\ (\bar{h}'' - \bar{h}''_c) + 2\zeta\bar{\omega}_n(\bar{h}' - \bar{h}'_c) + \bar{\omega}_n^2(\bar{h} - \bar{h}_c) = 0\end{aligned} \tag{8.16}$$

leading to

$$\begin{aligned}\bar{y}'' = \left[\bar{y}''_c - 2\zeta\bar{\omega}_n(\bar{y}' - \bar{y}'_c) - \bar{\omega}_n^2(\bar{y} - \bar{y}_c)\right] = \bar{D}_{\bar{y}}\\ \bar{h}'' = \left[\bar{h}''_c - 2\zeta\bar{\omega}_n(\bar{h}' - \bar{h}'_c) - \bar{\omega}_n^2(\bar{h} - \bar{h}_c)\right] = \bar{D}_{\bar{h}}\end{aligned} \tag{8.17}$$

Next step will be to define expressions for $(\ )''$ which will make sure that desired trajectory defined by $\bar{D}(\ )$'s are followed.

On the way of deriving necessary control commands, one can start with Eq.(2.22), where one time differentiation leads to

$$\bar{x}'' = \bar{V}'\cos\gamma\sin\Psi - \bar{V}\sin\gamma\gamma'\sin\Psi + \bar{V}\cos\gamma\cos\Psi\Psi' \tag{8.18}$$

Here using the expressions for $\bar{V}'$, Ψ' and γ' from Eqs.(2.19 - 2.21), results in

$$\begin{aligned}\bar{x}'' = \bar{D}_{\bar{x}} &= (\bar{P}/\bar{V} - \bar{D})\cos\gamma\sin\Psi - \bar{L}\cos\mu\sin\gamma\sin\Psi + \bar{L}\sin\mu\cos\Psi\\ \bar{y}'' = \bar{D}_{\bar{y}} &= (\bar{P}/\bar{V} - \bar{D})\cos\gamma\cos\Psi - \bar{L}\cos\mu\sin\gamma\cos\Psi + \bar{L}\sin\mu\sin\Psi\\ \bar{h}'' = \bar{D}_{\bar{h}} &= (\bar{P}/\bar{V} - \bar{D})\sin\gamma + \bar{L}\cos\mu\cos\gamma - 1\end{aligned} \tag{8.19}$$

Then, using

$$\begin{aligned} \bar{L} &= \bar{\rho}\bar{V}^2 C_L \\ \bar{D} &= \bar{\rho}\bar{V}^2 C_D = \bar{\rho}\bar{V}^2 (C_{D_0} + KC_L^2) \end{aligned} \tag{8.20}$$

and after several lengthy algebraic manipulations, it is possible to obtain the necessary control command inputs for trajectory tracking problem (as functions of desired trajectory states $\bar{D}_{\bar{x}}$, $\bar{D}_{\bar{y}}$ and $\bar{D}_{\bar{h}}$) as

$$\frac{\bar{P}}{\bar{V}} = \bar{\rho}\bar{V}^2 (C_{D_0} + KC_L^2) + \bar{D}_{\bar{h}} \sin\gamma + \bar{D}_{\bar{x}} \sin\Psi \cos\gamma + \bar{D}_{\bar{y}} \cos\Psi \cos\gamma \sin\gamma \tag{8.21}$$

$$C_L = \frac{\sqrt{(\bar{D}_{\bar{x}} \cos\Psi - \bar{D}_{\bar{y}} \sin\Psi)^2 + (\bar{D}_{\bar{h}} \cos\gamma + \cos\gamma - \bar{D}_{\bar{x}} \sin\Psi \sin\gamma - \bar{D}_{\bar{y}} \cos\Psi \sin\gamma)^2}}{\bar{\rho}\bar{V}^2} \tag{8.22}$$

$$\tan\mu = \frac{(\bar{D}_{\bar{x}} \cos\Psi - \bar{D}_{\bar{y}} \sin\Psi)}{(\bar{D}_{\bar{h}} \cos\gamma + \cos\gamma - \bar{D}_{\bar{x}} \sin\Psi \sin\gamma - \bar{D}_{\bar{y}} \cos\Psi \sin\gamma)} \tag{8.23}$$

where the detailed derivation can be investigated in further detail from Appendix-C.

Tracking of *inertial* or *constant* reference states (airspeed, heading angle and/or flight path angle) can also be adopted as a flight strategy, where necessary control commands should be used and applied accordingly. Here the complete derivation for the case of *tracking inertial reference states* and *tracking constant reference states* are also given in detail in Appendix-C.

Chapter 9

Simulation Evaluation and Results for Level Flight Strategies

In previous chapters, all the necessary components and control commands have been derived to execute *real-time guidance strategies in presence of winds*. when combined, all those components and commands will make sure that, once optimal adjustments (in airspeed, heading angle and/or flight path angle) are calculated, it will be possible to track those specified states, and through this tracking process, the power function will be minimized and endurance (i.e. flight time) will be maximized. With all these components, the derivation of all the necessary and key pieces are completed.

Next step will be to evaluate proposed flight strategies. Thus, in this chapter, the effectiveness, functionality and outcomes of the proposed guidance strategies will be demonstrated on five different level flight scenarios through extensive simulations.

Specifically speaking, those five level flight scenarios can be summarized as follows:

1. First, a reference flight scenario will be demonstrated which is defined as a function of constant airspeed and heading angle. In this scenario, airspeed is chosen as optimal level flight airspeed *with zero wind*, as given in Eq.(6.26). This will be the reference case which will be compared with other strategies.

2. Second, a case and outcomes will be shown where only allowed optimal adjustments are in heading angle. Here, airspeed will be kept constant.

3. Third, a scenario will be presented, where this time only optimal adjustments in airspeed will be allowed and heading angle will be kept constant.

4. Fourth, we will show a scenario in which optimal adjustments both in airspeed and heading angle are allowed.

5. Finally, as a fifth scenario, to demonstrate complete guidance strategy (i.e. the combination of *velocity strategy* and *trajectory tracking strategy*), a realistic daily application will be demonstrated in which optimal adjustments in both airspeed and heading angle are allowed, but the flight region is restricted as a 2D circular region, as given in Fig-8.1. With this course of action, UAV will be allowed to stay only within the specified geometric region (through *trajectory strategy*) and fly efficiently, by benefiting from the wind (through *velocity strategy*) while executing the assigned flight mission. Through this strategy it is also desired to demonstrate the outcomes of combination of *velocity strategy* together with *trajectory strategy*, which is the ultimate aim of this study.

A notional framework for the simulation studies of guidance strategies is shown in Fig-9.1. Here, the **Aircraft** dynamics is modeled by the previously described 3D point-mass equations. The UAV tracking logic, contained within the **Trajectory Tracking** box, is based on the reference trajectory methodology explained in Chapter 8. **Control** box includes the control commands derived through the method of feedback linearization as described in previous chapter. The **Velocity Strategy** box depicts the solution algorithms given in Chapter 6.

In general, the **Wind Gradients** and **Navigation** blocks represent sensors and algorithms for deriving estimates of the current wind states. This study mainly focuses on the development of algorithms for utilizing wind energies, and it is therefore assumed that accurate wind estimates can be made using on-board flight instruments and algorithms.

Fig-9.2 presents the main simulation flowchart for evaluating the proposed algorithms. In particular, it shows the required inputs to the proposed guidance algorithms for generating optimal airspeed and/or heading adjustments at a given time to minimize a projected power consumption at some terminal state.

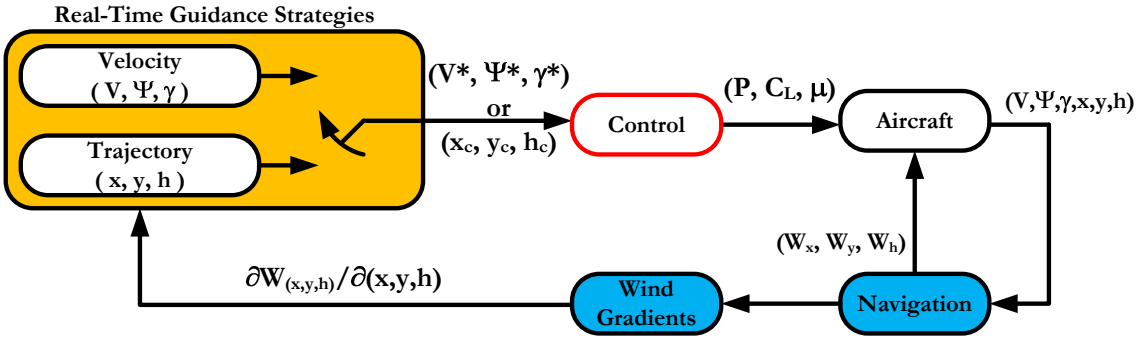

Figure 9.1: High-level architecture of combined guidance strategies: Velocity and Trajectory strategy.

9.1 Guidance Algorithm Parameters

Performance of the proposed level flight guidance strategies strongly depend on the following four parameters

$$\Delta\bar{V}_{\max}, \quad \Delta\bar{V}_{\min}, \quad \Delta\Psi_{\max}, \quad \Delta\Psi_{\min} \tag{9.1}$$

and it is crucial to come up with ranges of their appropriate values.

Actual values used in the guidance strategies can be smaller than the given bounds, but in this simulational study, we select $\Delta\bar{V}_{\max} \leq 5$ [ft/sec], $\Delta\bar{V}_{\min} = -\Delta\bar{V}_{\max}$, $\Delta\Psi_{\max} \leq 30°$, and $\Delta\Psi_{\min} = -\Delta\Psi_{\max}$. It is also important to note that those values are specific to an UAV and is subjected to vary from aircraft to aircraft.

9.2 Evaluation Criterion

Because of the reason that guidance strategies provided in this study are introduced to save power in UAV flights, a basic performance measure is defined as the *average power consumption* over a specified time interval,

$$\bar{P} = \frac{1}{\bar{t}_f} \int_0^{\bar{t}_f} \bar{T}\bar{V} d\bar{t} \tag{9.2}$$

where t_f is the time period of evaluation (i.e. flight/simulation time).

In the numerical results that are presented in the following sections, sampling time (integration step size) is selected as $50[Hz]$, (i.e. $0.02[sec]$).

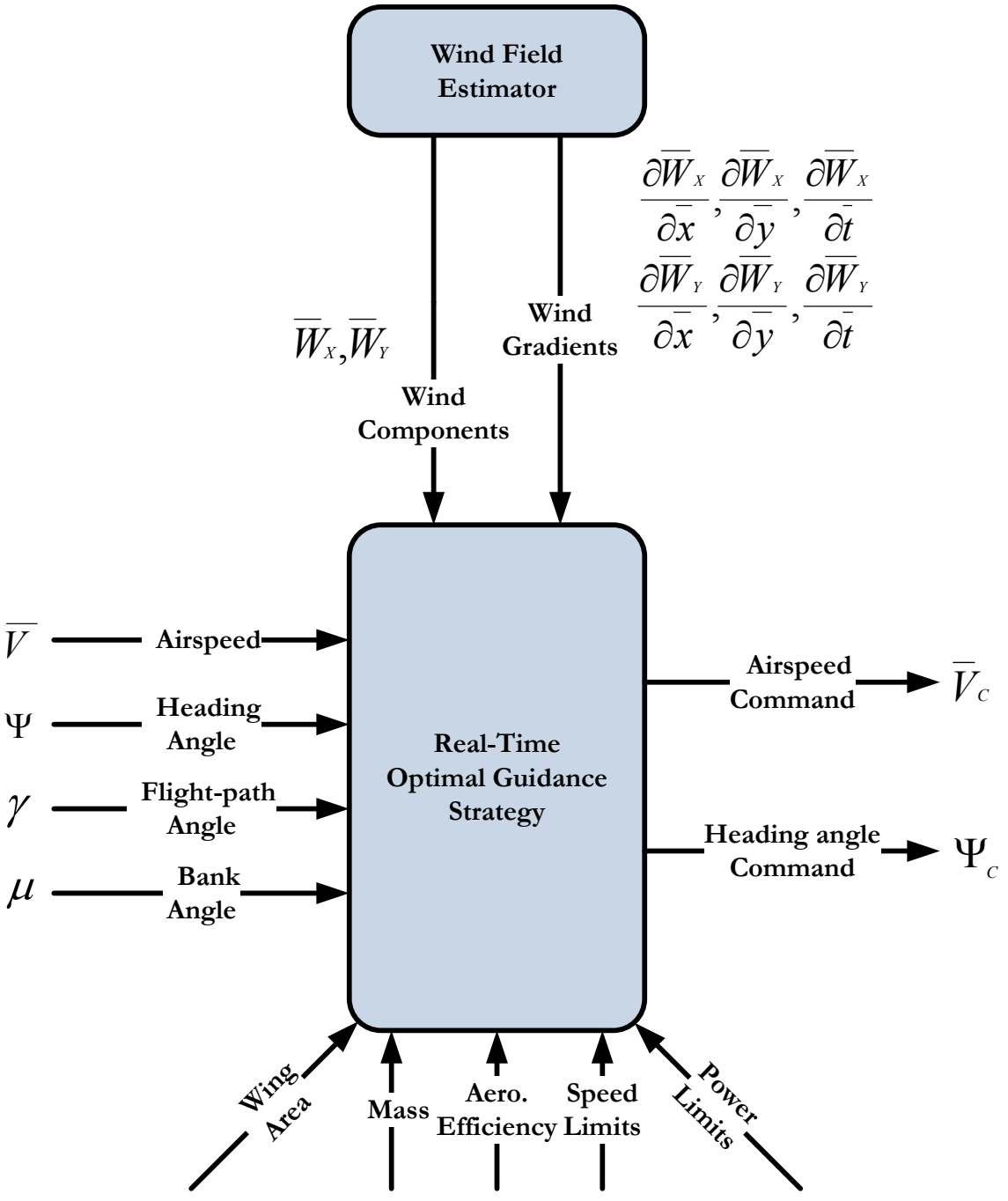

Figure 9.2: Simulation flowchart.

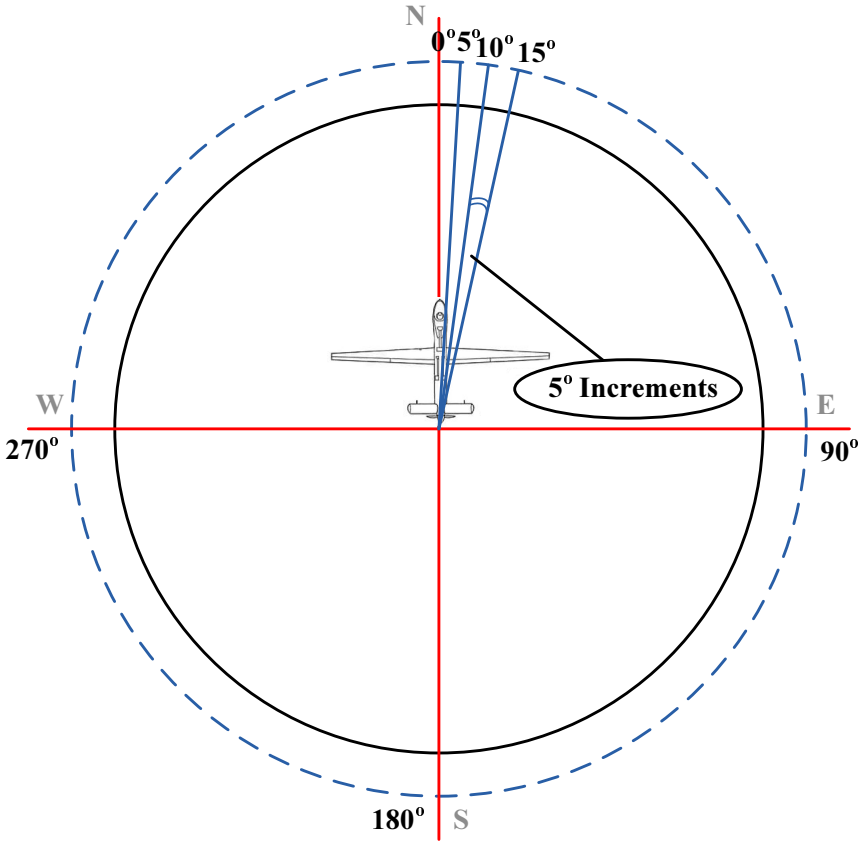

Figure 9.3: Average power concept for different initial heading angle (Ψ_0) settings.

Furthermore, different initial heading angles of the UAV result in different relative angles with respect to the wind field, and thus affect the resulting power saving benefit. In order to filter out these differences caused by different initial headings of UAV flights, and to have an estimate of global benefit, the above basic performance measure is further averaged within a set of different initial heading angles over $[0, 360^o]$. Here, a generic case of $\Delta\Psi_0 = 5^\circ$ increment is illustrated in Fig. 9.3. The mean of basic average power consumption over different initial heading conditions is defined as the measure of the performance

$$\bar{P}_{\text{avg}} = \frac{1}{N_\Psi} \sum_{i=1}^{N_\Psi} \bar{P}_{\Psi_0} \tag{9.3}$$

where each i corresponds to a different initial heading angle, and N_Ψ is the number of different initial heading angles used.

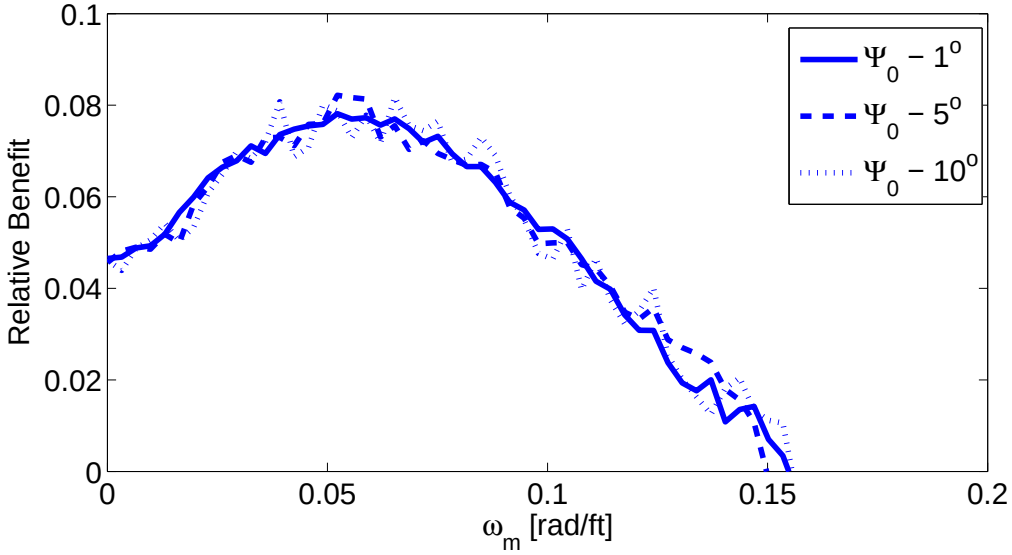

Figure 9.4: Effects of Ψ_0 sampling sizes for Strategy-4 ($\Delta\bar{V}$ & $\Delta\Psi$).

In the simulation studies, effects of different initial heading angle increments are also examined. Fig. 9.4 shows that $\Delta\Psi_0 = 5^o$ provides sufficiently accurate solutions as those with $\Delta\Psi_0 = 1^o$ at less computational loads, whereas it provides more accurate results than those with $\Delta\Psi_0 = 10^o$. Therefore, in the following simulational results, it is assumed that $\Delta\Psi_0 = 5^o$ for $\Psi_0 \in [0, 360^o]$.

To evaluate the proposed guidance strategies, following five scenarios are considered:

- **Scenario-0:** is the reference strategy that aims to follow the reference airspeed and a constant heading angle command set at the initial heading angle. This provides the reference average power consumption, $\bar{P}^0$.

- **Scenario-1:** In the second scenario, the commanded airspeed is adjusted periodically based on the current wind measurements wheres the heading angle command is set constant at the initial heading angle. The resulting average power consumption is denoted as $\bar{P}^1$.

- **Scenario-2:** In the third case, the heading angle is adjusted periodically based on the current wind measurements whereas the airspeed command is the same as the reference airspeed, and kept constant. The resulting average power consumption is denoted as $\bar{P}^2$.

- **Scenario-3:** In the fourth scenario, both airspeed and heading angle commands are adjusted periodically based on the current wind measurements. The resulting average power consumption is $\bar{P}^3$.

- **Scenario-4:** In fifth scenario, it is assumed that UAV is assigned to fly in a desired circular flight region (with a specific radius), and will maintain boundary control logics to stay within the specified region. While inside the region, both airspeed and heading angle commands are adjusted periodically based on the current wind measurements. When UAV gets close to the boundary and gets inside a buffer zone, decision making algorithm will take place to decide whether to track boundary or to head towards inside the specified flight region (in our case circular region). The resulting average power consumption is denoted as $\bar{P}^4$.

In all cases, airspeed and heading angle commands are tracked via closed-loop control logics derived in Chapter 8, where in fifth case in addition to *velocity strategy*, *trajectory tracking* control logics are also followed as well.

9.3 Benefit Criterion

To be able to come up with a decisive conclusion of the effectiveness of proposed strategies, it is essential to compare suggested scenarios with a reference scenario. In this case, reference scenario (Scenario-0) is the basis and is consisted of tracking optimal airspeed with constant heading angle. In Scenario-0, optimal airspeed is the optimal value of the airspeed in *zero winds*, as given in Eq.(6.26).

Therefore, the following benefit criterion is introduced as a relative measure of potential fuel savings of the proposed guidance strategies over the reference strategy

$$B_i = \frac{\bar{P}^0_{\text{avg}} - \bar{P}^i_{\text{avg}}}{\bar{P}^0_{\text{avg}}} \quad i = 1, 2, 3, 4 \tag{9.4}$$

9.4 Simulation Parameters

In simulations, UAV parameters similar to those of the ScanEagle UAV are used, where characteristic values of ScanEagle UAV, taken from Austin (2010), are given in Table-9.1.

Table 9.1: ScanEagle UAV parameters.

Name	Value
Weight	$W = 44[lbs]$
Wing Area	$S = 5.92[ft^2]$
Parasite Drag Coefficient	$C_{D_0} = 0.01$
Aerodynamic Efficiency	$E_{\max} = 25$
Max. power	$P_{\max} = 1400$[W]
Max. Airspeed	$V_{\max} = 134.5$ [ft/s]
Max. Lift Coefficient	$C_{L_{\max}} = 1.2$
Min. Lift Coefficient	$C_{L_{\min}} = 0$
Max. Bank Angle	$\mu_{\max} = 40^o$
Critical Lift Coefficient	$C_{L_{\text{cr}}} = 0.3$
Ceiling	$19,500[ft]$
Normalizing Airspeed	$V_n = V_{max} = 134.5[ft/sec]$

Here, the power available is assumed to be able to vary instantaneously (%100 change in 1sec for propeller-driven engines). In addition, available control rate bounds are taken into account as presented in Table-9.2.

Table 9.2: Normalized control rate bounds.

Name	Value
$(\bar{P}'_{max})$	6.216 (%100 change in 1sec)
$(C'_{L_{max}})$	1.865 ($\frac{1.2}{4}[1/sec]$)
(μ'_{max})	1.085 (10 [deg/sec])

Furthermore, the minimum airspeed constraint is selected to be close to the stall speed, whereas the maximum speed is selected to be close to a typical cruise speed, with allowances for transient dynamics in both cases. In terms of normalized quantities,

$$\bar{V}_{\min} = \frac{1.0}{\sqrt{\bar{\rho}C_{L_{\max}}}} \quad \text{and} \quad \bar{V}_{\max} = \frac{1.5}{\sqrt{\bar{\rho}C_{L_{\text{cr}}}}} \tag{9.5}$$

where $C_{L_{\text{cr}}}$ is a typical cruise lift coefficient, corresponding to an angle of attack of $3^o - 5^o$.

9.5 Simulation Results

For the conducted simulations in this section, a level flight at altitude of 15,000[ft] is assumed and a total flight time of $20[min] = 1200[sec]$ with a simulation step size of $0.02[sec] = 50[Hz]$ is taken into account. Normalization velocity, V_n, is taken as the maximum flight speed of the UAV ($V_n = 134.5[ft/sec]$). Wind magnitude ($\bar{W}_m$) and wind direction (Ψ_w), obtained from the stochastic wind model formulation (expressed in Chapter 3), is used. Wind frequency, throughout these equations is assumed to be constant and equal to $\omega_w = 0.05[rad/ft] \approx 9.4[deg/m]$. It is also assumed that periodic optimal adjustments are applied once in every $4[sec]$, which is the same as the measurement update time (i.e. $\Delta t = 4[sec]$).

The affect of varying wind magnitudes and wind frequencies is also taken into account and will be discussed in further details in the following sections.

9.5.1 Scenario-0: Constant airspeed, constant heading angle

In this scenario, it is desired to fly with optimal airspeed (determined in zero winds, as given in Eq.(6.26)) and constant heading angle, which is the initial heading angle given in the simulation settings. In other words, with this scenario, if the mission is

specified to fly with optimal airspeed and initial heading angle (say 90^o (with respect to true north)), UAV dynamics will execute these commands throughout the entire flight and will determine the power consumption during this specific flight routine. Obtained power consumption value is the *reference* power setting, $\bar{P}_0$, and will be compared with other outcomes to measure the efficiency of proposed strategies in given flight conditions.

For given UAV parameters in Table-9.1, obtained simulation results for Scenario-0 are presented in Figs.(9.5-9.8), where corresponding numerical results are given in Table-9.3.

In Table-9.3 $\bar{W}_m$ is mean wind magnitude, Ψ_W is mean wind direction, ω_W is wind frequency, $\bar{P}_{avg}$ is average power consumption, Ψ_0 is initial heading angle setting, $(C_L)_{max}$ is maximum obtained lift coefficient value and $(C_L)_{min}$ is minimum achieved lift coefficient value, throughout the conducted simulation.

As it is possible to see from Fig-9.5, for the given flight altitude $(15,000[ft])$, corresponding normalized optimal airspeed (in zero winds) is obtained as $\bar{V}^* = 0.7963$ which is equal to $V_{air} = 107.1[ft/sec]$. Given normalized power value in Table-9.3 is the amount of power required to maintain this flight for the given amount of time (20min) at the specified altitude (15,000ft). It is also possible to notice from Table-9.3 that, for the case of absence of winds in the equations, initial heading angle setting is not important and the average power setting is the same for different initial heading angle configurations. *But*, as it will be shown in further details in the following sections, this will not be true in presence of winds, and the initial heading angle setting will have an effect on the power consumption. This effect has to be taken into account and therefore it is necessary to average obtained power consumptions throughout different initial heading angle configurations.

9.5.2 Scenario-1: Optimal airspeed, constant heading angle case in presence of wind

This scenario finds several applications in routine mission assignments of UAVs. When an UAV is airborned and a mission is assigned, it is expected the UAV to travel from one location to another with given flight commands, and it is a very common practice to command the UAV to fly with a fixed heading angle. This scenario corresponds to this specific case, where UAV is flying with fixed heading angle. In the followings, we

Table 9.3a: Scenario-0: Numerical results.

Scenario	$\bar{W}_m$	$\Psi_W[deg]$	$\omega_W[rad/ft]$	$\bar{P}_{avg}$	$\Psi_0[deg]$	$(C_L)_{max}$	$(C_L)_{min}$
0	0.0000	0.0000	0.000	0.0368	0.0000	0.8660	0.8660
0	0.0000	0.0000	0.000	0.0368	5.0000	0.8660	0.8660
0	0.0000	0.0000	0.000	0.0368	10.0000	0.8660	0.8660
0	0.0000	0.0000	0.000	0.0368	15.0000	0.8660	0.8660
0	0.0000	0.0000	0.000	0.0368	20.0000	0.8660	0.8660
0	0.0000	0.0000	0.000	0.0368	25.0000	0.8660	0.8660
0	0.0000	0.0000	0.000	0.0368	30.0000	0.8660	0.8660
0	0.0000	0.0000	0.000	0.0368	35.0000	0.8660	0.8660
0	0.0000	0.0000	0.000	0.0368	40.0000	0.8660	0.8660
0	0.0000	0.0000	0.000	0.0368	45.0000	0.8660	0.8660
0	0.0000	0.0000	0.000	0.0368	50.0000	0.8660	0.8660
0	0.0000	0.0000	0.000	0.0368	55.0000	0.8660	0.8660
0	0.0000	0.0000	0.000	0.0368	60.0000	0.8660	0.8660
0	0.0000	0.0000	0.000	0.0368	65.0000	0.8660	0.8660
0	0.0000	0.0000	0.000	0.0368	70.0000	0.8660	0.8660
0	0.0000	0.0000	0.000	0.0368	75.0000	0.8660	0.8660
0	0.0000	0.0000	0.000	0.0368	80.0000	0.8660	0.8660
0	0.0000	0.0000	0.000	0.0368	85.0000	0.8660	0.8660
0	0.0000	0.0000	0.000	0.0368	90.0000	0.8660	0.8660
0	0.0000	0.0000	0.000	0.0368	95.0000	0.8660	0.8660
0	0.0000	0.0000	0.000	0.0368	100.0000	0.8660	0.8660
0	0.0000	0.0000	0.000	0.0368	105.0000	0.8660	0.8660
0	0.0000	0.0000	0.000	0.0368	110.0000	0.8660	0.8660
0	0.0000	0.0000	0.000	0.0368	115.0000	0.8660	0.8660
0	0.0000	0.0000	0.000	0.0368	120.0000	0.8660	0.8660
0	0.0000	0.0000	0.000	0.0368	125.0000	0.8660	0.8660
0	0.0000	0.0000	0.000	0.0368	130.0000	0.8660	0.8660
0	0.0000	0.0000	0.000	0.0368	135.0000	0.8660	0.8660
0	0.0000	0.0000	0.000	0.0368	140.0000	0.8660	0.8660
0	0.0000	0.0000	0.000	0.0368	145.0000	0.8660	0.8660
0	0.0000	0.0000	0.000	0.0368	150.0000	0.8660	0.8660
0	0.0000	0.0000	0.000	0.0368	155.0000	0.8660	0.8660
0	0.0000	0.0000	0.000	0.0368	160.0000	0.8660	0.8660
0	0.0000	0.0000	0.000	0.0368	165.0000	0.8660	0.8660
0	0.0000	0.0000	0.000	0.0368	170.0000	0.8660	0.8660
0	0.0000	0.0000	0.000	0.0368	175.0000	0.8660	0.8660
0	0.0000	0.0000	0.000	0.0368	180.0000	0.8660	0.8660

Table 9.3b: Scenario-0: Numerical results (continued).

Scenario	$\bar{W}_m$	$\Psi_W[deg]$	$\omega_W[rad/ft]$	$\bar{P}_{avg}$	$\Psi_0[deg]$	$(C_L)_{max}$	$(C_L)_{min}$
0	0.0000	0.0000	0.000	0.0368	185.0000	0.8660	0.8660
0	0.0000	0.0000	0.000	0.0368	190.0000	0.8660	0.8660
0	0.0000	0.0000	0.000	0.0368	195.0000	0.8660	0.8660
0	0.0000	0.0000	0.000	0.0368	200.0000	0.8660	0.8660
0	0.0000	0.0000	0.000	0.0368	205.0000	0.8660	0.8660
0	0.0000	0.0000	0.000	0.0368	210.0000	0.8660	0.8660
0	0.0000	0.0000	0.000	0.0368	215.0000	0.8660	0.8660
0	0.0000	0.0000	0.000	0.0368	220.0000	0.8660	0.8660
0	0.0000	0.0000	0.000	0.0368	225.0000	0.8660	0.8660
0	0.0000	0.0000	0.000	0.0368	230.0000	0.8660	0.8660
0	0.0000	0.0000	0.000	0.0368	235.0000	0.8660	0.8660
0	0.0000	0.0000	0.000	0.0368	240.0000	0.8660	0.8660
0	0.0000	0.0000	0.000	0.0368	245.0000	0.8660	0.8660
0	0.0000	0.0000	0.000	0.0368	250.0000	0.8660	0.8660
0	0.0000	0.0000	0.000	0.0368	255.0000	0.8660	0.8660
0	0.0000	0.0000	0.000	0.0368	260.0000	0.8660	0.8660
0	0.0000	0.0000	0.000	0.0368	265.0000	0.8660	0.8660
0	0.0000	0.0000	0.000	0.0368	270.0000	0.8660	0.8660
0	0.0000	0.0000	0.000	0.0368	275.0000	0.8660	0.8660
0	0.0000	0.0000	0.000	0.0368	280.0000	0.8660	0.8660
0	0.0000	0.0000	0.000	0.0368	285.0000	0.8660	0.8660
0	0.0000	0.0000	0.000	0.0368	290.0000	0.8660	0.8660
0	0.0000	0.0000	0.000	0.0368	295.0000	0.8660	0.8660
0	0.0000	0.0000	0.000	0.0368	300.0000	0.8660	0.8660
0	0.0000	0.0000	0.000	0.0368	305.0000	0.8660	0.8660
0	0.0000	0.0000	0.000	0.0368	310.0000	0.8660	0.8660
0	0.0000	0.0000	0.000	0.0368	315.0000	0.8660	0.8660
0	0.0000	0.0000	0.000	0.0368	320.0000	0.8660	0.8660
0	0.0000	0.0000	0.000	0.0368	325.0000	0.8660	0.8660
0	0.0000	0.0000	0.000	0.0368	330.0000	0.8660	0.8660
0	0.0000	0.0000	0.000	0.0368	335.0000	0.8660	0.8660
0	0.0000	0.0000	0.000	0.0368	340.0000	0.8660	0.8660
0	0.0000	0.0000	0.000	0.0368	345.0000	0.8660	0.8660
0	0.0000	0.0000	0.000	0.0368	350.0000	0.8660	0.8660
0	0.0000	0.0000	0.000	0.0368	355.0000	0.8660	0.8660
0	0.0000	0.0000	0.000	0.0368	360.0000	0.8660	0.8660

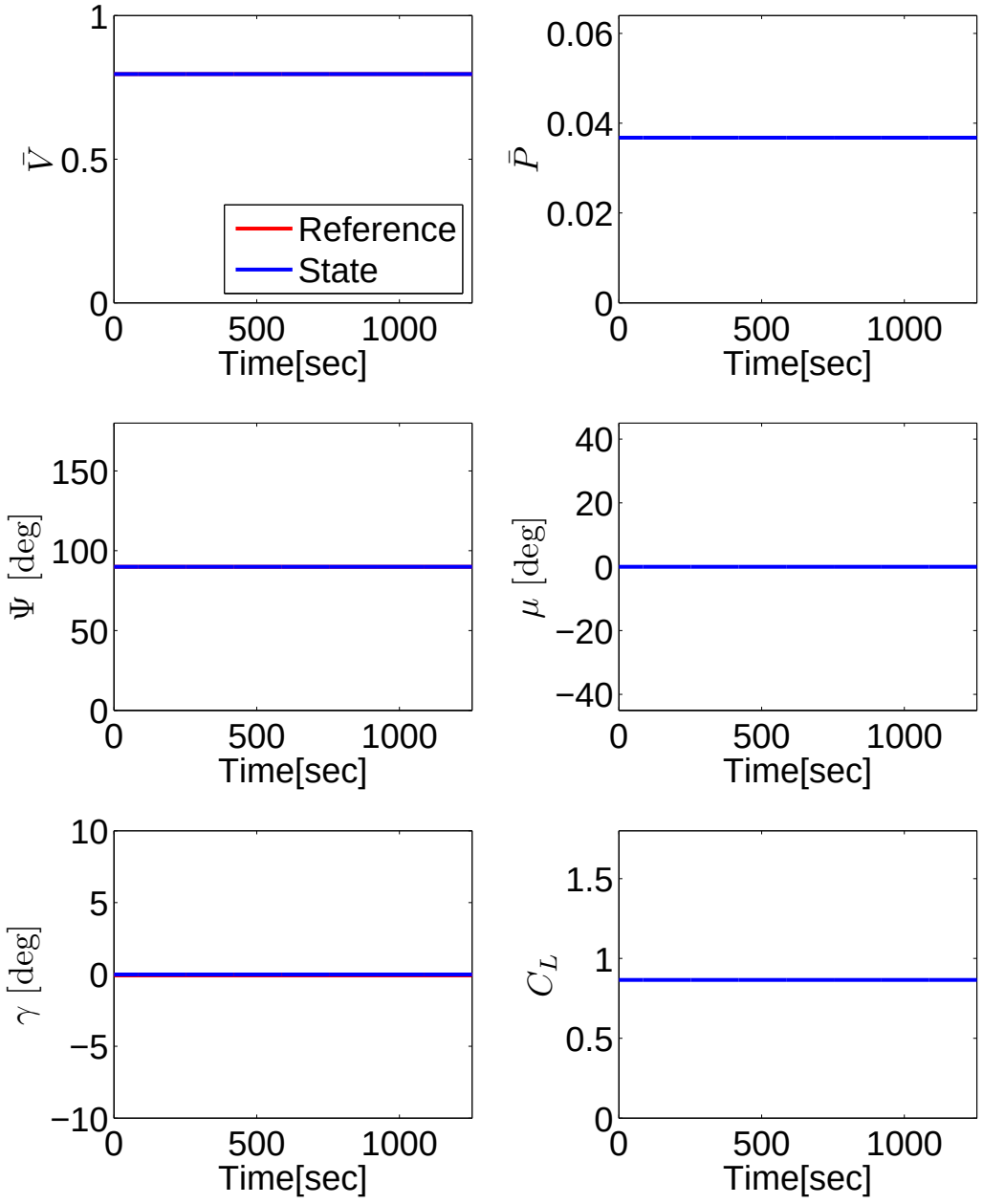

Figure 9.5: Scenario-0: Constant airspeed and heading angle flight results for $\Psi_0 = 90^o$.

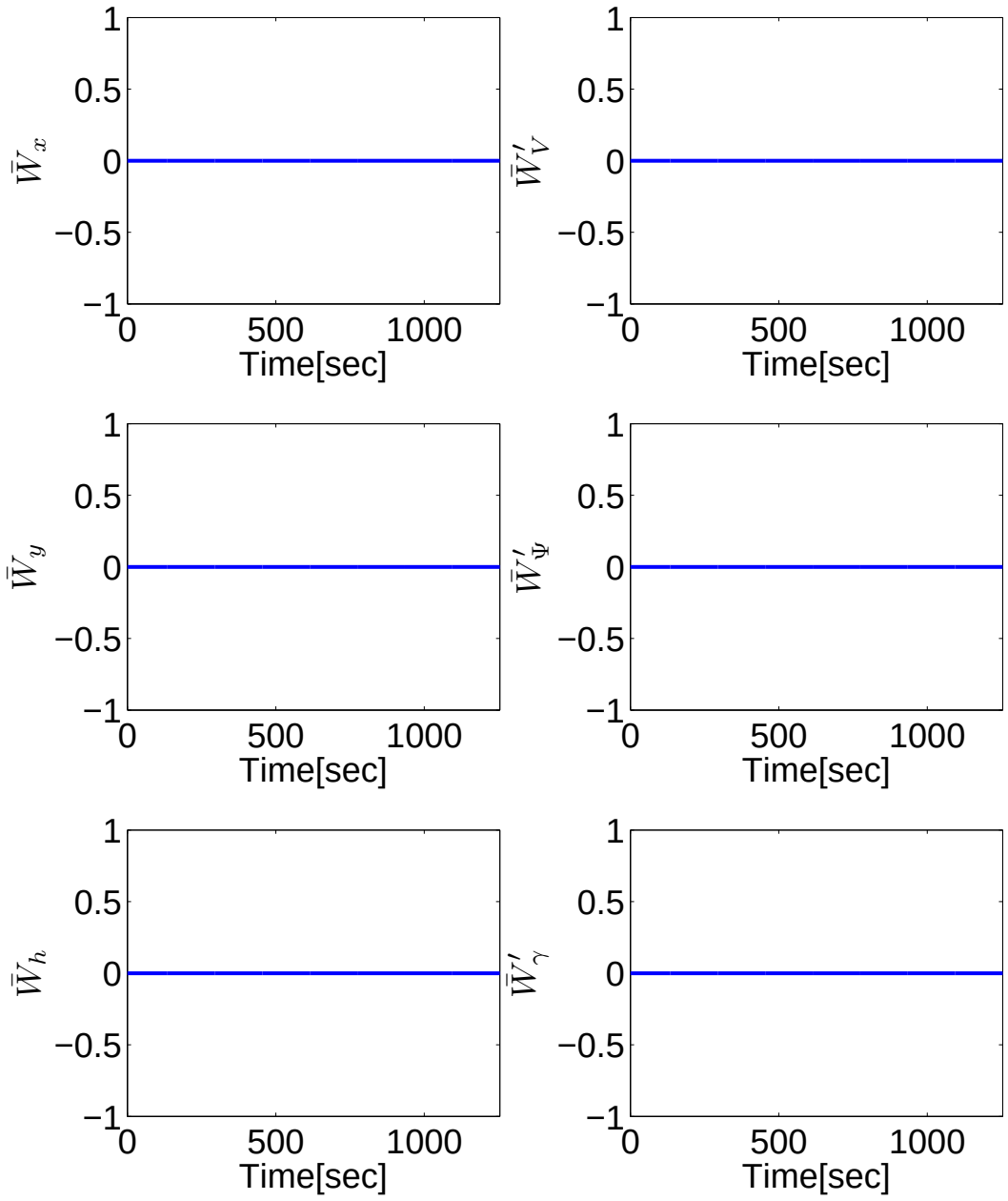

Figure 9.6: Scenario-0: Normalized wind speeds and accelerations.

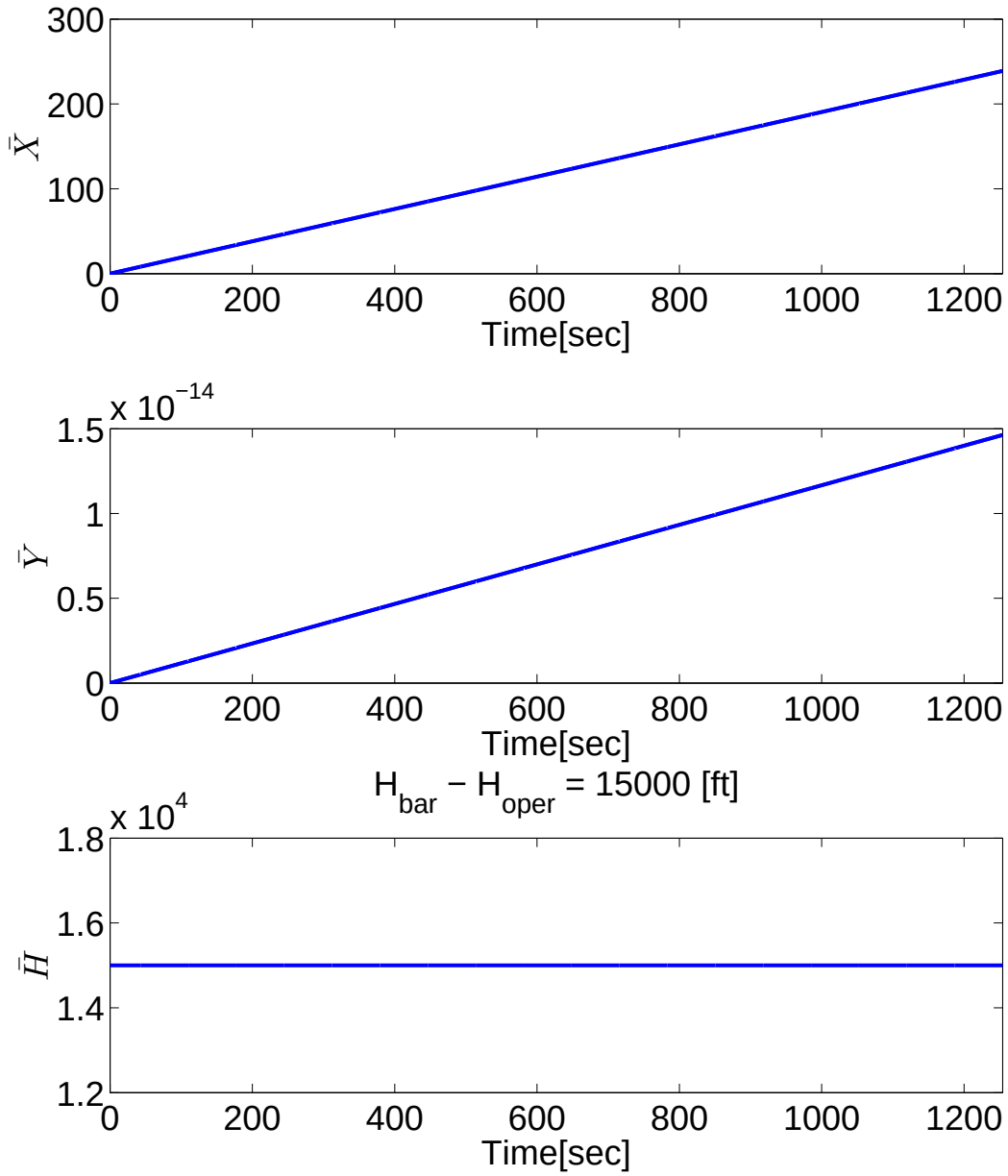

Figure 9.7: Scenario-0: Normalized positions.

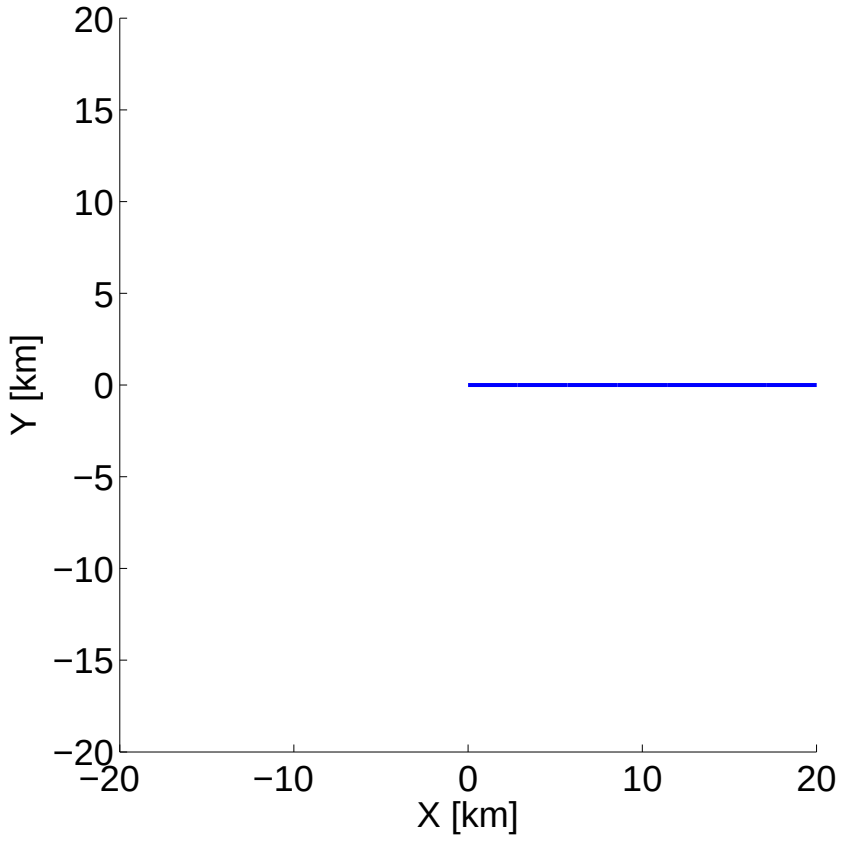

Figure 9.8: Scenario-0: Normalized flight path.

will be able to show that, when we are assigned with a mission of travelling from one point to another with fixed heading setting, by incorporating proposed power minimization strategies, and by varying airspeed with respect to local wind measurements, it is possible to introduce power savings and fly more efficiently, by increasing average flight time.

Therefore, in this scenario, the main goal will be to benefit from the local, instantaneous wind measurements to minimize our power consumption by *only adjusting our airspeed* and by tracking a reference airspeed value of ($\bar{V}^* = \bar{V}_0 + \Delta\bar{V}$). Thus, here, heading angle will be kept fixed at its initial setting.

Obtained simulation results are presented in Figs.(9.9-9.12) and corresponding numerical results are given in Table-9.4.

Further investigation of Table-9.4a shows that there is a clear trend of UAV minimizing its power when flying with *head-wind*, (i.e. flying in the opposite direction with the wind). In Table-9.4a we can also observe the effect that when initial heading setting gets close to the opposite of actual wind direction, the benefit we obtain maximizes. In other words, when the UAV is aligned with the *head-wind*, it is possible to maximize its lift through wind, minimize its power consumption and extract most benefit. On the other hand, results in Table-9.4b indicate that it is not possible to get the same effect when we fly with the *tail-wind* (i.e. flying in same direction with the wind).

In Fig-9.9, first figure shows the time history of the normalized airspeed. In this picture, red lines indicate reference command to be tracked and blue lines indicate the actual state history of the airspeed. It is possible to see from the airspeed plot that aircraft is able to track desired commands as expected and as a result, is able to maximize it is lift and able to minimize it power consumption. When control commands are further investigated, it is possible to see that bank angle-control command, (μ), is also actively working towards maintaining straight, level flight with desired heading angle. At first glimpse to the Fig-9.9, control efforts may seem very jittery and too intense, but this is due to the difference in scale of given simulations. The simulation time is 1200sec, while the update time is only 4sec, which in this case, each control state includes 300 control updates. When the control efforts are closely investigated, it is possible to see that the command tracking is smoothly executed.

It is also possible to see that, with this scenario, while we adjust airspeed and try

Table 9.4a: Scenario-1: Numerical results.

Scenario	$\bar{W}_m$	$\Psi_W[deg]$	$\omega_W[rad/ft]$	$\bar{P}_{avg}$	$\Psi_0[deg]$	$(C_L)_{max}$	$(C_L)_{min}$
1	0.2664	103.7914	0.050	0.0370	0.0000	1.2000	0.7908
1	0.2621	103.5347	0.050	0.0375	5.0000	1.2000	0.8358
1	0.2632	103.1844	0.050	0.0374	10.0000	1.2000	0.8343
1	0.2635	103.4688	0.050	0.0371	15.0000	1.2000	0.8241
1	0.2623	104.1140	0.050	0.0369	20.0000	1.2000	0.7876
1	0.2655	103.7317	0.050	0.0367	25.0000	1.2000	0.7826
1	0.2625	103.7389	0.050	0.0365	30.0000	1.2000	0.7672
1	0.2630	104.3226	0.050	0.0368	35.0000	1.2000	0.8646
1	0.2681	103.5741	0.050	0.0359	40.0000	1.2000	0.8695
1	0.2675	104.0844	0.050	0.0345	45.0000	1.2000	0.8690
1	0.2651	103.9083	0.050	0.0333	50.0000	1.2000	0.8666
1	0.2674	103.8922	0.050	0.0330	55.0000	1.2000	0.8274
1	0.2656	103.4750	0.050	0.0324	60.0000	1.2000	0.8679
1	0.2656	103.9638	0.050	0.0319	65.0000	1.2000	0.8675
1	0.2659	103.9538	0.050	0.0313	70.0000	1.2000	0.8672
1	0.2660	103.4803	0.050	0.0316	75.0000	1.2000	0.8668
1	0.2628	103.4258	0.050	0.0311	80.0000	1.2000	0.8529
1	0.2508	103.8261	0.050	0.0284	85.0000	1.2000	0.8663
1	0.2628	103.5466	0.050	0.0303	90.0000	1.2000	0.8208
1	0.2649	103.8885	0.050	0.0293	95.0000	1.2000	0.8533
1	0.2639	103.7432	0.050	0.0288	100.0000	1.2000	0.8263
1	0.2656	104.1163	0.050	0.0296	105.0000	1.2000	0.7940
1	0.2611	104.2402	0.050	0.0293	110.0000	1.2000	0.7940
1	0.2628	104.2502	0.050	0.0298	115.0000	1.2000	0.7942
1	0.2659	103.8849	0.050	0.0295	120.0000	1.2000	0.7961
1	0.2682	103.8093	0.050	0.0301	125.0000	1.2000	0.8051
1	0.2650	103.6727	0.050	0.0305	130.0000	1.2000	0.8572
1	0.2636	104.1124	0.050	0.0309	135.0000	1.2000	0.8661
1	0.2631	104.0384	0.050	0.0312	140.0000	1.2000	0.8660
1	0.2635	103.6999	0.050	0.0337	145.0000	1.2000	0.8660
1	0.2663	103.7011	0.050	0.0316	150.0000	1.2000	0.8660
1	0.2585	103.8607	0.050	0.0338	155.0000	1.2000	0.8660
1	0.2636	104.3998	0.050	0.0340	160.0000	1.2000	0.8661
1	0.2645	103.2442	0.050	0.0353	165.0000	1.2000	0.8661
1	0.2659	103.8258	0.050	0.0360	170.0000	1.2000	0.8661
1	0.2624	103.5342	0.050	0.0367	175.0000	1.2000	0.8661
1	0.2608	103.8032	0.050	0.0370	180.0000	1.2000	0.8660

Table 9.4b: Scenario-1: Numerical results (continued).

Scenario	$\bar{W}_m$	$\Psi_W[deg]$	$\omega_W[rad/ft]$	$\bar{P}_{avg}$	$\Psi_0[deg]$	$(C_L)_{max}$	$(C_L)_{min}$
1	0.2625	104.0601	0.050	0.0374	185.0000	1.2000	0.8660
1	0.2620	103.9337	0.050	0.0373	190.0000	1.2000	0.8082
1	0.2638	103.1240	0.050	0.0372	195.0000	1.2000	0.6985
1	0.2496	103.7207	0.050	0.0370	200.0000	1.2000	0.7677
1	0.2741	103.1897	0.050	0.0373	205.0000	1.2000	0.7631
1	0.2694	103.6089	0.050	0.0373	210.0000	1.2000	0.8184
1	0.2702	103.6052	0.050	0.0371	215.0000	1.2000	0.8451
1	0.2653	103.9671	0.050	0.0372	220.0000	1.2000	0.8205
1	0.2681	103.3695	0.050	0.0367	225.0000	1.2000	0.8015
1	0.2674	103.6040	0.050	0.0366	230.0000	1.2000	0.8674
1	0.2641	103.6644	0.050	0.0367	235.0000	1.2000	0.8387
1	0.2630	103.6290	0.050	0.0361	240.0000	1.2000	0.8199
1	0.2657	103.7466	0.050	0.0364	245.0000	1.2000	0.8126
1	0.2686	103.6782	0.050	0.0363	250.0000	1.2000	0.8665
1	0.2699	103.7006	0.050	0.0353	255.0000	1.2000	0.8663
1	0.2657	103.6119	0.050	0.0353	260.0000	1.2000	0.8662
1	0.2662	104.2083	0.050	0.0347	265.0000	1.2000	0.8661
1	0.2669	103.5151	0.050	0.0348	270.0000	1.2000	0.8661
1	0.2485	103.9996	0.050	0.0343	275.0000	1.2000	0.8478
1	0.2688	103.5697	0.050	0.0343	280.0000	1.2000	0.8660
1	0.2654	103.5963	0.050	0.0350	285.0000	1.2000	0.8660
1	0.2656	103.5815	0.050	0.0345	290.0000	1.2000	0.8593
1	0.2647	103.7219	0.050	0.0351	295.0000	1.2000	0.8660
1	0.2665	104.0994	0.050	0.0354	300.0000	1.2000	0.8660
1	0.2651	103.8834	0.050	0.0351	305.0000	1.2000	0.8660
1	0.2643	103.6135	0.050	0.0356	310.0000	1.2000	0.8660
1	0.2680	103.7382	0.050	0.0361	315.0000	1.2000	0.8660
1	0.2659	103.9467	0.050	0.0362	320.0000	1.2000	0.8661
1	0.2656	103.6693	0.050	0.0366	325.0000	1.2000	0.8661
1	0.2688	103.7638	0.050	0.0363	330.0000	1.2000	0.8661
1	0.2726	103.2074	0.050	0.0356	335.0000	1.2000	0.8264
1	0.2611	104.1114	0.050	0.0357	340.0000	1.2000	0.5979
1	0.2633	104.0043	0.050	0.0363	345.0000	1.2000	0.6827
1	0.2630	103.6010	0.050	0.0365	350.0000	1.2000	0.8243
1	0.2619	103.7724	0.050	0.0373	355.0000	1.2000	0.8650
1	0.2631	103.7189	0.050	0.0368	360.0000	1.2000	0.7889

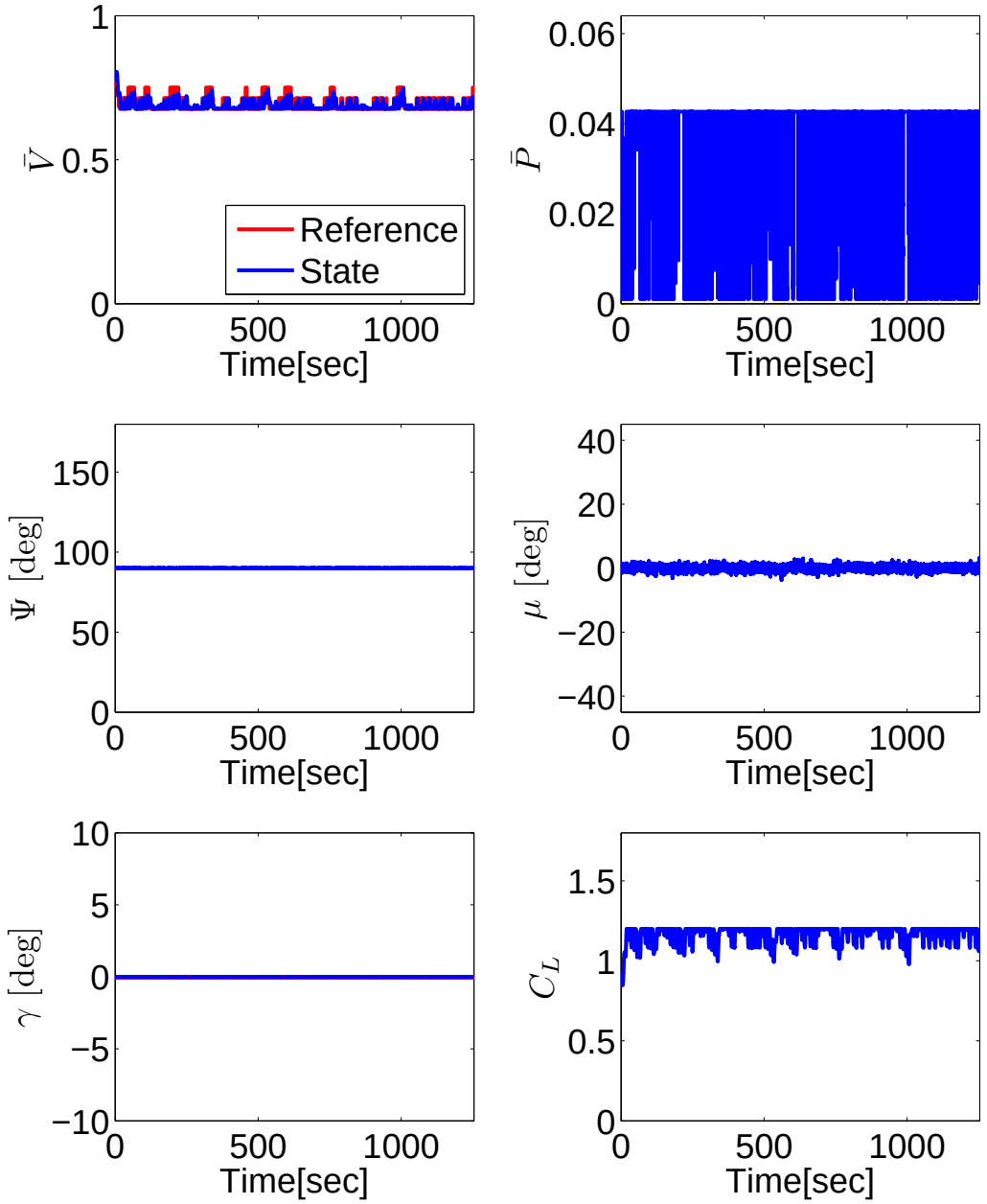

Figure 9.9: Scenario-1: Constant airspeed and heading angle flight results for $\Psi_0 = 90^o$.

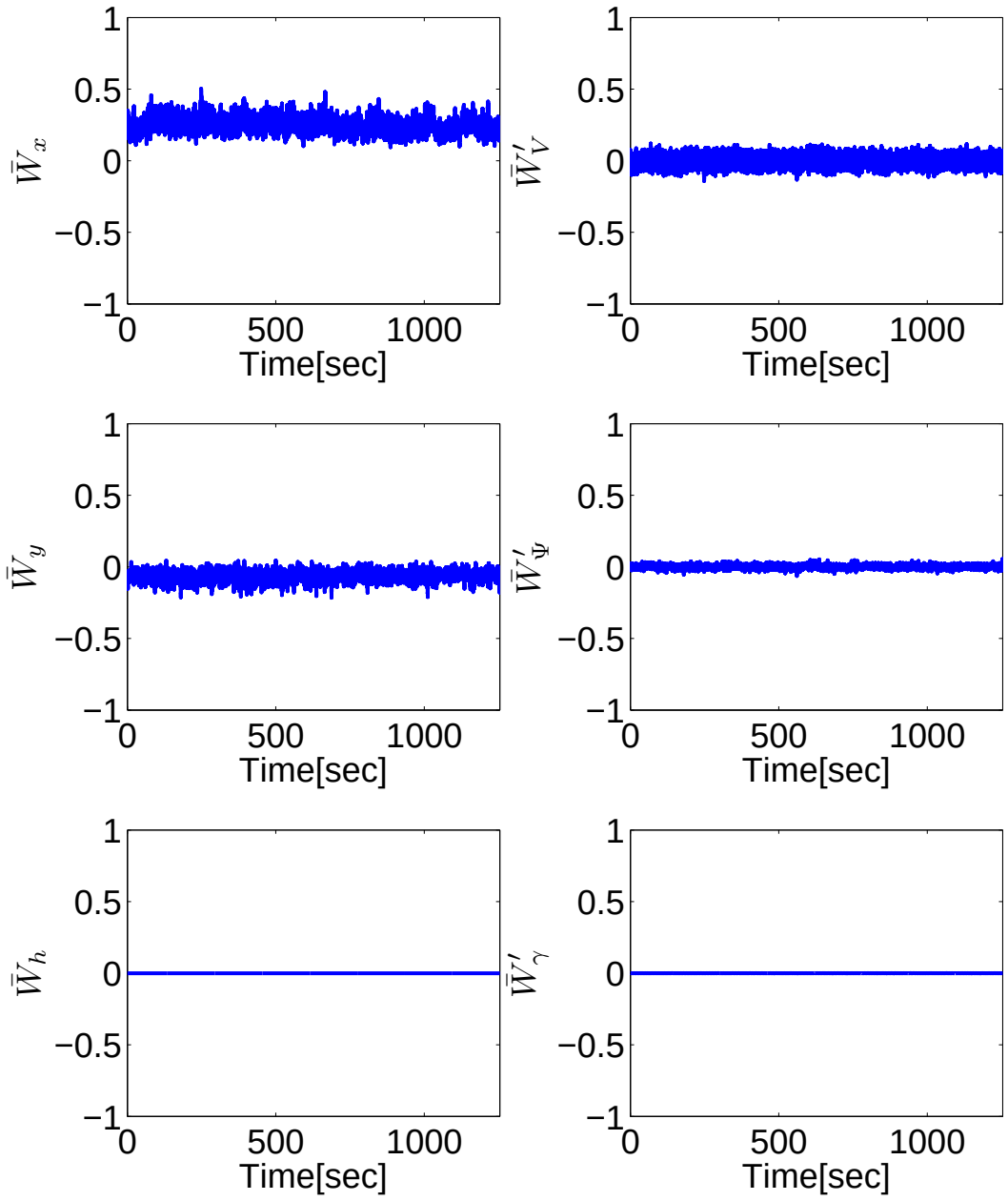

Figure 9.10: Scenario-1: Normalized wind speeds and accelerations.

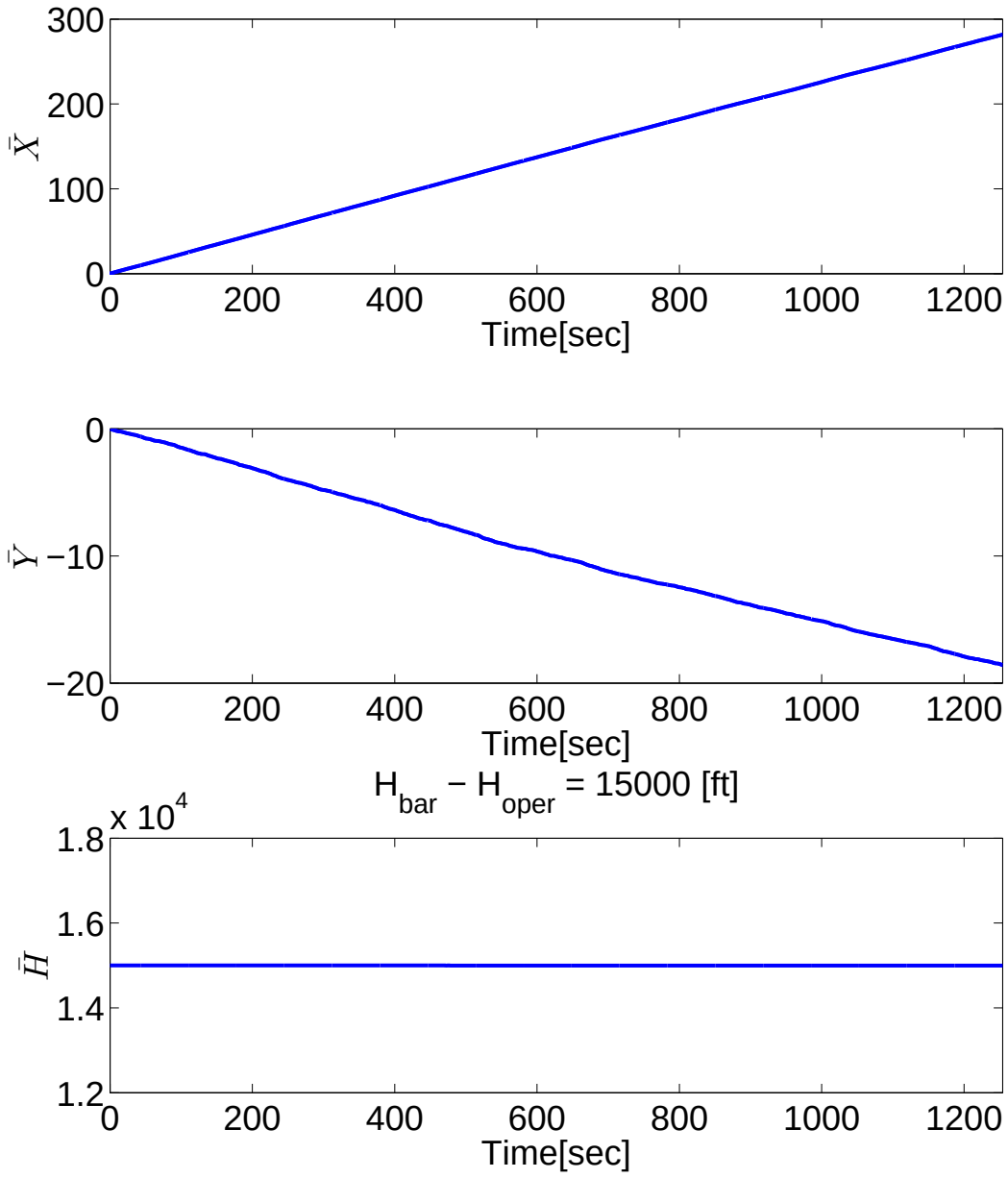

Figure 9.11: Scenario-1: Normalized positions.

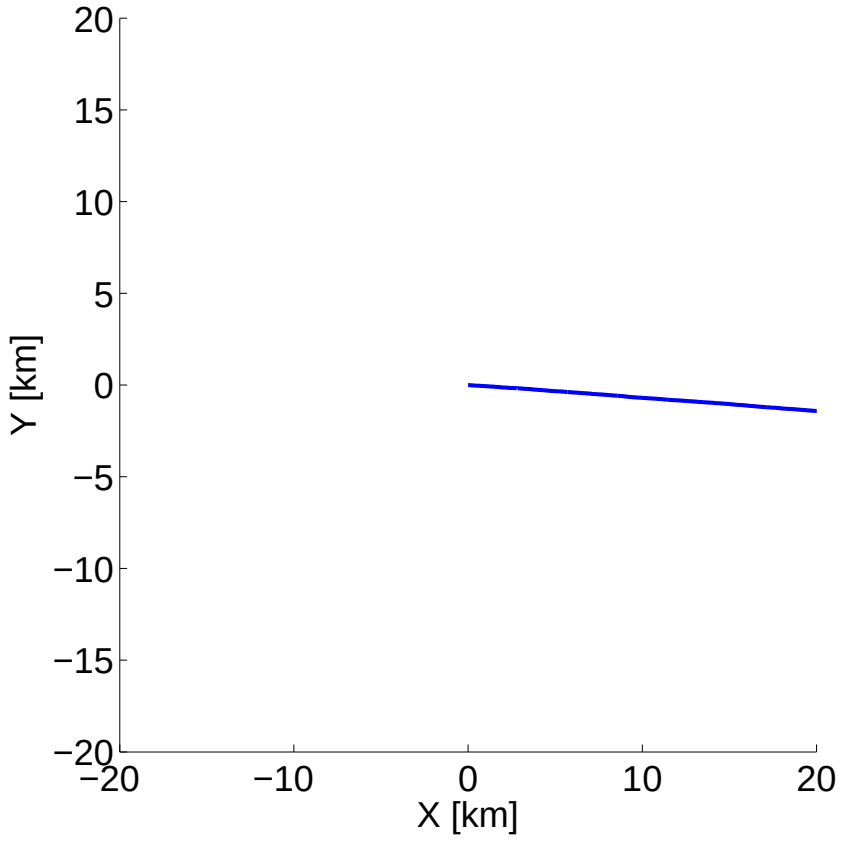

Figure 9.12: Scenario-1: Normalized flight path.

to minimize the power consumption, we also maximize lift (through control command C_L) and still able to maintain level flight with zero flight path angle (γ). In Fig-9.10 stochastic nature of the wind magnitudes and wind accelerations can be observed. In Fig-9.11 position of the UAV is given, while in Fig-9.12 flight path of the UAV can be observed.

Careful investigation of Fig-9.12 will lead to the fact, in existence of winds, even if aircraft is maintaining level flight with fixed heading angle, with time, UAV will be drifting towards the direction of the wind. This also shows the fact that, in presence of winds, only adjustments in airspeed is not desirable and optimal adjustments in heading angle is also necessary for correction of flying in the right direction (i.e. correct/desired heading angle with respect to true north). This effect will be investigated further in details the next two sections.

9.5.3 Scenario-2: Constant airspeed, optimal heading angle case in presence of wind

In previous section, it was witnessed that unless adjustments in airspeed are accompanied by heading angle, aircraft will always get drifted towards the wind direction. This is a crucial element in guidance strategies and should be address appropriately. Therefore in this and in the following sections, the effects of adjustments in heading angle commands will be investigated.

Before going any further and investigate the complete effects of combined adjustments in airspeed and heading angle, it is desired to first investigate the effects of adjustments only in heading angle, while maintaining a constant airspeed command. In this scenario, we will only apply periodic adjustments on heading angle and will keep airspeed constant at optimal airspeed obtained in presence of no winds, as given in Eq.(6.26).

Simulation results for this scenario are presented in Figs.(9.13-9.16) and corresponding numerical results are given in Table-9.5.

From Fig-9.13, one can clearly see the heading command change while UAV is trying to maintain fixed airspeed with minimal variations due to the wind and command effects. It is also possible to see from Fig-9.13 - C_L plot that adjustments only in heading angle is not able to bring much enhancement in terms of maximizing C_L, which is also reflected

Table 9.5a: Scenario-2: Numerical results.

Scenario	$\bar{W}_m$	$\Psi_W[deg]$	$\omega_W[rad/ft]$	$\bar{P}_{avg}$	$\Psi_0[deg]$	$(C_L)_{max}$	$(C_L)_{min}$
2	0.2532	103.7569	0.0500	0.0360	0	0.9417	0.8647
2	0.2523	103.7856	0.0500	0.0360	5.0000	0.9643	0.8647
2	0.2567	103.8085	0.0500	0.0361	10.0000	0.9514	0.8648
2	0.2493	103.7569	0.0500	0.0361	15.0000	0.9509	0.8647
2	0.2646	103.9632	0.0500	0.0361	20.0000	0.9667	0.8648
2	0.2530	103.9861	0.0500	0.0360	25.0000	0.9600	0.8648
2	0.2574	103.6251	0.0500	0.0363	30.0000	0.9381	0.8649
2	0.2552	103.8887	0.0500	0.0362	35.0000	0.9546	0.8650
2	0.2577	103.6251	0.0500	0.0368	40.0000	0.9582	0.8624
2	0.2664	103.4819	0.0500	0.0368	45.0000	0.9559	0.8567
2	0.2583	103.7168	0.0500	0.0362	50.0000	0.9864	0.8648
2	0.2584	104.2554	0.0500	0.0361	55.0000	0.9899	0.8651
2	0.2617	103.5850	0.0500	0.0369	60.0000	1.1016	0.8231
2	0.2583	103.5335	0.0500	0.0361	65.0000	1.1389	0.8267
2	0.2715	103.4475	0.0500	0.0369	70.0000	1.1111	0.8081
2	0.2683	103.7340	0.0500	0.0360	75.0000	1.0530	0.8433
2	0.2644	103.5965	0.0500	0.0361	80.0000	1.1254	0.8125
2	0.2657	104.0319	0.0500	0.0360	85.0000	1.0656	0.8425
2	0.2663	103.8085	0.0500	0.0361	90.0000	1.1113	0.8219
2	0.2598	103.3559	0.0500	0.0363	95.0000	1.0845	0.8304
2	0.2663	103.7455	0.0500	0.0367	100.0000	1.1136	0.8265
2	0.2681	103.3444	0.0500	0.0361	105.0000	1.1107	0.8247
2	0.2661	103.6996	0.0500	0.0368	110.0000	1.1218	0.8160
2	0.2635	103.7283	0.0500	0.0368	115.0000	1.0915	0.8357
2	0.2581	103.6882	0.0500	0.0365	120.0000	1.0994	0.8375
2	0.2629	103.7798	0.0500	0.0367	125.0000	1.0539	0.8238
2	0.2626	103.8543	0.0500	0.0368	130.0000	1.0974	0.8323
2	0.2619	103.8772	0.0500	0.0361	135.0000	1.0685	0.8412
2	0.2659	103.9517	0.0500	0.0361	140.0000	1.0511	0.8439
2	0.2669	104.3127	0.0500	0.0368	145.0000	1.0749	0.8565
2	0.2662	103.5449	0.0500	0.0360	150.0000	0.9719	0.8578
2	0.2682	103.3387	0.0500	0.0360	155.0000	1.0531	0.8512
2	0.2667	104.0950	0.0500	0.0362	160.0000	0.9941	0.8648
2	0.2594	103.3272	0.0500	0.0369	165.0000	0.9704	0.8589
2	0.2659	103.5621	0.0500	0.0363	170.0000	0.9939	0.8650
2	0.2685	103.8028	0.0500	0.0362	175.0000	0.9424	0.8581
2	0.2653	103.5507	0.0500	0.0360	180.0000	0.9627	0.8652

Table 9.5b: Scenario-2: Numerical results (continued).

Scenario	$\bar{W}_m$	$\Psi_W[deg]$	$\omega_W[rad/ft]$	$\bar{P}_{avg}$	$\Psi_0[deg]$	$(C_L)_{max}$	$(C_L)_{min}$
2	0.2644	103.6939	0.0500	0.0365	185.0000	0.9549	0.8562
2	0.2639	104.2611	0.0500	0.0360	190.0000	0.9578	0.8648
2	0.2694	103.2298	0.0500	0.0369	195.0000	0.9783	0.8648
2	0.2668	103.3387	0.0500	0.0361	200.0000	0.9872	0.8647
2	0.2712	104.2382	0.0500	0.0360	205.0000	0.9875	0.8649
2	0.2662	103.7397	0.0500	0.0369	210.0000	0.9839	0.8475
2	0.2704	103.8772	0.0500	0.0371	215.0000	0.9783	0.8651
2	0.2642	104.0319	0.0500	0.0371	220.0000	0.9742	0.8650
2	0.2681	103.7168	0.0500	0.0370	225.0000	0.9848	0.8652
2	0.2685	103.9976	0.0500	0.0370	230.0000	0.9655	0.8653
2	0.2694	103.8142	0.0500	0.0371	235.0000	1.0467	0.8653
2	0.2702	103.9116	0.0500	0.0367	240.0000	0.9963	0.8574
2	0.2655	104.0434	0.0500	0.0368	245.0000	1.0071	0.8651
2	0.2683	103.8371	0.0500	0.0372	250.0000	1.0076	0.8651
2	0.2666	103.6251	0.0500	0.0369	255.0000	0.9957	0.8648
2	0.2688	103.8543	0.0500	0.0372	260.0000	1.0269	0.8652
2	0.2673	103.7741	0.0500	0.0369	265.0000	1.0780	0.8625
2	0.2679	103.5507	0.0500	0.0369	270.0000	1.0536	0.8653
2	0.2683	104.1351	0.0500	0.0362	275.0000	1.0492	0.8628
2	0.2658	103.5277	0.0500	0.0360	280.0000	1.0369	0.8651
2	0.2645	104.4731	0.0500	0.0369	285.0000	1.0531	0.8601
2	0.2534	103.9059	0.0500	0.0363	290.0000	1.0466	0.8654
2	0.2585	103.8658	0.0500	0.0369	295.0000	1.0586	0.8647
2	0.2551	103.2814	0.0500	0.0360	300.0000	1.0492	0.8626
2	0.2555	103.2699	0.0500	0.0363	305.0000	1.0509	0.8653
2	0.2516	103.7856	0.0500	0.0361	310.0000	1.0560	0.8655
2	0.2513	104.0950	0.0500	0.0361	315.0000	1.0379	0.8654
2	0.2623	103.2814	0.0500	0.0360	320.0000	1.0011	0.8646
2	0.2534	103.6080	0.0500	0.0361	325.0000	0.9542	0.8653
2	0.2496	104.4960	0.0500	0.0360	330.0000	0.9586	0.8651
2	0.2527	103.9174	0.0500	0.0360	335.0000	0.9569	0.8648
2	0.2489	103.4418	0.0500	0.0362	340.0000	0.9592	0.8654
2	0.2561	104.1523	0.0500	0.0361	345.0000	0.9625	0.8652
2	0.2573	103.7512	0.0500	0.0364	350.0000	0.9575	0.8624
2	0.2473	104.1752	0.0500	0.0360	355.0000	0.9708	0.8649
2	0.2554	104.2382	0.0500	0.0370	360.0000	0.9534	0.8648

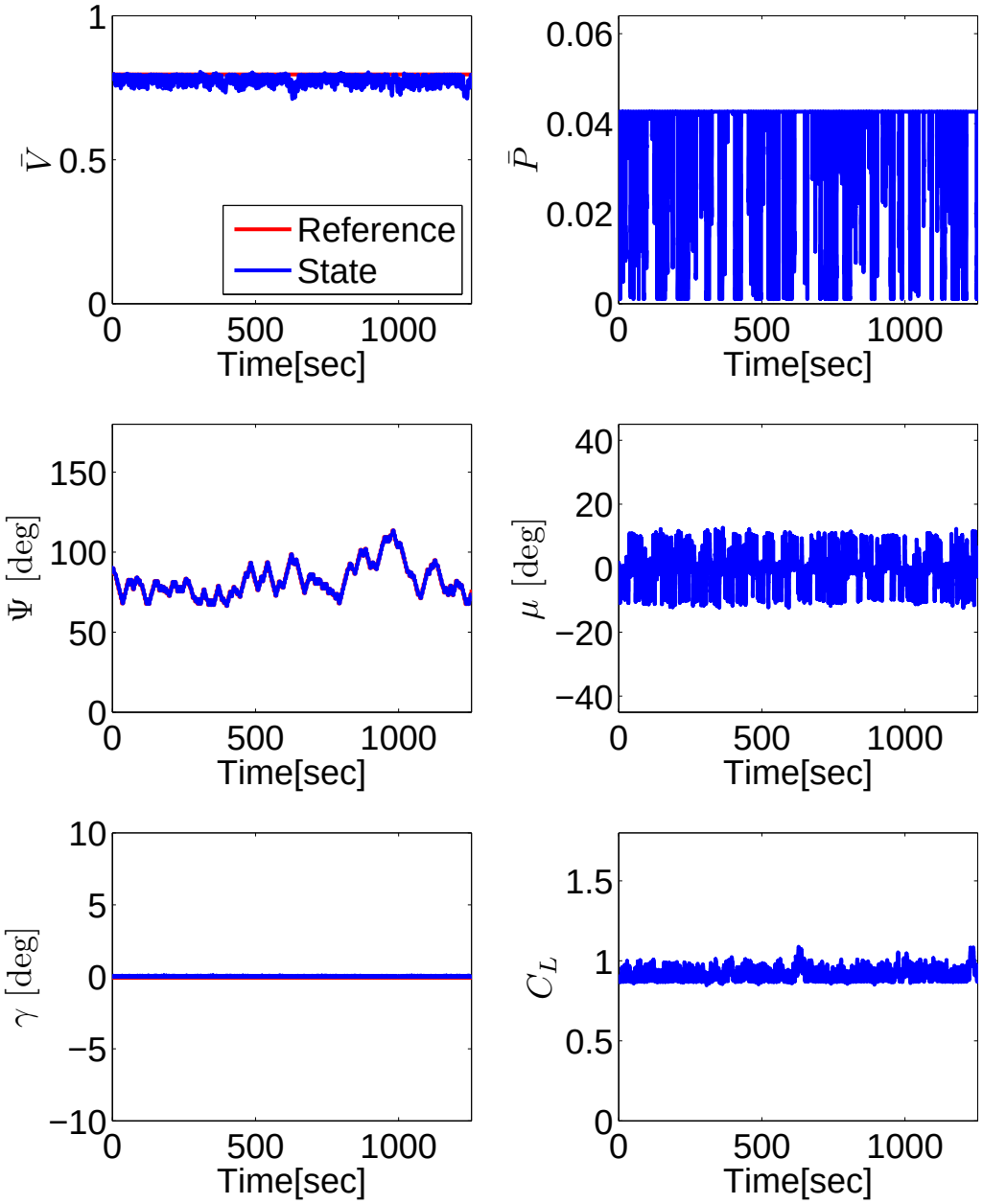

Figure 9.13: Scenario-2: Constant airspeed and heading angle flight results for $\Psi_0 = 90^o$.

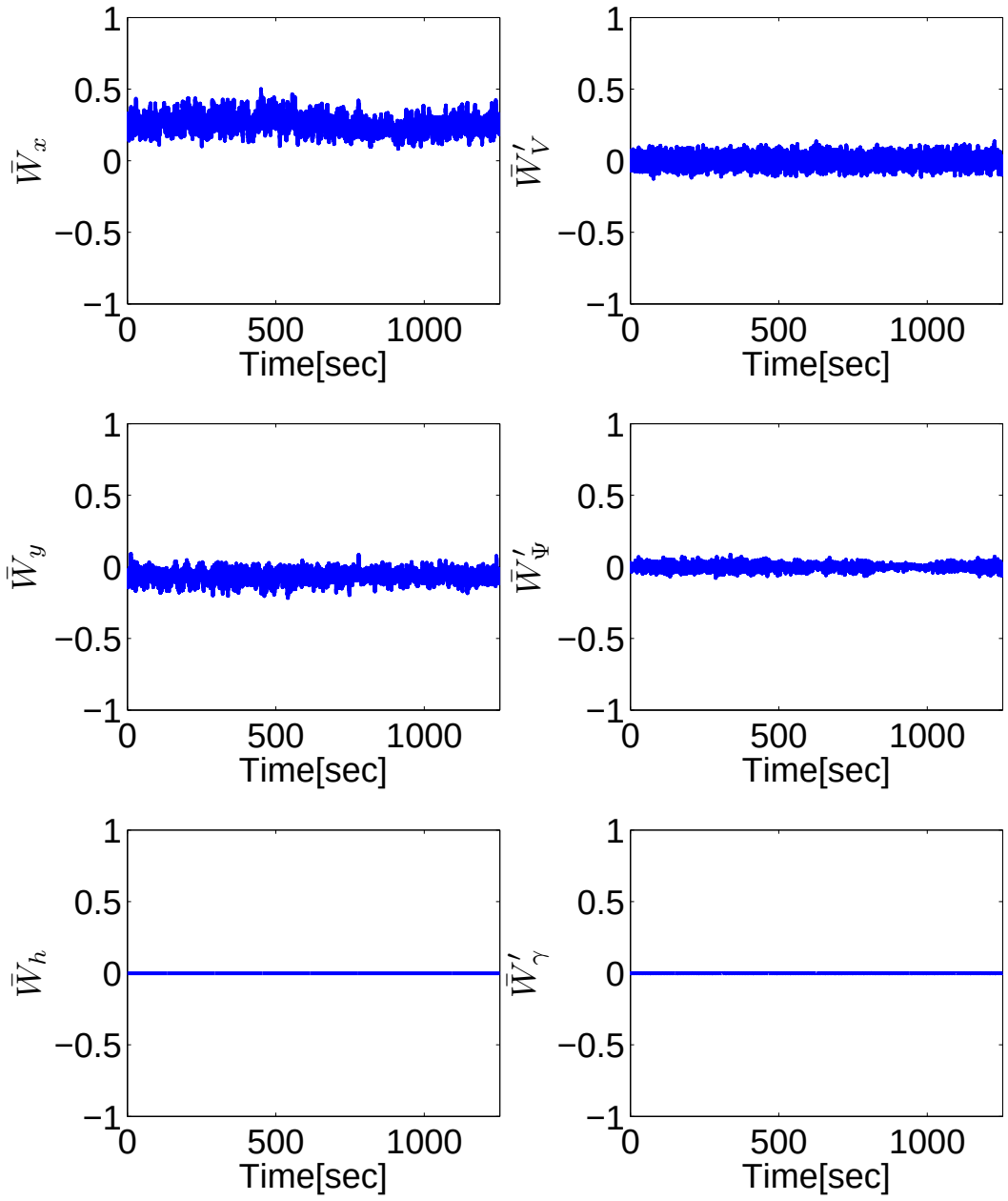

Figure 9.14: Scenario-2: Normalized wind speeds and accelerations.

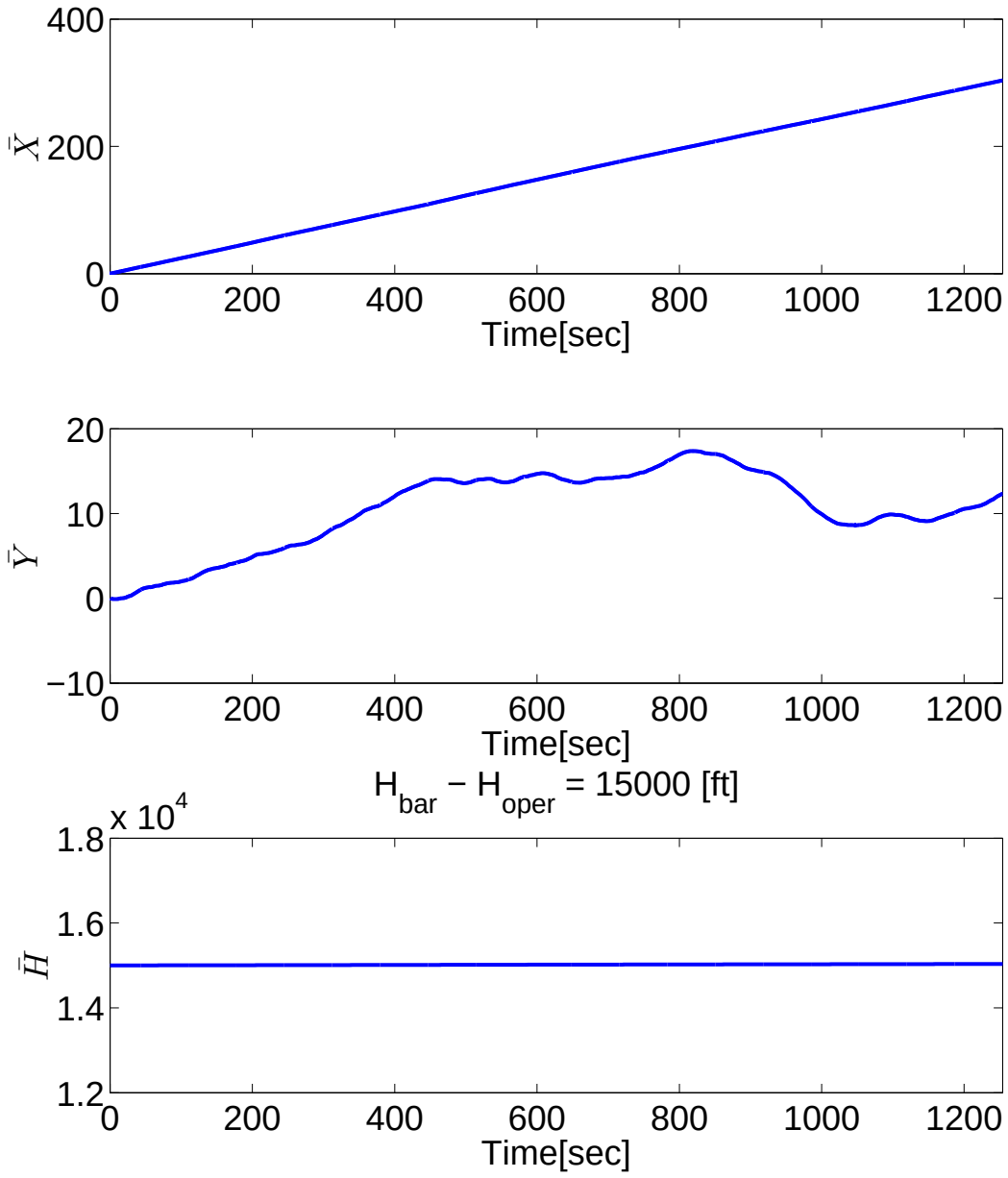

Figure 9.15: Scenario-2: Normalized positions.

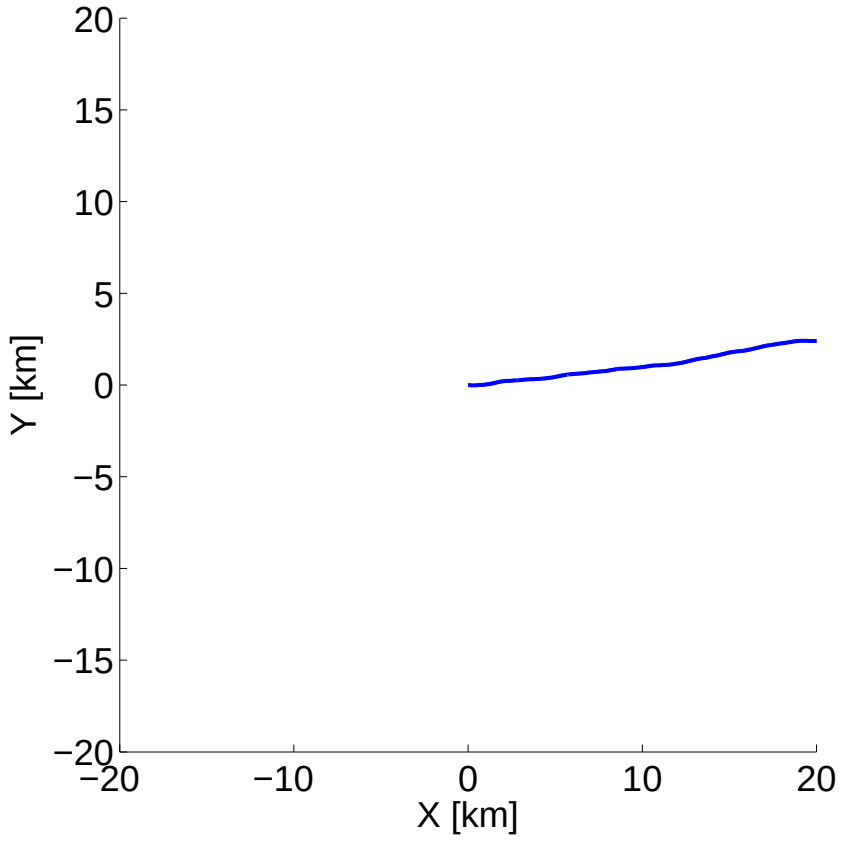

Figure 9.16: Scenario-2: Normalized flight path.

in the numerical results of $\bar{P}$ shown in Table-9.5. Table-9.5, simply tells that with only heading adjustments, it is not possible to provide any significant power minimization benefit, and airspeed adjustment will be necessary together with the heading angle adjustment.

Provided results clearly indicate that optimal adjustment only in heading angle provides very little benefit and needs to be combined with the optimal adjustments in airspeed. In this way, it will be possible not only to benefit from the wind magnitude, but also from the wind direction wherever and whenever it is possible. Combination of adjustments in heading angle and airspeed will help to reveal the real strength and effectiveness of the proposed guidance strategies. Next section will be discussing such combination and its effects on the flight path and state variables.

9.5.4 Scenario-3: Optimal airspeed, optimal heading angle in presence of wind

In previous sections, the affects of adjustment only in either heading angle or airspeed was demonstrated. It is straight forward from obtained results that combined affects of both (airspeed and heading) adjustments will help to harvest the maximum amount of benefit from the proposed guidance strategy and local wind conditions. This is also due to the fact that, in this way, it is not only possible to benefit from the power of the local wind magnitude (with adjustments on airspeed), but also will be possible to follow the wind pattern through adjustments in heading angle, stay with the wind as much as possible and extract maximum amount of benefit from the local wind patterns.

For this purpose, extensive simulations have been conducted, and obtained results are given in Figs.(9.17-9.20), whereas corresponding numerical results are given in Table-9.6.

Figs.(9.17-9.20) demonstrate the combined effect of applied adjustments in airspeed and heading angle. If Fig-9.17 is investigated further, one can spot the fact that we are not only able to maintain level flight through all these adjustments but also able to maximize (C_L) and minimize power consumption.

Fig-9.20 demonstrates flight path of the UAV. It is possible to notice from the flight trajectory that for different wind and atmospheric conditions flight path will also change. Eventually, while we seek to benefit from the wind currents and aim to entract energy

Table 9.6a: Scenario-3: Numerical results.

Scenario	$\bar{W}_m$	$\Psi_W[deg]$	$\omega_W[rad/ft]$	$\bar{P}_{avg}$	$\Psi_0[deg]$	$(C_L)_{max}$	$(C_L)_{min}$
3	0.2452	103.9517	0.0500	0.0352	0	1.2000	0.8239
3	0.2521	104.2783	0.0500	0.0353	5.0000	1.2000	0.7195
3	0.2647	103.4246	0.0500	0.0355	10.0000	1.2000	0.8068
3	0.2608	103.6194	0.0500	0.0348	15.0000	1.2000	0.8058
3	0.2510	103.7684	0.0500	0.0355	20.0000	1.2000	0.6275
3	0.2627	103.5793	0.0500	0.0346	25.0000	1.2000	0.7459
3	0.2515	104.0778	0.0500	0.0353	30.0000	1.2000	0.7562
3	0.2497	104.2611	0.0500	0.0348	35.0000	1.2000	0.6868
3	0.2615	103.7627	0.0500	0.0350	40.0000	1.2000	0.8150
3	0.2626	103.3043	0.0500	0.0345	45.0000	1.2000	0.7613
3	0.2597	103.4704	0.0500	0.0355	50.0000	1.2000	0.6237
3	0.2561	103.4590	0.0500	0.0345	55.0000	1.2000	0.7283
3	0.2653	103.3673	0.0500	0.0305	60.0000	1.2000	0.8680
3	0.2604	103.7798	0.0500	0.0298	65.0000	1.2000	0.8676
3	0.2729	104.0090	0.0500	0.0294	70.0000	1.2000	0.8594
3	0.2727	103.7970	0.0500	0.0295	75.0000	1.2000	0.8090
3	0.2762	104.1293	0.0500	0.0297	80.0000	1.2000	0.8665
3	0.2681	103.2527	0.0500	0.0294	85.0000	1.2000	0.8566
3	0.2711	103.6423	0.0500	0.0297	90.0000	1.2000	0.8535
3	0.2657	103.2126	0.0500	0.0299	95.0000	1.2000	0.8391
3	0.2691	103.7512	0.0500	0.0287	100.0000	1.2000	0.7937
3	0.2619	103.9689	0.0500	0.0284	105.0000	1.2000	0.8185
3	0.2666	103.4876	0.0500	0.0282	110.0000	1.2000	0.8058
3	0.2653	103.4246	0.0500	0.0294	115.0000	1.2000	0.7924
3	0.2643	103.7569	0.0500	0.0290	120.0000	1.2000	0.8402
3	0.2598	103.6710	0.0500	0.0288	125.0000	1.2000	0.8660
3	0.2622	103.7684	0.0500	0.0291	130.0000	1.2000	0.8661
3	0.2676	103.9976	0.0500	0.0292	135.0000	1.2000	0.8660
3	0.2622	103.8085	0.0500	0.0302	140.0000	1.2000	0.8660
3	0.2638	103.9403	0.0500	0.0304	145.0000	1.2000	0.8660
3	0.2592	104.0377	0.0500	0.0306	150.0000	1.2000	0.8660
3	0.2580	103.5392	0.0500	0.0304	155.0000	1.2000	0.8660
3	0.2630	103.5850	0.0500	0.0313	160.0000	1.2000	0.8661
3	0.2654	103.7512	0.0500	0.0321	165.0000	1.2000	0.8661
3	0.2604	103.3215	0.0500	0.0342	170.0000	1.2000	0.8661
3	0.2635	103.5621	0.0500	0.0333	175.0000	1.2000	0.8660
3	0.2613	103.6939	0.0500	0.0358	180.0000	1.2000	0.7601

Table 9.6b: Scenario-3: Numerical results (continued).

Scenario	$\bar{W}_m$	$\Psi_W[deg]$	$\omega_W[rad/ft]$	$\bar{P}_{avg}$	$\Psi_0[deg]$	$(C_L)_{max}$	$(C_L)_{min}$
3	0.2695	103.4418	0.0500	0.0359	185.0000	1.2000	0.8353
3	0.2645	103.8658	0.0500	0.0363	190.0000	1.2000	0.8168
3	0.2606	104.1236	0.0500	0.0358	195.0000	1.2000	0.8109
3	0.2654	103.8257	0.0500	0.0363	200.0000	1.2000	0.7496
3	0.2679	103.7913	0.0500	0.0361	205.0000	1.2000	0.8131
3	0.2659	103.6366	0.0500	0.0355	210.0000	1.2000	0.8112
3	0.2682	103.9976	0.0500	0.0362	215.0000	1.2000	0.8397
3	0.2593	104.2669	0.0500	0.0360	220.0000	1.2000	0.8238
3	0.2684	104.2497	0.0500	0.0352	225.0000	1.2000	0.7735
3	0.2646	103.8486	0.0500	0.0359	230.0000	1.2000	0.8448
3	0.2657	103.5392	0.0500	0.0357	235.0000	1.2000	0.8671
3	0.2684	103.8028	0.0500	0.0357	240.0000	1.2000	0.8134
3	0.2580	103.4533	0.0500	0.0357	245.0000	1.2000	0.7955
3	0.2652	103.6022	0.0500	0.0356	250.0000	1.2000	0.8665
3	0.2688	103.9002	0.0500	0.0352	255.0000	1.2000	0.8663
3	0.2655	103.3616	0.0500	0.0364	260.0000	1.2000	0.7831
3	0.2655	103.8887	0.0500	0.0360	265.0000	1.2000	0.8661
3	0.2661	103.4762	0.0500	0.0366	270.0000	1.2000	0.8520
3	0.2656	103.2012	0.0500	0.0357	275.0000	1.2000	0.8639
3	0.2696	103.3845	0.0500	0.0367	280.0000	1.2000	0.8464
3	0.2665	104.1580	0.0500	0.0348	285.0000	1.2000	0.8660
3	0.2607	103.6251	0.0500	0.0360	290.0000	1.2000	0.8319
3	0.2632	103.8944	0.0500	0.0361	295.0000	1.2000	0.8356
3	0.2660	103.7283	0.0500	0.0354	300.0000	1.2000	0.8660
3	0.2608	103.7455	0.0500	0.0361	305.0000	1.2000	0.8521
3	0.2515	104.1007	0.0500	0.0351	310.0000	1.2000	0.7368
3	0.2472	103.7798	0.0500	0.0356	315.0000	1.2000	0.8660
3	0.2511	104.1122	0.0500	0.0359	320.0000	1.2000	0.8567
3	0.2437	103.8887	0.0500	0.0354	325.0000	1.2000	0.8657
3	0.2492	103.8314	0.0500	0.0350	330.0000	1.2000	0.7577
3	0.2585	103.3960	0.0500	0.0352	335.0000	1.2000	0.8661
3	0.2425	104.1924	0.0500	0.0358	340.0000	1.2000	0.8135
3	0.2502	103.2814	0.0500	0.0357	345.0000	1.2000	0.6256
3	0.2526	103.5163	0.0500	0.0360	350.0000	1.2000	0.7064
3	0.2541	103.6080	0.0500	0.0355	355.0000	1.2000	0.8502
3	0.2475	104.0033	0.0500	0.0359	360.0000	1.2000	0.6119

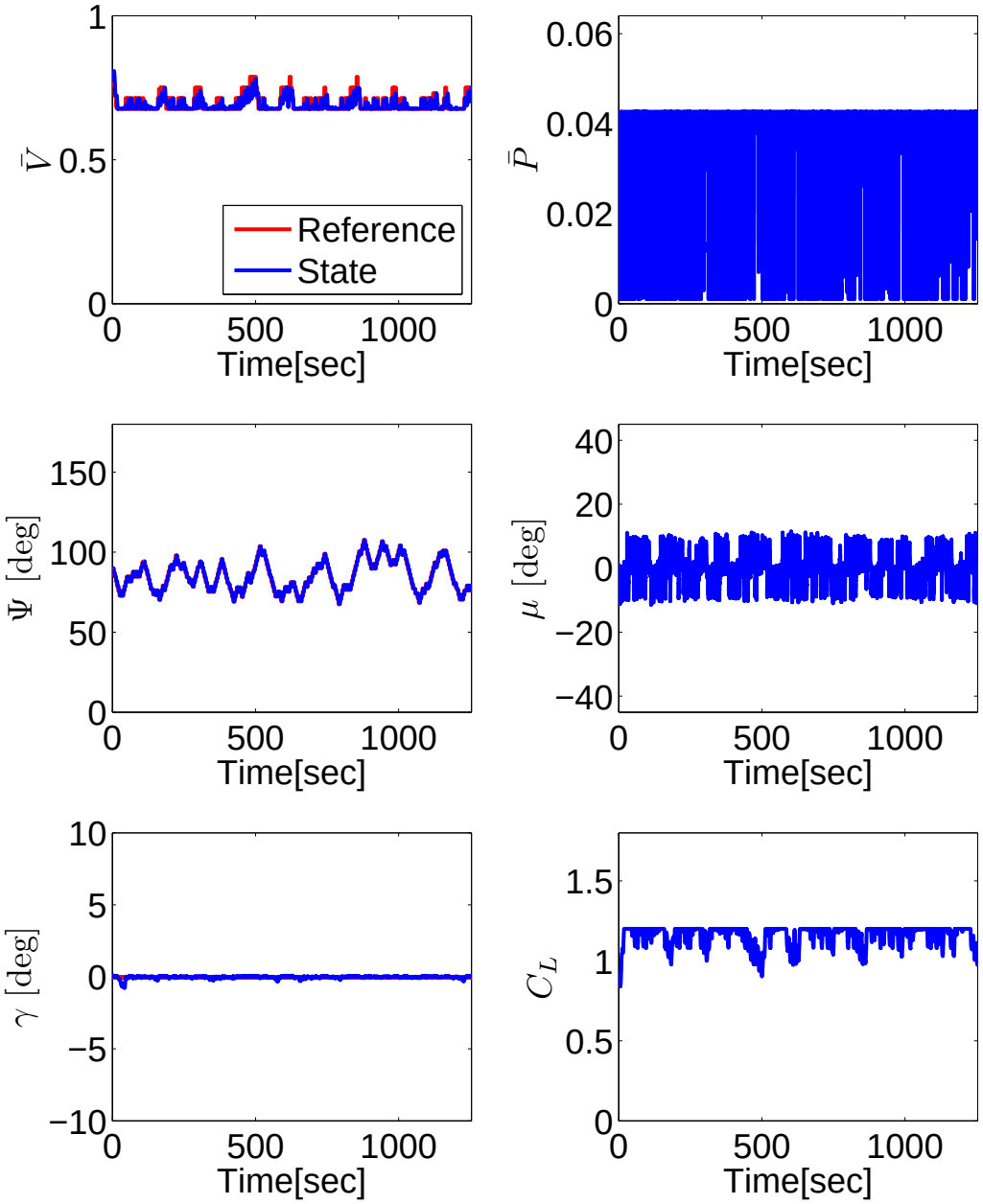

Figure 9.17: Scenario-3: Constant airspeed and heading angle flight results for $\Psi_0 = 90^o$.

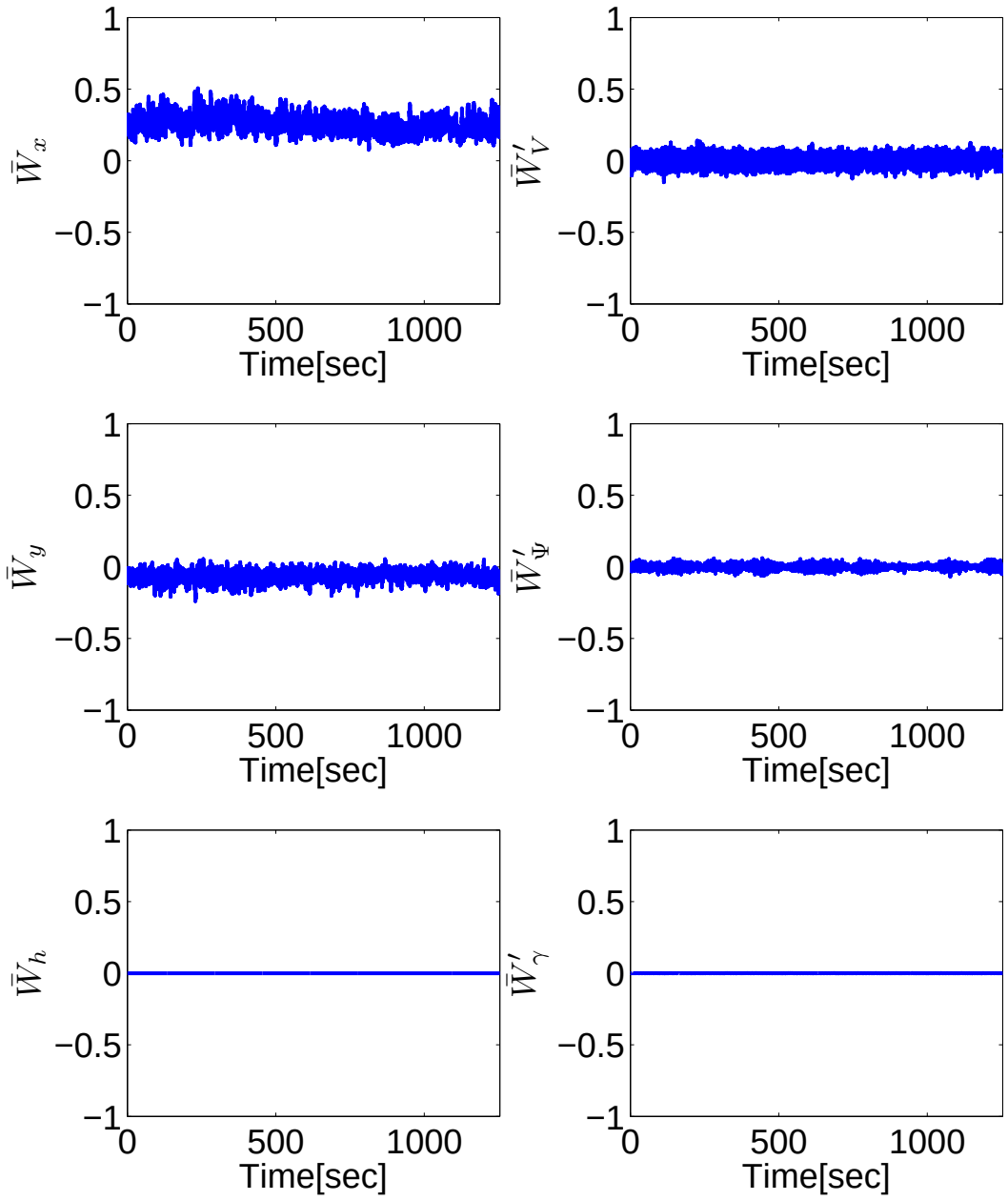

Figure 9.18: Scenario-3: Normalized wind speeds and accelerations.

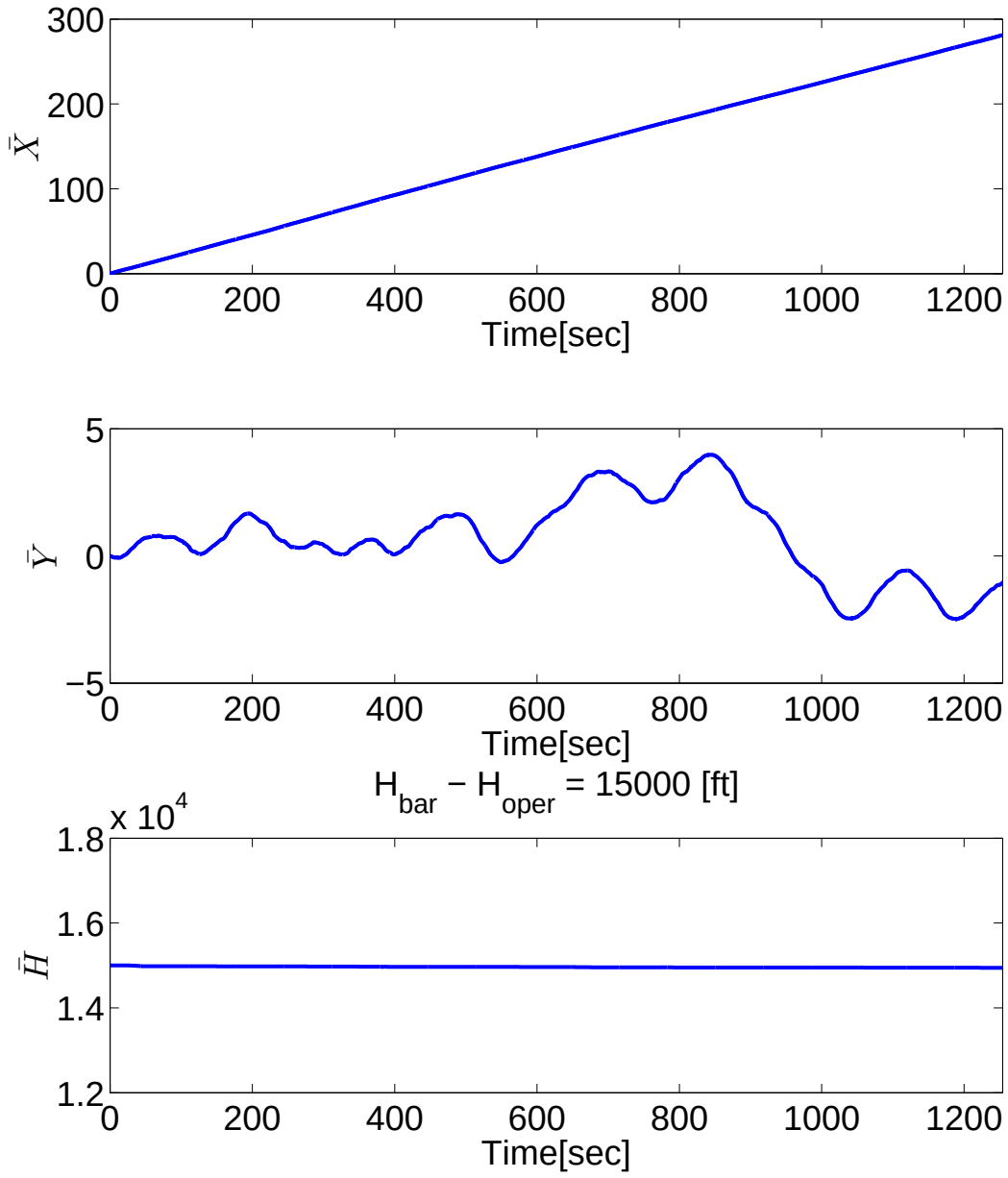

Figure 9.19: Scenario-3: Normalized positions.

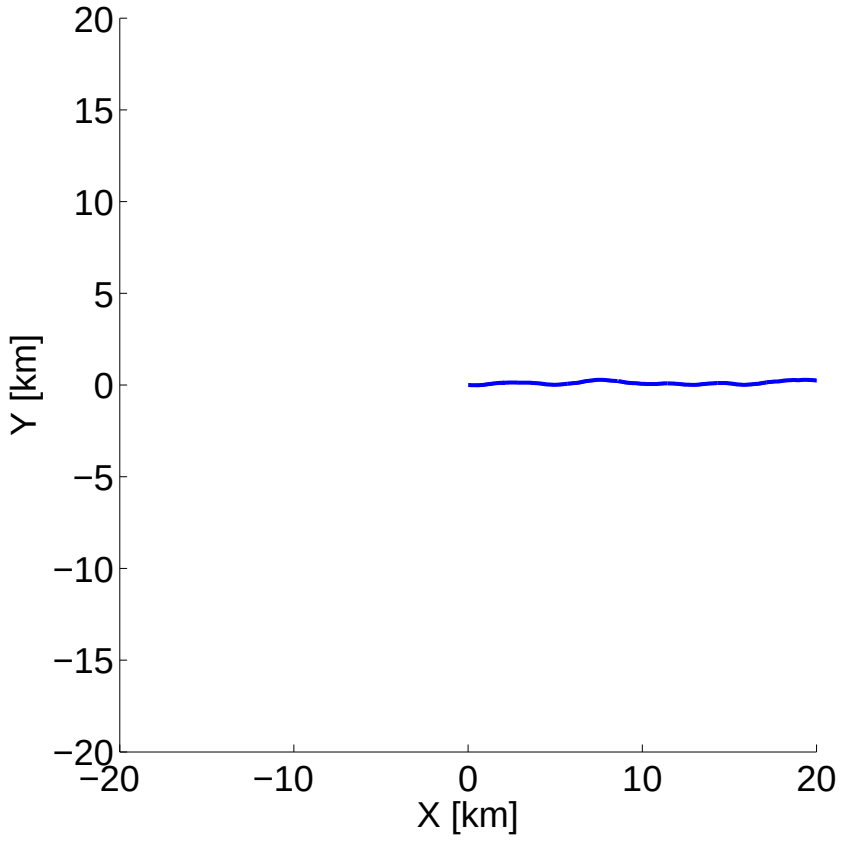

Figure 9.20: Scenario-3: Normalized flight path.

from the wind, this may potentially bring the UAV to a completely undesired location which is not related to the assigned flight mission. Therefore, it is essential to impose boundary control and restrict the flight region to complete the guidance strategies.

With the restricted flight region concept, it will be possible to stay within the restricted zone and execute the mission, but at the same time allows to benefit from the wind currents during the flight and minimize the corresponding power consumption. This concept has been introduced and has been discussed in further details in the next section. Due to the reason that UAVs often need to stay within a certain geometric boundary due to mission as well as operational requirements, effects of these flight constraints will be considered in the following section, as well.

9.5.5 Scenario-4: Optimal airspeed, optimal heading angle with a restricted circular flight zone in presence of wind

In all previously mentioned scenarios, UAV flights were not restricted in terms of the flight region and it was assumed that UAV could operate freely. This is not true in reality and when UAV is assigned a mission (data gathering, surveillance, investigation, ... etc.), it is restricted with a flight region and is expected to stay within this region until it executes the mission objectives. In that sense, it is essential to introduce and impose boundary constraints in terms of the flight zone.

Reference Trajectory

At this point, to assist a meaningful evaluation of any candidate strategies, a nominal reference trajectory is implemented where the UAV would fly in horizontal circles within the specified region at a fixed altitude $h_t \in [\bar{H}_{\min}, \bar{H}_{\max}]$, a radius of $\bar{r}_0 < \bar{R}$, and at a constant speed $\bar{V}_t$ that maximizes the endurance in steady-state flights with zero winds. This circular trajectory requires the UAV to fly at a constant bank angle when the wind is indeed zero. The period of the reference trajectory is given by

$$\bar{t}_r = \frac{2\pi \bar{r}_0}{\bar{V}_t} \tag{9.6}$$

Using this, we obtain

$$
\begin{aligned}
C_L &= \frac{1}{\bar{\rho}\bar{V}_t^2 \cos\mu_t} \\
\frac{\bar{P}}{\bar{V}} &= \bar{\rho}\bar{V}_t^2 C_{D_0} + \frac{1}{4\bar{\rho}C_{D_0}\bar{V}_t^2 E_{\max}^2 \cos^2\mu_t} \\
\Psi' &= \bar{\rho}\bar{V}_t C_L \sin\mu = \frac{1}{\bar{V}_t}\tan\mu_t \\
\bar{x}' &= \bar{V}_t \sin\Psi \\
\bar{y}' &= \bar{V}_t \cos\Psi
\end{aligned}
\tag{9.7}
$$

and the optimal constant reference speed can be determined from

$$
\min_{\bar{V}_t} \quad \bar{P} = \bar{\rho}\bar{V}_t^3 C_{D_0} + \frac{1}{4\bar{\rho}C_{D_0}\bar{V}_t E_{\max}^2 \cos^2\mu_t} \tag{9.8}
$$

where we have

$$
\begin{aligned}
\bar{V}_t &= \frac{1}{\sqrt{\bar{\rho}C_{L_t}\cos\mu_t}} = \frac{1}{\sqrt{2\sqrt{3}\bar{\rho}C_{D_0}E_{\max}\cos\mu_t}} \\
C_{L_t} &= 2\sqrt{3}C_{D_0}E_{\max} \\
\bar{P}_t &= \frac{2\bar{V}_t}{\sqrt{3}E_{\max}\cos\mu_t} = \frac{1}{3}\sqrt{\frac{2\sqrt{3}}{\bar{\rho}C_{D_0}}}\frac{1}{\sqrt{E_{\max}^3\cos^3\mu_t}}
\end{aligned}
\tag{9.9}
$$

Switching Algorithm in a Restricted Flight Zone

In a restricted flight zone, switching between *velocity* and *trajectory tracking* strategies is an important subject of matter. This basically determines if the UAV will stay within the region (and execute velocity strategy) or will switch the strategy and track the designated boundary conditions (via trajectory tracking strategy). This concept has been demonstrated as a flowchart in further detail in Fig-9.21.

As it is possible to see from Fig-9.21, switching between two strategies has been executed accordingly at the time of update and necessary action is taken following to the outcome of the algorithm.

The important question at this point is: *"What is the mathematical rule behind the switching algorithm?"*.

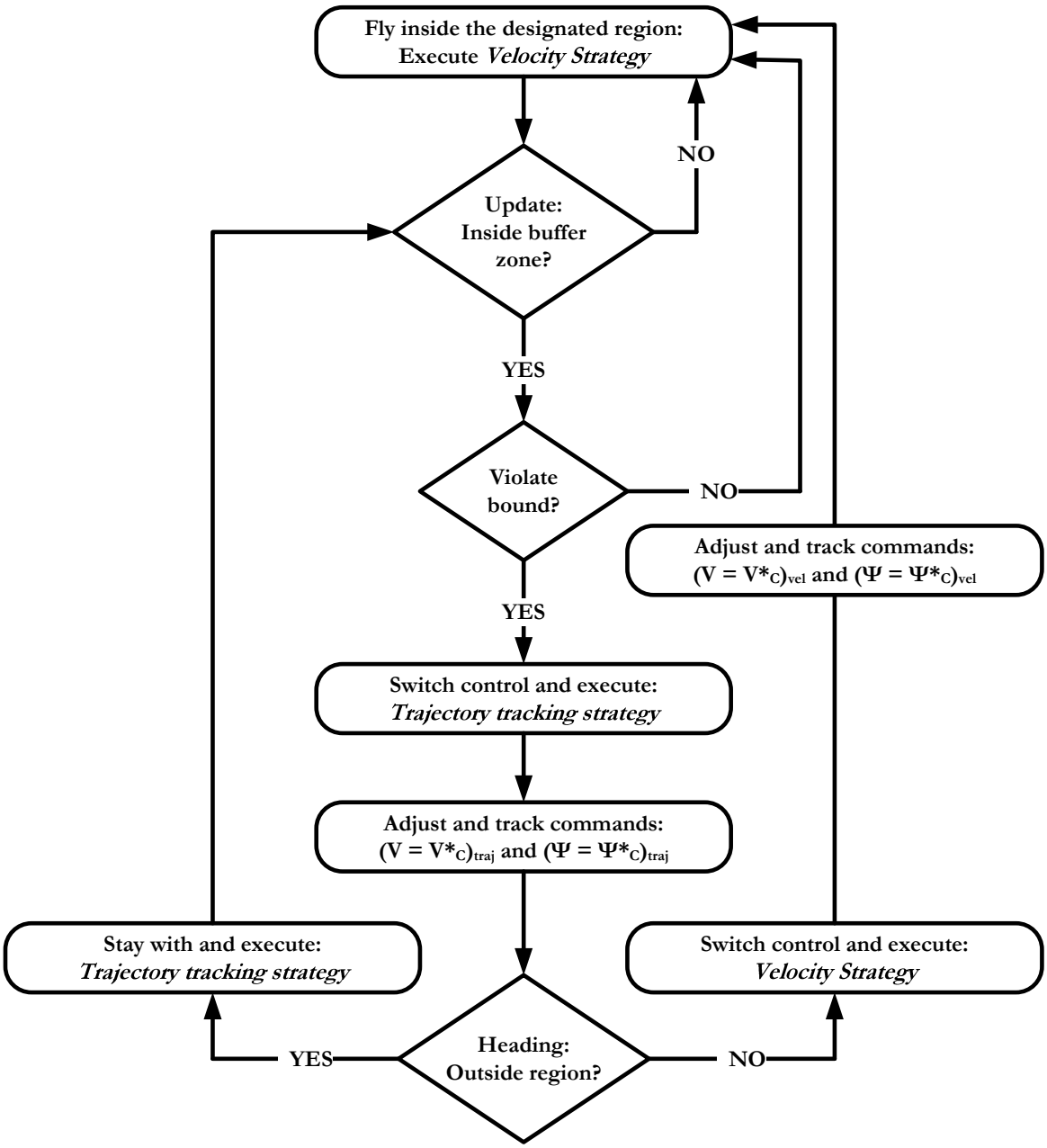

Figure 9.21: Switching algorithm flow chart for a restricted flight zone scenario.

Here, switching logic solely depends on the future approximations of the positions of the UAV ($\bar{x}$, $\bar{y}$) and on the definition of the buffer zone. In this specific section, buffer zone is defined as the geometric shape (in this case circular flight zone) which is smaller than the actual restricted flight zone and which defines the security zone for the execution of switching commands between velocity and trajectory tracking strategies. This concept is depicted in Fig-9.22. In other words, once the UAV gets inside the buffer zone the switching algorithm takes place and appropriate command is executed with respect to logic shown in Fig-9.21. The radius of the restricted circular flight zone is selected as $\sim$1mile(5200[ft]) and the buffer zone is selected as 1000ft away from the boundary (i.e. towards the center).

It is good to note that once the UAV is inside the buffer zone, there are three possible scenarios, as shown in Fig-9.22: (1) at the time of update (at $\bar{t}_0$), the prediction for positions dictates that UAV will leave the region (which requires the strategy to switch to trajectory tracking), (2) at the time of update, the prediction for positions dictates that UAV will stay within the buffer zone (which does not require any action and UAV will keep on flying with velocity strategy), (3) at the time of update, the prediction for positions foresees that UAV will fly towards inside the designated region, which (again) does not require any action, and UAV will keep on flying with the velocity strategy.

Since the matter of subject in this specific scenario is a circular flight zone pattern, the boundary constraints have been imposed as a circular flight region, as

$$\bar{x}(\bar{t}_0 + \Delta\bar{t})^2 + \bar{y}(\bar{t}_0 + \Delta\bar{t})^2 \leq \bar{R}^2 \tag{9.10}$$

where $\bar{x}(\bar{t}_0 + \Delta\bar{t})$ and $\bar{y}(\bar{t}_0 + \Delta\bar{t})$ are the position estimates for next time step $(\bar{t}_0 + \Delta\bar{t})$ based on the measurements taken at the time of update, $\bar{t}_0$. If the derivative of Eq.(9.10) is investigated, this leads to the second mathematical rule (also constraint) of switching algorithm as

$$2\bar{x}(\bar{t}_0 + \Delta\bar{t})\bar{x}'(\bar{t}_0 + \Delta\bar{t}) + 2\bar{y}(\bar{t}_0 + \Delta\bar{t})\bar{y}'(\bar{t}_0 + \Delta\bar{t}) \leq 0 \tag{9.11}$$

Therefore, through enforcing boundary constraints defined in Eq.(9.10) and Eq.(9.11), it is aimed to guide the UAV flight to stay within the restricted (circular) flight zone.

Here, it is known from previous derivations that the time rate of change of positions

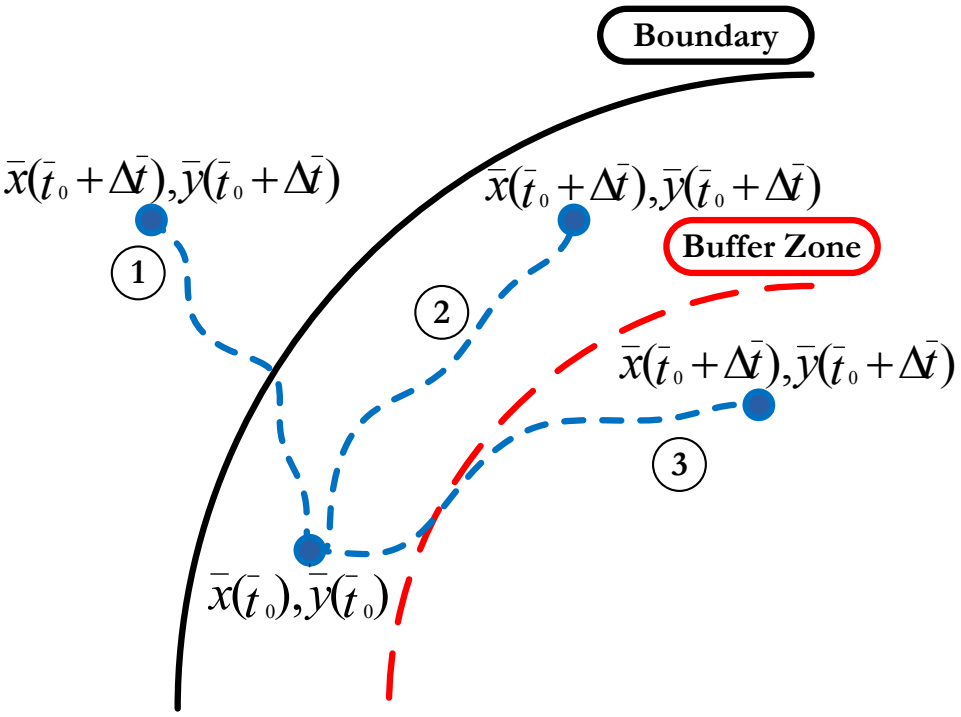

Figure 9.22: Buffer zone diagram for a restricted flight zone scenario.

$\bar{x}'(\bar{t}_0 + \Delta\bar{t})$ and $\bar{y}'(\bar{t}_0 + \Delta\bar{t})$ could be expressed as

$$\begin{aligned} \bar{x}'(\bar{t}_0 + \Delta\bar{t}) &= (\bar{V}_0 + \Delta\bar{V})\cos(\gamma_0 + \Delta\gamma)\sin(\Psi_0 + \Delta\Psi) + \bar{W}_x(\bar{t}_0\Delta\bar{t}) \\ \bar{y}'(\bar{t}_0 + \Delta\bar{t}) &= (\bar{V}_0 + \Delta\bar{V})\cos(\gamma_0 + \Delta\gamma)\cos(\Psi_0 + \Delta\Psi) + \bar{W}_y(\bar{t}_0\Delta\bar{t}) \end{aligned} \tag{9.12}$$

Furthermore, using the first order Taylor series approximation, the position expressions $[\bar{x}(\bar{t}_0 + \Delta\bar{t})$ and $\bar{y}(\bar{t}_0 + \Delta\bar{t})]$ at the next time step $(\bar{t}_0 + \Delta\bar{t})$ can be obtained as

$$\begin{aligned} \bar{x}(\bar{t}_0 + \Delta\bar{t}) &= \bar{x}_0 + \frac{\partial\bar{x}}{\partial\bar{x}}\Delta\bar{x} + \frac{\partial\bar{x}}{\partial\bar{y}}\Delta\bar{y} + \frac{\partial\bar{x}}{\partial\bar{t}}\Delta\bar{t} \\ \bar{y}(\bar{t}_0 + \Delta\bar{t}) &= \bar{y}_0 + \frac{\partial\bar{y}}{\partial\bar{x}}\Delta\bar{x} + \frac{\partial\bar{y}}{\partial\bar{y}}\Delta\bar{y} + \frac{\partial\bar{y}}{\partial\bar{t}}\Delta\bar{t} \end{aligned} \tag{9.13}$$

which simplifies to the final form of expressions

$$\begin{aligned} \bar{x}(\bar{t}_0 + \Delta\bar{t}) &= \bar{x}_0 + \bar{x}'_0\Delta\bar{t} \\ &= \bar{x}_0 + \left[\bar{V}_0\cos(\gamma_0)\sin(\Psi_0) + \bar{W}_x(\bar{t}_0)\right]\Delta\bar{t} \end{aligned} \tag{9.14}$$

and

$$\begin{aligned} \bar{y}(\bar{t}_0 + \Delta\bar{t}) &= \bar{y}_0 + \bar{y}'_0\Delta\bar{t} \\ &= \bar{y}_0 + \left[\bar{V}_0\cos(\gamma_0)\cos(\Psi_0) + \bar{W}_y(\bar{t}_0)\right]\Delta\bar{t} \end{aligned} \tag{9.15}$$

This finalizes the mathematical derivation of the switching rule, and with the help of previously obtained wind terms, the position estimates can be calculated and the switching rule could be applied accordingly.

Evaluation of complete guidance strategies in a restricted flight zone

Having defined all necessary components, simulation studies have been conducted and obtained results are provided in Fig-9.23.

From Fig-9.23 it is very easy to see that applied strategy is working as desired and whenever the UAV gets close to the boundary, it is enforced to give a decision and applies the appropriate flight logic. In case of Fig-9.23, whenever UAV gets very close to the boundary, it is enforced to give a decision: (i) it can be directed to fly towards inside the circular region to benefit from the wind currents, or (ii) it may track the boundary for some time, without getting out of the region and fly on the boundary until an optimal adjustment comes and dictates UAV to fly towards inside the circular

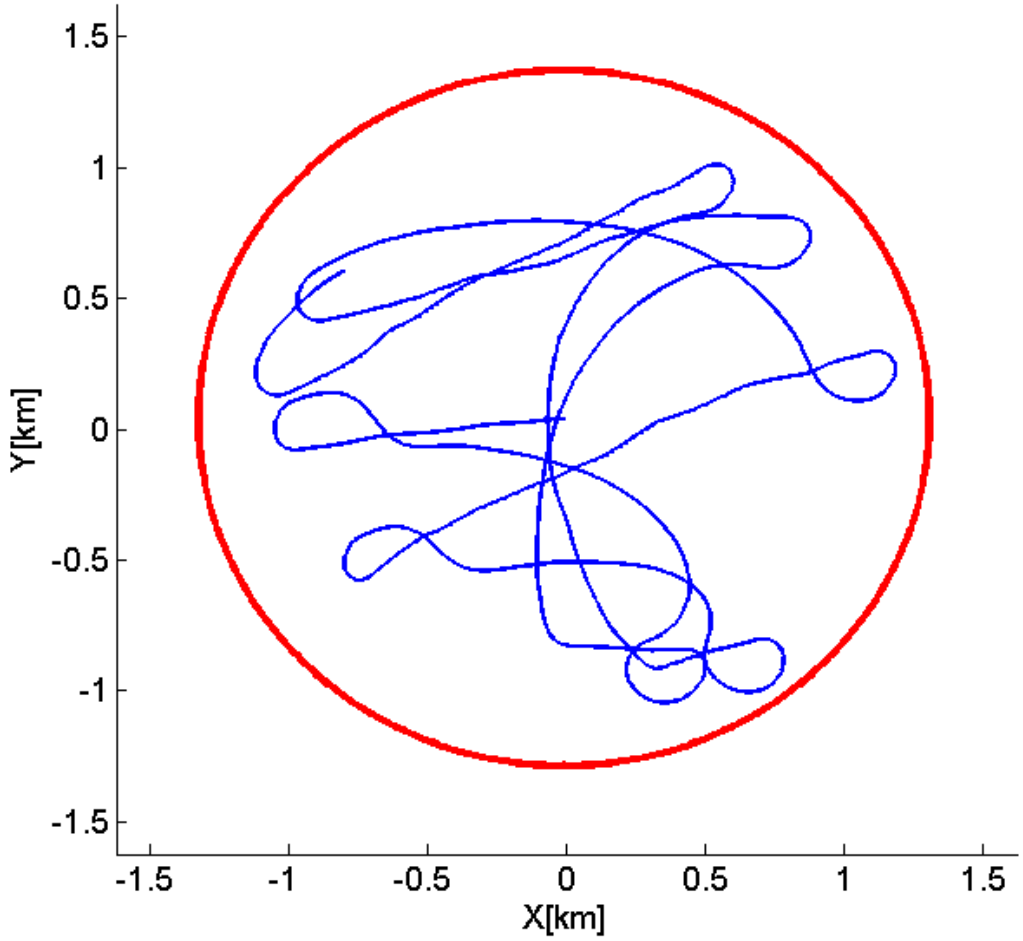

Figure 9.23: Scenario-4: Trajectory of UAV with optimal airspeed & heading strategy in a restricted circular level flight.

zone. This will make sure that power is minimized without violating assigned geometric region constraints and the mission objectives.

To sum up: when a mission is executed in a restricted flight zone, there are two things which may happen while UAV gets very close to (violate) the boundary:

- If it is beneficial to fly towards inside the given restricted region (in this case towards inside the circular zone)
  - apply *velocity guidance* strategy (i.e. necessary commands to achieve desired optimal airspeed and heading, thus minimize energy while flying inside the region)
  - Re-evaluate the decision at the next measurement update.
- If calculated optimal commands from *velocity strategy* are commanding aircraft to get out of the region
  - apply and stay with the *trajectory tracking* strategy, follow trajectory tracking commands to make sure you do not get out of the specified boundary until next measurement update.
  - Re-evaluate the decision at the next measurement update.

With this scenario, and given results, it is aimed to demonstrate the fact that, when UAV is assigned a mission such as to fly in a restricted zone, it is still possible to execute assigned mission without violating the geometric boundary constraints. Furthermore, it still will be possible to benefit from the wind patterns and minimize power consumption using periodic adjustments on airspeed and heading angle throughout the entire flight. As a result, obtained relative benefit in restricted flight case is given in Table-9.7.

Table 9.7: Scenario-3: Average power consumption results.

Altitude$[ft]$	$\bar{P}_{circ}$	$\bar{P}_4$	Avg. Benefit [%]
15,000	0.0439	0.0402	8.5

Here a sample scenario has been demonstrated on a circular restricted flight zone. Without the loss of generality, this can be expanded easily to several geometrical flight regions (such as ellipsoid, square, triangle, rectangular ... etc.), and benefits in power savings could still be demonstrated.

9.6 Relative Benefit vs. Wind Frequency

With the proposed optimal guidance strategies it is aimed to benefit from the global, low frequency wind behaviour. But at the same time, it is very important to know the limitations and short-comings of the strategies in terms of

- *"What are the feasible operation regions (i.e. feasible wind frequency regions)?"*,
- *"Where can we extract energy and fly efficiently?"*, and
- *"What are the bounds where the suggested optimal guidance strategy is not able to function as desired any more?"*.

and in this section above-mentioned issues will be addressed. It will be aimed to come up with possible trends to determine the wind frequency range where operations will be successful and energy extraction from the wind would be possible.

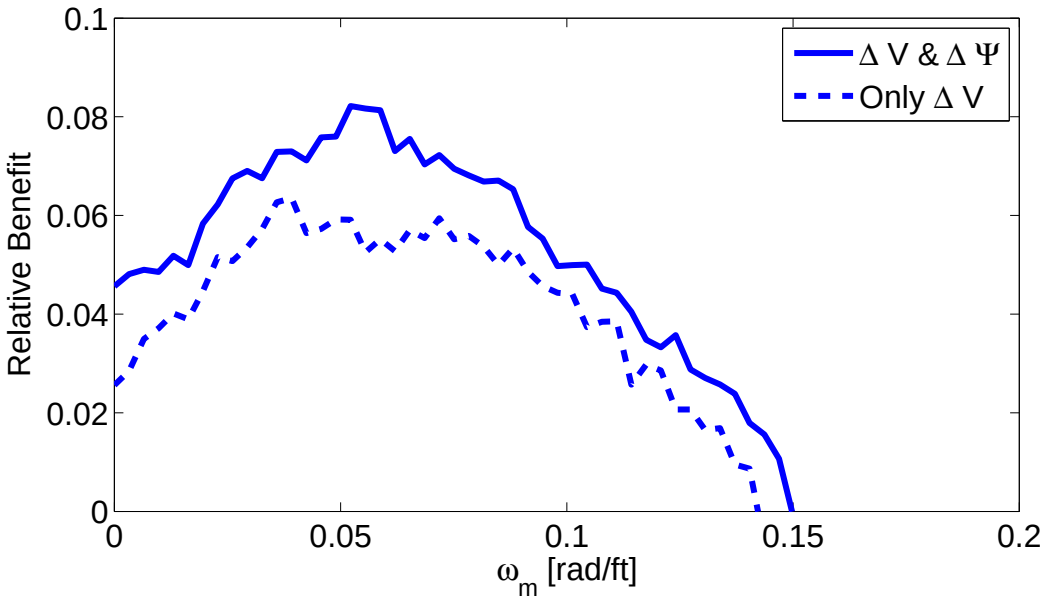

Figure 9.24: Relative benefit versus wind frequency response of Scenario-1 and Scenario-3.

Fig-9.24 compares the relative benefits of the two strategies in which periodic adjustments are made in the commands of airspeed alone (*dashed line*), and both airspeed

and heading (*solid line*), respectively, over the reference strategy.

Even in a constant wind field, the strategies of periodically varying airspeed and/or heading angle perform better than the constant airspeed reference trajectory. These benefits initially increase as the spatial frequency of the wind field gradually increases, but reaches a certain peak value at certain frequency and then starts to decrease beyond that frequency. As the spatial frequency exceeds a certain limit, the proposed strategies of varying airspeed and/or heading angles derived in this study are worse than the constant airspeed reference strategy. This is caused by the fact that as the spatial frequency exceeds a certain limit, the projected power consumption from which the airspeed and heading angle adjustments are derived starts to deviate significantly from the actual power consumption. Also when high frequency dynamics of the wind takes place, wind characteristics become too fast (turbulence-like), so that UAV cannot follow and execute desired commands as expected, in a timely fashion.

It seems that it is possible to obtain significant amount of benefit from varying the airspeed. Moreover, varying both airspeed and heading angle improves the benefit further. On the other hand, varying heading angle alone produces very little benefit (~ 0). For conducted simulations at given altitude, the peak benefit by varying both airspeed and heading angle is around $5 \sim 10\%$ savings of power consumptions over the reference strategy.

From the conducted simulation, it is also possible to deduct the result that when the periodic adjustments of airspeed and heading angle commands are tracked via closed-loop controls, UAV adjusts itself with respect to the wind conditions and varies its flight path to benefit optimally from wind conditions. In particular, the UAV flies along the wind direction most of the time either in tailwind or headwind, whereas it stays in cross wind conditions briefly.

9.7 Relative Benefit vs. Intensity of Stochastic Wind Model: θ

In previous section, relative benefit analysis has been conducted with respect to certain range of wind frequency. It should be noted that the results given in Section 9.6 and in Fig.9.24 are for a fixed value of intensity parameter-θ (which has been chosen as $\theta = 1$)

for the defined stochastic wind model, as shown in Eq.(3.8).

As it was explained beforehand in Chapter 3 and in Section 3.3, presented stochastic wind model was formulated as a *Mean-Reverting Ornstein-Uhlenbeck Process*. In this specific process when the system dynamics evolve with time, there is a force which will pull system dynamics back to a long term equilibrium point. The intensity of the pulling towards the equilibrium (or in other words, the intensity of mean-reverting) is controlled by the parameter θ, as shown in Eq.(3.8). Further investigation will help to realize that intensity parameter-θ is a term which has a unique impact on the nature of the stochastic wind model, and may have a significant influence on the outcomes of the proposed strategies. From this perspective, beside investigating the effects of change in wind frequency, it is also necessary to investigate the effects of change in intensity term (θ) characteristics.

Before proceeding any further, it should be kept in mind that an increasing value of θ will also increase the intensity of pulling towards the long term equilibrium, which will result in less deviations around the mean. Meanwhile, a decreasing value of θ will remove the intense attraction towards the long term equilibrium, and will cause the stochastic wind model to include excessive variations around the mean. These cases were discussed beforehand in Section 3.3 and were shown in Figs. 3.10 and 3.15.

In this section, the main desire is to demonstrate the outcomes of proposed guidance strategies for different values of intensity parameter-θ. Obtained results are shown in Fig.9.25, where wind frequency (ω_m) was kept constant at a value of $0.05[rad/ft]$.

As it is possible to see from Fig. 9.25, with an increasing value of intensity parameter (for both adjustment cases) the benefit increases to a certain value, and after that it reaches to *plateau effect* and pretty much stays constant. It should be kept in mind that every single simulation will provide slightly different results due to the stochastic nature of the wind model. *But*, even if the transient response characteristics are different, the long term behaviour and the trends should be the same, and the steady-state behaviour in higher values of θ should remain approximately constant. The reasoning behind this could be explained through Figs.3.10 and 3.15. As it is possible to see from Figs.3.10 and 3.15, with an increasing value of intensity parameter-θ, both wind magnitude and wind direction behaviours becomes more stable, and the deviations around the mean

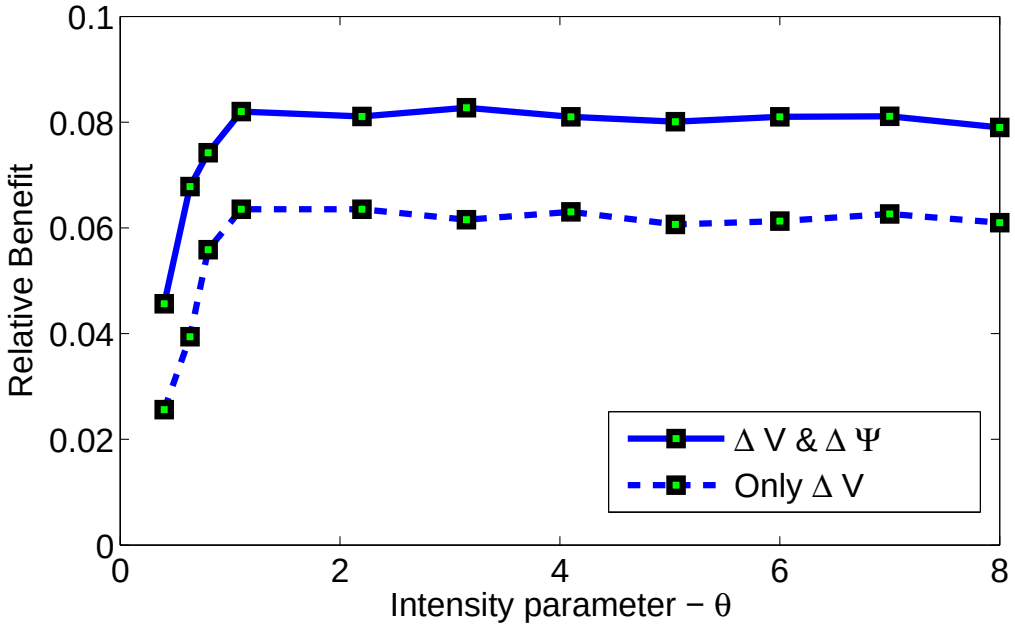

Figure 9.25: Effects of intensity term-θ on relative benefit with both airspeed and heading angle adjustment.

value becomes more invariant. This leads to the fact that with an increasing value of theta, there is a certain threshold where after this point, the change around the mean will not be significant, and therefore will not have a significant effect on relative benefit outcomes.

9.8 Relative Benefit vs. Measurement (Adjustment) Update Interval: $\Delta\bar{t}$

The choice of the update/measurement interval ($\Delta\bar{t}$) directly affects the performance of the proposed optimal guidance strategies.

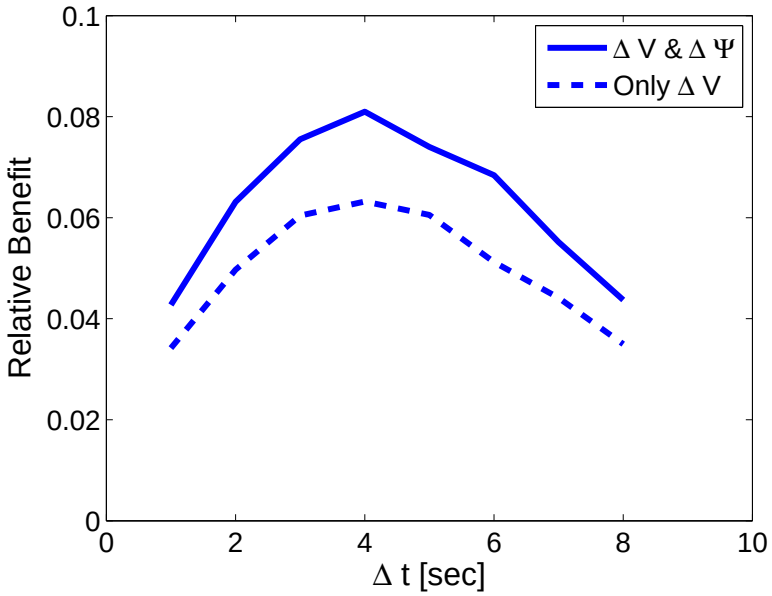

Figure 9.26: Effects of update time interval with both airspeed and heading angle adjustment.

Fig.9.26 illustrates the relative benefits achieved with different update intervals, using the strategy of varying both airspeed and heading angle. It shows that the relative benefit peaks around a certain optimal update interval, which is 4[sec], and is the value used for the examples provided in this thesis. The relative benefit decreases as the update interval either increases or decreases from this value. This is due to the fact

that waiting too long causes UAV to not be able to optimally adjusts (and align) itself with the existing wind patterns. At the same time, very fast and small update intervals causes UAV to change the tracking commands too early without reaching the steady state values, and executing commands appropriately.

9.9 Relative Benefit vs. Wind Variability: $\bar{W}_{m_0}/\bar{W}_m$

Wind variability can affect the relative benefits of UAV flights in winds. In this thesis, the wind variability is defined as the ratio of the constant wind term over the total wind magnitude: $\bar{W}_{m_0}/\bar{W}_m$. A smaller ratio corresponds to a larger wind variability and vice versa. Fig. 9.27 compares relative benefits in different wind variability ratios.

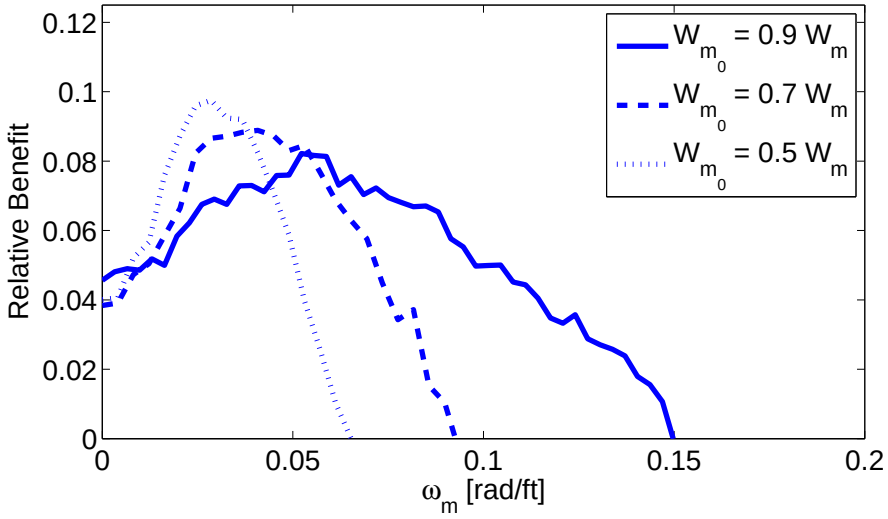

Figure 9.27: Effects of wind variability with both airspeed and heading angle adjustment.

While the basic trends of the relative benefits over spatial wind frequencies are the same, a more variable wind field enables the UAV to achieve higher relative benefits, albeit the range of spatial wind frequencies over which it can improve its endurance with *insitu* wind measurements becomes smaller.

In general, performance of the proposed guidance strategies depend on wind field models, vehicle performance characteristics, and parameters of the proposed strategies

in a complex, nonlinear way. In addition, errors in wind estimates can potentially degrade their performances. Nonetheless, results of the current thesis demonstrate that the proposed real-time guidance strategies can produce positive improvements in terms of average power consumptions over the reference strategy in a given stochastic wind field. They are easy to implement and can be incorporated in aerospace applications.

Chapter 10

Conclusions & Discussions

This thesis presents real-time UAV guidance strategies that utilize wind energies to improve flight endurance. In these strategies, airspeed and/or heading angle commands are periodically adjusted based on the on-board *insitu* measurements of local wind components and wind gradients. Through this, it has been aimed to show that using local, instantaneous wind measurements, without the knowledge of the wind field that the UAV is flying through, it is still possible to benefit from the wind energy and greatly enhance the performance and flight endurance of the UAVs. Throughout conducted research in this thesis, UAV has been modeled using 3D point-mass equations. Corresponding performance and practical constraints has been introduced to mimic a realistic flight of an UAV. A stochastic wind model has been derived through real data measurements taken from NOAA and IGRA stations from all around the continental US. With these data sets, first, a wind model characterizing wind behaviour with respect to altitude has been derived, and change of wind magnitude with respect to height has been modeled. Next, a sinusoidal wind model has been introduced to model horizontal wind behaviour which not only reflects temporal changes in the wind pattern, but also embeds spatial change in wind behaviour. Then, UAV flights were formulated as a non-linear optimization problem and a cost function has been introduced to model power characteristics at terminal state as a terminal state cost function, which will minimize power consumption. This static optimization problem has been solved using second-order gradient algorithms to find local, optimal solutions (adjustments) that will minimize the power with respect to taken local, instantaneous wind measurements. Specifically, the

amounts of airspeed and/or heading angle adjustments are derived to minimize a projected power consumption at some future time expressed at terminal state. Numerical simulations are used to evaluate the relative benefits of these strategies in saving average power consumptions over a reference strategy in which the UAV follows the constant optimal steady-level-flight-airspeed in zero wind. The average power consumption is defined over a specified interval and over different initial heading angles of the UAVs. Models of onboard closed-loop tracking logics that follow adjusted commands are developed using the method of feedback linearization.

Extensive simulations have been conducted to demonstrate the applicability and efficiency of the proposed algorithms and strategies. As a reference, optimal level flight conditions in zero wind has been used in comparison with the outcomes obtained from the proposed algorithms. Results indicate significant improvements in UAV flights can be achieved by adjusting airspeed and heading angles throughout the flight, without violating any flight constraints. Furthermore, it is shown that in case of a restricted flight zone mission, proposed strategies can still introduce enhancement in terms minimizing power and maximizing endurance during the flight of an UAV.

The proposed strategies offer improvements over the constant airspeed reference strategy in terms of average power consumptions even in a constant wind field. These benefits initially increase as the spatial frequency of the wind field gradually increases, but reaches a peak at certain frequencies and then start to decrease beyond these frequencies. As the spatial frequency exceeds a certain limit, the strategies of varying airspeed and/or heading angles become ineffective. The most benefit seems to come from varying the airspeed. Varying both airspeed and heading angle improves the benefit further. On the other hand, varying heading angle alone produces very little benefit. Changing the characteristics (intensity) of stochastic wind model also affects the outcomes. Higher intensity results in approximately constant average benefit, while smaller intensity parameter helps to show the trends of power savings more accurately. For a given spatial wind frequency, the relative benefit peaks for a certain update interval and would decrease for smaller or larger update intervals. In comparison, different levels of wind variability as measured by the percentage of the constant term in the wind expression also affect the performances of UAV flights. More variable wind leads to higher benefit peaks but a smaller spatial frequency range over which the proposed strategies

can recap energy from the wind.

In general, performance of the proposed guidance strategies depend on wind field models, vehicle performance characteristics, and parameters of the proposed strategies in a complex, nonlinear way. In addition, errors in wind estimates can potentially degrade their performances. Nonetheless, results of the current thesis demonstrate that the proposed real-time guidance strategies can produce significant positive improvements in terms of average power consumptions over the reference strategy in a given stochastic wind field. They are easy to implement and can be incorporated in UAV flights.

Chapter 11

Recommendations for Future Work

With this thesis, it has been aimed to study the possible ways to benefit from the global, low frequency characteristics of wind behaviour to enhance endurance of UAV flights through real-time guidance strategies. It has been assumed that only local, instantaneous, *in-situ* wind measurements are used to generate proposed real-time strategies.

Following arguments are considered as useful and beneficial research direction(s) for future studies:

- Throughout this study, it has been assumed that UAV performs some type(s) of level flight scenarios. It is beneficial to extend these level flight scenarios to 3D flights which will benefit not only from the horizontal wind pattern but also from the vertical wind patterns (such as thermals, microbursts, downdrafts, ... etc.)
- If 3D strategies are of interest of application, it is essential (and crucial) to have a more detailed and sophisticated (but yet realistic) stochastic wind model which will also be able to reflect the characteristics of thermals, microbursts, downdrafts, ... etc. This (with proper modeling) will further enhance the performance of UAVs in presence of winds.
- This study, has started with the idea in mind that (one day) this may be expanded and applied to commercial flights. It is known that on higher altitudes there are

extremely strong air currents (i.e. jet streams) and can provide a considerable amount of benefit in fuel/power savings. This thesis, was intended as a one of the steps towards implementing such real-time strategies further on harvesting energy from the wind in *commercial flights* to not only minimize power consumption (in that case fuel burn), but also minimize the fuel emissions and provide savings to commercial aviation companies. In long run, this may (and probably will) also have an impact on reducing ticket prices and travel costs as well. Therefore, investigating the real-time strategies on commercial flights is another topic of future interest.

- In this thesis, it has been assumed that no regional wind information is available and only local, instantaneous wind measurements has been used as inputs from the environment. In real-life, with the advancement of technology, it should be considered to use such advanced technology that can detect (and forecast to some extent) weather conditions in the flight zone of the UAV in the near future. Commercial aircraft can do this to some extent using their on board weather radars.

- In real life, wind measurements are taken using sophisticated GPS/INS algorithms which provide wind data measurements with certain estimation accuracy. It is also desired to study the effects of wind measurement errors on the path/trajectory of the UAV.

- As much as wind measurement errors, modeling errors are also of great importance. It is also very beneficial to study and consider the effect of modeling errors and its impacts on the optimization routine.

- It is without any doubt that, in case of a faulty sensor, or serious malfunction of any on-board (position or wind) measurement unit, optimization algorithm and therefore suggested real-time guidance strategy will perform poorly (if not fail). Therefore, fault detection algorithms can be implemented to work together with devised guidance strategies to bring further enhancement.

References

M. J. Allen. Autonomous Soaring for Improved Endurance of a Small Uninhabited Air Vehicle. In *43rd AIAA Aerospace Sciences Meeting and Exibit*, Reno, Nevada, 2005. American Institute of Aeronautics and Astronautics.

M. J. Allen and V. Lin. Guidance and Control of an Autonomous Soaring Vehicle with Flight Test Results. In *AIAA Aerospace Sciences Meeting and Exhibit*, volume AIAA Paper 2007-867, Reno, Nevada, 2007. American Institure of Aeronautics and Astronautics.

Jr. Anderson, J.D. *Introduction to Flight, 3rd Ed.* McGraw-Hill, 1989.

R. Austin. *Unmanned Aircraft Systems: UAVS Design, Development and Deployment.* John Wiley & Sons, 2010.

M. B. E. Boslough. Autonomous Dynamic Soaring Platform for Distributed Mobile Sensor Arrays. Technical report, Sandia National Laboratories, 2002.

P. J. Brockwell and R. A. Davis. *Time Series: Theory and Methods.* Springer-Verlag New York Inc., 1991.

B. Carnahan, H. A. Luther, and J. O. Wilkes. *Applied Numerical Methods.* Wiley, New York, 1969.

A.K. Dixit and R.S. Pindyck. *Investment Under Uncertainty.* Princeton University Press, Princeton, NJ., 1994.

Daniel J. Edwards. Implementation Details and Flight Test Results of an Autonomous Soaring Controller. In *AIAA Guidance, Navigation, and Control Conference*, 2008.

Lawrence C. Evans. *An Introduction to Stochastic Differential Equations*. Lecture Notes, UC Berkeley, 2010.

J. D. Holmes. *Wind Loading Structures*. Taylor & Francis, 2001.

M. R. Jackson, Y. J. Zhao, and R. A. Slattery. Sensitivity of Trajectory Prediction in Air Traffic Management. *Journal of Guidance, Control, and Dynamics*, 22(2): 219–228, 1999.

T. Kinoshita and F. Imado. The Application of an UAV Flight Simulator: The Development of a New Point Mass Model for an Aircraft. In *SICE-ICASE International Joint Conference*, 2006a.

T. Kinoshita and F. Imado. A Study on the Optimal Flight Control for an Autonomous UAV. In *Proceedings of the IEEE International Conference on Mechatronics and Automation*, 2006b.

P. E. Kloeden and E. Platen. *Numerical Solution of Stochastic Differential Equations*. Springer-Verlag, Berlin, 1992.

P. L. Krapivsky, S. Redner, and E. Ben-Naim. *A Kinetic View of Statistical Physics*. Cambridge University Press, 2010.

J. W. Langelaan. Gust Energy Extraction for Mini- and Micro- Uninhabited Aerial Vehicles. In *46th AIAA Aerospace Sciences Meeting and Exhibit*, 2008. AIAA-2008-0223.

Jack W. Langelaan. Gust Energy Extraction for Mini and Micro Uninhabited Aerial Vehicles. *Journal of Guidance, Control, and Dynamics*, 32(2):464–473, 2009.

N.R. Lawrance and S. Sukkarieh. A guidance and control strategy for dynamic soaring with a gliding UAV. In *Proceedings of the 2009 IEEE International Conference on Robotics and Automation (ICRA 2009)*, 2009.

D. Lawrence and S. Sukkarieh. Wind Energy Based Path Planning for a Small Gliding Unmanned Aerial Vehicle. In *AIAA Guidance, Navigation, and Control Conference*, 2009.

J. Lorenz. Numerical solution of the minimum-time flight of a glider through a thermal by use of multiple shooting methods. *Optimal Control Applications and Methods*, 6: 125–140, 1985.

T. G. McGee and J. K. Hedrick. Optimal Path Planning with a Kinematic Airplane Model. *Journal of Guidance, Control, and Dynamics*, 30(2):629–633, 2007.

R. L. McNeely, R. V. Iyer, and P. R. Chandler. Tour Planning for an Unmanned Air Vehicle Under Wind Conditions. *Journal of Guidance, Control, and Dynamics*, 30 (5):1299–1306, 2007.

J. Mueller, Y. J. Zhao, and W. L. Garrard. Optimal Ascent Trajectories for Stratospheric Airships Using Wind Energy. *Journal of Guidance, Control, and Dynamics*, 32, 2009.

G. Nachmani. Minimum Energy Flight Paths for UAVS Using Mesoscale Wind Forecasts and Approximate Dynamic Programming. Master's thesis, Naval Postgraduate School, 2007.

B. Oksendal. *Stochastic Differential Equations: An Introduction with Applications*. Springer-Verlag, New York, NY, 1995, 4th Ed.

C.K. Patel and I. Kroo. Control Law Design for Improving UAV Performance Using Wind Turbulence. 2006. AIAA-2006-0231.

B. L. Pierson and I. Chen. Minimum altitude-loss soaring in a specified vertical wind distribution. *Optimal Control Appl. Meth.*, 1:205–215, 1980.

B. L. Pierson and J. L. De Jong. Cross-country sailplane flight as a dynamic optimization problem. *Int. J. Num. Meth. Eng.*, 12:1743–1759, 1978.

M. A. Pinsky and S. Karlin. *An Introduction to Stochastic Modeling*. Academic Press, Elsevier, 2011.

W. Pisano and D. Lawrence. Control Limitations of Small Unmanned Aerial Vehicles in Turbulent Environments. In *AIAA Guidance, Navigation, and Control Conference*, 2009.

Y. C. Qi and Y. J. Zhao. Energy-Efficient Trajectories of Unmanned Aerial Vehicles Flying Through Thermals. *Journal of Aerospace Engineering*, 18(2):84–92, 2005.

H. Ruscheweyh. Practical experiences with wind-induced vibrations. *Journal of Wind Engineering and Industrial Aerodynamics*, 33:211–18, 1990.

R. Rysdyk. Course and Heading Changes in Significant Wind. *Journal of Guidance, Control, and Dynamics*, 30(4):1168–1171, 2007.

G. Sachs, A. Knoll, and K. Lesch. Optimal Utilization of Wind Energy for Dynamic Soaring. *Technical Soaring*, 15(2), 1991.

T. Sauer. Numerical Solution of Stochastic Differential Equations in Finance. Technical report, Department of Mathematics, George Mason University, 2010.

C. Scruton. *An Introduction to Wind Effects on Structures*. Oxford University Press, Oxford, 1981.

E. Simiu and R. H. Scanlan. *Wind Effects on Structures - Fundamentals and Applications to Design*. Wiley, New York, 1996.

J. J. E. Slotine and W. Li. *Applied Nonlinear Control*. Wil, 1991.

S. Sukkarieh and B. Lawrence. Autopiloted glider knows where to fly for a free ride. *New Scientist*, 2011.

G. N. Tiwari and M. K. Ghosal. *Renewable Energy Resources: Basic Principles And Applications*. Alpha Science International Ltd., 2010.

K. Turkoglu and Y. J. Zhao. Real-Time Insitu Strategies for Enhancing UAV Endurance by Utilizing Wind Energy. In *AIAA Guidance, Navigation, and Control Conference*, 2009.

J. M. Wharington. Autonomous Control of Soaring Aircraft by Reinforcement Learning. Technical report, Royal Melbourne Institute of Technology, 1998.

J. M. Wharington. Heuristic Control of Dynamic Soaring. In *5th Asian Control Conference*, 2004.

Y. J. Zhao. Optimal Patterns of Glider Dynamic Soaring. *Optimal Control Applications and Methods*, 24(2):67–89, 2004.

Y. J. Zhao. Extracting Energy from Downdraft to Enhance Endurance of Uninhabited Aerial Vehicles. *Journal of Guidance, Control, and Dynamics*, 32(4), 2009.

Y. J. Zhao and Y. C. Qi. Minimum Fuel Powered Dynamic Soaring of Unmanned Aerial Vehicles Utilizing Wind Gradient. *Optimal Control Applications and Methods*, 25:211–233, 2004.

Appendix A

Point-Mass Equations of Motion for an Aircraft in a Rotating Earth

A.1 Coordinate Systems

Descriptions:

($\hat{I}_s$, $\hat{J}_s$, $\hat{K}_s$): inertial (tatic), earth-centered equatorial

($\hat{I}$, $\hat{J}$, $\hat{K}$): earth-fixed, earth-centered equatorial

($\hat{e}$, $\hat{n}$, $\hat{u}$): topocentric, East, North, up

($\hat{i}$, $\hat{j}$, $\hat{k}$): c.g., wind-axis, $\hat{i}$ along airspeed, $\hat{j} \perp \hat{k}$ and points up, $\hat{j}$ forms right hand system

Assumption: spherical earth, and rotating

$$\begin{bmatrix} \hat{e} \\ \hat{n} \\ \hat{u} \end{bmatrix} = \begin{bmatrix} 0 & 1 & 0 \\ 0 & 0 & 1 \\ 1 & 0 & 0 \end{bmatrix} \begin{bmatrix} \hat{u} \\ \hat{e} \\ \hat{n} \end{bmatrix} \tag{A.1}$$

The following relations can be developed,

$\vec{\omega}_e = \omega_e \hat{K}$ rotational rate of $(\hat{I}, \hat{J}, \hat{K})$

Then the transformation between $(\hat{I}, \hat{J}, \hat{K})$ and $(\hat{e}, \hat{n}, \hat{u})$ can be developed

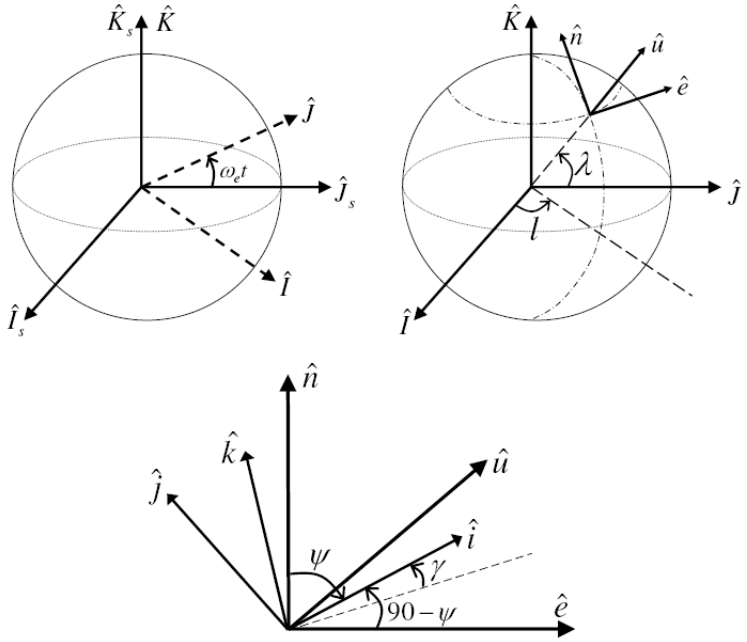

Figure A.1: Relations of frames of references

$$\begin{aligned}\begin{bmatrix}\hat{u}\\ \hat{e}\\ \hat{n}\end{bmatrix} &= \begin{bmatrix}\cos\lambda & 0 & \sin\lambda\\ 0 & 1 & 0\\ -\sin\lambda & 0 & \cos\lambda\end{bmatrix}\begin{bmatrix}\cos l & \sin l & 0\\ -\sin l & \cos l & 0\\ 0 & 0 & 1\end{bmatrix}\begin{bmatrix}\hat{I}\\ \hat{J}\\ \hat{K}\end{bmatrix}\\ &= \begin{bmatrix}\cos l\cos\lambda & \sin l\cos\lambda & \sin\lambda\\ -\sin l & \cos l & 0\\ -\cos l\sin\lambda & -\sin l\sin\lambda & \cos\lambda\end{bmatrix}\begin{bmatrix}\hat{I}\\ \hat{J}\\ \hat{K}\end{bmatrix}\end{aligned} \tag{A.2}$$

or

$$\begin{aligned}\begin{bmatrix}\hat{I}\\ \hat{J}\\ \hat{K}\end{bmatrix} &= \begin{bmatrix}\cos l\cos\lambda & -\sin l & -\cos l\sin\lambda\\ \sin l\cos\lambda & \cos l & -\sin l\sin\lambda\\ \sin\lambda & 0 & \cos\lambda\end{bmatrix}\begin{bmatrix}\hat{u}\\ \hat{e}\\ \hat{n}\end{bmatrix}\\ &= \begin{bmatrix}-\sin l & -\cos l\sin\lambda & \cos l\cos\lambda\\ \cos l & -\sin l\sin\lambda & \sin l\cos\lambda\\ 0 & \cos\lambda & \sin\lambda\end{bmatrix}\begin{bmatrix}\hat{e}\\ \hat{n}\\ \hat{u}\end{bmatrix}\end{aligned} \tag{A.3}$$

$\Rightarrow$

$$\hat{K} = \cos\lambda\hat{n} + \sin\lambda\hat{u} \tag{A.4}$$

In addition

$$\begin{aligned}
\begin{bmatrix} \hat{i} \\ \hat{j} \\ \hat{k} \end{bmatrix} &= \begin{bmatrix} \cos\gamma & 0 & \sin\gamma \\ 0 & 1 & 0 \\ -\sin\gamma & 0 & \cos\gamma \end{bmatrix} \begin{bmatrix} \cos(90-\Psi) & \sin(90-\Psi) & 0 \\ -\sin(90-\Psi) & \cos(90-\Psi) & 0 \\ 0 & 0 & 1 \end{bmatrix} \begin{bmatrix} \hat{e} \\ \hat{n} \\ \hat{u} \end{bmatrix} \\
&= \begin{bmatrix} \cos\gamma & 0 & \sin\gamma \\ 0 & 1 & 0 \\ -\sin\gamma & 0 & \cos\gamma \end{bmatrix} \begin{bmatrix} \sin\Psi & \cos\Psi & 0 \\ -\cos\Psi & \sin\Psi & 0 \\ 0 & 0 & 1 \end{bmatrix} \begin{bmatrix} \hat{e} \\ \hat{n} \\ \hat{u} \end{bmatrix} \\
&= \begin{bmatrix} \cos\gamma\sin\Psi & \cos\gamma\cos\Psi & \sin\gamma \\ -\cos\Psi & \sin\Psi & 0 \\ -\sin\gamma\sin\Psi & -\sin\gamma\cos\Psi & \cos\gamma \end{bmatrix} \begin{bmatrix} \hat{e} \\ \hat{n} \\ \hat{u} \end{bmatrix}
\end{aligned} \tag{A.5}$$

or

$$\begin{bmatrix} \hat{e} \\ \hat{n} \\ \hat{u} \end{bmatrix} = \begin{bmatrix} \cos\gamma\sin\Psi & -\cos\Psi & -\sin\gamma\sin\Psi \\ \cos\gamma\cos\Psi & \sin\Psi & -\sin\gamma\cos\Psi \\ \sin\gamma & 0 & \cos\gamma \end{bmatrix} \begin{bmatrix} \hat{i} \\ \hat{j} \\ \hat{k} \end{bmatrix} \tag{A.6}$$

$\Rightarrow$

$$\boxed{\begin{aligned}
\hat{i} &= \cos\gamma\sin\Psi\hat{e} + \cos\gamma\cos\Psi\hat{n} + \sin\gamma\hat{u} \\
\hat{e} &= \cos\gamma\sin\Psi\hat{i} - \cos\Psi\hat{j} - \sin\gamma\sin\Psi\hat{k} \\
\hat{u} &= \sin\gamma\hat{i} + \cos\gamma\hat{k} \\
\hat{j} &= -\cos\Psi\hat{e} + \sin\Psi\hat{n}
\end{aligned}} \tag{A.7}$$

A.2 Kinematics

A.2.1 Kinematics of Velocity

The position vector is given by, on a spherical earth,

$$\vec{r} = (R+h)\hat{u} = r\hat{u} \tag{A.8}$$

The rotational velocity of $(\hat{e}, \hat{n}, \hat{u})$ w.r.t. $(\hat{I}, \hat{J}, \hat{K})$ is

$$\vec{\Omega_{enu}} = \dot{l}\hat{K} - \dot{\lambda}\hat{e} \tag{A.9}$$

$$= -\dot{\lambda}\hat{e} + \dot{l}\cos\lambda\hat{n} + \dot{l}\sin\lambda\hat{u} \tag{A.10}$$

We want to find the vehicle velocity w.r.t. Earth

$$\vec{V_e} = (\frac{d\vec{r}}{dt})_{IJK} = \dot{h}\hat{u} + \vec{\Omega}_{enu} \times \vec{r} \tag{A.11}$$

$$= \dot{h}\hat{u} + (-\dot{\lambda}\hat{e} + \dot{l}\cos\lambda\hat{n} + \dot{l}\sin\lambda\hat{u}) \times (R+h)\hat{u} \tag{A.12}$$

$$= \dot{l}(R+h)\cos\lambda\hat{e} + \dot{\lambda}(R+h)\hat{n} + \dot{h}\hat{u} \tag{A.13}$$

On the other hand, the earth-relative velocity can be also expressed as

$$\vec{V_e} = \text{airspeed} + \text{windspeedw.r.t.earth} \tag{A.14}$$

$$= V\hat{i} + (W_e\hat{e} + W_n\hat{n} + W_u\hat{u}) \tag{A.15}$$

$$= V(\cos\gamma\sin\Psi\hat{e} + \cos\gamma\cos\Psi\hat{n} + \sin\gamma\hat{u}) + (W_e\hat{e} + W_n\hat{n} + W_u\hat{u}) \tag{A.16}$$

$$= (V\cos\gamma\sin\Psi + W_e)\hat{e} + (V\cos\gamma\cos\Psi + W_n)\hat{n} + (V\sin\gamma + W_u)\hat{u} \tag{A.17}$$

By comparing the two equations, we have

$$\dot{l}(R+h)\cos\lambda = V\cos\gamma\sin\Psi + W_e \tag{A.18}$$

$$\dot{\lambda}(R+h) = V\cos\gamma\cos\Psi + W_n \tag{A.19}$$

$$\dot{h} = V\sin\gamma + W_u \tag{A.20}$$

or

$$\dot{l} = \frac{V\cos\gamma\sin\Psi + W_e}{(R+h)\cos\lambda} \tag{A.21}$$

$$\dot{\lambda} = \frac{V\cos\gamma\cos\Psi + W_n}{(R+h)} \tag{A.22}$$

$$\dot{h} = V\sin\gamma + W_u \tag{A.23}$$

Additionally, the horizontal ground distance can be obtained as

$$\dot{s} = V\cos\gamma + W_e\sin\Psi + W_n\cos\Psi - \omega_e R\cos\gamma\sin\Psi \tag{A.24}$$

A.2.2 Different Expressions of Wind Components

The wind speed can be expressed in following ways

$$\vec{W} = W_i\hat{i} + W_j\hat{j} + W_k\hat{k} \tag{A.25}$$

$$= W_e\hat{e} + W_n\hat{n} + W_u\hat{u} \tag{A.26}$$

Using Eq. (7)

$$\begin{aligned}\begin{bmatrix} W_i & W_j & W_k \end{bmatrix}\begin{bmatrix} \hat{i} \\ \hat{j} \\ \hat{k} \end{bmatrix} &= \begin{bmatrix} W_e & W_n & W_u \end{bmatrix}\begin{bmatrix} \hat{e} \\ \hat{n} \\ \hat{u} \end{bmatrix} \\ &= \begin{bmatrix} W_e & W_n & W_u \end{bmatrix}\begin{bmatrix} \cos\gamma\sin\Psi & -\cos\Psi & -\sin\gamma\sin\Psi \\ \cos\gamma\cos\Psi & \sin\Psi & -\sin\gamma\cos\Psi \\ \sin\gamma & 0 & \cos\gamma \end{bmatrix}\begin{bmatrix} \hat{i} \\ \hat{j} \\ \hat{k} \end{bmatrix}\end{aligned} \tag{A.27}$$

$\Rightarrow$

$$W_i = \cos\gamma\sin\Psi W_e + \cos\gamma\cos\Psi W_n + \sin\gamma W_u \tag{A.28}$$

$$W_j = -\cos\Psi W_e + \sin\Psi W_n \tag{A.29}$$

$$W_k = -\sin\gamma\sin\Psi W_e - \sin\gamma\cos\Psi W_n + \cos\gamma W_u \tag{A.30}$$

A.3 Velocity Expressions

A.3.1 Earth-Relative Velocity

The earth-relative velocity can be expressed as

$$\vec{V}_e = \vec{V} + \vec{W} \tag{A.31}$$

In terms of $(\hat{e}, \hat{n}, \hat{u})$ system, the Eq. (21)

$$\vec{V}_e = (V\cos\gamma\sin\Psi + W_e)\hat{e} + (V\cos\gamma\cos\Psi + W_n)\hat{n} + (V\sin\gamma + W_u)\hat{u} \tag{A.32}$$

In terms of $(\hat{i}, \hat{j}, \hat{k})$ system

$$\vec{V} = V\hat{i} \tag{A.33}$$

so

$$\begin{aligned}
\vec{V}_e =& (V + W_i)\hat{i} + W_j\hat{j} + W_k\hat{k} && \text{(A.34)}\\
=& (V + W_e\cos\gamma\sin\Psi + W_n\cos\gamma\cos\Psi + W_u\sin\gamma)\hat{i} && \text{(A.35)}\\
&+ (-W_e\cos\Psi + W_n\sin\Psi)\hat{j} && \text{(A.36)}\\
&+ (-W_e\sin\gamma\sin\Psi - W_n\sin\gamma\cos\Psi + W_u\cos\gamma)\hat{k} && \text{(A.37)}
\end{aligned}$$

A.3.2 Inertial Velocity

Inertial velocity can be expressed as

$$\vec{V}_I = \vec{V}_e + \vec{V}_{e/I} \tag{A.38}$$

where

$$\begin{aligned}
\vec{V}_{e/I} &= (\omega_e\hat{K}) \times (R + h)\hat{u} && \text{(A.39)}\\
&= \omega_e(R + h)[\cos\lambda\hat{n} + \sin\lambda\hat{u}] \times \hat{u} && \text{(A.40)}\\
&= \omega_e(R + h)\cos\lambda\hat{e} && \text{(A.41)}
\end{aligned}$$

or

$$\vec{V}_{e/I} = \omega_e(R+h)\cos\lambda[\cos\gamma\sin\Psi\hat{i} - \cos\Psi\hat{j} - \sin\gamma\sin\Psi\hat{k}] \tag{A.42}$$

Define

$$W_e^R = W_e + \omega_e(R+h)\cos\lambda \tag{A.43}$$

Then, in terms of $(\hat{e}, \hat{n}, \hat{u})$ system

$$\vec{V}_I = (V\cos\gamma\sin\Psi + W_e^R)\hat{e} + (V\cos\gamma\cos\Psi + W_n)\hat{n} + (V\sin\gamma + W_u)\hat{u} \tag{A.44}$$

$$= V_{Ie}\hat{e} + V_{In}\hat{n} + V_{Iu}\hat{u} \tag{A.45}$$

Then, in terms of $(\hat{i}, \hat{j}, \hat{k})$ system

$$\vec{V}_I = (V + W_e^R\cos\gamma\sin\Psi + W_n\cos\gamma\cos\Psi + W_u\sin\gamma)\hat{i} \tag{A.46}$$

$$+ (-W_e^R\cos\Psi + W_n\sin\Psi)\hat{j} \tag{A.47}$$

$$+ (-W_e^R\sin\gamma\sin\Psi - W_n\sin\gamma\cos\Psi + W_u\cos\gamma) \tag{A.48}$$

$$= V_{Ii}\hat{i} + V_{Ij}\hat{j} + V_{Ik}\hat{k} \tag{A.49}$$

A.4 External Forces

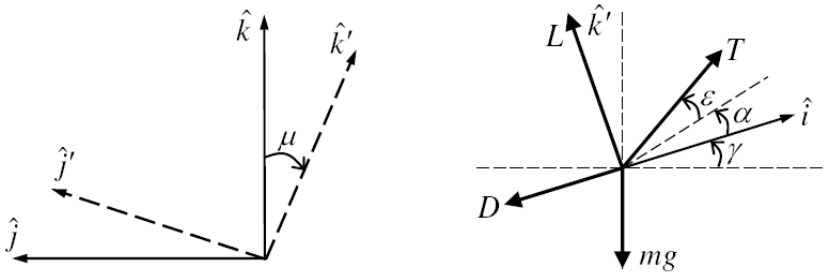

Figure A.2: External forces of aircraft

From the figure,

$$\hat{k}' = -\sin\mu\hat{j} + \cos\mu\hat{k} \tag{A.50}$$

Assuming zero slide force: $Y = 0$, then

$$\vec{F} = \vec{T} + \vec{D} + \vec{L} + m\vec{g} + \vec{Y} \tag{A.51}$$

where

$$\vec{T} = T\cos(\alpha+\epsilon)\hat{i} + T\sin(\alpha+\epsilon)\hat{k}' \tag{A.52}$$

$$= T\cos(\alpha+\epsilon)\hat{i} - T\sin(\alpha+\epsilon)\sin\mu\hat{j} + T\sin(\alpha+\epsilon)\cos\mu\hat{k} \tag{A.53}$$

$$\vec{L} = L\hat{k}' \tag{A.54}$$

$$= -L\sin\mu\hat{j} + L\cos\mu\hat{k} \tag{A.55}$$

$$\vec{D} = -D\hat{i} \tag{A.56}$$

$$m\vec{g} = -mg\hat{u} = -mg(\sin\gamma\hat{i} + \cos\gamma\hat{k}) \tag{A.57}$$

In terms of $(\hat{i},\hat{j},\hat{k})$ system

$$\vec{F} = F_i\hat{i} + F_j\hat{j} + F_k\hat{k} \tag{A.58}$$

$$=[T\cos(\alpha+\epsilon) - D - mg\sin\gamma]\hat{i} \tag{A.59}$$

$$-[L + T\sin(\alpha+\epsilon)]\sin\mu\hat{j} \tag{A.60}$$

$$+\{[L + T\sin(\alpha+\epsilon)]\cos\mu - mg\cos\gamma\}\hat{k} \tag{A.61}$$

In terms of $(\hat{e},\hat{n},\hat{u})$ system

$$\vec{F} = F_e\hat{e} + F_n\hat{n} + F_u\hat{u} \tag{A.62}$$

We have

$$\begin{bmatrix} F_e & F_n & F_u \end{bmatrix} = \begin{bmatrix} F_i & F_j & F_K \end{bmatrix} \begin{bmatrix} \cos\gamma\sin\Psi & \cos\gamma\cos\Psi & \sin\gamma \\ -\cos\Psi & \sin\Psi & 0 \\ -\sin\gamma\sin\Psi & -\sin\gamma\cos\Psi & \cos\gamma \end{bmatrix} \tag{A.63}$$

or

$$F_e = F_i\cos\gamma\sin\Psi - F_j\cos\Psi - F_k\sin\gamma\sin\Psi \tag{A.64}$$

$$F_n = F_i\cos\gamma\cos\Psi + F_j\sin\Psi - F_k\sin\gamma\cos\Psi \tag{A.65}$$

$$F_u = F_i\sin\gamma + F_k\cos\gamma \tag{A.66}$$

A.5 Kinetics

We are interested in the time rates of airspeed component, but the Newton's Law is given in inertial frame

A.5.1 Angular Rates

Angular velocity of $(\hat{I}, \hat{J}, \hat{K})$ w.r.t $(\hat{I}_s, \hat{J}_s, \hat{K}_s)$ is

$$\vec{\omega}_e = \omega_e \hat{K} \tag{A.67}$$

$$= \omega_e(\cos\gamma\hat{n} + \sin\gamma\hat{u}) \tag{A.68}$$

Angular velocity of $(\hat{e}, \hat{n}, \hat{u})$ w.r.t $(\hat{I}, \hat{J}, \hat{K})$ is

$$\vec{\Omega}_{enu} = \dot{l}\hat{K} - \dot{\lambda}\hat{e} \tag{A.69}$$

$$= -\dot{\lambda}\hat{e} + \dot{l}\cos\lambda\hat{n} + \dot{l}\sin\lambda\hat{u} \tag{A.70}$$

Angular velocity of $(\hat{i}, \hat{j}, \hat{k})$ w.r.t $(\hat{e}, \hat{n}, \hat{u})$ is

$$\vec{\omega}_{ijk} = \dot{\Psi}\hat{u} - \dot{\gamma}\hat{j} \tag{A.71}$$

$$= -\dot{\Psi}\sin\gamma\hat{i} - \dot{\gamma}\hat{j} - \dot{\Psi}\cos\gamma\hat{k} \tag{A.72}$$

$$= \dot{\gamma}\cos\Psi\hat{e} - \dot{\gamma}\sin\Psi\hat{n} - \dot{\Psi}\hat{u} \tag{A.73}$$

Angular velocity of of $(\hat{i}, \hat{j}, \hat{k})$ w.r.t $(\hat{I}, \hat{J}, \hat{K})$ is

$$\vec{\Omega}_{ijk} = \vec{\Omega}_{enu} + \vec{\omega_{ijk}} \tag{A.74}$$

$$= (-\dot{\lambda} + \dot{\gamma}\cos\Psi)\hat{e} + (\dot{l}\cos\lambda - \dot{\gamma}\sin\Psi)\hat{n} + (\dot{l}\sin\gamma - \dot{\Psi})\hat{u} \tag{A.75}$$

And

$$\vec{V}_{e/I} = \omega_e(R + h)\cos\lambda\hat{e} \tag{A.76}$$

$$\vec{\omega}_e + \vec{\Omega}_{enu} = -\dot{\lambda}\hat{e} + (\omega_e + \dot{l})\cos\lambda\hat{n} + (\omega_e + \dot{l})\sin\lambda\hat{u} \tag{A.77}$$

A.5.2 Velocity Relations

$$\vec{V}_e = \vec{V} + \vec{W} \tag{A.78}$$

$$\vec{V}_I = \vec{V}_e + \vec{V}_{e/I} = \vec{V} + \vec{W} + \vec{V}_{e/I} = \vec{V} + \vec{W}^R \tag{A.79}$$

where

$$\vec{V} = V\hat{i} = V\cos\gamma\sin\Psi\hat{e} + V\cos\gamma\cos\Psi\hat{n} + v\sin\gamma\hat{u} \tag{A.80}$$

$$\vec{W}^R = W_e^R\hat{e} + W_n^R\hat{n} + W_u^R\hat{u} \tag{A.81}$$

$$W_e^R = W_e + \omega_e(R+h)\cos\lambda \tag{A.82}$$

In terms of $(\hat{i},\hat{j},\hat{k})$

$$\vec{W}^R = (W_e^R\cos\gamma\sin\Psi + W_n\cos\gamma\cos\Psi + W_u\sin\gamma)\hat{i} \tag{A.83}$$

$$+ (-W_e^R\cos\Psi + W_n\sin\Psi)\hat{j} \tag{A.84}$$

$$+ (-W_e^R\sin\gamma\sin\Psi - W_n\sin\gamma\cos\Psi + W_u\cos\gamma) \tag{A.85}$$

$$= W_i^R\hat{i} + W_j^R\hat{j} + W_k^R\hat{k} \tag{A.86}$$

A.5.3 Newton's Law for Constant Mass

$$(\frac{d\vec{V}_I}{dt})_{I_sJ_sK_s} = \frac{\vec{F}}{m} \tag{A.87}$$

where

$$(\frac{d\vec{V}_I}{dt})_{I_sJ_sK_s} = (\frac{d\vec{V}_I}{dt})_{IJK} + \vec{\omega}_e \times \vec{V}_I \tag{A.88}$$

$$(\frac{d\vec{V}_I}{dt})_{IJK} = (\frac{d\vec{V}_I}{dt})_{enu} + \vec{\Omega}_{enu} \times \vec{V}_I \tag{A.89}$$

$\Rightarrow$

$$(\frac{d\vec{V}_I}{dt})_{enu} + (\vec{\omega}_e + \vec{\Omega}_{enu}) \times \vec{V}_I = \frac{\vec{F}}{m} \tag{A.90}$$

or

$$(\frac{d\vec{V}_I}{dt})_{enu} + (\frac{d\vec{W}}{dt})_{enu} + (\frac{d\vec{V}_{e/I}}{dt})_{enu} = \frac{\vec{F}}{m} - (\vec{\omega}_e + \vec{\Omega}_{enu}) \times \vec{V}_I \tag{A.91}$$

$\Rightarrow$

$$\boxed{(\frac{d\vec{V}_I}{dt})_{enu} = \frac{\vec{F}}{m} - (\frac{d\vec{W}}{dt})_{enu} - \vec{A}} \tag{A.92}$$

where

$$\boxed{\vec{A} = (\frac{d\vec{V}_{e/I}}{dt})_{enu} + (\vec{\omega}_e + \vec{\Omega}_{enu}) \times \vec{V}_I} \tag{A.93}$$

A.5.4 Expressing in $(\hat{i}, \hat{j}, \hat{k})$

$$(\frac{d\vec{V}_I}{dt})_{enu} = (\frac{d\vec{V}_I}{dt})_{ijk} + \vec{\omega}_{ijk} \times \vec{V} \tag{A.94}$$

$$= \dot{V}\hat{i} + [-\dot{\Psi}\sin\gamma\hat{i} - \dot{\gamma}\hat{j} - \dot{\Psi}\cos\gamma\hat{k}] \times V\hat{i} \tag{A.95}$$

$$= \dot{V}\hat{i} + V\dot{\gamma}\hat{k} - V\cos\gamma\dot{\Psi}\hat{j} \tag{A.96}$$

$$\vec{F} = F_i\hat{i} + F_j\hat{j} + F_k\hat{k} \tag{A.97}$$

$$(\frac{d\vec{W}}{dt})_{enu} = \dot{W}_e\hat{e} + \dot{W}_n\hat{n} + \dot{W}_u\hat{u} \tag{A.98}$$

$$= [\dot{W}_e\dot{W}_n\dot{W}_u] \begin{bmatrix} \cos\gamma\sin\Psi & -\cos\Psi & -\sin\gamma\sin\Psi \\ \cos\gamma\cos\Psi & \sin\Psi & -\sin\gamma\cos\Psi \\ \sin\gamma & 0 & \cos\gamma \end{bmatrix} \begin{bmatrix} \hat{i} \\ \hat{j} \\ \hat{k} \end{bmatrix} \tag{A.99}$$

$$= (\dot{W}_e\cos\gamma\sin\Psi + \dot{W}_n\cos\gamma\cos\Psi + \dot{W}_u\sin\gamma)\hat{i} \tag{A.100}$$

$$+ (-\dot{W}_e\cos\Psi + \dot{W}_n\sin\Psi)\hat{j} \tag{A.101}$$

$$+ (-\dot{W}_e\sin\gamma\sin\Psi - \dot{W}_n\sin\gamma\cos\Psi + \dot{W}_u\cos\gamma)\hat{k} \tag{A.102}$$

$$\boxed{\begin{aligned} \vec{A} &= (\frac{d\vec{V}_{e/I}}{dt})_{enu} + (\vec{\omega}_e + \vec{\Omega}_{enu}) \times \vec{V}_I \\ &= a_i\hat{i} + a_j\hat{j} + a_k\hat{k} \end{aligned}} \tag{A.103}$$

a_i, a_j, a_k are due to Earth rotation & Coriolis Force & spherical earth.

Then we have

$$\boxed{\begin{aligned}
\dot{V} &= \frac{T\cos(\alpha+\epsilon)-D}{m} - g\sin\gamma - \dot{W}_e\cos\gamma\sin\Psi - \dot{W}_n\cos\gamma\cos\Psi - \dot{W}_u\sin\gamma - a_i \\
V\cos\gamma\dot{\Psi} &= \frac{L+T\sin(\alpha+\epsilon)}{m}\sin\mu - \dot{W}_e\cos\Psi + \dot{W}_n\sin\Psi + a_j \\
V\dot{\gamma} &= \frac{L+T\sin(\alpha+\epsilon)}{m}\cos\mu - g\cos\gamma + \dot{W}_e\sin\gamma\sin\Psi + \dot{W}_n\sin\gamma\cos\Psi - \dot{W}_u\cos\gamma - a_k
\end{aligned}} \tag{A.104}$$

A.5.5 Derivations of the A term

$$\vec{A} = (\frac{d\vec{V}_{e/I}}{dt})_{enu} + (\vec{\omega}_e + \vec{\Omega}_{enu}) \times \vec{V}_I \tag{A.105}$$

$$= (\frac{d\vec{V}_{e/I}}{dt})_{enu} + \vec{\omega}_e \times (\vec{V} + \vec{W} + \vec{V}_{e/I}) + \vec{\Omega} \times \vec{V}_{e/I} + \vec{\Omega}_e \times (\vec{V} + \vec{W}) \tag{A.106}$$

where, the term $(\frac{d\vec{V}_{e/I}}{dt})_{enu} + \vec{\omega}_e \times (\vec{V} + \vec{W} + \vec{V}_{e/I})$ comes from earth rotation; $\vec{\Omega} \times \vec{V}_{e/I} + \vec{\Omega}_e \times (\vec{V} + \vec{W})$ comes from spherical earth

from Eq. (44)

$$(\frac{d\vec{V}_{e/I}}{dt})_{enu} = \omega_e[\dot{h}\cos\lambda - \dot{\lambda}(R+h)\sin\lambda]\hat{e} \tag{A.107}$$

$$= \omega_e[\dot{h}\cos\lambda - \dot{\lambda}(R+h)\sin\lambda](\cos\gamma\sin\Psi\hat{i} - \cos\Psi\hat{j} - \sin\gamma\sin\Psi\hat{k}) \tag{A.108}$$

$$\vec{\omega}_e + \vec{\Omega}_{enu} = -\dot{\lambda}\hat{e} + (\omega_e + \dot{l})\cos\lambda\hat{n} + (\omega_e + \dot{l})\sin\lambda\hat{u} \tag{A.109}$$

We have

$$(\vec{\omega}_e + \vec{\Omega}_{enu}) \times \vec{V}_I = \begin{bmatrix} \hat{e} & \hat{n} & \hat{u} \\ -\dot{\lambda} & (\omega_e + \dot{l})\cos\lambda & (\omega_e + \dot{l})\sin\lambda \\ V_{Ie} & V_{In} & V_{Iu} \end{bmatrix} \tag{A.110}$$

$$= (\omega_e + \dot{l})(V_{Iu}\cos\lambda - V_{In}\sin\lambda)\hat{e} \tag{A.111}$$

$$+ [(\omega_e + \dot{l})V_{Ie}\sin\lambda + \dot{\lambda}V_{Iu}]\hat{n} \tag{A.112}$$

$$- [\dot{\lambda}V_{In} + (\omega_e + \dot{l})V_{Ie}\cos\lambda]\hat{u} \tag{A.113}$$

$$= b_e\hat{e} + b_n\hat{n} + b_u\hat{u} \tag{A.114}$$

$$= b_i\hat{i} + b_j\hat{j} + b_k\hat{k} \tag{A.115}$$

$\Rightarrow$

$$\boxed{\begin{aligned} a_e &= \omega_e[\dot{h}\cos\lambda - \dot{\lambda}(R+h)\sin\lambda] + b_e \\ a_n &= b_n \\ a_u &= b_u \end{aligned}} \tag{A.116}$$

Also, substitute Eq. (47) into Eq. (117)-(119)

$$(\vec{\omega}_e + \vec{\Omega}_{enu}) \times \vec{V}_I \tag{A.117}$$

$$= (\omega_e + \dot{l})[\cos\lambda(V\sin\gamma + W_u) - \sin\lambda(V\cos\gamma\cos\Psi + W_n)]\hat{e} \tag{A.118}$$

$$+ [(\omega_e + \dot{l})\sin\lambda(V\cos\gamma\sin\Psi + W_e^R) + \dot{\lambda}(V\sin\gamma + W_u)]\hat{n} \tag{A.119}$$

$$- [\dot{\lambda}(V\cos\gamma\cos\Psi + W_n) + (\omega_e + \dot{l})\cos\lambda(V\cos\gamma\sin\Psi + W_e^R)]\hat{u} \tag{A.120}$$

$$= b_e\hat{e} + b_n\hat{n} + b_u\hat{u} \tag{A.121}$$

$$= b_i\hat{i} + b_j\hat{j} + b_k\hat{k} \tag{A.122}$$

$\Rightarrow$

$$\boxed{\begin{aligned} b_e &= (\omega_e + \dot{l})[\cos\lambda(V\sin\gamma + W_u) - \sin\lambda(V\cos\gamma\cos\Psi + W_n)] \\ b_n &= (\omega_e + \dot{l})\sin\lambda(V\cos\gamma\sin\Psi + W_e^R) + \dot{\lambda}(V\sin\gamma + W_u) \\ b_u &= -(\omega_e + \dot{l})\cos\lambda(V\cos\gamma\sin\Psi + W_e^R) - \dot{\lambda}(V\cos\gamma\cos\Psi + W_n) \end{aligned}} \tag{A.123}$$

using transformation

$$\begin{bmatrix} b_i & b_j & b_k \end{bmatrix} = \begin{bmatrix} b_e & b_n & b_u \end{bmatrix} \begin{bmatrix} \cos\gamma\sin\Psi & -\cos\Psi & -\sin\gamma\sin\Psi \\ \cos\gamma\cos\Psi & \sin\Psi & -\sin\gamma\cos\Psi \\ \sin\gamma & 0 & \cos\gamma \end{bmatrix} \tag{A.124}$$

we have

$$b_i = b_e\cos\gamma\sin\Psi + b_n\cos\gamma\cos\Psi + b_u\sin\gamma \tag{A.125}$$

$$b_j = -b_e\cos\Psi + b_n\sin\Psi \tag{A.126}$$

$$b_k = -b_e\sin\gamma\sin\Psi - b_n\sin\gamma\cos\Psi + b_u\cos\gamma \tag{A.127}$$

therefore

$$\boxed{\begin{aligned} a_i &= \omega_e[\dot{h}\cos\lambda - \dot{\lambda}(R+h)\sin\lambda]\cos\lambda\sin\Psi + b_i \\ &= \{\omega_e[\dot{h}\cos\lambda - \dot{\lambda}(R+h)\sin\lambda] + b_e\}\cos\gamma\sin\Psi + b_n\cos\gamma\cos\Psi + b_u\sin\gamma \\ a_j &= -\omega_e[\dot{h}\cos\lambda - \dot{\lambda}(R+h)\sin\lambda]\cos\Psi + b_j \\ &= -\{\omega_e[\dot{h}\cos\lambda - \dot{\lambda}(R+h)\sin\lambda] + b_e\}\cos\Psi + b_n\sin\Psi \\ a_k &= -\{\omega_e[\dot{h}\cos\lambda - \dot{\lambda}(R+h)\sin\lambda] + b_e\}\sin\gamma\sin\Psi - b_n\sin\gamma\cos\Psi + b_u\cos\gamma \end{aligned}} \tag{A.128}$$

A.5.6 Note

$$\omega_e[\dot{h}\cos\lambda - \dot{\lambda}(R+h)\sin\lambda] = \omega_e[(V\sin\gamma + W_u)\cos\lambda - (V\cos\gamma\cos\Psi + W_n)\sin\lambda] \tag{A.129}$$

Therefore

$$\boxed{\begin{aligned} \hat{b}_e &= \omega_e[\dot{h}\cos\lambda - \dot{\lambda}(R+h)\sin\lambda] + b_e \\ &= (2\omega_e + \dot{l})[(V\sin\gamma + W_u)\cos\lambda - (V\cos\gamma\cos\Psi + W_n)\sin\lambda] \end{aligned}} \tag{A.130}$$

and

$$a_i = \hat{b}_e\cos\gamma\sin\Psi + b_n\cos\gamma\cos\Psi + b_u\sin\gamma \tag{A.131}$$

$$a_j = -\hat{b}_e\cos\Psi + b_n\sin\Psi \tag{A.132}$$

$$a_k = -\hat{b}_e\sin\gamma\sin\Psi - b_n\sin\gamma\cos\Psi + b_u\cos\gamma \tag{A.133}$$

then combing with the wind acceleration terms,

$$\boxed{\begin{aligned} A_V &= (\dot{W}_e + \hat{b}_e)\cos\gamma\sin\Psi + (\dot{W}_n + b_n)\cos\gamma\cos\Psi + (\dot{W}_u + b_u)\sin\gamma \\ A_\Psi &= -(\dot{W}_e + \hat{b}_e)\cos\Psi + (\dot{W}_n + b_n)\sin\Psi \\ A_\gamma &= -(\dot{W}_e + \hat{b}_e)\sin\gamma\sin\Psi - (\dot{W}_n + b_n)\sin\gamma\cos\Psi + (\dot{W}_u + b_u)\cos\gamma \end{aligned}} \tag{A.134}$$

Then the kinetic equations become

$$\dot{V} = \frac{T\cos(\alpha+\epsilon) - D}{m} - g\sin\gamma - A_V \tag{A.135}$$

$$V\cos\gamma\dot{\Psi} = \frac{L + T\sin(\alpha+\epsilon)}{m}\sin\mu + A_\Psi \tag{A.136}$$

$$V\dot{\gamma} = \frac{L + T\sin(\alpha+\epsilon)}{m}\cos\mu - g\cos\gamma - A_\gamma \tag{A.137}$$

checks with Vinh's equations under zero winds. Note Ψ is defined from North here

A.5.7 Complete List of Equations

$$\boxed{\begin{aligned} \dot{V} &= \frac{T\cos(\alpha+\epsilon) - D}{m} - g\sin\gamma - A_V \\ V\cos\gamma\dot{\Psi} &= \frac{L + T\sin(\alpha+\epsilon)}{m}\sin\mu + A_\Psi \\ V\dot{\gamma} &= \frac{L + T\sin(\alpha+\epsilon)}{m}\cos\mu - g\cos\gamma - A_\gamma \\ \dot{l} &= \frac{V\cos\gamma\sin\Psi + W_e}{(R+h)\cos\lambda} \\ \dot{\lambda} &= \frac{V\cos\gamma\cos\Psi + W_n}{R+h} \\ \dot{h} &= V\sin\gamma + W_u \\ \dot{s} &= V\cos\gamma + W_e\sin\Psi + W_n\cos\Psi - \omega_e R\cos\gamma\sin\Psi \end{aligned}} \tag{A.138}$$

where

$$L = \frac{1}{2}\rho V^2 S C_L \tag{A.139}$$

$$D = \frac{1}{2}\rho V^2 S C_D \tag{A.140}$$

$$C_D = C_{D_0} + K C_L^2 \tag{A.141}$$

and

$$\boxed{\begin{aligned} W_e^R &= W_e + \omega_e(R+h)\cos\lambda \\ B_e &= \dot{W}_e + (2\omega_e + \dot{l})[(V\sin\gamma + W_u)\cos\lambda - (V\cos\gamma\cos\Psi + W_n)\sin\lambda] \\ B_n &= \dot{W}_n + (\omega_e + \dot{l})(V\cos\gamma\sin\Psi + W_e^R)\sin\lambda + \dot{\lambda}(V\sin\gamma + W_u) \\ B_u &= \dot{W}_u - (\omega_e + \dot{l})(V\cos\gamma\sin\Psi + W_e^R)\cos\lambda - \dot{\lambda}(V\cos\gamma\cos\Psi + W_n) \end{aligned}} \tag{A.142}$$

$$\boxed{\begin{aligned} A_v &= B_e\cos\gamma\sin\Psi + B_n\cos\gamma\cos\Psi + B_u\sin\gamma \\ A_\Psi &= -B_e\cos\Psi + B_n\sin\Psi \\ A_\gamma &= -B_e\sin\gamma\sin\Psi - B_n\sin\gamma\cos\Psi + B_u\cos\gamma \end{aligned}} \tag{A.143}$$

Assuming wind dependence $W_e(l,\lambda,h), W_n(l,\lambda,h), W_u(l,\lambda,h)$, then

$$A_V(V,\Psi,\gamma,l,\lambda,h;\omega_e,R) \tag{A.144}$$

$$A_\Psi(V,\Psi,\gamma,l,\lambda,h;\omega_e,R) \tag{A.145}$$

$$A_\gamma(V,\Psi,\gamma,l,\lambda,h;\omega_e,R) \tag{A.146}$$

1.
   - if winds also depend on time, $\Rightarrow$ time dependence included
   - if winds only depend on h, or both (λ,h), $\Rightarrow$ l dependence drops
   - in general,
   $$\dot{W}_e = \frac{\partial W_e}{\partial l}\dot{l} + \frac{\partial W_e}{\partial \lambda}\dot{\lambda} + \frac{\partial W_e}{\partial h}\dot{h} \tag{A.147}$$
2. non-rotating earth assumption, $\Rightarrow \omega_e = 0$
3. flat earth, $R \to \infty, \dot{l} \approx 0, \dot{\lambda} \approx 0$, then use
   $$\dot{x} = V\cos\gamma\sin\Psi + W_e \tag{A.148}$$
   $$\dot{y} = V\cos\gamma\sin\Psi + W_n \tag{A.149}$$
4. rotating earth, $\omega_e \neq 0$, V large or small, W large or small

Appendix B

Derivation of Normalized Wind Components:

The necessary terms of normalized wind components have been obtained through the definition of Laplacien,

$$\frac{(\ )}{\partial\bar{\Delta}} = \bar{W}_x\frac{(\ )}{\partial\bar{x}} + \bar{W}_y\frac{(\ )}{\partial\bar{y}} + \bar{W}_h\frac{(\ )}{\partial\bar{h}} + \frac{(\ )}{\partial\bar{t}} \tag{B.1}$$

where normalized wind components can be expressed as

$$\begin{aligned}
\frac{\partial\bar{W}_x}{\partial\bar{\Delta}} &= \bar{W}_x\frac{\partial\bar{W}_x}{\partial\bar{x}} + \bar{W}_y\frac{\partial\bar{W}_x}{\partial\bar{y}} + \bar{W}_h\frac{\partial\bar{W}_x}{\partial\bar{h}} + \frac{\partial\bar{W}_x}{\partial\bar{t}} \\
\frac{\partial\bar{W}_y}{\partial\bar{\Delta}} &= \bar{W}_x\frac{\partial\bar{W}_y}{\partial\bar{x}} + \bar{W}_y\frac{\partial\bar{W}_y}{\partial\bar{y}} + \bar{W}_h\frac{\partial\bar{W}_y}{\partial\bar{h}} + \frac{\partial\bar{W}_y}{\partial\bar{t}} \\
\frac{\partial\bar{W}_h}{\partial\bar{\Delta}} &= \bar{W}_x\frac{\partial\bar{W}_h}{\partial\bar{x}} + \bar{W}_y\frac{\partial\bar{W}_h}{\partial\bar{y}} + \bar{W}_h\frac{\partial\bar{W}_h}{\partial\bar{h}} + \frac{\partial\bar{W}_h}{\partial\bar{t}}
\end{aligned} \tag{B.2}$$

Then one can obtain the $\bar{W}_x'$,$\bar{W}_y'$ and $\bar{W}_h'$ as follows

$$
\begin{aligned}
\dot{W}_x &= \frac{\partial W_x}{\partial x}\dot{x} + \frac{\partial W_x}{\partial y}\dot{y} + \frac{\partial W_x}{\partial h}\dot{h} + \frac{\partial W_x}{\partial t} \\
\bar{W}'_x &= \frac{d\bar{W}_x}{d\tau} = t_n \frac{d\bar{W}_x}{dt} = t_n \frac{d(W_x/V_n)}{dt} = \frac{t_n}{V_n}\dot{W}_x \\
\bar{W}'_x &= \left(\frac{t_n}{V_n}\right)\left(\frac{\partial W_x}{\partial x}\dot{x} + \frac{\partial W_x}{\partial y}\dot{y} + \frac{\partial W_x}{\partial h}\dot{h} + \frac{\partial W_x}{\partial t}\right) \\
\bar{W}'_x = \left(\frac{1}{g}\right)&\left(\frac{\partial\left(\bar{W}_x V_n\right)}{\partial\left(\bar{x}\frac{V_n^2}{g}\right)}\left(V cos(\gamma) sin(\Psi) + W_x\right) + \frac{\partial\left(\bar{W}_x V_n\right)}{\partial\left(\bar{y}\frac{V_n^2}{g}\right)}\left(V cos(\gamma) cos(\Psi) + W_y\right)\right. \\
&\left. + \frac{\partial\left(\bar{W}_x V_n\right)}{\partial\left(\bar{h}\frac{V_n^2}{g}\right)}\left(V sin(\gamma) + W_h\right) + \frac{\partial\left(\bar{W}_x V_n\right)}{\partial(\bar{t}\ t_n)}\right)
\end{aligned}
\tag{B.3}
$$

$$
\begin{aligned}
\bar{W}'_x = \left(\frac{1}{g}\right)&\left[g\frac{\partial\bar{W}_x}{\partial\bar{x}}\left(\frac{V}{V_n}cos(\gamma)sin(\Psi) + \frac{W_x}{V_n}\right) + g\frac{\partial\bar{W}_x}{\partial\bar{y}}\left(\frac{V}{V_n}cos(\gamma)cos(\Psi) + \frac{W_y}{V_n}\right)\right. \\
&\left. + g\frac{\partial\bar{W}_x}{\partial\bar{h}}\left(\frac{V}{V_n}sin(\gamma) + \frac{W_h}{V_n}\right) + \left(\frac{V_n}{t_n}\right)\frac{\partial\bar{W}_x}{\partial\bar{t}}\right]
\end{aligned}
\tag{B.4}
$$

$$
\begin{aligned}
\bar{W}'_x =& \frac{\partial\bar{W}_x}{\partial\bar{x}}\left(\bar{V}cos(\gamma)sin(\Psi) + \bar{W}_x\right) + \frac{\partial\bar{W}_x}{\partial\bar{y}}\left(\bar{V}cos(\gamma)cos(\Psi) + \bar{W}_y\right) \\
&+ \frac{\partial\bar{W}_x}{\partial\bar{h}}\left(\bar{V}sin(\gamma) + \bar{W}_h\right) + \frac{\partial\bar{W}_x}{\partial\bar{t}}
\end{aligned}
\tag{B.5}
$$

Same analogy holds for $\bar{W}'_y$ as well

$$
\begin{aligned}
\dot{W}_y &= \frac{\partial W_y}{\partial x}\dot{x} + \frac{\partial W_y}{\partial y}\dot{y} + \frac{\partial W_y}{\partial h}\dot{h} + \frac{\partial W_y}{\partial t} \\
\bar{W}'_y &= \frac{d\bar{W}_y}{d\tau} = t_n\frac{d\bar{W}_y}{dt} = t_n\frac{d(W_y/V_n)}{dt} = \frac{t_n}{V_n}\dot{W}_y \\
\bar{W}'_y &= \left(\frac{t_n}{V_n}\right)\left(\frac{\partial W_y}{\partial x}\dot{x} + \frac{\partial W_y}{\partial y}\dot{y} + \frac{\partial W_y}{\partial h}\dot{h} + \frac{\partial W_y}{\partial t}\right) \\
\bar{W}'_y = \left(\frac{1}{g}\right)&\left(\frac{\partial\left(\bar{W}_y V_n\right)}{\partial\left(\bar{x}\frac{V_n^2}{g}\right)}\left(V cos(\gamma)sin(\Psi) + W_x\right) + \frac{\partial\left(\bar{W}_y V_n\right)}{\partial\left(\bar{y}\frac{V_n^2}{g}\right)}\left(V cos(\gamma)cos(\Psi) + W_y\right)\right. \\
&\left. + \frac{\partial\left(\bar{W}_y V_n\right)}{\partial\left(\bar{h}\frac{V_n^2}{g}\right)}\left(V sin(\gamma) + W_h\right) + \frac{\partial\left(\bar{W}_y V_n\right)}{\partial(\bar{t}\ t_n)}\right)
\end{aligned}
\tag{B.6}
$$

$$
\begin{aligned}
\bar{W}'_y = \left(\frac{1}{g}\right)&\left[g\frac{\partial\bar{W}_y}{\partial\bar{x}}\left(\frac{V}{V_n}cos(\gamma)sin(\Psi) + \frac{W_x}{V_n}\right) + g\frac{\partial\bar{W}_y}{\partial\bar{y}}\left(\frac{V}{V_n}cos(\gamma)cos(\Psi) + \frac{W_y}{V_n}\right)\right. \\
&\left. + g\frac{\partial\bar{W}_y}{\partial\bar{h}}\left(\frac{V}{V_n}sin(\gamma) + \frac{W_h}{V_n}\right) + \left(\frac{V_n}{t_n}\right)\frac{\partial\bar{W}_y}{\partial\bar{t}}\right]
\end{aligned}
\tag{B.7}
$$

$$
\begin{aligned}
\bar{W}'_y = &\frac{\partial\bar{W}_y}{\partial\bar{x}}\left(\bar{V}cos(\gamma)sin(\Psi) + \bar{W}_x\right) + \frac{\partial\bar{W}_y}{\partial\bar{y}}\left(\bar{V}cos(\gamma)cos(\Psi) + \bar{W}_y\right) \\
&+ \frac{\partial\bar{W}_y}{\partial\bar{h}}\left(\bar{V}sin(\gamma) + \bar{W}_h\right) + \frac{\partial\bar{W}_y}{\partial\bar{t}}
\end{aligned}
\tag{B.8}
$$

Finally, for $\bar{W}'_h$, one gets

$$
\begin{aligned}
\dot{W}_h =& \frac{\partial W_h}{\partial x}\dot{x} + \frac{\partial W_h}{\partial y}\dot{y} + \frac{\partial W_h}{\partial h}\dot{h} + \frac{\partial W_h}{\partial t} \\
\bar{W}'_h =& \frac{d\bar{W}_h}{d\tau} = t_n \frac{d\bar{W}_h}{dt} = t_n \frac{d(W_h/V_n)}{dt} = \frac{t_n}{V_n}\dot{W}_h \\
\bar{W}'_h =& \left(\frac{t_n}{V_n}\right)\left(\frac{\partial W_h}{\partial x}\dot{x} + \frac{\partial W_h}{\partial y}\dot{y} + \frac{\partial W_h}{\partial h}\dot{h} + \frac{\partial W_h}{\partial t}\right) \\
\bar{W}'_h = \left(\frac{1}{g}\right)&\left(\frac{\partial\left(\bar{W}_h V_n\right)}{\partial\left(\bar{x}\frac{V_n^2}{g}\right)}\left(V cos(\gamma) sin(\Psi) + W_x\right) + \frac{\partial\left(\bar{W}_h V_n\right)}{\partial\left(\bar{y}\frac{V_n^2}{g}\right)}\left(V cos(\gamma) cos(\Psi) + W_y\right)\right. \\
&\left. + \frac{\partial\left(\bar{W}_h V_n\right)}{\partial\left(\bar{h}\frac{V_n^2}{g}\right)}\left(V sin(\gamma) + W_h\right) + \frac{\partial\left(\bar{W}_h V_n\right)}{\partial(\bar{t}\ t_n)}\right)
\end{aligned}
\tag{B.9}
$$

$$
\begin{aligned}
\bar{W}'_h = \left(\frac{1}{g}\right)&\left[g\frac{\partial\bar{W}_h}{\partial\bar{x}}\left(\frac{V}{V_n}cos(\gamma)sin(\Psi) + \frac{W_x}{V_n}\right) + g\frac{\partial\bar{W}_h}{\partial\bar{y}}\left(\frac{V}{V_n}cos(\gamma)cos(\Psi) + \frac{W_y}{V_n}\right)\right. \\
&\left. + g\frac{\partial\bar{W}_h}{\partial\bar{h}}\left(\frac{V}{V_n}sin(\gamma) + \frac{W_h}{V_n}\right) + \left(\frac{V_n}{t_n}\right)\frac{\partial\bar{W}_h}{\partial\bar{t}}\right]
\end{aligned}
\tag{B.10}
$$

$$
\begin{aligned}
\bar{W}'_h =& \frac{\partial\bar{W}_h}{\partial\bar{x}}\left(\bar{V}cos(\gamma)sin(\Psi) + \bar{W}_x\right) + \frac{\partial\bar{W}_h}{\partial\bar{y}}\left(\bar{V}cos(\gamma)cos(\Psi) + \bar{W}_y\right) \\
&+ \frac{\partial\bar{W}_h}{\partial\bar{h}}\left(\bar{V}sin(\gamma) + \bar{W}_h\right) + \frac{\partial\bar{W}_h}{\partial\bar{t}}
\end{aligned}
\tag{B.11}
$$

B.1 General normalized wind components:

In general, $\bar{W}'_V$, $\bar{W}'_\Psi$ and $\bar{W}'_\gamma$ could be expressed in terms of $\bar{W}'_x$, $\bar{W}'_y$ and $\bar{W}'_h$ as follows

$$
\begin{aligned}
\bar{W}'_V =& \bar{W}'_x \cos\gamma \sin\Psi + \bar{W}'_y \cos\gamma \cos\Psi + \bar{W}'_h \sin\gamma \\
\bar{W}'_V =& \left[\frac{\partial \bar{W}_x}{\partial \bar{x}} \left(\bar{V} cos(\gamma) sin(\Psi) + \bar{W}_x \right) + \frac{\partial \bar{W}_x}{\partial \bar{y}} \left(\bar{V} cos(\gamma) cos(\Psi) + \bar{W}_y \right) \right. \\
& \left. + \frac{\partial \bar{W}_x}{\partial \bar{h}} \left(\bar{V} sin(\gamma) + \bar{W}_h \right) + \frac{\partial \bar{W}_x}{\partial \bar{t}} \right] \cos\gamma \sin\Psi \\
& + \left[\frac{\partial \bar{W}_y}{\partial \bar{x}} \left(\bar{V} cos(\gamma) sin(\Psi) + \bar{W}_x \right) + \frac{\partial \bar{W}_y}{\partial \bar{y}} \left(\bar{V} cos(\gamma) cos(\Psi) + \bar{W}_y \right) \right. \\
& \left. + \frac{\partial \bar{W}_y}{\partial \bar{h}} \left(\bar{V} sin(\gamma) + \bar{W}_h \right) + \frac{\partial \bar{W}_y}{\partial \bar{t}} \right] \cos\gamma \cos\Psi \\
& + \left[\frac{\partial \bar{W}_h}{\partial \bar{x}} \left(\bar{V} cos(\gamma) sin(\Psi) + \bar{W}_x \right) + \frac{\partial \bar{W}_h}{\partial \bar{y}} \left(\bar{V} cos(\gamma) cos(\Psi) + \bar{W}_y \right) \right. \\
& \left. + \frac{\partial \bar{W}_h}{\partial \bar{h}} \left(\bar{V} sin(\gamma) + \bar{W}_h \right) + \frac{\partial \bar{W}_h}{\partial \bar{t}} \right] \sin\gamma
\end{aligned}
\tag{B.12}
$$

$$
\begin{aligned}
\bar{W}'_V =& \frac{\partial \bar{W}_x}{\partial \bar{x}} \bar{V} cos^2(\gamma) sin^2(\Psi) + \frac{\partial \bar{W}_x}{\partial \bar{y}} \bar{V} cos^2(\gamma) sin(\Psi) cos(\Psi) + \frac{\partial \bar{W}_x}{\partial \bar{h}} \bar{V} sin(\gamma) cos(\gamma) sin(\Psi) \\
& + \left(\bar{W}_x \frac{\partial \bar{W}_x}{\partial \bar{x}} + \bar{W}_y \frac{\partial \bar{W}_x}{\partial \bar{y}} + \bar{W}_h \frac{\partial \bar{W}_x}{\partial \bar{h}} + \frac{\partial \bar{W}_x}{\partial \bar{t}} \right) cos(\gamma) sin(\Psi) \\
& + \frac{\partial \bar{W}_y}{\partial \bar{x}} \bar{V} cos^2(\gamma) sin(\Psi) cos(\Psi) + \frac{\partial \bar{W}_y}{\partial \bar{y}} \bar{V} cos^2(\gamma) cos^2(\Psi) + \frac{\partial \bar{W}_y}{\partial \bar{h}} \bar{V} sin(\gamma) cos(\gamma) cos(\Psi) \\
& + \left(\bar{W}_x \frac{\partial \bar{W}_y}{\partial \bar{x}} + \bar{W}_y \frac{\partial \bar{W}_y}{\partial \bar{y}} + \bar{W}_h \frac{\partial \bar{W}_y}{\partial \bar{h}} + \frac{\partial \bar{W}_y}{\partial \bar{t}} \right) cos(\gamma) cos(\Psi) \\
& + \frac{\partial \bar{W}_h}{\partial \bar{x}} \bar{V} sin(\gamma) cos(\gamma) sin(\Psi) + \frac{\partial \bar{W}_h}{\partial \bar{y}} \bar{V} sin(\gamma) cos(\gamma) cos(\Psi) + \frac{\partial \bar{W}_h}{\partial \bar{h}} \bar{V} sin^2(\gamma) \\
& + \left(\bar{W}_x \frac{\partial \bar{W}_h}{\partial \bar{x}} + \bar{W}_y \frac{\partial \bar{W}_h}{\partial \bar{y}} + \bar{W}_h \frac{\partial \bar{W}_h}{\partial \bar{h}} + \frac{\partial \bar{W}_h}{\partial \bar{t}} \right) sin(\gamma)
\end{aligned}
\tag{B.13}
$$

$$
\begin{aligned}
\bar{W}_V' = &\left(\frac{\partial \bar{W}_x}{\partial \bar{y}} + \frac{\partial \bar{W}_y}{\partial \bar{x}}\right) \bar{V} cos^2(\gamma) sin(\Psi) cos(\Psi) \\
&+ \left(\frac{\partial \bar{W}_x}{\partial \bar{h}} + \frac{\partial \bar{W}_h}{\partial \bar{x}}\right) \bar{V} sin(\gamma) cos(\gamma) sin(\Psi) \\
&+ \left(\frac{\partial \bar{W}_y}{\partial \bar{h}} + \frac{\partial \bar{W}_h}{\partial \bar{y}}\right) \bar{V} sin(\gamma) cos(\gamma) cos(\Psi) \\
&+ \frac{\partial \bar{W}_x}{\partial \bar{x}} \bar{V} cos^2(\gamma) sin^2(\Psi) + \frac{\partial \bar{W}_y}{\partial \bar{y}} \bar{V} cos^2(\gamma) cos^2(\Psi) + \frac{\partial \bar{W}_h}{\partial \bar{h}} \bar{V} sin^2(\gamma) \\
&+ \frac{\partial \bar{W}_x}{\partial \bar{\Delta}} cos(\gamma) sin(\Psi) + \frac{\partial \bar{W}_y}{\partial \bar{\Delta}} cos(\gamma) cos(\Psi) + \frac{\partial \bar{W}_h}{\partial \bar{\Delta}} sin(\gamma)
\end{aligned}
\tag{B.14}
$$

where $\partial \bar{W}_{(\ )}/\partial \bar{\Delta}$'s are given as

$$
\begin{aligned}
\frac{\partial \bar{W}_x}{\partial \bar{\Delta}} &= \bar{W}_x \frac{\partial \bar{W}_x}{\partial \bar{x}} + \bar{W}_y \frac{\partial \bar{W}_x}{\partial \bar{y}} + \bar{W}_h \frac{\partial \bar{W}_x}{\partial \bar{h}} + \frac{\partial \bar{W}_x}{\partial \bar{t}} \\
\frac{\partial \bar{W}_y}{\partial \bar{\Delta}} &= \bar{W}_x \frac{\partial \bar{W}_y}{\partial \bar{x}} + \bar{W}_y \frac{\partial \bar{W}_y}{\partial \bar{y}} + \bar{W}_h \frac{\partial \bar{W}_y}{\partial \bar{h}} + \frac{\partial \bar{W}_y}{\partial \bar{t}} \\
\frac{\partial \bar{W}_h}{\partial \bar{\Delta}} &= \bar{W}_x \frac{\partial \bar{W}_h}{\partial \bar{x}} + \bar{W}_y \frac{\partial \bar{W}_h}{\partial \bar{y}} + \bar{W}_h \frac{\partial \bar{W}_h}{\partial \bar{h}} + \frac{\partial \bar{W}_h}{\partial \bar{t}}
\end{aligned}
\tag{B.15}
$$

Following to this $\bar{W}_\Psi'$ becomes

$$
\begin{aligned}
\bar{W}_\Psi' =& \bar{W}_x' cos(\Psi) - \bar{W}_y' sin(\Psi) \\
\bar{W}_\Psi' =& \left(\frac{\partial \bar{W}_x}{\partial \bar{x}} \left(\bar{V} cos(\gamma) sin(\Psi) + \bar{W}_x\right) + \frac{\partial \bar{W}_x}{\partial \bar{y}} \left(\bar{V} cos(\gamma) cos(\Psi) + \bar{W}_y\right)\right. \\
&\left. + \frac{\partial \bar{W}_x}{\partial \bar{h}} \left(\bar{V} sin(\gamma) + \bar{W}_h\right) + \frac{\partial \bar{W}_x}{\partial \bar{t}}\right) cos(\Psi) - \left(\frac{\partial \bar{W}_y}{\partial \bar{x}} \left(\bar{V} cos(\gamma) sin(\Psi) + \bar{W}_x\right)\right. \\
&\left. + \frac{\partial \bar{W}_y}{\partial \bar{y}} \left(\bar{V} cos(\gamma) cos(\Psi) + \bar{W}_y\right) + \frac{\partial \bar{W}_y}{\partial \bar{h}} \left(\bar{V} sin(\gamma) + \bar{W}_h\right) + \frac{\partial \bar{W}_y}{\partial \bar{t}}\right) sin(\Psi)
\end{aligned}
\tag{B.16}
$$

And finally $\bar{W}_\gamma'$ turns out to be

$$
\begin{aligned}
\bar{W}'_{\gamma} =& \bar{W}'_{x} sin(\gamma) sin(\Psi) + \bar{W}'_{y} sin(\gamma) cos(\Psi) - \bar{W}'_{h} cos(\gamma) \\
\bar{W}'_{\gamma} =& \left(\frac{\partial \bar{W}_x}{\partial \bar{x}} \left(\bar{V} cos(\gamma) sin(\Psi) + \bar{W}_x \right) + \frac{\partial \bar{W}_x}{\partial \bar{y}} \left(\bar{V} cos(\gamma) cos(\Psi) + \bar{W}_y \right) \right. \\
& \left. + \frac{\partial \bar{W}_x}{\partial \bar{h}} \left(\bar{V} sin(\gamma) + \bar{W}_h \right) + \frac{\partial \bar{W}_x}{\partial \bar{t}} \right) sin(\gamma) sin(\Psi) + \left(\frac{\partial \bar{W}_y}{\partial \bar{x}} \left(\bar{V} cos(\gamma) sin(\Psi) + \bar{W}_x \right) \right. \\
& \left. + \frac{\partial \bar{W}_y}{\partial \bar{y}} \left(\bar{V} cos(\gamma) cos(\Psi) + \bar{W}_y \right) + \frac{\partial \bar{W}_y}{\partial \bar{h}} \left(\bar{V} sin(\gamma) + \bar{W}_h \right) + \frac{\partial \bar{W}_y}{\partial \bar{t}} \right) sin(\gamma) cos(\Psi) \\
& - \left(\frac{\partial \bar{W}_h}{\partial \bar{x}} \left(\bar{V} cos(\gamma) sin(\Psi) + \bar{W}_x \right) + \frac{\partial \bar{W}_h}{\partial \bar{y}} \left(\bar{V} cos(\gamma) cos(\Psi) + \bar{W}_y \right) \right. \\
& \left. + \frac{\partial \bar{W}_h}{\partial \bar{h}} \left(\bar{V} sin(\gamma) + \bar{W}_h \right) + \frac{\partial \bar{W}_h}{\partial \bar{t}} \right) cos(\gamma)
\end{aligned}
\tag{B.17}
$$

Appendix C

Derivation of Control Commands

C.1 Control Inputs for Tracking Inertial velocity, Inertial Heading angle and Inertial Flight Path angle ($\bar{V}_{(IN)}$, $\Psi_{(IN)}$, $\gamma_{(IN)}$):

In this section, the derivation of control inputs will be shown which will make sure that once the inertial speed is defined, it will be possible to track those specific commands. For this purpose, it is started with the slightly modified version of normalized velocity EoM, as

$$\bar{x}'_{c_{(IN)}} = \bar{V}_{(IN)} \cos\gamma_{(IN)} \sin\Psi_{(IN)} \tag{C.1}$$

where inertial (ground) speed (by definition [$\vec{V}_{ground} = \vec{V}_{air} + \vec{V}_{wind}$]) already includes wind information. This leads to an expression as

$$\bar{x}''_{c_{(IN)}} = \bar{V}'_{(IN)} \cos\gamma_{(IN)} \sin\Psi_{(IN)} - \bar{V}_{(IN)} \sin\gamma_{(IN)} \gamma'_{(IN)} \sin\Psi_{(IN)} + \bar{V}_{(IN)} \cos\gamma_{(in)} \cos\Psi \Psi'_{(IN)} \tag{C.2}$$

Next, using the same analogy described in previous sections, one can obtain an expression for the rate of change of velocity for each $\bar{x}$, $\bar{y}$, $\bar{h}$ component. This turns out to be an approximation to a second order tracking problem, as follows:

$$\begin{aligned} \bar{x}'' &= \left[-2\zeta\bar{\omega}_n(\bar{x}' - \bar{x}'_{c_{(IN)}})\right] = \bar{D}_{\bar{x}_{(IN)}} \\ \bar{y}'' &= \left[-2\zeta\bar{\omega}_n(\bar{y}' - \bar{y}'_{c_{(IN)}})\right] = \bar{D}_{\bar{y}_{(IN)}} \\ \bar{h}'' &= \left[-2\zeta\bar{\omega}_n(\bar{h}' - \bar{h}'_{c_{(IN)}})\right] = \bar{D}_{\bar{h}_{(IN)}} \end{aligned} \tag{C.3}$$

Following the steps defined in previous sections, necessary control actions for tracking **inertial speed strategy** can be derived as:

$$\frac{\bar{P}_{(IN)}}{\bar{V}} = \bar{\rho}\bar{V}^2(C_{D_0} + KC^2_{L_{(IN)}}) + \bar{D}_{\bar{h}_{(IN)}} \sin\gamma + \bar{D}_{\bar{x}_{(IN)}} \sin\Psi \cos\gamma + \bar{D}_{\bar{y}_{(IN)}} \cos\Psi \cos\gamma \sin\gamma \tag{C.4}$$

$$C_{L_{(IN)}} = \frac{\sqrt{(Numer_1)^2 + (Numer_2)^2}}{\bar{\rho}\bar{V}^2} \tag{C.5}$$

$$\tan\mu_{(IN)} = \frac{(\bar{D}_{\bar{x}_{(IN)}} \cos\Psi - \bar{D}_{\bar{y}_{(IN)}} \sin\Psi)}{(\bar{D}_{\bar{h}_{(IN)}} \cos\gamma + \cos\gamma - \bar{D}_{\bar{x}_{(IN)}} \sin\Psi \sin\gamma - \bar{D}_{\bar{y}_{(IN)}} \cos\Psi \sin\gamma)} \tag{C.6}$$

where terms $Numer_1$ and $Numer_2$ are defined as

$$\begin{aligned} Numer_1 &= (\bar{D}_{\bar{x}_{(IN)}} \cos\Psi - \bar{D}_{\bar{y}_{(IN)}} \sin\Psi) \\ Numer_2 &= (\bar{D}_{\bar{h}_{(IN)}} \cos\gamma + \cos\gamma - \bar{D}_{\bar{x}_{(IN)}} \sin\Psi \sin\gamma - \bar{D}_{\bar{y}_{(IN)}} \cos\Psi \sin\gamma) \end{aligned} \tag{C.7}$$

In the light of given derivations above, "Control Inputs for Tracking Inertial velocity, Inertial Heading angle and Inertial Flight Path angle ($\bar{V}_{(const)}$, $\Psi_{(const)}$, $\gamma_{(const)}$)" can also be defined accordingly, which uses the same control commands as defined in Chapter-8.